REGULATION OF MHC CLASS II EXPRESSION IN COLORECTAL CANCER

BY

OLIVER JAMES PICKLES

A thesis submitted to the University of Birmingham

for the degree of DOCTOR OF PHILOSOPHY



UNIVERSITY OF BIRMINGHAM

Institute of Immunology and Immunotherapy

College of Medical and Dental Sciences

University of Birmingham

May 2021

UNIVERSITY OF
BIRMINGHAM

University of Birmingham Research Archive

e-theses repository

This unpublished thesis/dissertation is copyright of the author and/or third parties. The intellectual property rights of the author or third parties in respect of this work are as defined by The Copyright Designs and Patents Act 1988 or as modified by any successor legislation.

Any use made of information contained in this thesis/dissertation must be in accordance with that legislation and must be properly acknowledged. Further distribution or reproduction in any format is prohibited without the permission of the copyright holder.

ABSTRACT

The vast majority of colorectal cancers (CRC) fail to respond to immune checkpoint blockade (ICB). Tumour MHC Class II expression correlates with improved response to ICB and survival in other cancers. Most pMMR CRC does not express Class II and half of CRC cell lines exhibit promoter methylation of the Class II transactivator (*CIITA*).

A collection of fifteen CRC organoids was established, eight were found to be strongly-inducible for Class II after 24 hours. Of the remaining tumours, 3 were Class II non-inducible and were deficient in IFNγ signalling and four displayed only weak Class II expression. *CIITA* methylation was not found in any organoids, in contrast to cell lines. Class II expression correlated with *CIITA* mRNA expression and ChIP PCR confirmed *CIITA* promoter histone acetylation in responsive lines, histone methylation was again not observed. Weakly-inducible lines had evidence of EZH2 occupancy of *CIITA*, however, most could strongly express Class II with prolonged IFNγ exposure for 72 hours, with responses further enhanced with EZH2 inhibition.

Deficiency of activated T cells within the CRC microenvironment is likely to explain the absence of Class II expression in many tumours. Organoids should be the standard tissue culture method for assessing epigenetics in cancer.

ACKNOWLEDGEMENTS

This work would not have been possible without the teamwork and collaboration of many of my colleagues, who have always been willing to give their time and expertise.

Firstly I must thank my supervisors Prof Gary Middleton, Prof Andrew Beggs and Prof Ben Willcox. Gary, you have always provided an unalterable drive and enthusiasm for the science, underpinned by a genuine desire to improve outcomes for our patients. Your early morning texts at the weekend have helped me stay motivated throughout. Andrew, I don't think I've ever seen anybody take on as many tasks and projects at once and yet always have time for the small details when needed. Without a doubt, you're the smartest surgeon I've ever met. Ben, thanks for guiding my formative years and always providing a calm head and eye for detail. You've often provided the balance for the project and helped keep everything grounded.

Next, I must thank Cancer Research UK for funding this work. The fantastic opportunity they have provided me and future students through establishing the Birmingham Centre has been truly invaluable. I hope the dividends will benefit the West Midlands and further afield for many years to come through creating a generation of academic cancer physicians to bring through future therapeutic advances.

Growing organoids is challenging and time-consuming at the best of times and would not have been possible without several people. Firstly, Kasun Wanigasooriya, who I've spent several months of my life with in tissue culture, had an equal share in maintaining all the organoids and took on the specialist ordering responsibilities. To all those who taught me initial organoid culture and/or helped with tissue processing when samples invariably arrived at 4pm on Fridays including João Silva, Agata Stodolna, Louise Tee, Yash Sinha, Helen Bermingham, Toju Sillo and Samita Patel.

To Nabil Quraishi and the Flow Cytometry facility (mainly Adriana Flores-Langarica) who brought me up to speed with flow cytometry. The genomics team including Claire Bryer and Celina Whalley, for putting aside their very busy service role to help design that one last experiment. Setting up the COVID testing service at the

university was pleasantly diverting at a stressful time, I'm available for another thousand RNA extractions anytime. To Anetta Ptasinska, who provided vital assistance with the ChIP work, you moved to the group at just the right time (for me!) and your 5 AM data analysis was always more accurate than mine. Aneta Drozd, congratulations on your excellent MSc. You carried the BRAF project over the line and will make an excellent PhD student.

Finally to all my NHS colleagues, both in the acute assessment areas and the cancer departments, you have been incredible throughout with your professionalism and adaptability. Not least to my wife Ali, who has taken on more than most in respiratory medicine. The last twelve months have taken a heavy toll and I couldn't have done it without your support.

COVID-19 has impacted many, but cancer patients have suffered more than most, from delayed diagnosis and cancelled curative surgery, breaks from chemo, suspension of clinical trials and the simple fear of being more vulnerable to infection. We have many things to be hopeful for and I'm sure this decade will see even greater improvements in patient outcomes. We owe it to all of them to rebuild cancer services as rapidly as possible.

TABLE OF CONTENTS

Chapter 1: Introduction 1
1.1 An introduction to colorectal cancer and rationale for the project 1
1.1.1 Colorectal cancer background: epidemiology 3
1.1.2 Colorectal cancer background: anatomy and histology 4
1.1.3 Colorectal cancer background: aetiology and molecular carcinogenesis 5
1.1.3.1 The adenoma-carcinoma sequence and chromosomal instability and new insights from organoid technology 5
1.1.3.2 Mismatch repair deficiency and microsatellite instability 8
1.1.3.3 Risk factors for the development of CRC 11
1.1.3.3 Molecular and immune characterisation 12
1.2 Treatment and Staging of Colorectal Cancer 13
1.2.1 Systemic treatment of colorectal cancer and molecular implications 14
1.2.2 Immunotherapy in malignancy 16
1.2.3 Immunotherapy in CRC 18
1.3 Barriers to immunotherapy response 21
1.3.1 Tumour intrinsic resistance: tumour mutational burden 22
1.3.2 Tumour intrinsic resistance: antigen presentation and interferon resistance 24
1.3.3 Tumour intrinsic resistance: oncogenic regulation of immunity 25
1.3.4 Tumour microenvironmental: immune contexture 27
1.3.5 Tumour microenvironmental: microbiome 29
1.4 Major histocompatibility complex (MHC) Class II 30
1.4.1 Normal biology and function of Class II 31
1.4.2 Regulation of Class II via CIITA 34
1.4.3 Class II expression and cancer including CD4+ T cell activity 36
1.4.4 Functionality of Class II in non-APCs 38
1.4.5 Mechanisms of Class II loss in tumour 42
1.4.6 Epigenetic regulation of CIITA 44
1.5 Colorectal organoids as models of disease 50
1.6 Aims and Objectives 54
Chapter 2: Materials and Methods 56
2.1 Tissue culture 56
2.1.1 Cell Line culture 56
2.1.1.1 Cell Line freezing and reviving 57
2.1.2 Organoid culture 58

2.1.2.1 Ethics and tissue collection....59
2.1.2.2 Organoid derivation....60
2.1.2.3 Organoid passaging....62
2.1.2.4 Thawing cryopreserved organoids....63
2.1.2.5 Cryopreserving organoids....63
2.1.2.6 Generation of single-cell suspensions from organoids....64
2.1.3 Mycoplasma testing....64
2.1.4 Cell viability assessment....65
2.1.4.1 GSK126 experiments....66
2.1.4.2 Entinostat....68
2.1.4.3 Interferon-gamma....68
2.2 Protein assessment....68
2.2.1 Protein extraction from cell lines....68
2.2.2 Protein extraction from organoids....69
2.2.3 Protein processing and gel electrophoresis....69
2.2.3.1 Western Blotting....70
2.2.3.2 Western buffers....72
2.3 DNA and RNA methodology....73
2.3.1 DNA/RNA extraction from cell lines and organoids....73
2.3.1.1 QUBIT quantification of RNA/DNA....73
2.3.1.2 TapeStation assessment of DNA/RNA quality....74
2.3.2 RNA procedures....74
2.3.2.1 DNAse treatment....74
2.3.2.2 Quantitative reverse transcription PCR (RT-qPCR): reverse transcription 75
2.3.2.3 Quantitative reverse transcription PCR (RT-qPCR): SYBR green PCR 75
2.3.2.4 Quantitative reverse transcription PCR (RT-qPCR): TaqMan....76
2.3.2.5 Total RNA sequencing....78
2.3.2.6 Total RNA sequencing analysis....80
2.3.3 DNA procedures: pyrosequencing analysis of DNA CpG methylation....81
2.3.3.1 Bisulfite conversion....81
2.3.3.2 Pyrosequencing PCR primer design and quality assessment....83
2.3.3.3 Pyrosequencing PCR....84
2.3.3.4 Pyrosequencing....84
2.3.4 DNA Procedures: whole-genome sequencing....86
2.3.5 DNA Procedures: Chromatin Immunoprecipitation (ChIP)....87

2.3.5.1 ChIP: cross-linking (single and dual) 87
2.3.5.2 ChIP: chromatin sonication and immunoprecipitation 88
2.3.5.3 ChIP: reverse cross-linking 91
2.3.5.3 ChIP qPCR 92
2.4 Flow cytometry 93
2.4.1 Fluorescence-activated cell sorting (FACS) 95
Chapter 3: Establishment of a collection of human colorectal cancer organoids 97
3.1 Introduction 97
3.2 Processing Tissue Samples 99
3.2 Patient characteristics of lines 102
3.3 Transcriptional subtypes 109
3.4 Summary 110
Chapter 4: Characterisation of MHC Class II inducibility in colorectal cancer organoids 111
4.1 Introduction 111
4.1.1 Aims and Objectives 113
4.2 Validation of IFNγ stimulation experiments 113
4.2.1 Dosing and timing of IFNγ stimulation 113
4.2.2 Dose-response assessment 114
4.2.3 Validation of Class II antibody and flow cytometry methodology 117
4.3 Cell line assessment 118
4.3.1 Cancer cell line IFNγ inducibility 120
4.3.2 Cancer Cell Line Summary 126
4.4 Organoid assessment 126
4.4.1 Characterisation of organoid IFNγ responses by flow cytometry 127
4.4.2 Characterisation of organoid IRF1/STAT1 responses following IFNγ 135
4.4.3 Evaluation of higher doses of IFNγ on organoid Class II expression 140
4.5 Conclusions 143
Chapter 5: Understanding the Mechanisms of MHC Class II Loss in Colorectal Cancer 145
5.1 Introduction 145
5.1.1 Revision of MHC Class II presentation 145
5.1.2 Aims and objectives 147
5.2 Tumour Characteristics and IFNγ responsiveness 148
5.2.1 Primary tumour Class II expression and organoid expression 151
5.3 Assessment of *CIITA* mRNA expression 152

5.3.1 Validation of RT-qPCR 153
5.3.2 RT-qPCR (TaqMan) for *CIITA* mRNA 154
5.4 Cell sorting of positive and negative sub-populations from organoids 158
5.5 Assessment of cell lineages comprising organoids 162
5.6 Assessment of CpG methylation of CIITA-pIV 166
5.7 Assessment of H3K9ac and H3K9me2 of CIITA-pIV 171
5.8 Assessment of EZH2 occupancy 181
5.9 Genetic determinants of Class II inducibility in organoids 184
5.10 Summary and discussion 195
Chapter 6: Reversing loss of Class II inducibility 199
6.1 Introduction 199
6.1.1 Aims and Objectives 201
6.2 Validation of EZH2 inhibitor (GSK126) and HDACi (Entinostat) dose 201
6.3 Assessment of longer exposures of IFNγ 204
6.4 Pharmacological reversal of Class II loss in organoids 207
6.5 Genomic determinants of differential EZH2 responses 214
6.6 Conclusions 217
Chapter 7: General Discussion 219
7.1 Development of the organoid collection 219
7.2 Class II is frequently inducible in CRC tumours and absence likely represents IFNγ deficiency within the TME 220
7.2.1 Therapeutic consequences of IFNγ deficiency 223
7.3 Tumour-specific Class II expression: a biomarker for ICB responsiveness? 224
7.4 Tumour-specific Class II expression: the in-situ vaccination approach? 226
7.4 Epigenetics: the pitfalls of 2D cell culture and epigenetic modifiers 227
7.5 Summary 230
Chapter 8: Appendix-flow cytometry gating 232
Chapter 9: References 235

LIST OF TABLES

Table 1.1 Reported trials of immunotherapy in CRC. 20
Table 2.1 Cell Lines 57
Table 2.2 Antibodies for Western Blot experiments 72
Table 2.3 Antibody details for flow cytometry experiments 95
Table 3.1 Characteristics of derived organoids. 104
Table 3.2 CMS Classification of organoids. 109
Table 4.1 Summary of known cell line class II inducibility with IFNγ and underlying methylation status of promoter IV of CIITA. 119
Table 4.2 Summary of Flow Cytometry Class II inducibility of colorectal cancer cell lines +/- IFNγ stimulation. 121
Table 4.3 Summary of Flow Cytometry Class II inducibility of colorectal cancer organoids +/- IFNγ stimulation 127
Table 5.1 Clinicopathological characteristics of organoids and Class II expression. 150
Table 5.2 Summary of CIITA RT-qPCR results. 155
Table 5.3 Bisulfite conversion efficiency. 167
Table 5.4 Pyrosequencing results for CIITA-pIV methylation. 170
Table 5.5 H3K9ac changes with IFNγ. 179
Table 5.6 H3K9me2 changes with IFNγ. 180
Table 5.7 KEGG pathway enrichment 192

LIST OF FIGURES

Figure 1.1 Anti-CTLA-4 and anti-PD-1 immunotherapy……..18

Figure 1.2 Immunotherapy response by tumour type and mutation rate……..22

Figure 1.3 Antigen presentation via MHC Class II……33

Figure 1.4 Regulation of CIITA-pIV expression……36

Figure 1.5 Example morphology of human colorectal organoids……..52

Figure 2.1 Bisulfite conversion……82

Figure 2.2 Optimisation of ChIP Covaris shearing times……90

Figure 2.3 Flow cytometry gating……95

Figure 3.1 Derivation of organoids……101

Figure 4.1 Western blot for IFNγ dose confirmation……..116

Figure 4.2 Flow Cytometry Class II Antibody Validation in HEK293 ± CIITA cells...118

Figure 4.3 Western blot of IFNγ response in colorectal cell lines……122

Figure 4.4 Flow cytometry assessment of Class I and Class II expression in four colorectal cancer cell lines...……..123

Figure 4.5 Summary of flow cytometry Class II inducibility for colorectal cancer cell lines……124

Figure 4.6 Flow cytometry assessment of Class II expression following prolonged IFNγ exposure in three minimally responsive colorectal cell lines……..125

Figure 4.7 Flow cytometry assessment of Class I and Class II expression in three non-inducible organoids lines……129

Figure 4.8a Flow cytometry assessment of Class I and Class II expression in four weakly-inducing organoid lines……130

Figure 4.8b: Summary of Class II expression in four weakly-inducing lines……..131

Figure 4.9a Flow cytometry assessment of Class I and Class II expression in strongly-inducing organoid lines……132

Figure 4.9b Flow cytometry assessment of Class I and Class II expression in strongly-inducing organoid lines……133

Figure 4.9c Summary of Class II expression in eight strongly-inducing lines……134

Figure 4.10 Western blot of IFNγ response in non-responding organoid lines…….136

Figure 4.11 Western blot of IFNγ response in weakly-inducing organoid lines…….137

Figure 4.12 Western blot of IFNγ response in strongly-inducing organoid lines…...138

Figure 4.13 Flow cytometry assessment of IFNγ Receptor surface expression…...140

Figure 4.14a Flow cytometry assessment of Class II responses with higher IFNγ doses in strongly inducible lines……141

Figure 4.14b Flow cytometry assessment of Class II responses with higher IFNγ doses in weakly inducible lines……142

Figure 5.1 Melt Curve from CIITA/GAPDH SYBR Green Validation……...154

Figure 5.2 RT-qPCR for CIITA mRNA expression following IFNγ stimulation……..155

Figure 5.3 Flow cytometry assessment of Class II sorted organoids……..161

Figure 5.4 Western blot of IFNγ response in Class II sorted lines……..162

Figure 5.5 Flow cytometry assessment of cell populations within organoids……164

Figure 5.6 Flow cytometry assessment of sorted organoid lines for goblet cell populations……165

Figure 5.7 Pyrosequencing of CIITA-pIV in organoids and cell lines……..169

Figure 5.8 CIITA-pIV H3K9 acetylation in cell lines and organoids……173

Figure 5.9 CIITA-pIV H3K9me2 in cell lines and organoids……176

Figure 5.10 CIITA-pIV occupancy by EZH2……182

Figure 5.11 RNA expression of IFNγ response pathway genes……..186

Figure 5.12 Differential RNA expression in non-inducible organoids……188

Figure 5.13 Hierarchical clustering of expression data for non-inducible organoids. ……189

Figure 5.14 Principal Component Analysis (PCA)……190

Figure 5.15 Gene Ontology analysis of Class II inducible (strong/weak) vs non-inducible organoids……193

Figure 5.16 KEGG pathway display for retinol metabolism……..194

Figure 6.1 GSK126 viability across colorectal cancer organoids……203

Figure 6.2 Treatment of non-responsive organoids with longer duration of IFNγ….206

Figure 6.3a Pharmacological reversal of Class II loss and longer IFNγ exposure in weakly inducible organoids……209

Figure 6.3b Pharmacological reversal of Class II loss and longer IFNγ exposure in weakly inducible organoids……210

Figure 6.3c Pharmacological reversal of Class II loss and longer IFNγ exposure in weakly inducible organoids……211

Figure 6.3d Pharmacological reversal of Class II loss and longer IFNγ exposure in weakly inducible organoids……212

Figure 6.4 Class II expression with longer duration IFNγ, GSK126 and Entinostat. 213

Figure 6.5 RNA expression of PRC2 and SWI/SNF complex proteins……...216

LIST OF ABBREVIATIONS

ACT	adoptive cell transfer
APCs	antigen presenting cells
ATP	adenosine triphosphate
CAR T cell	Chimeric Antigen Receptor T cell
ChIP	chromatin immunoprecipitation
CIITA	class II transactivator
CIMP	CpG methylator phenotype
CMS	consensus molecular subtypes
CRC	colorectal cancer
CRIS	CRC intrinsic subtypes
CTLA-4	cytotoxic T-lymphocyte-associated protein 4
DC	dendritic cell
diH20	deionised water
DMSO	dimethyl sulfoxide
DNMT	DNA methyltransferase
EGFR	epidermal growth factor receptor
EZH2	enhancer of zeste homolog 2
FMO	fluorescence minus one
HATs	histone acetyltransferases
HDAC	histone deacetylase
HLA	human leukocyte antigen
IBD	inflammatory bowel disease
ICB	immune checkpoint blockade
IEC	intestinal epithelial cell
lFNγ	interferon-gamma
IHC	immunohistochemistry
MDSC	myeloid-derived suppressor cells
MHC	major histocompatibility complex
d/pMMR	mismatch repair deficient/proficient
MSI(-Hi)	microsatellite instability (high)
MSS	microsatellite stable

nf-H20	nuclease-free water
OHS	organoid harvesting solution
OS	overall survival
PBS	phosphate-buffered saline
PBSO	Dulbecco’s phosphate-buffered saline (without Ca2+, Cl- and Mg2+)
PCR	polymerase chain reaction
PD-1	programmed cell death protein 1
PD-L1/2	programmed cell death ligand 1/2
PDO	patient-derived organoids
PFS	progression-free survival
PRC2	polycomb repressive complex 2
TCR	T cell receptor
TDB	tumour digestion buffer
Th1	type 1 T cell helper
TIL	tumour-infiltrating lymphocyte
TMB	tumour mutation burden
TME	tumour microenvironment
TNM	tumour/nodal/metastasis staging
Treg	regulatory T cell
UHB	University Hospitals Birmingham

Chapter 1: Introduction

1.1 An introduction to colorectal cancer and rationale for the project

Colorectal cancer (CRC) remains a significant cause of mortality and morbidity globally. Despite the multiple advances in targeted medicine and immuno-oncology over the last decade, these new therapeutic options remain limited to small sub-groups of CRC patients or have limited efficacy. The backbone of therapy for the patient diagnosed with metastatic colorectal cancer in 2021 remains traditional cytotoxic chemotherapy, with treatment regimens that have remained largely unchanged for over ten years (1).

The immune system has been postulated to have a key role in controlling cancers, however, it is only with the advent of immune checkpoint blockade (ICB) that the full potential of this approach has been realised. Discovery of the Programmed Cell Death Protein 1 (PD-1) axis, through which cancer can evade activated T cell responses, led to the development of compounds that block the pathway (2). This has been best demonstrated in metastatic melanoma, a tumour that had previously been close to untreatable. With immunotherapy, however, it has been possible to achieve durable clinical benefit and even cure in significant numbers of these patients (3). CRC by contrast, has a dismal response to ICB, except for the few percent of metastatic patients who have Mismatch Repair Deficient (dMMR) disease, likely as a result of the very high numbers of neoantigens in these hypermutated tumours (4). The overarching purpose of this work is to explore the mechanisms limiting the responsiveness of microsatellite stable (MSS) CRC to immunotherapy, and where possible to counter this phenomenon.

Tumour-specific major histocompatibility complex (MHC) Class II expression has previously been shown to correlate with improved prognosis and predict response to ICB (5, 6). Work by this group established that MHC Class II could be used to stratify MSS colorectal tumours into different levels of immunogenicity, potentially identifying a biologically unique subgroup that could benefit from ICB (7). This fundamentally clinical question is currently being assessed in the phase II clinical trial, ANICCA, which is the first trial to prospectively select patients to be treated with ICB (Nivolumab) based on MHC class II expression (Gary Middleton CI; ClinicalTrials.gov Identifier: NCT03981146).

Our understanding of MHC class II and the role it plays in modulating the disease course and survival largely comes from retrospective analysis of resection specimens and cell line work. Several weaknesses exist with these approaches, however. Resection specimens are predominantly obtained from patients whose cancers have not metastasised, and therefore represent a predetermined biological group which is likely to be fundamentally different from a group of patients who present with metastases. Cell lines are a simplification of cancer, grown in isolation of the tumour microenvironment (TME) or immune system and issues such as clonal selection based on growth characteristics favoured in the plastics and media chosen by the laboratory. Additionally, cell lines lack the complex subclonal heterogeneity of a ‘complete’ cancer. They rapidly diverge from their original biology and it has been demonstrated that the same cell line e.g. MCF7 grown in different research groups can be transcriptionally and genetically distinct (8), or even incorrectly characterised as a different tumour type (9). Alternative methods of studying cancers have included animal modelling, with limitations assessing the immune responses to human

cancers in immuno-competent animals, as well as the cost, time and ethical considerations.

Technological improvements in 3D tissue culture has seen the establishment of patient-derived organoids (PDO) in the last few years. These systems retain morphological and clinicopathological features of the tissues they are derived from, including subclonal heterogeneity and unlike 2D models, are stable genetically and epigenetically over time (10, 11). As a method for studying cell-autonomous cancer biology, for example, the inducibility of MHC Class II in CRC, organoids provide a bridge between in vivo models and an ex vivo system that can be manipulated whilst maintaining fidelity to the original tumour. This thesis encompasses the development of a collection of PDOs from local patients and the study of Class II biology within these models.

1.1.1 Colorectal cancer background: epidemiology

Colorectal cancer is one of the four most common cancers affecting patients in the UK. In 2017, there were approximately 40000 new cases diagnosed. Whilst age-standardised incidence has largely been stable, there has been an increasing rate in younger patients under the age of 50 (12). This increase in younger patients remains poorly understood, however many have poor prognostic features and most do not have a readily identifiable hereditary cancer syndrome (13). Mortality from CRC accounts for just over 16000 deaths per year in the UK and is therefore the second most common cause of cancer death (12).

1.1.2 Colorectal cancer background: anatomy and histology

Colorectal cancer encompasses a heterogeneous group of malignancies arising from the colon and rectum. Despite many similarities between tumours, differences in embryological origin, lymphatic system and blood supply exist through the length of the large intestine. These differences are increasingly recognised as biologically relevant when considering the treatment of colorectal cancer systemically. The start of the colon is defined proximally by the ileocaecal valve, which serves to minimise retrograde reflux of bowel contents into the terminal ileum. The ascending colon and the majority of the transverse colon are supplied by the superior mesenteric artery, with arterial supply to the distal transverse and descending colon coming from the inferior mesenteric artery. The rectum is also supplied by the inferior mesenteric artery, with the more inferior portion additionally supplied by branches of the internal iliac artery (14).

On histology, the vast majority of colorectal tumours are adenocarcinomas, with a low single-figure percentage of neuroendocrine tumours (both high and low grade). Other types of colon tumour are rare, including squamous (typical of anal lesions below the dentate line but very rare within the colon), sarcomas and lymphomas. For the avoidance of doubt, where CRC is discussed in this document, it refers to adenocarcinomas.

Immunohistochemistry (IHC) can be performed to further characterise colorectal lesions as bowel origin, with CK20 and CDX2 positivity and CK7 negativity most commonly observed. Molecular pathology assessment of colorectal biopsies and resections has expanded in the last decade and is now an important part of patient

stratification. MMR deficiency should be assessed in all newly-diagnosed patients and extended-spectrum RAS (Exon 2-4 of *KRAS* and *NRAS*) and *BRAF* V600 mutations should be assessed in any patients being considered for anti-EGFR antibody therapy (15, 16).

1.1.3 Colorectal cancer background: aetiology and molecular carcinogenesis

Colorectal tumours have been shown to develop through several mechanisms of molecular carcinogenesis. CRC can be classified as demonstrating either chromosomal instability (CIN) or microsatellite instability (MSI). Much of our knowledge of these two forms of CRC come from two hereditary syndromes. Although the pathways involved in these inherited forms typically leads to tumours in younger patients, the same molecular pathogenesis is found to underpin sporadic CRC cases (17).

1.1.3.1 The adenoma-carcinoma sequence and chromosomal instability and new insights from organoid technology

Vogelstein described the classic model of adenoma-carcinoma sequence in the 1980s, defining the carcinogenesis of CRC with CIN (18). This sequence was based on the observation that most CRC tumours arose from adenomas (or polyp; a pre-malignant dysplastic lesion), in a process that frequently took many years for an invasive tumour to form. Similarly, a relatively rare familial syndrome had previously been identified where patients presented with many polyps from a young age, developing invasive CRC by their early forties. This syndrome, known as familial adenomatous polyposis (FAP), was found to have an underlying genetic cause, with a heterozygous germline loss of the long arm of chromosome 5 bearing the

adenomatous polyposis coli (*APC*) gene (19). Interestingly, many sporadic CRCs were also found to have a double hit (missense, stop-gain or other deleterious geneic event) affecting both copies of the *APC* tumour suppressor gene (TSG) (20), although the patients with these sporadic cancers had no evidence of germline APC mutation. Instead, it was postulated that these patients acquired two independent mutations within copies of *APC* within the same cell, a process recognised by Knudson in retinoblastoma (with the TSG, in this case, the *RB1* gene) and subsequently referred to as the 'two-hit hypothesis (21).'

Vogelstein sought to identify if a defined order of genetic aberrations led to CRC, examining tissue samples from multiple patients with increasingly malignant lesions from early adenomas in patients with FAP, adenomas (both with and without small malignant foci) in non-FAP patients and finally resected invasive tumours (18). Four known mutations were assessed across this range of adenomas and tumours: 1) *RAS* mutation, 2) loss of 5q chromosome; subsequently confirmed as *APC*, 3) 17p chromosomal loss; subsequently determined to be *TP53* loss and 4) loss of 18q; containing the Deleted in Colorectal Carcinoma (*DCC*) putative TSG. As adenomas enlarged or developed small areas of adenocarcinoma, an increasing number of molecular aberrations were detected. Generally, 5q/*APC* loss and *RAS* mutations were found to be early events, with 18q and p53 loss seen to a greater extent in developed cancers (17, 18, 22).

APC loss is therefore an important early event in the formation of adenomas and cancers. *APC* functions as a TSG in Wnt/APC/β-Catenin signalling, a pathway that is of vital importance to intestinal stem cell (ISC) biology and control of proliferation. APC loss leads to an accumulation of β-Catenin both in the nucleus and at cadherin

junctions, activating the TCF/LEF transcription factors and destabilising cell-cell adhesions respectively and is detected in the majority of CRC (23, 24). In cancers without evidence of *APC* loss, other Wnt pathway-activating mutations are frequently found, including loss of *RNF43* which normally serves to internalise and degrade Frizzled, the canonical pathway receptor for Wnt (25).

Until recently, the lack of a stem cell model limited the ability to test the effect of each potential driver mutation on carcinogenesis. Cell lines by definition have to be immortalised to grow in vitro and therefore will have acquired many of the mutations and adaptations required to grow independently. Additionally, driver mutations must be contained within ISCs, as the daughter cells of these stem cells rapidly migrate through crypts and terminally differentiate before undergoing anoikis, an apoptotic shedding into the gut lumen. Differentiated cells from ISCs have only around a one-week lifespan, therefore mutations must arise within and be maintained in ISCs during the months and years required for a polyp to become malignant (26, 27). With organoid culture, it has been possible to support ISC growth from non-malignant bowel, with culture conditions requiring Wnt, R-Spondin, epidermal growth factors and several other factors to propagate (10).

Established ISC cultures (from normal bowel) have previously undergone sequential genome editing with CRISPR-Cas9 to assess which genetic events led to independence from growth factor signalling in culture media and to attempt to recreate the adenoma-carcinoma sequence. Normal bowel stem cells with *APC* loss (or constitutively active β-catenin) become independent of Wnt and R-Spondin requirements, *TP53* and *SMAD4* deleted organoids grow without Noggin and TGFβ inhibition. $KRAS^{G12V}$ mutation allows for some attenuated growth in EGF depleted

media, however, additional *PI3KCA*^{E545K} mutation was required for complete independence from EGF. Normal bowel organoids with all five of these features grow in completely unsupplemented media. However, the requirements for true tumorigenicity remain more complex, with the five-mutation (*APC, SMAD4, TP53, KRAS* and *PI3KCA*) engineered organoids able to form only minimally invasive tumours in mice and the metastases formed from these tumours also failed to progress to greater than 1 mm in size. By contrast, organoids derived from CRC freely formed tumours in mice and gave rise to large volume metastasis. The genome-edited normal bowel organoids remained largely well-differentiated and failed to develop CIN. Interestingly, when repeating the process with low-grade adenoma derived organoids, deletion of *TP53* and *SMAD4* led to similar behaviours in mice as the five-mutation normal organoids, but the addition of either a *KRAS* or *PI3KCA* mutation to the organoids led to the development of aggressive cancers with large volume metastasis. It, therefore, seems possible to engineer driver mutations in normal gut epithelium to model Wnt/Niche-independent stem cell behaviour, but without fully recapitulated tumour characteristics (28). Drost et al also performed a near-identical version of these experiment during the same period, with highly concordant findings (29).

1.1.3.2 Mismatch repair deficiency and microsatellite instability

An alternate pathway of colorectal carcinogenesis has been described, affecting around 15% of patients diagnosed with CRC. Defects in the mismatch repair proteins (MMR; typically annotated as either pMMR or dMMR for proficient or deficient respectively) confers a ‘hypermutator phenotype,’ leading to the accumulation of large numbers of mutations within dMMR tumours. The MMR genes (*MLH1, MSH2,*

MSH3, MSH6, PMS1 and *PMS2*) encode proteins responsible for the detection of errors of replication, typically seen in areas of microsatellites (30). Microsatellites are repetitive sequences of between one and six nucleotides. DNA polymerase is prone to slippage in these repetitive areas, which if not recognised and repaired, leads to a variable number of repeats in that region, frameshift and insertion/deletion (indels) mutations. This variable read length observed within defined microsatellites is termed microsatellite instability (MSI) (31).

Assessment of patients for dMMR has traditionally been performed in two ways. Firstly, MMR protein expression can be stained for using IHC in a tumour sample, with loss of protein expression typically followed up with confirmatory genetic (germline) testing. This is the current means of assessing patients in standard clinical practice (32, 33). The second option is to use a PCR and sequencing-based approach, amplifying five representative microsatellite loci. The most commonly used has been the Bethesda panel, with tumours defined as MSI-H (high) if three or more regions demonstrate length discrepancies, MSI-L (low) if one or two regions have evidence and microsatellite stable (MSS) if all of the regions are uniform (34). More recently, next generation sequencing (NGS) approaches, including the TruSight Oncology 500 assay, have become more standardised and are beginning to enter clinical utility. Generally, the terms MSI-H and dMMR are used interchangeably when discussing this unique subgroup of tumours.

Clinically, dMMR tumours can arise both as part of a hereditary syndrome known as Hereditary Nonpolyposis Colorectal Cancer (HNPCC, also known as Lynch syndrome) or as a sporadic form. In HNPCC, patients present with colorectal cancers from around the mid-forties and can also develop other organ tumours, most typically

endometrial, with an underlying germline loss of a single copy of an MMR gene. These familial clusters are important to identify, with affected relatives offered enhanced endoscopic surveillance, aspirin and earlier curative diagnosis. Most dMMR tumours, however, arise spontaneously, with around 80% having no familial component and no evidence of germline mutation. The most common route of spontaneous dMMR is promoter methylation of *MLH1*, which causes loss of both *MLH1* and *PMS2* expression, with the expression of the latter dependent on *MLH1*. These tumours are observed more frequently observed in right-sided, *BRAF* mutant tumours (35, 36).

dMMR CRC tumours have been known to be a biologically distinct entity for some time, with better outcomes following surgery as well as reduced benefits (or potentially even harm in the case of single-agent fluoropyrimidine) from chemotherapy in the adjuvant setting (37, 38). More recently these differential responses have been observed in the neoadjuvant FOxTROT study, with significantly lower radiological and histopathological responses in dMMR tumours with chemotherapy (39). Although around 15% of all CRC will be dMMR, this prevalence drops to only 3% in the metastatic patient cohort. The improved prognosis conferred by dMMR has been linked with enhanced immune recognition of the very high neoantigen burden (40, 41). The TME of dMMR CRC is frequently characterised by the presence of a CD8+ T cell and CD4+ Th1 polarised immune infiltrate, in stark contrast to the majority of pMMR CRC tumours. These inflamed tumours are often balanced with the expression of multiple inhibitory immune checkpoints and the interplay of Immune Checkpoint Blockade (ICB) with this disease group will be considered subsequently (42, 43).

It is worth noting that a second group of hypermutated CRC have been identified, with DNA polymerase ε and δ (*POLE* and *POLD1*) mutations. These genes are responsible for base excision and repair and loss of function leads to the accumulation of mutations at an even higher rate than in dMMR CRC. Though a relatively rare subgroup of pMMR CRC (around 1%), they appear to behave similarly to dMMR tumours, in particular concerning ICB response. Typical mutation rates observed in dMMR, *POLE* and *POLD1* mutated CRC range from 30-60, 100-200 and >200 mut/MB respectively.(44, 45).

1.1.3.3 Risk factors for the development of CRC

The familial syndromes of FAP and HNPCC make up a small percentage of the total cases of CRC, around 1 and 5% respectively. However, around a fifth of patients will have some hereditary component, as assessed by the Amsterdam criteria (46), based around the age of diagnosis in first- and second-degree relatives. The vast majority of cases will have no significant genetic component, with risk factors including age, male gender, western diet (red meat, low fruit and vegetable consumption and processed foods), obesity, type II diabetes mellitus and alcohol all linked (47). A sedentary lifestyle has been increasingly recognised as important in the development of many cancers, with this effect particularly pronounced in CRC, with a postulated mechanism of insulin resistance. There is a growing body of evidence that exercise can prevent CRC (primary prevention), improve long term outcomes after surgery in the adjuvant setting as well as improving outcomes and enabling higher chemotherapy intensity in those with recurrent disease (48). Patients with Inflammatory Bowel Disease (IBD), including Ulcerative Colitis (UC) and Crohn's disease, have chronic inflammation in their bowel, which is carcinogenic (49). IBD

patients have a significantly increased lifetime risk of developing CRC, with the risk particularly pronounced in UC, those with greater extent and duration of inflammation and those who also develop Primary Sclerosing Cholangitis (PSC; which is strongly associated with UC). As with hereditary syndromes like HNPCC, IBD patients should be offered enhanced endoscopic surveillance and prophylactic surgery (ideally panproctocolectomy) can be considered in the higher risk groups (50).

1.1.3.3 Molecular and immune characterisation

In recent years our understanding of the molecular and immune context of CRC has improved substantially. By 2015, six separate but highly interconnected transcriptionally subtype classifications had been proposed. To unify these approaches, a combined analysis was performed in 2015 to generate the Consensus Molecular Subtypes (CMS) (51). The CMS divided CRC into 4 subgroups: 1) CMS 1; immune activated, largely comprised of MSI-H, 2) CMS2; canonical, with a strong epithelial component and activation of Wnt and *KRAS* mutations, 3) CMS3; metabolic, similar to CMS2 but with a substantially deranged metabolic component and 4) CMS 4; mesenchymal, marked by stromal infiltration, TGFβ signalling and epithelial-mesenchymal transition. Survival varied between groups, with increased survival in CMS1 and worst survival in CMS4 (51). Interestingly, both CMS1 and CMS4 are marked by immune infiltration, with CMS4 typically displaying an inflamed TME, with inhibitory cytokine expression and polarisation towards tolerant populations compared with the Th1 cytotoxic polarisation in CMS1 (52, 53). One potential weakness with the molecular stratification is that many systems use whole tumour samples, including stroma and immune infiltrates. Arguably these microenvironmental fractions are also vital to treatment response and prognosis. A

separate stratification has been proposed called the CRC intrinsic subtypes (CRIS), which analyses just the epithelial component and transcription profile of the cancer cells, resulting in five sub-classifications (54).

It has been known for some time that CRC tumours with an increased presence of Tumour Infiltrating Lymphocytes (TILs) have a better prognosis and are less likely to develop distant metastasis (55) and are also more commonly seen in MSI-H CRC (43). A more nuanced approach to assessing TIL populations was developed by Galon et al. IHC quantification of CD3+ and CD8+ cells in both the core and invasive front of the tumour using an automated algorithm to calculate Immunoscore, with higher scores identifying more immune infiltrated tumours. Immunoscore better predicts overall and recurrence-free survival following resection of CRC than standard TNM staging and grading, and has the potential to supplement traditional staging information, allowing for improved selection of patients to undergo adjuvant chemotherapy (56).

1.2 Treatment and Staging of Colorectal Cancer

Patients presenting with a new diagnosis of CRC should be reviewed on a Multidisciplinary Team (MDT) meeting at a centre specialising in CRC (57). Staging of patients should be performed, initially based on radiographic images (typically CT scan with additional MRI for rectal cancer) and final pathological staging based on the resection specimen. TNM staging, most recently updated to version 8, is used to classify tumours by the extent of their local and distant spread and has largely replaced the older Dukes' staging. Tumour (T) staging encompasses the level and depth of invasion of the primary tumour through the bowel wall and into the

surrounding structures. Nodal (N) staging reports the number of involved lymph nodes, whilst Metastasis (M) staging denoting radiologically diagnosed distant metastatic deposits (58).

Patients who present with early-stage resectable disease should proceed straight to surgery (57). Locally advanced rectal cancers may require pre-operative chemo/radiotherapy to allow for adequate margins at resection, typically this is performed as chemoradiotherapy. Post-operative patients with evidence of lymph node involvement (stage III) will be offered adjuvant chemotherapy, as will those with stage II (T3/4 N0) with other risk factors including extramural vascular invasion, perforation and T4 primary (57, 59). A subgroup of patients who present with isolated synchronous liver metastasis can benefit from synchronous or staged resection of these deposits and this approach is commonly taken for metachronous liver disease, often following a period of systemic treatment (60, 61).

1.2.1 Systemic treatment of colorectal cancer and molecular implications

Standard of care treatment of colorectal cancer has remained largely unchanged over the last decade. Chemotherapy, almost exclusively used as a doublet combination of two drugs is administered every two to three weeks, with response assessment with a CT scan performed every three months. Fluoropyrimidines, including 5-fluorouracil (5-FU) and the pro-drug capecitabine, form the backbone to treatment rotas and are given alongside either oxaliplatin (e.g. CAPOX/FOLFOX for the combination with capecitabine or 5-FU/folinic acid respectively) or irinotecan (usually given as FOLFIRI) (1). All patients being considered for systemic treatment should be tested for *BRAF* and *RAS* mutation, as well as MMR status (57). These

mutations are relatively common in CRC, making up around 10% and 45% of patients respectively (62). The importance of these mutations is that they predict resistance to anti-EGFR monoclonal antibody therapy with cetuximab or panitumumab. The Epidermal growth factor receptor (EGFR) is a receptor tyrosine kinase (RTK) and is commonly overexpressed in CRC (63, 64). RAS and BRAF operate immediately downstream of EGFR and under physiological conditions, EGFR activates RAS (RAS-GTP), which leads to dimerization of RAF isomers (ARAF/BRAF/CRAF) with subsequent phosphorylation of MEK and then ERK (62). In the presence of constitutively active BRAF or RAS, blockade of the upstream receptor is therefore ineffective (65). Patients who are wild-type can receive a combination of an anti-EGFR monoclonal antibody with their first-line doublet chemotherapy regime on current NHS funding arrangements (1, 57).

Worldwide, aside from anti-EGFR targeted therapy, bevacizumab has been used to target vascular endothelial growth factor (VEGF) receptor signalling, which plays an important role in tumour angiogenesis and survival (66-69). Bevacizumab (and aflibercept) have been shown to improve overall survival in some studies, however, this data is insufficient for the National Institute for Health and Care Excellence (NICE) to approve funding in the UK currently (70).

Three recent developments have led to changes in practice in colorectal oncology. Firstly, Trifluridine/Tipiracil chemotherapy has been approved as a third-line agent (71). Secondly, the BEACON CRC study, assessing combination targeted treatment in *BRAF* V600E mutant CRC, reported for the first time an overall survival improvement over chemotherapy of a regime consisting of encorafenib (a BRAF inhibitor) with cetuximab (72). *BRAF* mutant disease is known to confer significantly

poorer prognosis, resistance to chemotherapy and previous attempts with both BRAF monotherapy and combination strategies with MEK and EGFR inhibition have been of limited efficacy and this study, therefore, represents a long-needed improvement (73, 74). The most significant change, however, has been the treatment of CRC with immunotherapy and identification of responsive disease subtypes.

1.2.2 Immunotherapy in malignancy

Over the last decade, immunotherapy has become increasingly common in the treatment of malignancies. Whilst cellular therapies, including Chimeric Antigen Receptor (CAR) T-cells, have failed thus far to make an impact in the solid tumour groups (75), monoclonal antibody inhibition of immune checkpoints has expanded rapidly. A large number of immunoregulatory checkpoint molecules have been identified that are likely to be important to cancer immune evasion. The most recognised classes are the cytotoxic T-lymphocyte-associated protein 4 (CTLA-4) and programmed cell death protein 1 (PD-1) / ligand (PD-L1), and it is these two classes that are routinely targeted with cancer immunotherapy. Whilst many compounds are in clinical development, the approved ICB agents consist of anti-CTLA-4 drugs (ipilimumab and tremelimumab) and drugs targeting PD-1 (pembrolizumab and nivolumab) and PD-L1 (avelumab, atezolizumab and durvalumab) (76, 77).

These two groups of drugs have fundamentally different mechanisms and frequently they are utilised in combination for synergy, for example in melanoma and renal cancer (3, 78). CTLA-4 is expressed on naïve T-cells at the stage of priming with antigen presenting cells (APCs) including dendritic cells. These professional APCs

collect primarily exogenous antigen from dying tumour cells and return to regional lymph nodes where they encounter naïve T cells. Antigen is presented through both Major Histocompatibility Complex (MHC) Class I and II, with sensing of antigen by naïve T cells through the T cell receptor (TCR), providing the 'first signal' for priming. A complex interaction of co-stimulatory (CD28, CD40, OX40) and co-inhibitory (CTLA-4, LAG3, TIM3) signals occurs, influenced by external factors including the presence of cytokines, providing the 'second signal.' CTLA-4 is potently upregulated on the cell surface of T cells following TCR engagement and is therefore targetable to enhance priming and increasing the likelihood of T cell activation occurring (79). Once primed, T cells return to the tumour and again through TCR/MHC interaction detect antigen on tumour cells, resulting in the production of Interferon-gamma (IFNγ). IRF1, a downstream interferon-stimulated response element (ISRE) of IFNγ, binds to the promoter of the genes for PD-L1 and PD-L2, which are subsequently expressed on the tumour surface, binding the PD-1 receptor on T cells with the potential to cause inactivation of that T cell (79, 80) (**Figure 1.1)**.

ICB agents therefore can increase T cell activation at the site of antigen presentation and priming (CTLA-4), as well preventing inactivation and exhaustion of T cells in the TME (PD-1). Additionally, as these mechanisms are non-specific and likely to be common means of immune evasion, the applicability of these compounds to multiple tumour types has occurred (81). Despite this, the responses between tumour types varies substantially.

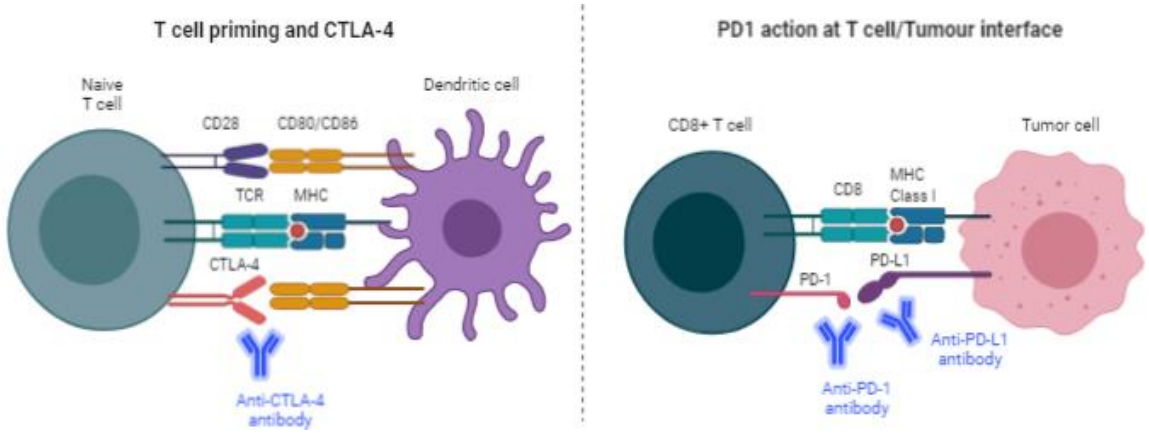


Figure 1.1 Anti-CTLA-4 and anti-PD-1 immunotherapy. Site of action and mechanism of common ICB agents. Priming of T cells (**left**) largely occurs in lymphoid structures. Recognition of MHC-expressed antigens by naïve TCR leads to competition between co-inhibitory (e.g. CTLA-4; which is upregulated following TCR engagement) and co-stimulatory (e.g. CD28) molecules expressed by T cells. Blockade of CTLA-4 pushes the balance towards activation of naïve T cells. Primed T cells then traffic back towards the tumour, utilising chemokine signalling and cytokine gradients. Once T cells re-enter the tumour (**right**), antigen on tumour MHC molecules is again recognised through TCR interaction. Engagement with the tumour MHC leads to production of IFNγ, causing tumours to upregulate PD-L1/2 which binds to the PD-1 receptor on T cells, causing inactivation and apoptosis. Anti-PD1 axis compounds block the signal, either through binding to ligand on tumour or the receptor on T cells. Diagram adapted from Pardoll et al, with image creation in BioRender.

1.2.3 Immunotherapy in CRC

For a tumour to respond to ICB, the first requirement is that mutated proteins are present to be recognised by the immune system as foreign. It is reasoned that if there is a greater number of neoantigens within a tumour, that the chances of immunogenic peptide being identified would be higher. ICB in non-small cell lung cancer (NSCLC) is more effective in smokers compared with non-smokers. This effect is caused by the high number of clonal mutations (e.g. in the majority of cells that make up that cancer) produced by the mutagens in tobacco smoke (82). Melanoma, the archetypal immunotherapy responsive tumour, is similarly caused by mutagen exposure (UV light) with a high average tumour mutation burden (TMB) (83). Indeed, TMB is a strong independent predictor of response and outcome with

ICB. In head and neck, bladder and NSCLC tumours, the threshold for response to ICB was around 200 mutations (84). Another study looked across a range of cancers, grouping tumours as high, intermediate or low TMB based on >20 mutations/mb, 6-19 mutations/mb and 1-5 mutations/mb respectively. Improved responses rates, progression-free (PFS) and overall survival (OS) were again observed with the high TMB in NSCLC and melanoma (the typically responsive tumours) treated with anti-PD-1 therapies (85).

dMMR tumours, with high TMB and microenvironments characterised by immune infiltrates and the expression of immune checkpoints are highly responsive to ICB (42). The US Food and Drug Administration (FDA) granted accelerated approval for pembrolizumab in all dMMR tumours in 2017, an unusual biomarker specific approval (86). A formative phase II study was performed by Le et al, comparing dMMR CRC, pMMR CRC and other tumours with dMMR treated with single-agent pembrolizumab. Responses were high in both of the dMMR groups (40% in CRC and 71% in non-CRC, n=10 and 7 respectively). The response rate of 0% in pMMR CRC was if anything the more interesting result, with this substantially lower than expected. TMB was higher in dMMR disease (mean 1782 mutations compared with 73 in pMMR) (4). Expansion of this study (n=86) in dMMR cancers was performed, confirming excellent outcomes with durable responses (21% complete response, 53% objective response, 2-year PFS 53% and 2-year OS 64%) (87).

The findings of these relatively small studies have been consistently replicated in CRC. Initial studies were not selected by MMR status and were disappointing, unsurprising given only around 3% of patients with metastatic disease will have dMMR (88). Results from reported studies have been summarised in **Table 1.1**.

Several phase III studies are ongoing in dMMR CRC, particularly in the first-line metastatic and adjuvant setting with atezolizumab and pembrolizumab (88, 89).

Study	Treatment/Characteristics	Response Rate	PFS (months)	OS (months)
	dMMR CRC			
Le et al (87)	Pembrolizumab Mixed dMMR tumours (47% CRC) N=86	53% 21% CR	Median NR 2-year 53%	Median NR 2-year 64%
Checkmate 142 (90, 91)	Nivolumab and Ipilimumab dMMR CRC N=119	60% 9% CR	Median NR 15 month 75%	Median NR 15 month 84%
	pMMR CRC			
Le et al (4)	Pembrolizumab MSS CRC N=28	0%	2.2 20 week 11%	5.0
Checkmate 142 (89, 90)	Nivolumab and Ipilimumab MSS CRC N=23	5%	Not given	Not given

Table 1.1 Reported trials of immunotherapy in CRC. Adapted from Ganesh et at and Boland et al. Results stratified by MMR status. CR: Complete Response, NR: Not Reached.

Thus, ICB is highly effective in patients with dMMR CRC but has little to no activity in pMMR CRC. This differential efficacy presents an ideal tumour type to study de novo resistance to ICB. The dichotomy of response can be assessed, whilst still using tumours derived from the same organ, similar oncogenic drivers (more *BRAF* mutations in dMMR) and wider TME factors, such as the unique interplay of the gut microbiome and colorectal tumours.

1.3 Barriers to immunotherapy response

Despite impressive results in some patients, a significant number of patients display primary resistance to ICB. In NSCLC for example, even when stratified by tumour PD-L1 expression of greater than 50%, a biomarker for ICB sensitivity, only around 45% of patients respond (92). Acquired, or secondary resistance has been reported in patients following initial responses and disease control for over a year with ICB. Tumour intrinsic mechanism including loss-of-function mutations in *JAK1* and *JAK2*, as well as loss of beta-2-microglobulin (*B2M*), are well recognised, causing a functional loss of MHC expression (93). Any of these secondary routes to resistance are also likely to be invaluable to the tumour in escaping immunosurveillance, an important step in carcinogenesis (94). Many of these mechanisms have been implicated in parallel in both primary and secondary resistance (95), *JAK1/2* mutations are also identified in primary resistance to ICB in melanoma for example (96).

In order to understand how a tumour can resist immunotherapy, a series of factors are important. Firstly, the availability and recognition of neoantigens, followed by tumour intrinsic mechanisms that can prevent the presentation of that antigen or tumour cell insensitivity to immune effectors including IFNγ production. Next, the interaction between the tumour and the microenvironment including the specific immune contexture of the tumour and wider expression of immune checkpoints. Finally, the TME itself, including interactions with the microbiome (95). These factors will be considered in more detail next.

1.3.1 Tumour intrinsic resistance: tumour mutational burden

Previously we have considered how TMB can predict responses to ICB and the stark difference between hypermutated dMMR CRC and MSS CRC when treated with ICB. It is therefore important to assess neoantigen burden in MSS disease, could it be that the lack of immunotherapy response is as a result of a low mutation rate? Assessment of TMB is complex and several different approaches have been adopted in pursuit of a reliable method, though none have yet been established as a prospective predictive biomarker for ICB responsiveness (84).

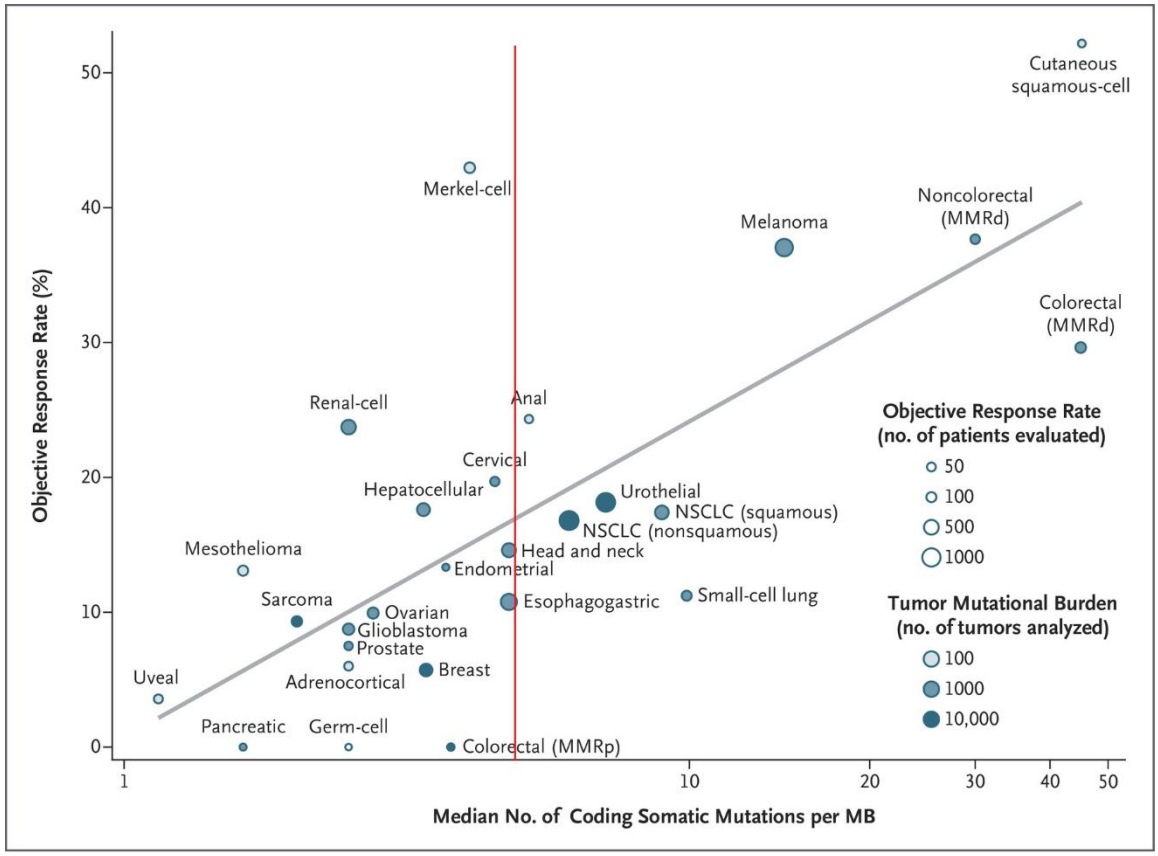


Figure 1.2 Immunotherapy response by tumour type and mutation rate. Response rate from published data ICB usage in each tumour type plotted against tumour-type specific mutation rates. Correlation (grey line) coefficient 0.74, suggesting 55% contribution to response from TMB. Figure taken from Yarchoan et al and adapted. Red line added to display approximate point of 7 mut/MB.

The MSK-Impact NGS approach found a mutation rate of 7 mut/MB predicted response in NSCLC (84). Yarchoan et al performed a broad comparison of TMB across different tumour types and correlated the known responses to ICB in that tumour type, demonstrating a correlation (P<0.001) between mutation rate and response (**Figure 1.2**) (83). This data illustrates some important points. Firstly, that melanoma and dMMR tumours have a much higher TMB than corresponding common tumours and that they respond as expected based on this mutation rate. The other ICB responsive tumours, including renal, NSCLC and Head & Neck are generally in the 5-10 mut/MB range. MSS colorectal cancer is also in this group and has a higher mutation burden than renal, but despite this is a notable outlier, with a response rate of close to zero rather than a predicted response rate of 10-20% (83). Therefore a lack of neoantigens and low TMB is unlikely to completely explain this lack of ICB efficacy in MSS CRC.

Interestingly, a study last year looked specifically at the effects of TMB within the MSI-H CRC group and response to ICB. A significantly higher threshold (37-40 mut/MB) was found for prediction of response, with all patients above this responding to ICB and only 33% responding in the lower TMB group. Similarly, after 18 months the median PFS was not reached in the TMB high group, compared with only 2 months median PFS in TMB low patients. Median OS was also significantly different, around 14 months in TMB low patient and not reached in TMB high (all TMB patients were alive at 36 months) (97). The mutation threshold for ICB response is, therefore, an order of magnitude higher in MSI-H CRC compared to other solid organ tumours and may explain why MSS CRC, with comparable mutation rates to lung and renal cancer, fails to respond. This observational data suggest that CRC

may have biology that is unique and fundamentally immunologically adverse and one hypothesis is that the very high neoantigen burden in MSI-H CRC is necessary to overcome this barrier.

1.3.2 Tumour intrinsic resistance: antigen presentation and interferon resistance

The presence of neoantigens within a cancer cell is not sufficient to induce an immune response independently and antigens must be presented on the cell surface (tumour or APCs) through specialised MHC molecules to elicit a T cell response. MHC molecules are encoded by a variety of human leukocyte antigen (HLA) molecules and have differing roles. MHC Class II will be considered subsequently. MHC Class I is a heterodimer composed of an alpha chain (encoded by *HLA-A, B* or *C*) and β2M and is expressed on all nucleated cells. Endogenous proteins undergo proteolysis in endosomes into short lengths (around 8-10 amino acids) before surface presentation to cytotoxic T cells via the CD8 receptor. Loss of functional Class I has been reported in a proportion of tumours arising from multiple organs. Loss of Class I can arise through several mechanisms including epigenetic and genetic loss of the *HLA* genes and *B2M*, genes involved in the endoplasmic reticulum transport (TAP) genes and can also occur reversibly through post-translational regulation (98, 99). MHC Class I loss is accompanied by enhanced NK (natural killer) cell activation, where Class I normally serves as an inhibitory ligand, however, these NK responses are typically circumvented by tumours (98, 100). Within colorectal cancer, HLA mutations are found in at least one allele in just over 10% of patients. Interestingly, HLA mutations were strongly enriched for in hypermutated tumours and all tumours bearing multiple HLA mutations were hypermutated. Tumours with

greater cytotoxic lymphocyte infiltration were also more likely to have HLA mutations, suggesting an important role in immune escape, particularly in hypermutated tumours (101).

Antigen presentation pathways are substantially enhanced by the presence of IFNγ, produced by T cells in the TME. IFNγ is responsible for upregulation of Class II in all epithelial tissues, to a lesser degree enhances Class I presentation and is also necessary for the expression of PD-L1/2 in many tumours. A signalling cascade following IFNγ binding to the surface IFNγR (IFNγ receptor) causes JAK1/JAK2 activation and STAT1 homodimerisation. STAT1 is an important transcription factor, initiating transcription of many of the IFNγ response genes including *IRF1* (80, 102-104). CRISPR screens of genes conferring ICB resistance in mice treated with immunotherapy and in melanoma/T cell co-culture models identify multiple genes within this pathway (*IFNGR1/2, JAK1/2, STAT1* and IFN enhancing genes including the Apelin receptor and *PTPN2*) (105, 106). Most of these events lead to irreversible loss of action through mutation, however, there is also an important relationship between oncogenic drivers and their ability to regulate the immune context of the cell. Many of these pathways are important, not only as they are common (e.g. RAS) but also have the potential to be druggable, with both anti-proliferative effects as well as enhancing immune action against the tumour.

1.3.3 Tumour intrinsic resistance: oncogenic regulation of immunity

We have previously studied the immunological consequences of *KRAS* mutation in CRC, using an immune metagene termed the Co-ordinate Immune Response Cluster (CIRC). This was derived from Cancer Genome Atlas (TCGA) expression data,

subject to unsupervised hierarchical clustering and identified a 28 gene signature predominantly involving a subset of Th1-related genes, including multiple Class II alleles. Interestingly, within MSS CRC there is a subgroup of patients with comparable CIRC expression to MSI-H CRC, an effect that is independent of TMB and which therefore may represent a subgroup of MSS sensitive to ICB (7). Across all CRC studied, *KRAS* mutation was weakly predictive of a lower CIRC expression. Further analysis studied the effects of *KRAS* within different CMS groups, demonstrating the importance of the broader transcriptional profile when assessing these effects (51). Within CMS2 patients, the canonical group characterised by MAPK signalling and already showing very low CIRC expression, *KRAS* mutants were further significantly repressed. Unsurprisingly, KRAS mutations arising in CMS1 cancers (largely synonymous with MSI-H) made very little difference to CIRC expression, as these tumours are already highly immunogenic (107).

KRAS mutations have been shown to reduce IRF1 and STAT1 responses following IFNγ stimulation, with mutant *KRAS* inducing a programme of transcriptional silencing of these genes (108). Gene level activating mutations in the MAPK pathway and transcriptional activity (e.g. MEK signature) are both correlated with reduced T cell infiltrates and worse outcome in triple-negative breast cancer, an effect that is independent of TMB (109). Furthermore, *KRAS* mutations have been shown to increase expression of CXCL3 and CXCR2 (chemoattractant for Myeloid-Derived Suppressor Cells; MDSCs) via repressing IRF2 in a mouse model of MSI-H CRC with inducible KRAS mutation. Mice with mutant *KRAS*, induced via a Cre-recombinase construct, were found to have significantly reduced CD4+ and CD8+ T cells and increased MDSC infiltrates in the TME and had attenuated responses to anti-PD-1

ICB compared to wild-type mice without induced KRAS expression (110). In *BRAF* mutant melanoma, combined MEK and BRAF inhibition led to enhanced MHC Class -I and -II expression and increased T cell infiltration (111). *BRAF* mutation in melanoma has also been shown to induce a tolerant TME through production of IL-1 (112).

Wnt activation is fundamental to crypt biology and normal IEC development and function. Independence from Wnt signalling, including through *APC* loss, is an essential early process in CRC carcinogenesis. There is evidence that activation of Wnt increases stemness and resistance to chemotherapeutics in cancer cells (113). TCGA analysis of 'non-inflamed' tumours from multiple sites of origin showed a strong correlation with Wnt/β-Catenin signalling (114). Wnt expression has additionally been shown to increase regulatory T cells and polarise intestinal dendritic cells towards generating regulatory responses (113).

1.3.4 Tumour microenvironmental: immune contexture

The role of inflammatory infiltrates in CRC has already been discussed, particularly the role of CTLs in disease control. It is increasingly apparent that many of these infiltrates may contain exhausted effector T cell populations, as a result of immune checkpoint expression in the TME, as well as suppressive populations of immune cells. These inhibitory cell populations include regulatory T cells (Treg), MDSCs, Tumour Associated Macrophages (TAMs) and Cancer-Associated Fibroblasts (CAFs) (115-117). Regulatory cells play an important role in preventing damage to normal healthy tissue caused by immune cell activation and are therefore vital in preventing autoimmune disease. Their role in cancer is often deleterious to immune system

control of the tumour. MDSCs suppress tumour immune-mediated rejection through several mechanisms including the generation of reactive oxygen species (ROS; inhibiting TCR-MHC interactions and peptide binding to MHC), production of suppressive cytokines including arginase, TGFβ and IL10, as well as preventing T cell traffic into tumours by downregulating L-selectin on T cells (115). Tregs similarly act through the production of immune-suppressive cytokines but also express immune checkpoints and generate tolerogenic DCs (117). Interestingly, Tregs have frequently been shown to confer better prognosis in CRC in contrast to nearly all other solid organ malignancies. This phenomenon remains poorly understood but may relate regulatory responses toward gut microbiota rather than anti-tumour activity (118-120).

A major problem with tumour resident T cells is that they often display signs of inactivity and exhaustion, induced by immune checkpoints and regulatory cell populations. Frequently, they are resistant to reactivation even in the presence of ICB. An epigenetic mechanism has been postulated for T cell exhaustion, particular limiting the development of adequate memory T cells (121). There has been some limited success with epigenetic modifiers in combination with ICB, including DNA methyltransferase inhibitors (DMNT e.g. 5-azacytidine) and histone deacetylase inhibitors (HDAC e.g. entinostat) (95). Similarly, inhibition of MEK (122) and MEK with BRAF (111) has been demonstrated to reduce T cell exhaustion and increase T cell infiltration respectively and has demonstrated synergy with immunotherapy. The difficultly with epigenetic and MAPK pathway modification is that the off-target effects of these drugs are wide-ranging. MEK inhibition for example reduces T cell priming and BRAF monotherapy reduces T cell infiltrates in the two previous studies. HDAC

inhibition decreases CXCL10 expression, a critical chemokine for T cell ingress into tumour (123). The conflicting actions of these medications have meant that pharmacological adjuvants to enhance TME immune response have been limited thus far.

1.3.5 Tumour microenvironmental: microbiome

Colorectal tumours are uniquely exposed to large numbers of potentially pathogenic bacteria, with a direct interface between tumour cells and microbiota. Normal gut homeostasis requires that these bacteria are prevented from translocating into the bloodstream, whilst at the same time minimising chronic inflammation, requiring a limited and tolerogenic response (124). Observational studies have shown that certain bacteria appear to have a causative role in inflammation (e.g. IBD) and the formation of cancers, including *Fusobacterium nucleatum* (*F. nucleatum*), certain strains of *Escherichia coli* and *Bacteroides fragilis* (125). An overabundance of *F. nucleatum* has been shown to correlate with the presence of lymph node metastasis and is inversely correlated with CD3+ T cell infiltration (126). Associations between groups of gut bacteria and both enhanced responses to ICB and the risk of subsequent development of immunotherapy-related colitis have begun to emerge (127). Antibiotics are known to alter the composition of gut bacteria and reduce the diversity of the microbiome, with studies suggesting lower responses and reduced survival in ICB-treated patients who receive antibiotics prior to immunotherapy (128). Fascinatingly, it has been possible to culture viable *F. nucleatum* from distant liver metastasis from colorectal tumours, suggesting that these bacteria are transported with clusters of cancer cells when undergoing metastasis and may have a role in

establishing the metastatic niche. Antibiotics against *F. nucleatum* reduced cancer growth and cell proliferation in these cases (129).

Bacterial sensing and defence is primarily directed by innate Toll-like receptors (TLR), with a number including TLR3, TLR4 and TLR9, along with the downstream adapter protein MyD88, pro-tumorigenic culminating in NF-κB activation. TLR activation in tumours caused by infectious agents including Epstein Barr virus (EBV) and Helicobacter pylori has also been linked to carcinogenesis, most characteristically in head and neck and gastric cancers respectively (130). IRAK-M is a TLR regulator that is important in colorectal carcinogenesis and is associated with worse prognosis in CRC. It is activated by both TLR2/4 and Wnt, inhibiting cellular anti-microbial defences and activating oncogenic signalling through STAT3 (131).

1.4 Major histocompatibility complex (MHC) Class II

The potential obstacles to immunotherapy response are therefore present at multiple levels, including both the cancer cell and surrounding microenvironment which can be influenced by tumour factors as well as external factors including microbiome. MHC Class II expression is potentially important in immunotherapy responses for several reasons. Firstly, there are prognostic links to Class II expression and response to ICB. Secondly, Class II expression within epithelial tumours including CRC, is inducible rather than constitutive, implying that an active T cell infiltrate and relevant tumour-directed immune action is likely to be ongoing in those tumours expressing Class II. This is in contrast to Class I expression which is largely non-inducible and binary, it is either present or lost and therefore Class II may serve as a biomarker to predict patients likely to benefit from ICB. This hypothesis is subject to

our ongoing Phase II ANICCA clinical trial (Gary Middleton CI; ClinicalTrials.gov Identifier: NCT03981146). Finally, cell-autonomous loss of Class II inducibility has been reported in around half of colorectal cell lines, suggesting that this mechanism of immune escape may be conserved and important in CRC. Class II biology will be considered in more detail next.

1.4.1 Normal biology and function of Class II

MHC Class II has many similarities in structure and function with Class I. The crystal structure was first described in 1993, comprising a heterodimer of αβ chains encoded by *HLA-DR, DP and DQ* isomers on chromosome 6. MHC Class II is characterised by an open-ended peptide-binding groove (132-134). This open conformation facilitates the binding of longer peptide sequences to Class II, typically 15-18 amino acids in contrast to the 9-11 amino acids afforded by the closed conformation of Class I (135, 136). For many years, Class II expression was thought to be the preserve of professional antigen-presenting cells (APCs) including DCs and B cells, where the Class II is expressed constitutively. It is however now known that Class II expression is seen in many cancers and disease states. Low-level expression is seen in many epithelial tissues and nearly all cells are Class II inducible with IFNγ (137-139). In healthy bowel, increasing expression of Class II is seen from duodenum to the ileum with weak expression seen in the large bowel with a decreasing gradient from the caecum to the rectum. IBD is associated with significant Class II expression in the colon in many cases and is commonly seen in areas of inflamed mucosa (138).

Class II molecules primarily associate with exogenous peptides that are endocytosed into the cell (140). Class II is combined with these peptides prior to assembly and cell surface expression via the endoplasmic reticulum. The presence of the Invariant Chain (Ii) occupying the peptide-binding groove limits association with cell-derived protein (141). Ii is proteolytically degraded during the combination of peptides with the MHC molecules to form class II-associated invariant chain peptide (CLIP) (142). Catalysis of peptide binding and stabilisation of unbound MHC molecules is performed by the HLA-DM chaperone protein, negatively regulated by HLA-DO which acts as a competitive inhibitor of HLA-DM (143, 144). Transport of peptide bound Class II molecules occurs in a highly regulated fashion, including distribution by cell polarity in epithelial surfaces (apical vs basolateral surfaces) and molecules are stably expressed unless targeted for degradation by ubiquitination (145). Unlike Class I, which is recognised by CD8+ T cells, Class II presentation is detected by CD4+ T helper cells which assist and promote activation of CD8+ cells, but also can act directly to cause cytotoxicity (139). Antigen presentation via MHC Class II is summarised in **Figure 1.3.**

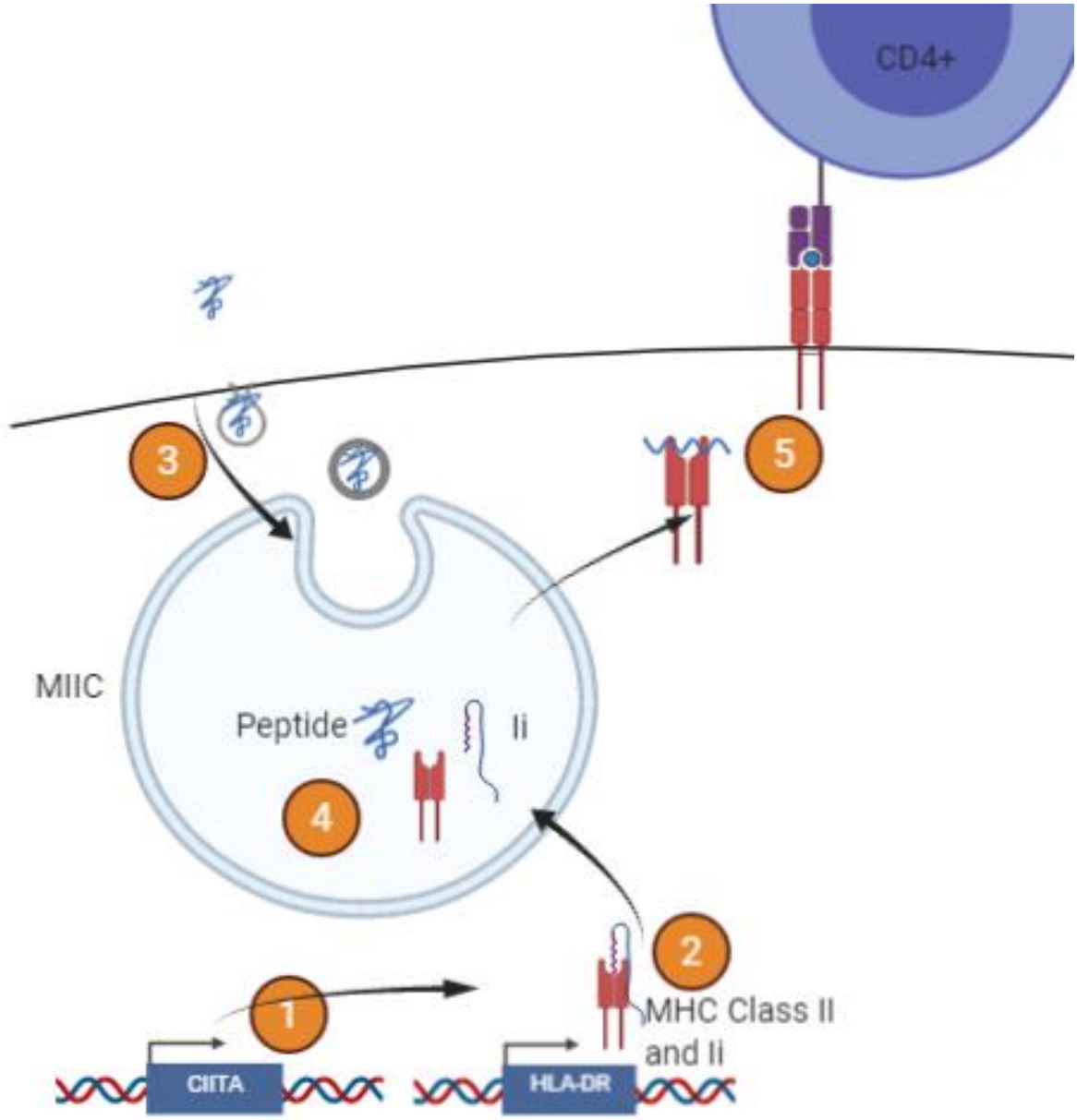


Figure 1.3 Antigen presentation via MHC Class II. 1. Class II proteins (HLA-DR/DP/DQ and accessory molecules including Ii, HLA-DM and HLA-DO) are expressed following CIITA activation, either constitutively in APCs or through IFNγ-mediated pathways. 2. MHC Class II is initially associated with Ii to prevent endogenous peptide binding. Class II is transported to endosomal compartments (MIIC) associated with endoplasmic reticulum. 3. Exogenous peptides are endocytosed into the cell and vesicles fuse with the MIIC compartment. 4. Proteolytic breakdown of exogenous protein and Ii (leaving CLIP) occurs, with chaperone proteins including HLA-DM facilitating combination of MHC Class II with peptides. 5. MHC-peptide complexes are transported to the cell surface, presenting antigen to CD4+ T cells. Ii- Invariant Chain; MIIC- MHC class II-containing compartment; CIITA- Class II Transactivator. Image created in BioRender.

1.4.2 Regulation of Class II via CIITA

The expression of Class II on the cell surface requires the activation of the Class II Transactivator (*CIITA*). CIITA protein itself is non-DNA binding but coordinates the required events for Class II expression, including engagement of the RFX-AP and RFX-5 proteins. *CIITA* is regulated by four independent promoters, the activation of which varies between cells with constitutive and induced Class II expression. Promoter I is active in dendritic cells, promoter III in mature B cells and promoter IV (with a lesser contribution via pIII) in IFNγ induced states. Little is known about promoter II function (146). In addition to IFNγ, IL-12 produced by Th1 cells causes increases Class II expression through induction of CIITA-pIV (147).

CIITA was first discovered by the Accolla lab, who initially demonstrated that hybridisation of the Raji B cell lymphoma line (which lacks Class II expression) with normal splenocytes could restore Class II inducibility in the lymphoma line in some of the hybrids, an effect that was independent of any loss of Chromosome 6 (e.g. the *HLA-DR,DP,DQ* loci) (148). The hybrids with restored Class II were found to have gained a region of chromosome 16 compared with the lines that still lacked Class II (149). These findings were extrapolated into B cell lines derived from children with Bare Lymphocyte syndrome (BLS), a rare congenital absence of Class II, associated with severe combined immunodeficiency and death in infancy from infection. Previously it was known that BLS patients had preserved expression of RFX family proteins, but that they failed to bind to the HLA-DR promoters and therefore failed to express Class II. These BLS lines were all found to have mutations or loss in a 4.5kb region of chromosome 16, reintroduction of cDNA for these region restored Class II and the gene, encoding an 1130 amino acid protein, was designated *CIITA* (150).

IFNγ leads to activation of CIITA-pIV through a combination of transcription factor and chromatin remodelling events (**Figure 1.4**) (151). Three regulatory regions of CIITA-pIV termed GAS, E-box and IRE are bound by STAT1 homodimers, USF-1 and IRF1 respectively. The first step, STAT1 binding, requires the ATP-dependent BRG-1 (*SMARCA4*) SWI/SNF chromatin remodelling complex to maintain an accessible chromatin structure. IRF1 binding is critical to the recruitment of histone acetyltransferases (HATs) including p300 and CBP (151). The BRG-1/SWI/SNF complex is an interesting gene enhancer. It is non-sequence specific in its activity and instead is attracted to other DNA bound proteins (152). Loss of BRG-1 has been reported in around a quarter of cancers and causes unresponsiveness to IFNγ in experimental models. In direct opposition to the SWI/SNF complex is the polycomb repressive complex 2 (PRC2) which comprises SUZ12 and the Enhancer of zeste homolog 2 (EZH2). The role of PRC2, of which EZH2 is a principle catalytic component and histone methyltransferase, is the (tri)-methylation of Histone 3 Lysine 27 (H3K27me3), a histone mark associated with significant transcriptional repression. In cells with functional BRG-1, *CIITA* expression is seen rapidly following IFNγ in around 6 hours, with expression accompanied by a reduction in EZH2 and SUZ12 occupancy at *CIITA*, an increase in H3 acetylation and decreasing H3K27 methylation (153).

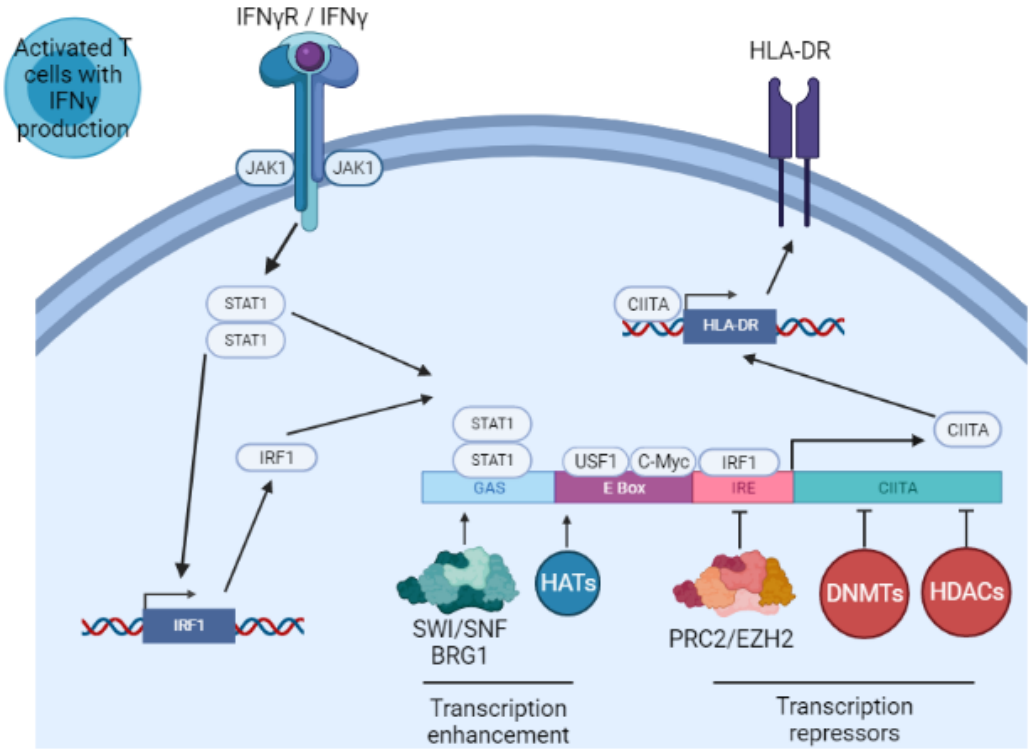


Figure 1.4 Regulation of CIITA-pIV expression. Binding of STAT1, IRF1, USF-1 transcription factors is required for CIITA expression following IFNγ. In addition, chromatin structure must be maintained in an open conformation by recruitment of the BRG-1 complex and Histone Acetyltransferases (HATs). Negative regulation can occur through DNA methyltransferase (e.g. DNMT1) activity, causing promoter methylation) and Histone deacetylase (HDAC), causing loss of acetylation. Figure adapted from Wright KL and Ting JP, Trends Immunol, 2006. Image created in BioRender

1.4.3 Class II expression and cancer including CD4+ T cell activity

Class II expression in tumours has been associated with better disease outcomes in several studies of CRC. An important paper from Lovig et al in 2002 examined Class II (HLA-DR) expression in resected colorectal tumours. Surprisingly, given the age of the study, they also stratified tumours as MSS or MSI-H. IHC staining of HLA-DR was divided into three groups: high (>50% of cells), medium (5-49%) and absent (<5%). In MSS CRC, only around 10% of tumours exhibited high Class II, with weak expression seen in a further 37% and 52% were absent. In contrast, 53% of MSI-H tumours had strong HLA-DR expression, with weak expression observed in a

further 20%. Both MSI-H and MSS tumour had improved survival with either weak or strong Class II expression compared with absent, with this effect greater in MSS CRC and independent of TIL density (5). A second study in resected rectal cancer found two-thirds of tumours lacked Class II expression. Patients with any Class II expression had a significantly lower 5-year recurrence rate (9.1% vs 1.6%), though MMR status was not assessed (154). Another series of colorectal resection samples confirmed increased survival and lower stage tumours in tumours with Class II expression and the presence of IFNγ mRNA in the TME. IFNγ expression also correlated with decreased c-myc activation, with the hypothesis that this might be suppressed through STAT1 activation. Again MMR status was not assessed in this study (155). Sconocchia et al utilised tissue microarrays to assess a range of bowel resections including normal bowel, adenoma and tumours demonstrating an increasing Class II positivity of 5, 19 and 25% respectively. Class II expression was found to be both prognostic for overall survival and lower Class II expression was associated with higher tumour stage (TNM). Survival data, when controlled by TNM staging, demonstrated a hazard ratio of 0.43 (0.24-0.8, p=0.0075) for Class II expression (156).

Similar findings have been replicated in other tumour sites. Laryngeal squamous cell cancers (SCC) with Class II expression were lower grade (well-differentiated), marked by strong T cell infiltrates and had significantly better prognosis (157). Cervical cancers with Class II positivity have increased CD4+ and CD8+ infiltrates, independent of MHC Class I status (158) and in a separate study of cervical adenocarcinomas, Class II expression was again associated with lower stage disease and significantly higher median disease-free survival (211 vs 53.3 months)

(159). In mice transplanted with the MDA-MB-435 cell line (a melanoma line, though misclassified as triple-negative breast cancer in this and several related papers (9)), mice who developed more aggressive metastatic disease were found to have lower Class II expression. Furthermore, when these metastatic deposits were removed and grown again in 2D culture, IFNγ inducibility in vitro was reduced. This suggested a role for Class II loss as an adaptive means of immune escape and the development of more aggressive tumour phenotype (160).

In clinical trial data for patients treated with ICB, retrospective analysis for potential biomarkers of responsiveness has been performed. In both melanoma and Hodgkin Lymphoma treated with anti-PD-1 immunotherapy, tumour-specific Class II was shown to be predictive for response and survival. Interestingly, PD-L1 and Class I expression was not predictive (6, 161). A subsequent planned follow-up study by the melanoma group examined pre-treatment biopsies for PD-1, PD-L1, Class II and IDO-1. IDO-1 is upregulated in response to high concentrations IFNγ and is another immune checkpoint. Multispectral IHC revealed that close spatial co-localisation of PD-1/PD-L1 or Class II/IDO-1 both predicted response, PFS and OS to anti-PD-1 monotherapy, with the hypothesis that these spatial relationships predicted functional immune activation and early mechanism of suppression in response. Importantly, the survival improvement was only seen in the immunotherapy treated patients, with untreated control samples not exhibiting any survival difference, suggesting a clear causal role (162).

1.4.4 Functionality of Class II in non-APCs

There is evidence that Class II expression in epithelial organs, including the gut and respiratory tract, is functional and highly relevant in a number of pathologies. Epithelial surfaces represent the point of contact between the body, microbiota and the outside world and functionality as a non-professional antigen-presenting cell has been proposed (163). Some of the earliest evidence for this surrogate APC role was found in coeliac disease, where intestinal Class II expression significantly decreased in patients on gluten-free diets. In patients with active disease, there was evidence of Class II presentation of gliadin, a known antigenic protein derived from wheat (164). T cell hybridomas have been shown to recognise tetanus toxin presented via Class II in colorectal cell lines. High levels of antigen, or low concentrations with co-treatment with IFNγ, both lead to functional and stable expression via MHC Class II with evidence of T cell recognition and activation. When these lines were grown as monolayers, polarity of response was evident with intake of antigen only on the apical surface with predominantly basolateral Class II expression (165, 166). The basolateral surface, in contact with the lamina propria, is enriched with CD4+ T cells in contrast to intraepithelial lymphocytes which are predominantly CD8+ (167). Human small intestinal derived (non-cancer) organoid cultures were shown to upregulate Class II following IFNγ stimulation and that functional evidence of antigen presentation was present, including Class II localisation to endosomes and functional HLA-DM (168).

Gut Class II expression is also sufficient to prime novel CD4+ responses in situ and can generate lethal cytotoxic responses, in the absence of support from professional APCs including DCs. Gut graft versus host disease (GVHD) occurs following bone marrow transplant and conditioning with TBI (total body irradiation) or chemotherapy.

In a mouse model of GVHD, Koyama et al demonstrated that gut microbiota, via TLR signalling (MyD88 and TRIF) and presentation via Class II to lamina propria IFNγ-producing lymphocytes caused a feed-forward amplification of Class II expression in gut tissue. This increase in Class II expression was sufficient to prime naïve CD4+ T cells, causing severe inflammation of IECs and lethal GVHD in the mice. When haematopoietic APC and stromal lineage Class II expression was eliminated, leaving IECs as the only source of Class II, priming and GVHD continued to occur. Deletion of Class II in IECs completely abrogated toxicity (169).

Microbiota was critical to the Class II expression and immune activation; mice with dysbiosis had higher Class II expression and an expanded CD4+ compartment following BMT, sterile mice failed to develop GVHD or significant Class II expression and antibiotics reduced severity of GVHD. Radiation was found to decrease the thickness of the mucous layer overlying IECs, which is present to prevent the direct interface between bacteria and IECs. Interestingly evidence of this phenomenon is present in normal physiology, where the colonic mucous layer is much thicker (and colon is normally Class II negative) than the relatively thin small intestinal mucous layer (with evidence of Class II expression unless germ-free) (169).

There is further evidence that naïve CD4+ T cells can directly eradicate established tumours. When naïve CD4+ T cells harvested from mice with established melanoma are reintroduced by adoptive transfer following lymphodepletion (ensuring the deletion of regulatory populations), they are primed in the tumour, differentiate into activated intratumoural Th1 cells and eradicate the tumour. This occurs independent of CD8+ or any other cytotoxic cell population and requires neither exogenous cytokines nor prior vaccination (170). Similarly, a Class II presented neoantigen in

cholangiocarcinoma (ERBB2IP) was recognised by endogenous CD4+ TILs. Ex vivo expansion and reintroduction of the CD4+ TIL led to rapid tumour regression and long-term disease control (171). This is consistent with a recent tumour-specific RNA vaccination approach, which developed a bioinformatics pipeline to predict which mutations would be most immunogenic and form the basis of the vaccine. They demonstrated that that majority of the immunogenic antigens were Class II-restricted, possibly related to the longer peptide-binding groove in Class II, allowing cross-presentation of the same antigen to multiple TCRs, as well as the immunogenicity of certain peptide flanking regions associated with Class II antigens (172, 173). A significant proportion of activated T cells from melanoma tumours were CD4+, recognising specific Class II neoantigens (174). During tumorigenesis across multiple tumour types, there is an evolutionary selection of driver mutations that are predicted to bind poorly to Class II, suggesting a critical role of Class II neoantigens in successful immunosurveillance (175).

CD4+ T cells are vitally important, even if the primary tumour is Class II negative, with roles polarising anti-tumour responses and facilitating innate and CD8+ immunity. There is evidence that this can occur both through direct tumour Class II detection on tumours, through presentation on professional APCs or even through secreted Class II antigen. In the case of secreted antigen, tumour control occurred even when Class II expression was deleted, via the IFNγ production by macrophages activated by CD4+ cells (176, 177). Whilst CD4+ T cells exhibit broad anti-tumour activity even in Class II negative cancers, there is evidence that tumour-specific Class II expression can further enhance immune responses (178).

Studies have assessed the effect of introducing Class II into tumour-bearing mouse models, through constitutive expression of CIITA. This stable expression of CIITA is more representative of a professional APC than IFNγ-induced Class II expression in a tumour and has been suggested that it could function as an in situ 'vaccination.' Results from these CIITA expression experiments demonstrate rapid ingress of CD4+ T cells, followed by CD8+ cells and elimination of even established tumours. Animals developed a CD4+ memory pool and resisted rechallenge with the same tumour, even when a Class II negative version is used. Similarly, adoptive transfer of the resultant immune cell populations led to tumour control in mice with Class II negative tumours. CD4/CD8 combined ACTs gave superior tumour control, however, CD4+ only transfers were effective and offered improved tumour rejection compared with CD8+ alone, even in the Class II negative tumours (179, 180). Again it was shown that cancer cells primed T cells within the tumour and prove that Class II expression can cause potent immunological control of the tumour (179). Furthermore, animal models with deletion of DC or macrophages were as effectively controlled with tumour *CIITA* transduction than their wild-type counterparts, demonstrating that CD4+ priming and activation can adequately occur at the level of Class II positive tumour cell and in the absence of professional APCs (181).

1.4.5 Mechanisms of Class II loss in tumour

Loss of inducibility of Class II expression within tumours has been reported through several mechanisms. Integrity of JAK/STAT signalling is required for IFNγ-dependent Class II expression and mutations in this pathway cause loss of Class II expression as previously discussed. In primary resistance, these are however not felt to be that common (96, 182). Also reported is the role of *KRAS* mutation and MAPK pathway

activation causing transcriptional silencing of *STAT1*, with evidence that MEK inhibitors can increase expression of MHC Class I and II and enhance response to anti-PD-1 therapy. This latter effect is accompanied with increased traffic of TILs into tumour and therefore could be secondary rather than causal (108, 109). Post-translational regulation of Class II appears to occur in *RB1* mutants, where Class II is expressed but not present on the cell surface, an effect that can be reversed with reconstitution of Rb (183).

The majority of reports concerning the loss of Class II inducibility focus on loss of function of the pathway at the level of CIITA. A small number of studies identify direct mutation and loss of functional *CIITA* including gene fusions, deletion and frameshift mutation focussed in exon 1 of pIV, however, these studies are all in B cell lymphomas, which have distinct Class II biology and regulation compared with solid organ tumours (178, 184). In a series of 34 Class II negative MSI-H CRC (only around 25% of which should be negative (5)), only one tumour (3%) was found to have a direct mutation of *CIITA*, however, up to 27% had evidence of mutation in *RFX5* (185). *ASCL1* (also known as HASH-1) has a role in neurological and neuroendocrine development and has been identified in small cell lung cancer (a high-grade neuroendocrine tumour) and neuroblastoma as responsible for reducing *CIITA* transcripts through binding of the CIITA-pIV E-box domain. Transcription of *ASCL1* was shown to increase following IFNγ in these cells. There is no evidence of *ASCL1* mediated silencing of *CIITA* outside of neurological tissues, however (186).

1.4.6 Epigenetic regulation of CIITA

Epigenetic regulation can occur at a number of different levels. Direct CpG methylation of DNA promoter sites, mediated through DNMT1 and DNMT3B, causes silencing of gene expression. Additionally, modification of histone tails, primarily through acetylation and methylation can alter chromatin accessibility and transcription. Acetylation is an activating mark (e.g. at H3K9ac, H3K27ac and H3K14ac) and methylation is generally seen as repressive (H3K9me3 and H3K27me3), though notably, H3K4me3 is activating (187). H3K9 mono- and demethylation is performed by the G9a histone methyltransferase, with trimethylation catalysed through SUV39H1 (188, 189). H3K27 trimethylation is the result of the PRC2 complex, including EZH2 (190). CpG methylation and H3K9 methylation are closely linked, with histone modifications facilitating recruitment of DNMT1 and DNMT3B to chromatin. The combination of these two marks therefore reinforces an inaccessible chromatin state (191).

Of note, G9a inhibitors including CM-272 (a combined G9a/DNMT1 inhibitor) have recently been developed, demonstrating cytotoxicity and enhancing responses in combination with anti-PD-1 therapy (192). The enhancement of immune response is secondary to the de-repression of Endogenous Retroviral (ERV) sequences, many of which are repressed through promoter methylation, with subsequent activation of cytosolic viral defence pathways including MAVS-RIG1-STING leading to the production of type 1 interferons (193-195).

Several cell line studies have interrogated regulation and inducibility of Class II in cancer. A 2004 study by Satoh et al assessed IFNγ stimulation followed by HLA-DR

expression in 20 cell lines (8 CRC, 12 gastric). They demonstrated that a significant number of these cancer lines (3/8 CRC and 4/12 gastric) were unable to upregulate Class II following IFNγ treatment, with an absence of CIITA mRNA on RT-qPCR. All cell lines, except one gastric line, were Class II negative at (IFNγ unstimulated) baseline. All lines without inducibility had evidence of CpG methylation of CIITA-pIV, with dense methylation of the vast majority of CpG sites. They also assessed the role of histone modification, namely H3 acetylation and H3K9me2 dimethylation utilising chromatin immunoprecipitation (ChIP) PCR, across four regions of CIITA-pIV (around 500 bp). Inducible lines had convincing increases in acetylation, whereas non-inducible lines were unchanged. H3K9me2 changes appeared less convincing with a greater total amount of H3K9me2 in the non-inducible lines, although this was seen to decrease with IFNγ in the one line they provided results for in the paper. Finally, knockout of both DNMT1 and DNMT3B was found to reverse CpG methylation and restored HLA-DR expression in IFNγ stimulated cells (196).

Similar findings have been replicated in other cell line studies. Four hepatocellular carcinoma (HCC) lines were assessed, with all found to be Class II non-inducible. CpG methylation of CIITA-pIV was found, although this was only assessed in one line (197). In a series of neuroblastoma cell lines, all but one atypical line were found to be Class II non-inducible. However in contrast to the Satoh paper, around half exhibited *CIITA* mRNA expression and were not CpG methylated (possibly as a result of neuronal HASH-1 expression as described above, though this was not assessed (186)). The remaining lines were CpG methylated (198). In a collection of 26 haematological cell lines (largely T cell ALL and B cell ALL and myeloma), ten lines were non-inducible for Class II with nine of these exhibiting CpG methylation of

CIITA-pIV. Nearly all the CpG methylated lines were T cell in origin (in contrast to B cell lineages which do constitutively express Class II). Interestingly they did compare primary samples to exclude tissue culture phenomenon and evidence of CpG was found in a much smaller proportion of patients (~20%) (199).

CpG methylation of CIITA-pIV has also been described in two sites of immune privilege, the eye (and uveal melanoma) and trophoblast (choriocarcinoma). Both of these sites are known to favour tolerance and avoidance of inflammation through several mechanisms including anatomical segregation of immune cells, suppressor/regulatory populations and downregulation of HLA expression (200). The bowel also exhibits features of immune tolerance, including responses to microbiome (119). It is, therefore, a possibility that these cancers may arise from tissue or cells with epigenetic programming in favour of immune privilege, which during carcinogenesis facilitates immune escape. Uveal melanocytes and ocular melanoma cell lines both exhibit an inability to express Class II or *CIITA* mRNA following IFNγ, with this partially reversed with 5-azacytidine (201). Similarly, both trophoblast and developmental tumours including choriocarcinoma lines exhibit transcriptional repression of CIITA-pIV via methylation (202, 203). In ovarian cancer lines, a combination of HDAC and DNMT1 inhibition partly reversed loss of Class II inducibility, though *CIITA* methylation was not specifically assessed as causal (204).

There should however be some caution when interpreting these results. The assessment of epigenetic changes, particularly methylation in 2D culture cell lines is mechanistically unreliable. A comparison between cancer cell lines and corresponding tissue of origin reveals many cell lines exhibit substantially increased and aberrant CpG island methylation. Of the described CpG methylation events, 57%

were never found in corresponding primary tissue samples (205). In colorectal cell lines specifically, CpG island methylator phenotype is substantially overrepresented compared to the primary tissues, with these effects either acquired in vitro or preferentially selected for in tumours that it is possible to derive into cell lines (206). The effects of establishing cultures from primary cells has been studied from a number of cells types of origin. A rapid (within days) loss of global DNA methylation, accompanied by promoter-specific gain in methylation is observed characteristically (207).

These concerns have a basis in the literature for CIITA-pIV specifically. Primary trophoblast cells and choriocarcinoma cell lines were both shown to be non-inducible for Class II in a study by Holtz et al, however, in contrast to the long-term cultured lines, primary cells were not CpG methylated. These primary cells instead exhibited a failure to acetylate *CIITA* following IFNγ, suggesting a distinct epigenetic mechanism for loss of *CIITA* expression, such as binding of a remote regulator (208). Studies in squamous cell carcinoma (SCC) cell lines found three out of nine lines were Class II non-inducible, again with failure to acetylate *CIITA*, but that none of these lines were CpG methylated. Expansion to a broader panel of 22 SCC lines failed to find a single line with CIITA-pIV methylation (209). Interestingly, the same group derived an SCC line with a paired reactive autologous CD4+ T cell population, which they used to study co-culture immune reactivity. The SCC line was initially Class II positive in the presence of either the CD4+ cells or exogenous IFNγ, however over time in culture the cells became non-inducible for Class II with either condition. CpG methylation was not assessed, however, this represents a tissue culture acquired mechanism of Class II repression (210). In a study of Class II negative, MSI-H colorectal tumours,

evidence of *CIITA* promoter methylation in primary tumour tissue was not found in any patient sample (and contrary to CRC cell lines run alongside), casting significant doubt on the biological relevance of this mechanism in CRC patients (185).

Finally, several papers report silencing of *CIITA* via recruitment of EZH2/PRC2 to *CIITA* (initially described in section 1.4.2), with resultant H3K27 trimethylation. Holling et al assessed *CIITA* regulation in a group of uveal melanoma cell lines, three of which displayed non-inducibility for Class II following IFNγ. Two of these lines had evidence of CpG methylation and accompanying H3K9 methylation. The final line was not CpG methylated but exhibited increasing EZH2 binding and H3K27me3 of CIITA-pIV. Interesting, all lines had evidence of H3 acetylation following IFNγ, however, this was insufficient to overcome the repressive marks (211). Truax et al studied Class II inducibility in variable metastatic clones of MDA-MB-435 derived from mice. As previously described, the variants with the least Class II inducibility exhibited the greatest metastatic potential. Interestingly, they provide one of the few quantitative accounts of Class II expression, giving a percentage of cells with Class II surface expression by flow cytometry, rather than simple presence or absence. Notably, all lines were able to upregulate Class II, but with significantly delayed characteristics, with some lines taking 72 hours to reach full levels of expression. There was no evidence of CpG or H3K9 methylation of *CIITA* in any of the lines. Instead, increasing EZH2 occupancy at CIITA-pIV (and H3K27me3) was seen with time following IFNγ, with the largest amount of EZH2 binding in the lines with lowest Class II inducibility. In contrast, lines with rapid Class II inducibility demonstrated a decreased occupancy of CIITA-pIV by EZH2 following IFNγ (212). A detailed assessment of CIITA-pIV in HeLa cells confirmed a regulatory role of EZH2 and

competition with BRG-1/SWI/SNF as an activator (153). EZH2/H3K27me3 silencing of *CIITA* has been reported in the normal biological process of B cell differentiation into pre-plasmablasts (213)

Regulation of *CIITA* via several different mechanisms has therefore been reported. Cancer cells may use all of these methods (JAK1/STAT1/IRF1 pathway mutation, *CIITA* CpG/H3K9 methylation, *CIITA* H3K27/EZH2/BRG-1 and post-translational blocking of Class II surface expression) with redundancy as means to immune escape. The best characterised of these mechanisms in the literature is CIITA-pIV CpG methylation, however, as discussed there should be some caution as this data has been derived almost exclusively from 2D cell culture. It is also important to note that a phase II study of pembrolizumab (anti-PD-1) in combination with 5-azacytidine in MSS CRC was a complete failure, with no evidence of enhanced efficacy (214). A randomised Phase II trial (with 100 patients recruited) of pembrolizumab plus 5-azacytidine or placebo in NSCLC also had concerning results, with the 5-azacytidine patients having significantly shorter PFS, with the trial stopped early due to concerns that the combination appeared to be antagonistic (215). The study authors hypothesised that the potential negative effects of 5-azacytidine on T cell immunity or possibly the upregulation of other checkpoints in the TME could have contributed to this deleterious result (215). It may well be therefore given these results that CpG methylation is not important in tumour biology, however, it is difficult to use epigenetic modifiers as their effects are wide-ranging and often conflicting. There have been concerns for example that they may worsen tumour control through de-repressing oncogenes and other genes leading to ‘stemness,’ thereby worsening outcomes for patients (216).

To definitively answer the question of whether there is a cancer cell-autonomous loss of Class II inducibility and to understand the underlying mechanisms of this, there is a need for a different model system. Given the postulated mechanisms of Class II dysregulation converge on epigenetic control of *CIITA*, this is particularly difficult to reliably assess in 2D cultures. One such system that could improve on 2D culture models is 3D patient-derived organoids.

1.5 Colorectal organoids as models of disease

Intestinal organoids can be cultured from both small and large human bowel, using methods developed around ten years by Hans Clevers group from Utrecht, Netherlands (10, 217). Organoids are self-replicating cultures of Lgr5+ stem cells, which normally are found at the base of crypts within the intestine. In the small bowel, they are supported by Wnt-producing Paneth cells, though these are not found in the colon. Within the crypts, a gradient of Wnt is present, with high concentrations at the base decreasing towards the tips of the villi. Stem cells undergoing cell division, preserving a copy of the original stem cell and also produce a daughter cell which has the potential to differentiate into the full range of mature gut cell types. The reducing Wnt concentration drives the differentiation and migration of cells up the crypt. Initially, transit-amplifying cells are formed, before differentiation into mature functional intestinal cells which eventually undergo anoikis, the sheading of dying cells into the gut lumen. This whole process typically lasts only 5-7 days, with constant renewal from Lgr5+ ISCs required to maintain homeostasis (10). From the isolation of a single Lgr5+ stem cell, it is possible to grow a simple crypt-like structure (218). In contrast to small bowel (which is maintained largely independently in organoid cultures by Wnt from Paneth cells), the prolonged culture of large bowel

requires several other growth factors to be present in media. These include Wnt3a, Noggin, R-spondin-1 (Lgr5 agonist and Wnt co-factor), nicotinamide, EGF and inhibitors of p38 and ALK. Colon cancer organoids to not generally require Wnt3a/noggin/R-spondin as they are typically Wnt-independent e.g. through APC loss. In addition, cultures require the presence of a basement membrane extract such as Matrigel, which is rich in laminin-α1/2, found at the crypt base and supports stem cell survival. The second role of matrigel, which polymerises at 37°C to form a semi-solid scaffold, is to provide a structure for organoids to grow and expand in (10).

The establishment of protocols to allow the stable culture of intestinal organoids has been a significant technological improvement in tissue culture and has enabled researchers to establish collections of organoids, both from normal organ and disease states, including cancer, both from primary and metastatic sites. Collections of CRC organoids have demonstrated appropriate proportions of disease markers such as MMR status, *KRAS* mutation and tumour grade, and are felt to be largely free of bias or selection of certain characteristics favoured in the culture system (219, 220). Organoids also appear to closely model and predict in vivo chemo- and radio-responsiveness and biologically relevant drug sensitivities are present e.g. *KRAS* mutants are resistant to anti-EGFR therapy (221-225). One of the key advantages of cancer organoids over cell lines is the presence of heterogeneity, with multiple subclonal populations present within a culture. The genetic and transcriptional composition remains highly stable over time, comparisons with primary tissue show faithful replication of tumour in most lines. A small number of organoid lines have been shown to lose certain subclonal populations, which may represent the size of the tumour that is processed (e.g. a biopsy sized specimen from an 8 cm tumour will

not contain all populations) or a clone that fails to grow in the culture conditions, however, these limitations have been fairly minor (221).

Similar technologies including tumourspheres and tumouroids have been described as earlier 3D cultures. These cultures lack the morphological complexity and cell-cell interaction found in organoids, though can model heterogeneity. Tumoursphere (TS) cultures typically fail after around 6-8 weeks in continued culture and therefore are more limited models in which to study disease. Confusingly, the terms for some of these 3D cultures are used inaccurately and interchangeable and there can be a substantial difference in composition and methodology between different models. More importantly, TSs when compared with organoids derived from the same tissue sample, show a lack of stability over time, with increasing proportions of stem cells present. Implanting organoids into mice leads to the development of morphologically faithful tumours, which does not occur with TS. Finally, chemoresistance was found to dramatically increase over time (only 1-3 passages) in TSs, whilst remaining completely stable with time in organoids (226, 227).

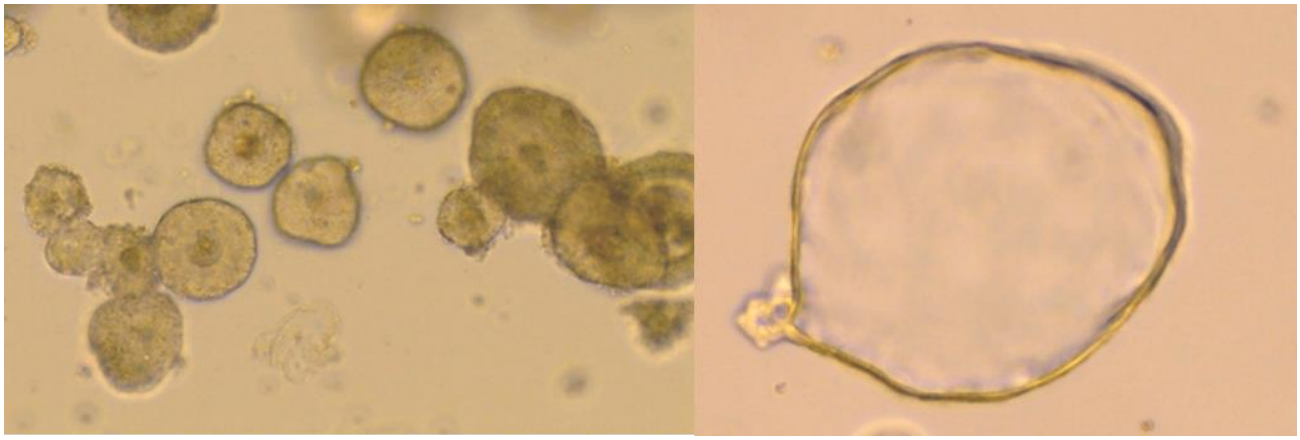


Figure 1.5 Example morphology of human colorectal organoids. Organoids on the **left** are derived from colorectal cancer sample and form generally solid structures with a small central lumen. In comparison, organoids from normal large bowel, shown **right**, form simple large cystic organoids.

Organoids, therefore, represent a model that bridges the gap between the biological faithfulness of animal models and a tissue culture-based, high-throughput system that can be manipulated ex vivo. Additionally, they can be characterised with the clinicopathological data for the patient they were derived from; data that is rarely available for cell lines. Theoretically, as organoid banks increase, it will be relatively simple to select a range of lines to study a given problem, choosing, for example, right-sided, MSS, low immune (minimal TILs, low immunoscore), *BRAF*-mutant colorectal tumours. Further research in refining organoid technology is ongoing, for example adding matched fibroblasts to provide stroma and patient lymphocytes (peripherally sourced or derived from TILs if present). These combinations are far from standard and are at the limit of technological feasibility at present, but could be valuable in the future to study immune actions against tumour (+/- ICB) and stromal contributions to chemotherapy sensitivity (for example the stromal component of pancreatic cancer provides significant resistance) (228, 229).

Previously, the role of epigenetic modification of *CIITA* in cancers has been discussed, alongside the biology of 2D cell lines, which are known to have the potential to diverge substantially during culture epigenetically. In reality, current 2D cultures should be increasingly seen as screening tools and it is increasingly important to validate epigenetic findings from cell lines in patient samples to prove relevance to disease. Organoids, by contrast, are remarkably faithful epigenetically to the tissues they are derived from. A study comparing primary tissue from both adult, paediatric and fetal populations found that age and anatomical (e.g. ileum vs caecum vs rectal) specific patterns of methylation were maintained with high fidelity over prolonged periods of organoid culture. The most remarkable features were observed

in the fetal lines. In normal embryogenesis, methylation patterns change dramatically between global hypo- and hypermethylation, before the acquisition of tissue-specific promoter hypermethylation. These normal developmental stages were found to occur over time in fetal organoid lines, in the absence of external factors to control the process and were dependent on *TET1*. Over time these fetal lines became increasingly similar to the lines derived from paediatric patients (230, 231). Furthermore, disease-specific methylation patterns have been proven to be maintained in organoid, for example, methylation in IBD derived from inflamed epithelium (232). Assessment of a range of cancer organoids with matched normal tissue (healthy background bowel) and primary tumour, found that established organoids maintained a consistent state of methylation with the primary tissue (e.g. the original non-tumour), as well as faithfully representing the tumour specific changes (233).

The epigenetic stability and modelling of developmental methylation changes have therefore established organoid models as the leading method for studying epigenetics in laboratory-based culture. This work, therefore, sets out to establish the biology of MHC Class II (dys)regulation using a collection of human colorectal cancer organoids.

1.6 Aims and Objectives

- Derive a collection of organoid models from human colorectal tumours, complete with characterisation of the primary tumour clinicopathological features and primary tumour Class II expression

- Assess Class II expression in colorectal organoids, both at baseline and with IFNγ stimulation, using flow cytometry to characterise responses.
- Relate lab inducibility of Class II with primary Class II expression
- In non-inducible lines examine factors leading to loss of Class II expression, including STAT1/IRF1 signalling integrity, CIITA-pIV CpG methylation, *CIITA* mRNA expression following IFNγ
- Assess the role of histone modification, including H3 acetylation and H3K9 methylation and EZH2 occupancy
- Assess the use of epigenetic modifiers to reverse Class II loss within colorectal organoids, reassessing response with flow cytometry

Chapter 2: Materials and Methods

2.1 Tissue culture

2.1.1 Cell Line culture

All cell lines were grown as adherent monolayers in vented T75 flasks (Corning, UK) in a humidified incubator at 37°C supplemented with 5% CO_2. Cells were maintained with media changes every three days and were split once at 80% confluence. Cells used in experiments were sub-confluent and low passage number (below 20^{th} for all cell lines). Media was supplemented with 10% Fetal Calf Serum (FCS, Sigma-Aldrich, USA) and Penicillin-Streptomycin (final concentration of 50 units/ml and 50 µg/ml respectively. Life Technologies, USA).

For splitting of cells approaching confluence, media was removed and cells were washed twice with Phosphate Buffered Saline (PBS, Sigma-Aldrich, USA). Following this, 2 ml 0.25% (w/v) pre-warmed Trypsin-EDTA solution (Life Technologies, UK) was added and incubated at 37°C for around five minutes or until all cells had detached. Trypsin was inactivated with 4 ml of media and cells mixed, before centrifuging at 200 x g for five minutes. Cell pellets were re-suspended in desired volume and dilution of media and restored to a fresh flask. When cells were required for experiments, cell counts were determined prior to centrifugation. 10 µl suspended cells were mixed with 10 µl Trypan Blue (Sigma-Aldrich, UK) and counted using a TC20™ Automated Cell Counter (Bio-Rad) taking the average of at least two values. All cell lines used and media conditions are detailed in **Table 2.1**. All cells were obtained from the American Type Culture Collection (ATCC), except for HCT116 wild-type and isogenic line (Horizon Discovery, UK) and RKO (AMS Biotechnology

Europe Ltd, UK). Additionally, the HEK293 +/- *CIITA* transfection (used as a Class II expressing positive/negative control during validation) was kindly provided by Dr Heather Long (University of Birmingham).

Cell Line	Media Conditions	Origin
DLD1 (CCL-221)	RPMI 1640 with L-Glutamine (Life Technologies, UK) 10 % FCS	Colorectal adenocarcinoma Adult Male
HEK293±CIITA (CRL-1573)	DMEM (Dulbecco's Modified Eagle's Medium; Life Technologies, UK) 10% FCS	Human Embryonic Kidney Two isoforms of this line, parental and a stable transfection with *CIITA*
HT-29 (HTB-38)	Modified McCoys 5A with L-Glutamine (Life Technologies, UK) 10 % FCS	Colorectal adenocarcinoma, Female, 44
HCT116 (CCL-247)	RPMI 1640 with L-Glutamine 10 % FCS	Colorectal adenocarcinoma, Adult Male
HCT116 (+/-) Isogenic KRAS	RPMI 1640 with L-Glutamine 10% FCS	Commercially available isogenic cell line with knock out of mutant *KRAS* allele from the parental line
RKO (CRL-2577)	DMEM 10% FCS	Colorectal adenocarcinoma

Table 2.1 Cell Lines. List of cell lines used for subsequent experiments, including media conditions and details of origin. ATCC cell line registry number given after each cell name in brackets.

2.1.1.1 Cell Line freezing and reviving

Cell stocks were frozen to allow for replenishment with low passage stock and maintenance of line fidelity. Detached cells were suspended in media supplemented with 5-10% Dimethyl Sulfoxide (DMSO; Sigma-Aldrich, UK) according to the ATCC protocol for each line. Cells were placed in cryovials and transferred to -80°C freezer initially in a Mr Frosty (Nalgene) before long term storage in the liquid-vapour phase

of liquid nitrogen. To revive cells from frozen, cryovials were thawed in a water bath and then slowly re-suspended in 10 ml warmed media. Cells were centrifuged at 200 x g for five minutes, with pellets re-suspended in media to dilute DMSO before transferring to vented flasks for continued culture.

2.1.2 Organoid culture

Organoid culture technology has been developed over the last decade and is rapidly expanding both in terms of utilisation and application of newer and more complex technologies such as CRISPR-Cas9 genome editing. Cultures can be derived from almost any tissue type, replicating both normal organ structure and function, or model disease (e.g. inflammatory bowel, cystic fibrosis, cancer) (11). Colorectal organoids are derived from a self-renewing population of Lgr5+ stem cells, found in the base of crypt structures in the small and large bowel, with the daughter cells produced by cell division forming the full population of representative cell types from the tissue, including enterocytes, goblet cells, and enteroendocrine cells. In contrast to other 3D culture model systems, including tumourspheres, organoids recapitulate the highest degree of structural hierarchical cell-cell interaction. Basement membrane extracts (e.g. matrigel) providing the source of extracellular interaction and structure, with matrigel polymerising to form a semi-solid pellet at 37°C, providing a scaffold for growing organoids to embed within (10, 234). Cancer-derived organoids have been shown to capture tumour heterogeneity, are stable both genetically and epigenetically and can be used to accurately predict in vivo treatment responses (223, 231).

2.1.2.1 Ethics and tissue collection

All organoids were derived under local ethical approval (Beggs 17-287) from the University of Birmingham Human Biomaterials Resource Centre (HBRC). The HBRC itself has approval from the North West - Haydock Research Ethics Committee (Ref 15/NW/0079). All patients provided informed consent (utilising HBRC standard consent forms) for the inclusion of both normal bowel and tumour samples for the purpose of organoid derivation and downstream analysis including genetic applications. We are indebted to these patients for their kind support, particularly coming at a time when they face a life-changing diagnosis.

Potential patients were identified from the colorectal Multidisciplinary Team (MDT) meetings. Patients from University Hospitals Birmingham, firstly from Queen Elizabeth Hospital Birmingham (QEHB) and later additionally from Birmingham Heartlands Hospital were included. The vast majority of patients were consented in surgical outpatient clinics before resection of their primary tumours, with clinicians with current Good Clinical Practice (GCP) certification and study-specific consent training. Local NHS pathologists, on receipt of tissue from theatre, were able to process samples promptly to include a section of normal bowel tissue and a representative tumour sample for collection by the HBRC, whilst maintaining sample integrity for accurate staging and standard pathological reporting. Samples were transferred to HBRC for registration and anonymization and were stored at 4°C in DMEM/F12 (Life Technologies, UK) supplemented with Primocin antibiotic at 100 µg/ml (Invivogen, France) until processing, with almost all samples processed within 24 hours of surgery.

2.1.2.2 Organoid derivation

Original protocols for the processing of intestinal samples to form organoid cultures were developed by Prof Hans Clevers at the Hubrecht Institute, Netherlands (10). Over time they have been adapted and refined (221). This group (Beggs PI) forms part of the Cancer Research UK (CRUK) supported Human Cancer Model Initiative (HCMI). This international collaboration serves to facilitate the development of the technology and collaboration between groups, sharing of protocols and resources. A close working relationship has been formed with the Wellcome Trust Sanger Institute (WTSI, Cambridge, UK). In addition to the organoid lines derived 'in-house,' several Birmingham patient samples were processed in WTSI, with the return of established lines to this group. Protocols established are therefore the result of local application and refinement of these established protocols.

Tumour samples from HBRC arriving in the laboratory were removed from storage media into a petri dish, with larger samples cut into moderate-sized (<5 mm) pieces before adding to a 50 ml centrifuge tube. Next, tumour pieces were washed thoroughly in Dulbecco's Phosphate Buffered Saline without Ca2+, Cl- and Mg2+ (PBSO, Sigma-Aldrich, UK) supplemented with primocin at 100 µg/ml and shaken vigorously. PBSO/primocin was then carefully removed, leaving tumour fragments behind. The wash step was repeated at least two further times until the wash supernatant appeared clear.

The overnight primocin incubation and vigorous cleaning protocol were introduced based on earlier experience of establishing cultures, with a high risk of infection in the first days of culture. Microbiological assessment of culture media suggested

infection with multi-drug resistant *Enterococci sp.* and therefore likely contamination from the sample itself. No further cultures have been infected in the two years following this protocol change.

Once cleaned, tumour fragments underwent mechanical and chemical digestion with pre-warmed 37°C tumour digestion buffer (TDB), consisting of 2.5% FCS, 75 U/ml collagenase IX (Sigma, USA) and 125 µg/ml dispase II (Fisher Scientific, UK) dissolved in DMEM media. Fragments were suspended in 2 ml TBD in a bijou tube and finely cut with tissue processing scissors for fifteen minutes. The mixture was frequently agitated and incubated at 37°C for one hour. The sample was then filtered through a sterile 20 µm filter to isolate crypt stem cells. The undigested material was incubated for a further thirty minutes in 1 ml TBD, and then filtered and rinsed thoroughly with PBSO to collect remaining cells. The cells were then centrifuged at 300G for four minutes, rinsed in PBSO and centrifuged again and the supernatant discarded. The cell pellet was taken up in matrigel (Corning, USA) and then transferred at 50 µl/well into a pre-warmed 24-well plate (Corning, USA). Matrigel was then allowed to polymerase at 37°C for at least thirty minutes, before the addition of 500 µl/well Intesticult Human Organoid growth complete A+B media (Stemcell Technologies, Canada) supplemented with Primocin, and maintained in a humidified incubator at 37°C with 5% CO2. For longer-term culture of cancer organoids, Intesticult Human Organoid media A component was combined with 50% volume DMEM/F12, as the B component primarily contains Wnt pathway factors and is not required for cancers with APC loss. Normal lines were maintained in complete (A+B) media. Following digestion and first plating of new lines, the ROCK (Rho kinase) inhibitor Y-27632 (Stratech, UK) was included in the media at a final

concentration of 10 µM/ml for the first two to three days of culture. ROCK inhibitors have been demonstrated to improve stem cell survival under conditions of stress, including freeze/thaw events, tissue processing and Fluorescence-activated cell sorting (FACS) and have become generally widespread across organoid protocols in recent years (235).

For more recent lines, an updated TBD has been utilised (221) consisting of 20 µg/ml Hyaluronidase (Fisher Scientific, UK), 1.5 mg/ml Collagenase II (Sigma, UK), 10 µM Y-27632, 2.5% FCS and primocin 100 µg/ml dissolved in DMEM/F12 media. Generally, this has been felt to provide more complete digestion of the tissue compared with the old buffer. Larger samples, and normal bowel samples when processed, would occasionally block the filters and prove difficult to process, with the updated buffer ameliorating this factor.

2.1.2.3 Organoid passaging

Organoids were passaged to remove dead cells, reduce confluence and to maintain matrigel structural consistency approximately every seven days. The majority of lines required a 1:2 passaging ratio (e.g. 4 wells replated into 8). Media was aspirated and 500 µl ml organoid harvesting solution (OHS; Bio-Techne, USA) was added to each well. Matrigel pellets were disrupted using a 3 ml Pasteur pipette and organoids transferred to a 15 ml centrifuge tube. Organoid/matrigel suspensions were incubated for 30-60 minutes on ice with frequent mixing to dissolve matrigel, before being further diluted with PBSO and organoids pelleted at 400 x g for four minutes at 4°C. OHS was then aspirated and organoids were partly broken up with a combination of mechanical digestion (by passing through a no-filter 10 µl pipette tip

inserted on the end of 1 ml pipette tip, for a maximum of three passes) and chemical digestion using 1 ml pre-warmed TrypLE Express (Gibco, Denmark) for three minutes. TrypLE was inactivated by the addition of 9 ml ice-cold PBSO, prior to centrifuging at 300-400 x g for four minutes at 4°C. PBSO was aspirated, and organoids were taken up in matrigel and replated in pre-warmed 24-well plates, with subsequent addition of media as previously described.

2.1.2.4 Thawing cryopreserved organoids

Cryovials were thawed in a 37°C waterbath until just a small crystal of ice remained. Organoids were transferred to a fresh 15 ml centrifuge tube using a Pasteur pipette and 10 ml of warm DMEM/F12 was slowly added. Organoids were centrifuged at 200 x g for five minutes at room temperature and supernatant aspirated off the organoid pellet. The pellet was resuspended in matrigel and plated as previously described. 10 µM Y-27632 was added to media for the first three days of culture.

2.1.2.5 Cryopreserving organoids

For each cryovial, six wells of established organoids (around day 3 since plating) were harvested in OHS to dissolve matrigel. Further digestion of organoids was not performed and instead, formed organoids were suspended in 1 ml DMEM/F12. An equal volume of 80% FCS / 20% DMSO was slowly added, with primocin and Y-27632 added at previously documented final concentrations. Organoids were transferred to 2 ml Cryovials and placed at -80°C in a Mr Frosty for a minimum of two hours. Long term storage was in liquid nitrogen vapour phase.

2.1.2.6 Generation of single-cell suspensions from organoids

Many of the downstream applications of organoids require the generation of single-cell suspensions. This was performed by aspirating media, dissolving matrigel in OHS and then performing combined mechanical/chemical digestion as described in 2.1.2.3. In contrast to the partial digestion performed when passaging organoids, a more rigorous approach was used for single-cell production, with TrypLE incubation times of 10-15 minutes and approximately ten passages through 10 µl pipette tip performed. Following digestion, confirmation of single cells was performed with microscopy and cell viability and counting performed as described in 2.1.1.

2.1.3 Mycoplasma testing

Cell lines and organoids were regularly tested for mycoplasma contamination using an EZ-PCR Mycoplasma Test Kit (Biological Industries, Israel). 1 ml of media was removed and briefly centrifuged at 250 x g to remove larger cell debris and supernatant removed into a fresh tube. Media then underwent high-speed centrifugation (17000 x g) for 10 minutes. The supernatant was discarded and the pellet re-suspended in 50 µl buffer solution (kit supplied) and placed on heat block at 95°C for three minutes. Polymerase chain reaction (PCR) amplification of a mycoplasma specific 16S region was performed in a PCR tube strip or plate. The reaction was performed using 35 µl nuclease-free water (nf-H20; Amresco, USA), 10 µl reaction mix (kit supplied) and 5 µl of the sample. A positive control (kit supplied) and negative control (nuclease-free water) were also run. The following programme was used: 94°C for 30s; 35 cycles of 94°C for 30 s, 60°C for 120 s, 72°C for 60 s; and finally 94°C for 30 s, 60°C for 120 s and held at 72°C for 300 s.

An agarose gel was prepared using 10x TBE buffer (0.89 M Tris Borate pH8.3, 20 mM Na2EDTA. Geneflow, UK), 2% w/v agarose (Lonza, USA) and 1:10000 SYBR Safe DNA Gel Stain (Invitrogen, USA) dissolved in deionised water. The solution was gently heated to solubilise and poured into a gel cassette to set before sample loading. 20 µl of PCR product was loaded on the gel and electrophoresis performed for 30 minutes at 120 V, with detection of DNA bands using a UV reader (U:genius 3, Syngene).

2.1.4 Cell viability assessment

Organoid drug screens were performed as previously described in the literature (222, 225), using an Adenosine Triphosphate (ATP)-based luminescence reporter assay (CellTiter-Glo® 3D Cell Viability Assay, Promega, USA). Single-cell suspensions of organoids were generated (see 2.1.2.6), counted and were resuspended in matrigel at a reduced volume of 30 µl/well in 96 well, white-walled, clear bottomed assay plates (Corning, USA). After 30 minutes, 200 µl Intesticult media was added and small organoids allowed to reform over 72 hours. At 72 hours, 100 µl media was carefully removed without disturbing the matrigel at the bottom of the well. 100 µl fresh media with 2x desired drug concentration was added, giving a final concentration of 1x in 200 µl. Organoids were incubated with the drug for a further 72 hours. The 3D CellTiter assay was thawed overnight at 4°C and then brought to 22°C in a water bath. 100 µL media was removed from each well and 100 µL assay added. Cells were lysed by placing on an orbital shaker for five minutes and plates were incubated at room temperature for 25 minutes, prior to recording luminescence on an EnSpire microplate reader (PerkinElmer). For drug response experiments, a minimum of five wells were used for each condition in each cell line, including an

untreated condition using vehicle (e.g. 0.2% DMSO). Results were processed in GraphPad Prism (version 8.3.0).

A potential limitation of ATP-reporter assays is that it is possible to exceed the maximum linearity range, e.g. where increasing amounts of cells (ATP) no longer produce an increase in the luminescence value recorded. As per the manufacturer directions, an ATP standard curve was performed using ATP disodium salt (Promega, USA) at concentrations between 10 µM and 100 nM and run on each experimental plate to ensure the assay was in working range. Using ATP is recommended because of the complexity and volume of biomass relative to 2D culture methods, where typically a cell count alone is used. A final cell count of 1000 cells/well was selected for the organoid lines, which provided both a strong luminescence readout and was within the assay linearity parameters.

2.1.4.1 GSK126 experiments

GSK126 is a direct selective inhibitor of EZH2. EZH2 forms part of the polycomb repressive complex 2 (PRC2) which is responsible for trimethylation of lysine 27 on histone 3 (H3K27me3). Overexpression of EZH2 has been found across multiple cancer types and is associated with worse prognosis (236). Previous experiments in cell lines have demonstrated significant cytotoxicity at doses above 5 µM, however this also varies substantially line-to-line. Interestingly, at lower doses, some lines exhibit increased growth kinetics (237). Studies using colorectal cancer organoids remain fairly limited in the literature, however surprisingly an assessment of GSK126 in twenty CRC organoids was published in 2016, confirming a differential sensitivity across different tumour models (238). Transcriptional changes and reductions in

H3K27me3 have been demonstrated at relatively low GSK126 doses (1.5 µM), with changes occurring following four days of treatment, but maximal by eight days (239). A second study using colorectal cell lines used 0-5 µM GSK126 for 72 hours, demonstrating minimal cytotoxicity at 2 µM which increased markedly at 5 µM. At 2 µM, decreased H3K27me3 total protein expression and a small increase in mRNA of an EZH2 regulated gene occurred (240).

A dose of 2 µM GSK126 for six days was chosen for epigenetic modification in experiments in this project, based on the effect on H3K27me3 and gene expression at this dose with minimal cytotoxicity. Cytotoxicity assay (CellTiter 3D) was performed in organoids with a range of doses between 0-10 µM to confirm line-specific sensitivities, given the large therapeutic range of the compound (as described in **2.1.4**).

GSK126 was purchased from Stratech Scientific (UK) and reconstituted in warmed DMSO to a stock concentration of 10 mM. Subsequent dilutions were performed in DMSO to give 500x final concentration, before being added to media at 1:500 to give a final DMSO concentration of 0.2%. Drug aliquots were stored at -20°C. For the experiments on organoid cultures, drugs were added to 500 µl organoid media for each well, typically with 3-4 wells combined for each condition to be utilised for flow cytometry. For the six day GSK126 culture, media and drug was replaced after 72 hours. Where a combined treatment with both entinostat (see subsequent paragraph for entinostat details) and GSK126 was utilised, 2 µM GSK126 was added alone for 72 hours before media change and addition of both GSK126 and 5 µM entinostat for a further 72 hours.

2.1.4.2 Entinostat

Entinostat is a synthetic benzamide inhibitor with activity against histone deacetylase (HDAC). It is relatively toxic in colorectal cells (241), however, it has demonstrated efficacy in reversing the loss of MHC-Class II expression in ovarian lines following IFNγ (204). Most frequently, a dose of 5 μM has for 72 hours has been used in the literature for the purpose of epigenetic modification. Entinostat was purchased from Stratech Scientific (UK) and was supplied at 10 mM in DMSO. Subsequent dilutions were again performed in DMSO to give a 500x concentration, with final 1:500 dilution into media to give final concentrations of 5 μM entinostat in 0.2% DMSO, with 72 hours treatment used in combination with 6 days of GSK126. Drug aliquots were stored at -20°C.

2.1.4.3 Interferon-gamma

Interferon-gamma (IFNγ) was purchased from Stratech Scientific (UK). Dilutions were performed in PBSO with 0.1% Bovine Serum Albumin (BSA; Sigma-Aldrich, USA) with batch-specific activity used to produce aliquots at 500x desired concentration with storage at -80°C and replacement every six months. Specifics of IFNγ dose and duration of stimulation are given in results chapter 4.2.

2.2 Protein assessment

2.2.1 Protein extraction from cell lines

Cell lines were plated at 8-10x10^6 cells per well in six-well plates, before IFNγ stimulation or drug treatment. At the time of lysis, cells were not more than 80-90% confluent. Lysis was performed on ice with ice-cold reagents. Media was aspirated and cells were washed twice using PBS. 100-140 μl Radioimmunoprecipitation assay

buffer (RIPA buffer; Thermo Scientific, USA) with 1x Protease/Phosphatase inhibitor cocktail (Cell Signalling Technology, USA) was added directly to wells and a cell scraper was used to detach and lyse cells. Lysates were further incubated in RIPA buffer on ice with occasional pipetting for 15 minutes prior to boiling at 100°C for five minutes on a heat block.

2.2.2 Protein extraction from organoids

Organoids were treated embedded in matrigel with the required drug or IFNγ. Once treated, media was aspirated and matrigel was dispersed in OHS for 60 minutes on ice with frequent pipetting. Organoids were centrifuged at 400 x g for four minutes, the supernatant discarded and the resulting pellet washed in 10 ml PBSO and centrifuged again. Two to three wells of organoids were normally combined for each condition. The organoid pellets were resuspended in RIPA buffer with protease/phosphatase inhibitor, with subsequent processing as the cell line lysates.

2.2.3 Protein processing and gel electrophoresis

Once extracted, lysates were sonicated (23 KHz, 15-20 µm) twice for ten seconds, placing on ice between sonication steps to reduce the temperature. Cell debris was removed by centrifuging at 13000 x g for five minutes, before removing supernatants into fresh Eppendorf tubes. Protein was quantified using the Pierce BCA Protein Assay Kit (Thermo Scientific, USA), which calculates protein concentration by comparison with a known concentration of bovine serum albumin (BSA) in a dilution series. 10 µl of standard or sample was added to 190 µl of the working solution, incubated at 37°C for thirty minutes, before absorbance at 562 nm was recorded on an Enspire microplate spectrophotometer (PerkinElmer). Protein concentrations for

lysates were calculated and normalised on each gel for protein quantity and volume (e.g. typically 20 µg in 20 µl) with 1:6 loading buffer (Lane Marker Reducing Sample Buffer, Thermo Scientific USA) made up to the required volume with nf-H20.

Samples were heated with the loading buffer at 95°C for 5 minutes before immediately loading onto gels (10-12%, Mini-PROTEAN TXG Precast Gel, Bio-Rad, USA). Precision Plus Protein WesternC Standard (Bio-Rad, USA) was run alongside samples to provide molecular weight. Electrophoresis was performed using Mini Trans-Blot Cell system (Bio-Rad, USA) in running buffer at 80 V for ten minutes and then 140 V until the gel front had sufficiently resolved. Wet transfer of the resolved proteins onto Amersham Hybond PVDF membrane (GE Healthcare, Germany) was then performed in transfer buffer at 90 V for ninety minutes at 4°C. Running, transfer and other buffers are listed below in Western Blot Reagents.

2.2.3.1 Western Blotting

Once transferred, membranes were blocked in 5% Dried Skimmed Milk powder (Marvel, UK) diluted in 1x TBST, for one hour at room temperature with gentle agitation on a rocker. After blocking, membranes were briefly rinsed in TBST prior to incubation in primary antibody overnight at 4°C on a roller. All antibodies and dilutions are listed in **Table 2.2**.

The next day, membranes were rinsed four times in TBST for five minutes. Detection of primary antibodies was performed with a peroxidase-conjugated Affinipure goat anti-rabbit antibody (Jackson ImmunoResearch, USA) in 5% skimmed milk/TBST at 1:10000 dilution, for one hour at room temperature with gentle agitation on a rocker. Following secondary incubation, four further TBST washes of five minutes were

performed. Blots were developed using a chemiluminescence method. Membranes were covered in a fine layer of Amersham ECL Western Blotting Detection Reagent (GE Healthcare, UK) and left for five minutes before excess ECL reagent was removed. Digital capture of blot images was performed using a Fusion FX6XT digital imaging system (Vilber Lourmat, Germany)

Membranes were re-probed for other proteins of interest and GAPDH loading control by a stripping method. Two rinses in Mild Stripping Buffer for ten minutes, followed by two washes of ten minutes in PBS and finally two washes in TBST for five minutes were performed. Completeness of stripping was assessed by repeating blocking, secondary antibody binding and ECL detection.

Band densitometry was performed using ImageJ version 1.52a (National Institutes of Health, USA) with data presentation and statistical analysis performed in GraphPad Prism version 8.4.1. Protein expression levels were corrected for GAPDH expression and where relevant expressed as relative expression compared with a control condition. Differences in protein expression were analysed using an unpaired two-tailed T test.

Target/Clone/ #Catalogue	Source Species	Supplier	Diluent	Dilution
P-ERK (P-P44/42) #9101S	Rabbit	Cell Signalling Technology	5% BSA/TBST	1:1000
GAPDH (D16H11) #5174S	Rabbit	Cell Signalling Technology	5% Skimmed Milk/TBST	1:1000
STAT1 (42H3) #9175S	Rabbit	Cell Signalling Technology	5% BSA/TBST	1:1000
IRF1 #GTX129134	Rabbit	Source Bioscience	5% BSA/TBST	1:1000

Table 2.2 Antibodies for Western Blot experiments. Source and experimental details for antibodies used in Western experiments, with clone number (where available) and catalogue number for each given supplier.

2.2.3.2 Western buffers

Transfer buffer: 10x Tris/Glycine buffer (Bio-Rad, Germany). Made up to 1 L with 700 ml deionised water (diH20) and 200 ml Methanol (VWR Chemicals, France) to give 1x solution with final concentrations of 25 mM Tris, 192 mM Glycine, pH 8.3.

Running buffer: 10x Tris/Glycine/SDS buffer (Bio-Rad, Germany). Made up to 1 L with 900 ml diH20 to give 1x solution with final concentrations of 25 mM Tris, 192 mM Glycine, 0.1% w/v SDS, pH 8.3.

10x TBS solution: 24 g TRIS-HCl, 5.6 g TRIS Base, 88 g Sodium Chloride (all supplied by Sigma-Aldrich, USA), diH20 to 1L volume, pH 7.6.

1x TBST solution: 100 ml 10x TBS, 899 ml diH20, 1 ml Tween20 (VWR Chemicals, France).

Mild Stripping buffer: 15 g Glycine (Sigma-Aldrich, USA), 1 g SDS (Sigma-Aldrich, Japan), 10 ml Tween20, pH 2.2. Total volume 1 L made up with diH20.

2.3 DNA and RNA methodology

2.3.1 DNA/RNA extraction from cell lines and organoids

Simultaneous extraction of DNA and RNA was performed from cell lines and organoids utilising a spin column-based protocol (AllPrep DNA/RNA Mini Kit; QIAGEN, Germany). All reagents listed were kit-supplied and procedure performed as per manufactures instructions. Cell lines were detached with TrypLE, pelleted, rinsed twice in PBS before resuspending in 600 µl RLT Plus Buffer. Organoids were removed from matrigel using OHS for 60 minutes, before rinsing twice in PBSO and resuspending in RLT Plus and then processed as per cell lines. Cells were homogenised and lysed using a 1 ml / 10 µl tip for mechanical agitation. DNA was collected on an AllPrep DNA spin column, with the flow-through containing RNA combined with an equal volume of 80% ethanol before addition to an RNeasy spin column. DNA was washed with 500 µl AW1 buffer, followed by 500 µl AW2 buffer, before elution with 100 µl EB (elution buffer). The RNA was washed with 700 µl RW1 buffer, followed by two washes with 500 µl RPE buffer. Elution from the filter was performed with 50 µl nf-H20.

2.3.1.1 QUBIT quantification of RNA/DNA

QUBIT is a rapid and reproducible fluorescence-based method to quantify nucleic acids, produced by Thermofisher (USA). Kits for both RNA and double-stranded (ds) DNA were used, with both available in a High Sensitivity (HS) and Broad Range (BR) version. DNA and RNA samples were first processed with the BR assay, with any out-of-range low values repeated with the HS kit. Working buffer was prepared (1:200 mix of dye and dilution buffer) and kit-supplied standards were measured

before each run. 1 µl sample (and 10 µl standard) were made up to 200 µl total volume in working buffer, vortexed briefly and then analysed on a QUBIT fluorometer 3.0.

2.3.1.2 TapeStation assessment of DNA/RNA quality

TapeStation assays were used for DNA/RNA quality assessment (Aligent Technologies, Germany). The technology utilises ScreenTapes containing multiple miniaturised electrophoresis channels to replace many of the functions that traditionally would have been performed with agarose gel electrophoresis or Bioanalyser, in a rapid, digital and automated format. DNA was assessed using the D1000 system (detecting up to 1000BP), combining 1 µl sample with 3 µl sample buffer. Samples and molecular weight ladder with were vortexed at 2000 RPM for one minute before loading on a TapeStation 4200 for automated analysis. RNA assessment using RNA ScreenTapes was performed identically, except sample buffer volume was 5 µl to 1 µl sample/ladder. Data output from the TapeStation includes a pseudo-representation of an agarose gel, used to confirm library generation or PCR amplification at given molecular weights as well as the calculation of RNA Integrity Number (RIN).

2.3.2 RNA procedures

2.3.2.1 DNAse treatment

RNA for downstream experiments was purified with DNA removal (DNAse treatment). The TURBO DNA-free kit (ThermoFisher Scientific, Lithuania) was used, which uses an inactivation agent to remove the DNAse at the end of the procedure. 1 µl (2 U) of TURBO DNAse was added to each sample, with 5 µl 10x TURBO DNAse buffer, into

a final volume with sample RNA of 50 µl. The sample was mixed before proceeding to a heat block incubation of thirty minutes at 37°C. 5 µl DNase Inactivation Reagent was added and incubated for five minutes at room temperature, mixing the tube by flicking several times. Samples were then centrifuged at 10000 x g for 90 s to pellet the inactivation reagent and the supernatant was carefully removed into fresh Eppendorf tubes.

2.3.2.2 Quantitative reverse transcription PCR (RT-qPCR): reverse transcription

Quantification of *CIITA* mRNA expression was assessed following IFNγ stimulation. A two-step protocol was utilised, with an initial reverse transcription step followed by separate qPCR. A High-Capacity RNA-to-cDNA (ThermoFisher Scientific, Lithuania) was used to produce single-stranded cDNA from the sample RNA. A range of RNA inputs from 10 ng to 100 ng were assessed initially to identify the best signal for *CIITA* mRNA expression, with 50 ng being used for all subsequent experiments.

The reverse transcription reaction was performed with 10 µl RT buffer mix and 1 µl RT reaction mix combined with the DNAse treated RNA. Samples were mixed before performing the RT reaction on a thermocycler (37°C for 60 minutes, 95°C for 5 minutes, 4°C hold). A final quantity of 50 ng cDNA in 4 µl volume was obtained.

2.3.2.3 Quantitative reverse transcription PCR (RT-qPCR): SYBR green PCR

SYBR Green technology uses a dye that binds non-specifically to dsDNA, with a structural change caused by binding increasing the fluorescence of the dye markedly. As the sequence of interest is amplified during PCR, the amount of DNA will increase exponentially and therefore more SYBR green binding will occur. A melt curve is

performed at the end of the PCR reaction to confirm the specificity of SYBR green binding, which when bound only to the target sequence will result in a sharp discrete curve.

Processed cDNA was made up in a 10 µl reaction volume with 2x PowerUp SYBR Green Master Mix (ThermoFisher Scientific, Lithuania) and forward/reverse primers for *CIITA* at 500 nM final concentration. Primers were based on previously published data (196) and were purchased from Sigma-Aldrich (UK), with the following sequences:

CIITA Forward: 5'-AGACTTGCCGCGGCCCCAGAG-3'
CIITA Reverse: 5'-GTAGAGGCACAGGGGGTCAGC-3'

Reactions were plated in quadruplet on MicroAmp plates with optical seals (ThermoFisher Scientific, China) and qPCR was performed on a ThermoFisher QuantStudio 5 with the following cycling conditions: 50°C for 2 mins, 95°C for 2 mins, 40 cycles of denature at 95°C for 15 s, anneal/extend at 60°C for 1 min. A melt curve stage was completed following qPCR: 1.6°C/s ramp to 95°C for 15 s, 1.6°C/s ramp to 60°C for 1 min, 0.15°C/s ramp to 95°C for 15 s. The analysis was performed in Thermofisher Cloud Design and Analysis package. Analysis of the melt curve, unfortunately, revealed likely non-specific binding (see 5.3.1) and therefore experiments were redesigned using a TaqMan-based approach.

2.3.2.4 Quantitative reverse transcription PCR (RT-qPCR): TaqMan

TaqMan-based PCR uses fluorescence resonance energy transfer (FRET) to quantify DNA during the PCR reaction. Each primer contains two probes, one which fluoresces and the second which quenches the fluorescent signal of the first when in

close proximity by FRET. When the primer anneals to template DNA, Taq polymerase releases the fluorescent probe which is no longer inhibited by the quencher. TaqMan is therefore highly sequence specific, overcoming the problems of non-specific binding that can be seen with SYBR green.

Validated off-the-shelf ThermoFisher TaqMan Gene Expression arrays were selected for *CIITA* (Hs00172106_m1) and *GAPDH* (Hs02786624_g1). A range of RNA concentrations (10-100 ng) was again validated and again 50 ng was used for experiments. The qPCR reaction was prepared in 20 µl total volume comprised of 10 µl TaqMan Fast Advanced Mastermix, 1 µl Gene Expression array primer (*GAPDH* or *CIITA*), 4 µl cDNA and 5 µl nf-H20 and run using a fast cycling protocol. Each line was plated in quadruple replicate for *CIITA* (with and without IFNγ) and *GAPDH* (with and without stimulation). Reactions were plated in MicroAmp Fast 96 well plates with optical seals (ThermoFisher Scientific, China) and run on a ThermoFisher QuantStudio 5 with the following cycling conditions: 50°C for 2 mins, 95°C for 2 mins, 40 cycles of denature at 95°C for 1 s, anneal/extend at 60°C for 15 s. Analysis was performed in Thermofisher Cloud Design and Analysis package, with automated determination of Cycle Threshold (Ct). Relative quantification was performed by the ΔΔCt method (242), *GAPDH* Ct values were subtracted from *CIITA* Ct values to normalise to total RNA, before determination of the difference in *CIITA* Ct values (*CIITA* IFNγ – *CIITA* Control) and calculation of relative increase using the formula (2^-(ΔΔCt)). Mean values for the four replicates were plotted logarithmically with standard deviation values in GraphPad Prism (version 8.3.0).

2.3.2.5 Total RNA sequencing

Total RNA sequencing of organoid RNA was performed. RNA underwent quality assessment (TapeStation) to ensure a satisfactory RIN (>7) prior to sequencing. 150 ng of DNAse-treated RNA was aliquoted for input in a 12 µl volume. Under normal cellular conditions, around 80-90% of extracted RNA is ribosomal in origin (rRNA), therefore the sample underwent ribo-depletion with the NEBNext rRNA Depletion Kit (New England BioLabs, USA).

The rRNA was hybridised with a DNA probe (1 µl NEBNext rRNA Depletion Solution in 2 µl Probe Hybridisation buffer) specific for ribosomal sequences, mixed, centrifuged and underwent the following thermocycler reaction: 95°C for 2 min, 95°C to 22°C at 0.1°C/s, 22°C for 5 min. Next, RNase H was used to breakdown the rRNA hybridised to the DNA probes (2 µl NEBNext RNase H diluted in 2 µl RNase H Reaction Buffer and 1 µl nf-H20). The sample was again mixed, centrifuged and then incubated at 37°C for 30 minutes. The remaining DNA probes were digested using 2.5 µl DNase I diluted in 5 µl DNase I Reaction Buffer with 22.5 µl nf-H2O and again mixed and incubated at 37°C for 30 minutes. Finally, RNA purification was performed using 110 µl NEBNext RNA Sample Purification Beads. Beads were added to RNA and rinsed twice in 200 µl 80% ethanol, using a magnet to bind beads in between washes. RNA was eluted in 8 µl nf-H20 before proceeding to library preparation.

RNA library prep was performed using the NEBNext Ultra II Directional RNA Library Prep Kit for Illumina (New England BioLabs, USA). The full protocol is available from https://international.neb.com/protocols/2017/02/07/protocol-for-use-with-purified-

mrna-or-rrna-depleted-rna-and-nebnext-ultra-ii-directional-rna-library-prep-kit-for-illumina-neb-e7760-e7765 .

The initial step requires the generation of a cDNA two stranded library and clean up. Firstly, RNA was fragmented and primed for first-strand synthesis, adding 4 µl NEBNext First Strand Synthesis Reaction Buffer and 1 µl random primers to 5 µl RNA, incubating at 94°C for 15 minutes. First-strand cDNA synthesis was performed with the addition of 8 µl Strand Specificity Reagent and 2 µl First-Strand Synthesis Enzyme Mix, cycling through 25°C for 10 min, 42°C for 15 min, 70°C for 15 min. Second strand cDNA synthesis was performed next, with the addition of 8 µl Second Strand Synthesis Reaction Buffer with dUTP Mix (10X) and 4 µl Second Strand Synthesis Enzyme Mix with 48 µl nf-H2O, incubating at 16°C for 60 min. Finally, cDNA was purified using NEBNext Sample Purification Beads. The beads were vortexed and 144 µl added to the cDNA, mixing well. Following a five minute incubation at room temperature, beads were washed twice in 200 µl 80% ethanol (using a magnetic rack to retain beads), before elution in 53 µl 0.1% TE buffer.

50 µl of the prepared cDNA was removed and combined with sequencing adapters. Firstly, the cDNA ends were prepared for adapter ligation, adding 7 µl Ultra II End Prep Reaction Buffer and 3 µl Ultra II End Prep Enzyme Mix, mixing well and incubating at 20°C for 30 min followed by 65°C for 30 min. 2.5 µl adapters were combined with 1 µl Ligation Enhancer and 30 µl Ultra II Ligation Master Mix, mixed well and incubated for 15 minutes at 20°C and then a further 15 minutes at 37°C following the addition of 3 µl Uracil DNA glycosylase (UDG) and the DNA glycosylase-lyase Endonuclease VIII (USER) enzyme. Finally, the library was purified using a further pulldown with NEBNext Sample Purification Beads, adding 87 µl for

10 minutes, before performing two 200 µl 80% ethanol washes and eluting in 17 µl 0.1x TE buffer.

The sample-specific index primers were added during the PCR enrichment of adaptor-ligated DNA. 15 µl of eluted DNA was combined with 5 µl forward (i7) and 5 µl reverse (i5) index primer, along with 25 µl NEBNext Ultra II Q5 Master Mix. PCR was performed under the following conditions: Initial denaturation 98°C for 30 s, 7 cycles of denaturation followed by annealing/extension (98°C for 10 s, 65°C for 75 s), final extension 65°C for 5 minutes. Finally, the library was purified again with 45 µl NEBNext Sample Purification Beads, added for five minutes, washed twice in 200 µl 80% ethanol and eluted in 23 µl 0.1x TE buffer. Library presence was confirmed with TapeStation and QUBIT DNA quantification. Libraries were pooled before running on the Illumina NextSeq500 platform using 75 paired-end reads, with a 1% PhiX spike. The library was split evenly across two flow cells (e.g. all samples run on both flow cells to avoid any potential bias), with run metrics showing high-quality data acquisition. The PF percentage (passed filter; the number of clusters that could be individually read without loss to background from densely packed clusters) was 94.09%, % >Q30 was 95.7% (Q30 being the 1:1000 individual base call error rate, therefore 95.7% of base calls were made with at 1:1000 or better error rate) and samples were equally represented in the number of reads.

2.3.2.6 Total RNA sequencing analysis

Sequencing FASTQ files were downloaded from the Illumina Basespace cloud server. FASTQ files from both flow cells were combined for each sample on Partek Flow (a cloud-based semi-automated workstream for bioinformatics analysis).

Alignment of reads was performed using STAR index aligner (version 2.7.3a; Spliced Transcripts Alignment to a Reference) and human genome assembly GRCh38 (hg38). Transcript counting and normalisation were performed prior to GSA (gene-specific analysis), with filtering for expression fold changes of +2 or -2 fold with $p<0.05$. Each sample was annotated by characteristic e.g. strong responder to IFNγ stimulation, allowing for pathway (KEGG) and gene set enrichment analysis (gene ontology) and unsupervised hierarchical clustering across the characteristics of interest.

2.3.3 DNA procedures: pyrosequencing analysis of DNA CpG methylation

2.3.3.1 Bisulfite conversion

Sodium bisulfite is commonly used in the study of DNA methylation. Addition of bisulfite to DNA causes unmethylated cytosine bases to undergo chemical modification to uracil. The presence of methyl groups ‘shields’ cytosine bases from modification, so remaining unchanged (243). During PCR reactions, complementary base pairing will lead to uracil being replaced with thymine and therefore a comparison of cytosine to thymine ratio obtained during sequencing allows calculation of the percentage methylation at that base **(Figure 2.1)**.

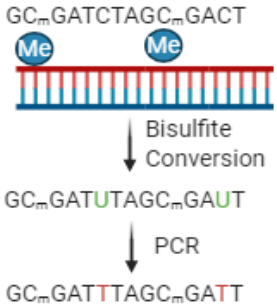


Figure 2.1 Bisulfite conversion. Schematic of bisulfite conversion. Sodium bisulfite causes unmethylated cytosine residues to be converted to uracil, complementary base pairing results in a thymine base being detected during sequencing. Single strand effects shown only. C_m represent methylated cytosine bases. Image created in Biorender.

Bisulfite conversion was performed with the EZ DNA methylation kit (Zymo, USA). The CT conversion reagent was reconstituted in nf-H20 and M-dilution buffer, vortexing for ten minutes to dissolve. 500 ng DNA was prepared, adding 5 µl M-dilution buffer and making up the volume to 50 µl with nf-H20, before incubating for 15 minutes at 37°C. 100 µl CT Conversion Reagent was added to each sample, mixed well and then incubated on a heat block for 16 hours at 50°C whilst protected from light. Samples were transferred to ice for ten minutes, diluted in 400 µl M-Binding Buffer and transferred to kit-supplied spin columns. Columns were centrifuged at max speed for 30 seconds, follow-through discarded and the filters rinsed in 100 µl M-wash buffer, repeating the centrifuge step. 200 µl M-Desulphonation Buffer was added to the filter and incubated at room temperature for 30 minutes, before centrifuging for 30 seconds at max speed. Two washes with 200 µl M-wash buffer were performed, before finally eluting the bisulfite converted DNA into a fresh tube in 10 µl M-Elution Buffer.

2.3.3.2 Pyrosequencing PCR primer design and quality assessment

Before sequencing, it is necessary to amplify the area of interest (CIITA-pIV) using PCR. The sequence for CIITA-pIV was downloaded from the University of California Santa Cruz Genome Browser (UCSC; available from https://genome.ucsc.edu/), with the region chr16:10,972,877-10,973,234 selected, encompassing the main CpG island. Raw sequence data was input into PyroMark Assay Design software (QIAGEN, version 2.0.2.5), which performs in silica bisulfite conversion, followed by computer modelling of available primer configurations based on size, annealing temperatures and predicted looping with other primer sequences or mispriming. A forward primer, biotinylated reverse primer (the biotin allows capture of the single strand for the pyrosequencing reaction) and a sequencing primer were designed. The sequence targeted contained eight individual CpG sites/variable regions. Final primer sequences (Sigma-Aldrich) were as follows:

CIITA Forward: 5'-GGGGGATGGAATATGTAAAATGTAG-3'

CIITA Reverse-Biotin: 5'-CCCCCAAACTCTAAACACAACAAACC-3'

CIITA Sequencing: 5'-GGAATATGTAAAATGTAGGG-3'

Before undergoing PCR for pyrosequencing, the conversion efficiency of bisulfite conversion was assessed using qPCR. A previously described methodology (244) was used with two primer pairs targeting β-Actin both with unconverted/methylated sequences (*ACTB*(-)) as well as converted/unmethylated (*ACTB*(+)) DNA. The qPCR was run using SYBR green with a dissociation step as previously described (see 2.3.2.3). Primer (Sigma-Aldrich) sequences were as follows:

ACTB(-) F: 5-TGGTGATGGAGGAGGCTCAGCAAGT

ACTB(-) R: 5-AGCCAATGGGACCTGCTCCTCCCTTGA

ACTB(+) F: 5-TGGTGATGGAGGAGGTTTAGTAAGT

ACTB(+) R: 5-AACCAATAAAACCTACTCCTCCCTTAA

TapeStation analysis was performed following Pyrosequencing PCR to confirm band presence at the correct molecular weight.

2.3.3.3 Pyrosequencing PCR

Amplification of the CIITA-pIV region was performed using the PyroMark PCR kit (QIAGEN, Germany). 0.5 µl of bisulfite converted DNA was used as input into the reaction in a 25 µl reaction mix for each sample. The remaining reaction mixture (for each 25 µl) was comprised of 12.5 µl PyroMark PCR master mix, 5 µl Q solution, 2.5 µl coral load concentrate, forward/reverse primers at 0.2 µM final concentration for both, with remaining volume made up with nf-H20. PCR was performed on a thermocycler with the following conditions: 95°C for 15 minutes, 45 cycles (94°C for 30 s denature, 56°C for 30 s annealing, 72°C for 30 s extension) and a final extension at 72°C for 10 minutes.

2.3.3.4 Pyrosequencing

Pyrosequencing reactions provide rapid, high-throughput and reliable sequencing over a short distance (up to a few hundred base pairs). The technology uses deoxyribonucleotide triphosphate (dNTP) bases bound to pyrophosphate (PPi). Each base is individually fed into the reaction mix, and if complementary to the next base in the template strand is incorporated by DNA polymerase, causing the release of PPi. Released PPi is converted to ATP, driving a luciferase-catalysed release of light

that is proportional to the number of bases sequenced (e.g. three consecutive cytosine bases will yield a 3x signal) (245). For methylation analysis, a predicated sequence is known and therefore a planned dispensation order of dNTPs can be utilised to maximise efficiency, both in terms of time and reagent usage. Unknown sequences can be determined but required the addition of potentially all four dNTPs until a signal is detected for a given nucleotide. With variable regions, such as the cytosine/thymine ratio in a bisulfite-converted sample, represented by the 'Y' symbol, both bases can be sequentially used to give a ratio of methylated to unmethylated nucleotide.

The sequencing reaction was set up on the PyroMark Q48 (QIAGEN) sequencer. The required reagents were loaded into injector cartridges using PyroMark Q48 Advanced Reagents (QIAGEN, Germany). Sequencing primer was diluted to 4 µM in annealing buffer, with a resulting final concentration of 800 nM in the reaction mix. An absorber strip was fitted to the Q48 and a new sample disc fixed in place. 10 µl bisulfite converted DNA was loaded into each well on the disc, followed by 3 µl QIAGEN Magnetic Beads (Germany). Beads were vortex frequently during pipetting to reduce settling. In addition to the samples, 5 recommended primer negative controls were run as specified by QIAGEN to exclude non-specific sequencing:

1. PCR without template DNA
2. PCR with template DNA but no sequencing primer
3. Sequencing primer without PCR product
4. Biotinylated primer without PCR product
5. Biotinylated primer and sequencing primer without PCR product

Run setup was performed in PyroMark Q48 Autoprep software (Version 2.4.2, QIAGEN, Germany). The sequence to analyse was:

TYGGGAAATA TTTYGTTTTT AGTATTTTYG TAAYGATTTT GYGYGGGAAT TAGGAGTYGG GAATTYGGAG TTTGGTTTGT TGTGTTTAGA GTT.

The calculated dispensation order based on this sequence was:

ATCTGACTGATTCTGTTAGTGATTCTGTGATCGATTAGTCAGTCGATAGATGTCT GTATCTGAG

Each sample was run in triplicate and in addition EpiTect Methylated and Unmethylated Control DNA (already bisulfite converted; QIAGEN, Germany) was run alongside samples. Analysis of C/T ratio was performed by the automated algorithm on the PyroMark Q48 AutoPrep software.

2.3.4 DNA Procedures: whole-genome sequencing

Whole-genome sequencing of organoid lines was outsourced to Nonacus Ltd. 500 ng of DNA was supplied frozen for PCR-free library preparation. The MGI-Seq G400 platform was used with 50x coverage supplied. As only tumour material was supplied, basecalled FASTQ files were merged per sample, trimmed with Trimmomatic (246). Trimmed reads were then aligned to the GRCh38.3 reference genome using BWA-MEM (Burrow-Wheeler Aligner, v0.7.17-r1188, please see https://arxiv.org/abs/1303.3997), PCR duplicates were marked using Picard (Picard Toolkit 2019, v4.0.12.0, the Broad Institute, available from http://broadinstitute.github.io/picard/) and reads were realigned locally around Indel sites. Variant calling was performed using Pisces (247) (a tumour only variant caller, v5.2.9.122) with standard settings. VCF files were then annotated using VEP (248)

(Variant Effect Predictor; v97.3, Ensembl, available from https://www.ensembl.org/info/docs/tools/vep/index.html) and SNPs present from 1000Genomes (249), GnOMAD (250) and dbSNP (251) at a MAF of > 0.01 were excluded. Pathogenicity of SNPs was assessed using dbSNP. Copy number calling was called using CNVNator (v0.4.1) (252) and structural variants using Manta (v1.6.0) (253). HLA typing was performed using HLA*LA (v1.0.1) (254).

2.3.5 DNA Procedures: Chromatin Immunoprecipitation (ChIP)

Chromatin Immunoprecipitation (ChIP) is a methodology for studying DNA-binding proteins and other epigenetic modifications including histone modification. DNA binding proteins are first cross-linked to DNA, using agents such as formaldehyde. The DNA is then fragmented using sonication, followed by an antibody-based selection of the sheared DNA bound to the protein of interest. The DNA is then released from the protein by reverse cross-linking and can be assessed either by PCR or sequencing.

2.3.5.1 ChIP: cross-linking (single and dual)

Cell lines and organoids were treated with IFNγ for the required time and were subsequently digested into single-cell suspensions (see 2.1.2.6). $1x10^7$ cells were used for each cross-linking condition, collecting in a 15 ml centrifuge tube and were washed three times in PBS. Cells were resuspended in 10 ml PBS containing 1% methanol-free formaldehyde (ThermoFisher Scientific, USA) and incubated at room temperature for ten minutes on a roller. Cross-linking was terminated with the addition of 2.5 ml 2M Glycine (Sigma-Aldrich, USA), incubating at room temperature

for five minutes, before centrifuging at 400 x g for 5 minutes at 4°C and then washing twice in PBS. Chromatin pellets were frozen at -80°C.

For *EZH2* ChIP, a dual cross-linking protocol was followed. Cells were prepared and washed as above, but prior to the addition of formaldehyde, cells were instead resuspended at $3.3x10^6$ cells/ml. Di(N-succinimidyl) glutarate (DSG; Sigma-Aldrich, Germany) was reconstituted in DMSO and added to the cell suspension at a final concentration of 2.5 mM, with cells incubated for 45 minutes at room temperature on a roller. Following the DSG cross-linking, cells were washed four times in PBS before immediately continuing to the second cross-linking step with formaldehyde as detailed above.

2.3.5.2 ChIP: chromatin sonication and immunoprecipitation

Sonication was performing with a Covaris E220 Evolution and according to the truChIP Chromatin Shearing Kit (Covaris, USA) protocol. Covaris utilises highly focused acoustic ultrasonication to shear nucleic acids. It produces highly consistent results between samples and is therefore an ideal method for sample preparation for use with ChIP.

Cross-linked cells underwent lysis to isolate nuclei using 300 µl Lysis Buffer B (containing 1:100 protease inhibitor; kit supplied), incubating cells for 10 minutes at 4°C on a roller. Cells were centrifuged at 500 x g for 5 minutes at 4°C, before removing the supernatant. This step was then repeated with 300 µl Wash Buffer C (containing 1:100 protease inhibitor; kit supplied) incubating for 10 minutes at 4°C on a roller, followed by two rinses in Shearing buffer D3 (containing 1:100 protease inhibitor; kit supplied) without an incubation step. Each pellet was resuspended in

130 µl Shearing Buffer D3 and transferred into microTUBES for shearing on the Covaris for ten minutes per sample.

Before performing chromatin shearing, a range of sonication conditions were assessed as described in the protocol. Briefly, nuclei were resuspended in Shearing Buffer D3 (kit supplied) and 130 µl aliquots were prepared in microTUBES (Covaris, USA) to allow for assessment of different shearing times, aiming to yield 200-700 BP fragment. Six separate time points (2, 4, 6, 8, 10 and 12 minutes) were programmed, using the Low Cell Shearing Protocol (Peak power 105 W, duty factor 2%, 200 cycles per burst, 6°C temperature setpoint). Once sonication was completed, 1 µl DNA was analysed by TapeStation and the most efficient time point (10 minutes) was chosen for future experiments based on the 200-700 BP enrichment observed **(Figure 2.2)**.

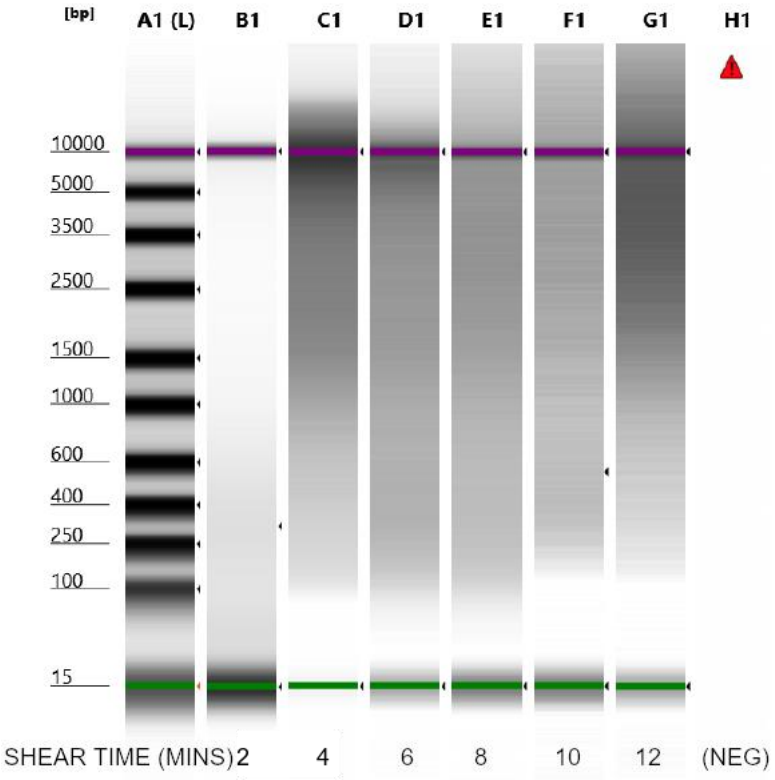


Figure 2.2 Optimisation of ChIP Covaris shearing times. TapeStation of DNA product following a range of sonication times between 2 and 12 minutes, loaded lane B to G. Optimal enrichment at 200-700 BP seen in lane F (10 minutes). Negative control in lane H.

Once the shearing was complete, samples were removed from microTUBES into fresh Eppendorf tubes, centrifuged at 16000 x g for ten minutes at 4°C to pellet any insoluble chromatin and 130 µl sheared chromatin was removed and diluted with 260 µl (two volumes) ChIP dilution buffer (containing 1:100 protease inhibitor; kit supplied). Five percent of the total chromatin volume was taken off and kept at 4°C to assess for total loading quantification (input). Meanwhile, antibodies for H3K9ac (Abcam, UK, #ab4441), H3K9me2 (Abcam, UK, #ab195482) and *EZH2* (Abcam, UK, #ab195409) were conjugated with magnetic Dynabeads Protein G (Thermo Fisher Scientific, Norway). 10 µl Dynabeads were prepared for each immunoprecipitation (IP), first washing beads in PBS before combining with 2 µg/IP antibody in 0.5% BSA

in PBS, incubating on a wheel for two hours at 4°C. Sheared chromatin was combined with 10 µl of antibody-bead conjugate for each IP and incubated at 4°C overnight on a wheel.

2.3.5.3 ChIP: reverse cross-linking

Following incubation, samples underwent a series of washes, the constituents of the buffers are described subsequently, with each washed performed with the aid of a magnetic rack to clear solution and pull down the beads. Beads were washed with 500 µl Wash buffer 1, two washes with 500 µl Wash buffer 2, one wash in 500 µl LiCl buffer before two final washes with TE/NaCl. Chromatin was eluted in two 50 µl volumes of elution buffer, vortexing and incubating for 15 minutes at room temperature with each elution. Input DNA (collected prior to IP) was brought to 100 µl total volume in elution buffer. Input and IP samples were then incubated at 65°C overnight with 3 µl Proteinase K (50 mg/ml, Roche, Germany) and 3 µl 5 M NaCl to reverse cross-link. DNA was purified with the addition of 180 µl AMPure XP beads (1.8:1 volume; Beckman Coulter, USA), incubating at room temperature for 15 minutes, before washing twice with 500 µl 80% ethanol. After the last wash, beads were left to air dry for ten minutes and DNA was eluted in 90 µl nf-H20.

Buffer constituents were as follows: Wash Buffer 1 (20 mM Tris-HCl pH 8.0, 150 mM NaCl, 2 mM EDTA pH 8.0, 1% Triton X-100 and 0.1% SDS); Wash Buffer 2 (20 mM Tris-HCl pH 8.0, 500 mM NaCl, 2 mM EDTA, 1% Triton X-100, and 0.1% SDS); LiCl Buffer (10 mM Tris-HCl pH 8.0, 250 mM LiCl, 1 mM EDTA, 0.5% NP-40 and 0.5% Na-deoxycholate); TE/NaCl Buffer (10 mM Tris-HCl pH 8.0, 50 mM NaCl and 1 mM EDTA pH 8.0; Elution buffer (100 mM NaHCO3 and 1% SDS).

2.3.5.3 ChIP qPCR

Four primers were used to cover the CIITA-pIV for ChIP PCR, based on previously published sequences (196):

CIITA-pIV region 1 Forward: 5'-GCCTGAAAAGGGAAAGTGACCACCTC-3'

CIITA-pIV region 1 Reverse: 5'-CACACCCCCAGCCGTGGCAA-3'

CIITA-pIV region 2 Forward: 5'-ACAAGCTCCCTGCAACTCAG-3'

CIITA-pIV region 2 Reverse: 5'-CCACCACGTGCTTTATCAGA-3'

CIITA-pIV region 3 Forward: 5'-GGGCTGAGAATCGAGGCTCCGAGAC-3'

CIITA-pIV region 3 Reverse: 5'-GCGGGGATGCTGGAAACGAGGTG-3'

CIITA-pIV region 4 Forward: 5'-TCCTGCAGAGGTGCGCGCCCTTC-3'

CIITA-pIV region 4 Reverse 5'-CCGCCTGGAGAGCCCAATACCCAAGA-3'

Additional quality control was performed by performing PCR for the SP1 and Involucrin (IVL) region; SP1 being an open acetylated conformation, with IVL methylated. 1 µM of forward and reverse primer for each region was combined with 2x PowerUp SYBR Green Master Mix (ThermoFisher Scientific, Lithuania) and nf-H20 to a total volume of 7.5 µl and combined with 2.5 µl immunoprecipitated DNA in a 384 well PCR plate. For each region input DNA, acetylation and methylation were plated in technical duplicate and *EZH2* in quadruplet. A standard curve dilution was plated using genomic DNA at 0.04, 0.2, 1 and 5 ng/µl (from Kasumi-1 cell line; kindly provided by Dr Anetta Ptasinska) for each region and negative controls were run for all primers. PCR was performed under the SYBR Green cycling conditions as detailed in 2.3.2.3, on an Applied Biosystems 7500 qPCR machine. Analysis of melt

curves and Ct determination was performed using SDS software (Applied Biosystems). Quantification was performed relative to the standard curve and data from each region was normalised by input control. Finally, a comparison of each region was performed with and without IFNγ stimulation to give a relative change.

2.4 Flow cytometry

Flow cytometry allows the rapid characterisation of large numbers of heterogeneous cells by using fluidics to generate a stream of single cells. Cells pass through a laser and data on the forward and side scatter (broadly representing size and complexity/granularity respectively) of light can be collected by detectors. In addition to this basic data, fluorochrome-conjugated antibodies against both surface and internal antigens can allow simultaneous detection of up to 16 characteristics, providing detailed phenotyping of cells of interest.

In order to analyse cells from 2D and organoid culture, lines were treated with IFNγ and/or drugs of interest for the desired time-frame in standard culture conditions, before being dissociated into single cells (2.1.2.6). Cells were filtered through a 70 µl filter before washing in PBSO and divided into 96 well V bottom polypropylene plates. First cells were stained with eBioscience Fixable Viability Dye eFluor 780 (1 µl/ml diluted in PBSO, ThermoFisher Scientific, USA), incubating at 4°C for 30 minutes in the dark, before washing three times with 200 µl PBSO. Cell surface markers were stained for with antibody conjugates **(Table 2.3)** in Flow Cytometry Staining buffer containing 1% Bovine Serum Albumin (Roche, Germany) and 0.1% sodium azide (G Biosciences, USA) dissolved in PBSO and incubated at room temperature for 30 minutes in the dark. Cells were again rinsed three times with 200 µl PBSO. Cells

were fixed with the eBioscience™ Foxp3 / Transcription Factor Staining Buffer set (ThermoFisher, USA). One-part Fixation Concentrate was dissolved in three-parts Fixation diluent and 100 µl added to each well for 30 minutes at room temperature in the dark. If intracellular stains were required, cells were taken up in Permeabilization buffer (one-part dissolved in nine-parts distilled water) and centrifuged at 400 x g for five minutes, discarding the supernatant, before resuspending in Permeabilization buffer containing intracellular antibodies. Cells were washed three times in PBSO buffer resuspending cells in 150-200 µl in Flow Cytometry Staining buffer.

Samples were analysed using an LSR Fortessa X-20 flow cytometer (BD), with data analysis performed using FlowJo (Version 10.5.3, BD). Compensation was performed with either single-stained cells (with negative comparison with unstained cells) or UltraComp eBeads (ThermoFisher, USA), with one drop beads combined with 1 µl antibody for 30 minutes and compared with unstained beads. Fluorescence minus one (FMO, cells stained for viability and all other antibodies other than the target of interest) stains were performed for Class II and MUC2. An example of the standard gating strategy is displayed below **(Figure 2.3)**, initially selecting singlets (FSC-A vs FSC-H), followed by selection of cells (FSC-A vs SSC-A) and finally live cells in the APC-Cy7^{lo} fraction (APC-Cy7 vs SSC-A). Class II gating was performed with the aid of FMO cells. Individualised gating for all experiments is provided in the **Chapter 8 appendix.**

Target (Clone)	Conjugate	Source	Supplier	Dilution
HLA-A,B,C (W6/32)	APC	Mouse IgG2a	Biolegend	1:100
HLA-DR,DP,DQ (Tü39)	PE-Cy7	Mouse IgG2a	Biolegend	3:100
Epcam/CD326 (9C4)	Pacific Blue	Mouse IgG2b	Biolegend	5:100
LGR5 (8F2)	BV510	Rat IgG2b	BD Biosciences	5:100
MUC2 (MLP/842)	FITC	Mouse IgG1	Bio-Techne	5:100
Chromogranin A	PE	Mouse IgG1	BD Biosciences	5:100
IFNγ Receptor α chain CD119 (GIR-94)	PE	Mouse IgG2b	Biolegend	5:100

Table 2.2 Antibody details for flow cytometry experiments

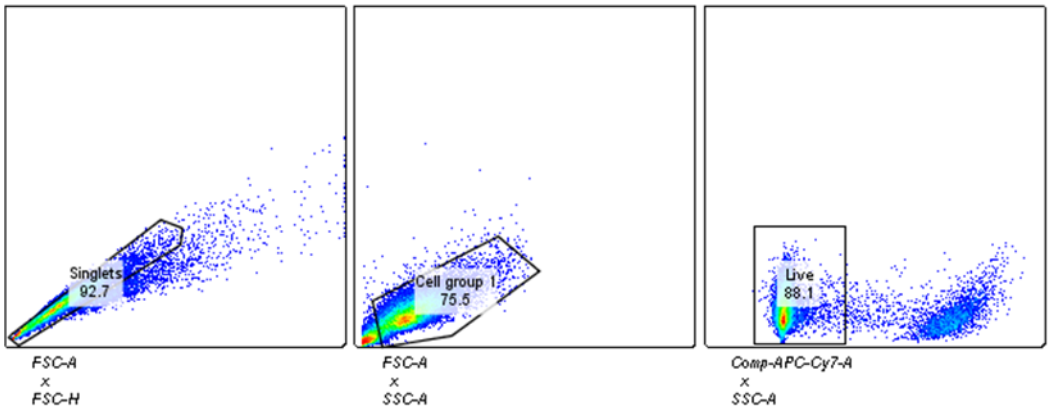


Figure 2.3 Flow cytometry gating

2.4.1 Fluorescence-activated cell sorting (FACS)

Organoids with weakly-inducible Class II expression were treated with 24 hours IFNγ and ROCK inhibitor (Y-27632, to preserve viability during sorting). Staining for live-dead, Class II and single stains were performed, in sodium azide-free Flow Cytometry Staining Buffer. Cells were sorted with a stringent gating strategy for Class

II positive and negative cells, selecting only strongly positive cells. Sterile sorting was performed on a BD FACSAria Cell-Sorting System within a category 2 tissue culture hood and was kindly performed by Dr Adriana Flores-Langarica from the University of Birmingham Flow Cytometry Service. Cells were sorted into organoid media, were returned to tissue culture, washed in PBSO and then resuspended in a single well of matrigel. Organoids were seen to reform over the following week, with usual growth kinetic restored after around five days.

Chapter 3: Establishment of a collection of human colorectal cancer organoids

3.1 Introduction

Recent technological advances have allowed the establishment of self-sustaining organoid models. These 3D cultures can be derived from almost all known tissue types (for example brain and thyroid), replicating structure and function of that tissue with a high degree of fidelity. Furthermore, cells from diseased tissues including cancer can be established into culture, providing an unrivalled cell-based system for studying disease. The clinical application of these models is already being observed and it is known that colorectal cancer organoids can predict the in vivo sensitivity to chemotherapy and radiotherapy (221, 223-225), potentially providing an 'avatar' to select effective anti-cancer therapies for patients, improving outcomes and minimising unnecessary toxicity. Within this group, current work includes setting up a clinical trial to assess the effectiveness of chemotherapy selection based on the results of 3D cultures derived from colorectal cancer patient biopsies (collaboration between 2cureX (Denmark) and Dr Helen Bermingham/Prof Andrew Beggs locally).

Rectal organoids have been used in the prediction of drug sensitivity in rare variants of cystic fibrosis, a disease with over 2000 known mutations in the CFTR gene. Before this organoid screening approach, it was simply not feasible to study the effectiveness of the compound in all these rare variants, with only the common mutations enrolled in clinical trials. The simple technique uses rectal biopsy to study chloride channel dynamics in the lab, with drug funding agreed for patients with evidence of drug response in the organoid model (255).

Aside from clinical applications, organoids allow fundamental disease biology to be explored in greater depth and accuracy. Organoids from cancer, for example, replicate tumour heterogeneity and are stable over prolonged periods transcriptionally and at genome level (11, 221). This offers an advantage of 2D cancer cell cultures, which are known to change over time in culture, with the same cell lines displaying hugely variable responses to drugs between passages and different lab groups (8). It is also known the 2D cultures become epigenetically altered with time, with methylation in particular disparate from the primary tissue (205). Organoids, by contrast, are highly faithful to the original sample, including disease-specific epigenetic patterns and even physiological epigenetic changes, for example in embryogenesis. Given the concerns over 2D culture, organoids are now established as the gold standard for cell-based assessment of epigenetics in disease (230, 231).

Beyond these technological advantages over cell lines, organoids allow the context of the native tumour biology to be considered in parallel with the cell-autonomous behaviours that are observed under experimental conditions. The establishment of a pathologically and microenvironmentally annotated collection of patient-derived organoids is a core aim of this project. The regulation of MHC Class II will be assessed, but the additional strength will be the potential to know what is happening in the tumour of the patient. This context is fundamental to understanding the relevance of findings, is there tumour Class II expression or the presence of tumour infiltrating lymphocyte populations on primary tumour IHC? The further contextual information around tumour pathology (e.g. sidedness, stage, grade, mutation and transcriptional context) can be assessed in conjunction with any experimental

hypothesis. Whole-genome and total RNA data will be produced for each organoid, again allowing interpretation of experimental findings, in this and future projects.

3.2 Processing Tissue Samples

Between October 2017 and December 2019, tissue collection was performed on patients from University Hospitals Birmingham undergoing cancer surgery. Patients were identified by clinicians in surgical clinics and multidisciplinary meetings and consented to use of their tissue for research according to protocols and ethical approval of the University of Birmingham HBRC (see section 2.1.2.1). Tissue from both colon and rectal primary tumours resections, metastasectomy (removal of metastases) including liver and peritoneal and matched normal bowel samples were sampled and anonymised by the HBRC and were subsequently processed in dedicated tissue culture hoods for organoid lines.

A total of 12 organoids were developed, with the following criteria used for declaring a line as established:

1. Survives long term culture e.g. >10 passages
2. Organoids are frozen and survive thawing
3. DNA/RNA extracted and sequenced to confirm tumour origin
4. Histologically sectioned to prove tumour morphology

A number of lines were terminated during the first six months of sample collection due to infection, usually within the first few days of processing the sample. It was felt likely that carryover of bowel bacteria was the likely source of these infections, which occurred despite the presence of Penicillin/Streptomycin as originally described (10). The methodology was adapted to include primocin, a combination of broad-spectrum

anti-fungal and antibiotics. This was included in the storage media used to contain the samples overnight before processing the next day. Additionally, a cleaning step at the beginning of processing was included consisting of vigorously shaking the segments of bowel in PBSO/primocin until the solution became clear. Since the adaptation of the new protocol, a reduction in new lines being terminated from infection has occurred, from around 50% to zero.

In addition to the 12 lines derived in this laboratory, a further 3 lines were processed from UHB patients and established at the WTSI and returned to this facility, complete with whole-genome sequencing data, as part of a reciprocal arrangement under the Human Cancer Model Initiative (HCMI). Initially, some normal bowel samples were processed for organoid culture in parallel to tumour samples, however, due to cost constraints, the majority of samples were only processed for tumour organoids. The matched normal bowel underwent DNA/RNA extraction for subsequent analysis. Samples received for processing were between 139-638 mg in weight.

A total of 94 samples were received over the collection period from HBRC. Of these, 54 samples were either not processed and were disposed of or did not form organoids in the initial two weeks following processing. Of the 40 samples that it was possible to derive organoid cultures from, 28 were terminated due to failure of the culture to propagate or infection. 26 of these were terminated before the antibiotic change, with the vast majority of these lost to infection. Only two lines were lost after the antibiotic change occurred. Summarised in **Figure 3.1**.

A second important change has been the use of ROCK inhibitors in freezing, thawing and derivation of new lines. Two of the earlier lines derived (647 and 658) had failed multiple thaw attempts, however, the addition of the inhibitor to thaw media and for the first three days of culture, allowed successful reconstitution of these lines. Since adding the inhibitor for both freezing and thawing, very high success rates have been observed during the thawing process (>90% of vials and all established lines).

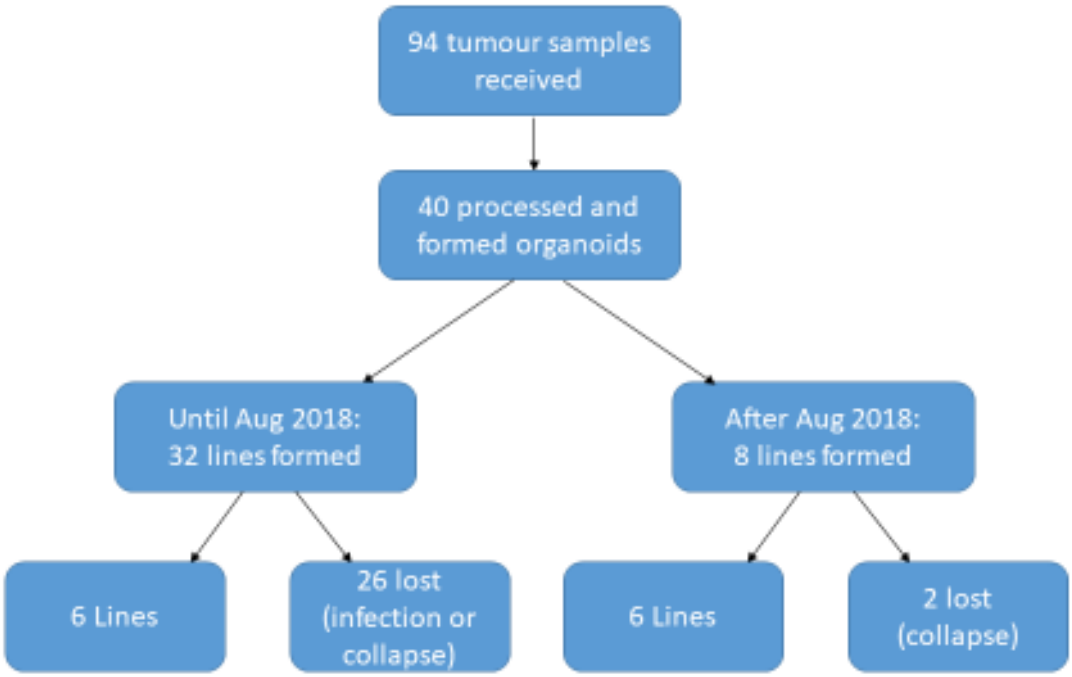


Figure 3.1 Derivation of organoids. Flow chart of samples received and processed over the sample collection period. Following change in antibiotic protocols in August, a dramatic decrease in loss of lines due to infection was observed.

3.2 Patient characteristics of lines

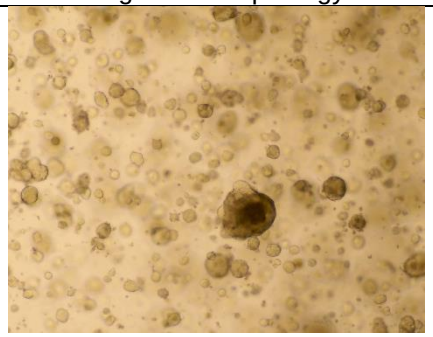
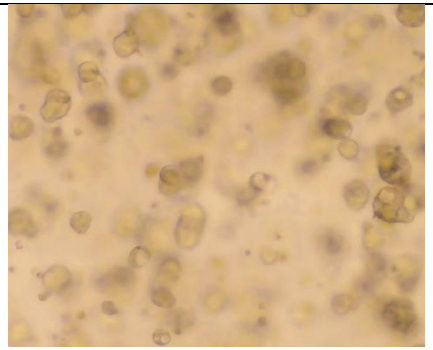
Samples selected for this project were all specimens from any colorectal (adenocarcinoma) primary. Metastatic deposits, e.g. liver metastases were excluded from this project, although they were often processed by the lab. Two of the patients had metastatic disease, e.g. those undergoing combined colectomy and metastasectomy, where organoids derived from the primary site only were used in these experiments. Five rectal tumours were included in the data, all of which had undergone prior treatment in order to downstage them for curative resection. Four of these patients underwent standard radiotherapy (one received short-course radiotherapy with 25 Gy in 5 fractions, three with long course chemoradiotherapy with 45 Gy in 25 fractions with capecitabine). A final patient had long course chemoradiotherapy followed by systemic chemotherapy (FOLFIRI 3 cycles and FOLFOX 6 cycles). None of the patients presenting with colon tumours (e.g. excluding rectal) had undergone chemotherapy or radiotherapy for either downstaging or neoadjuvant intent, before their resections.

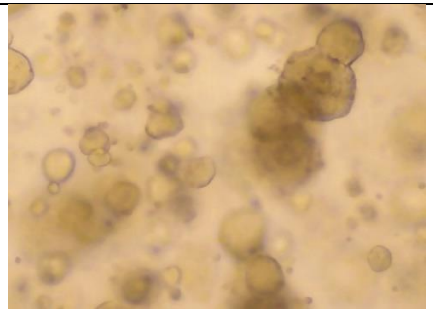
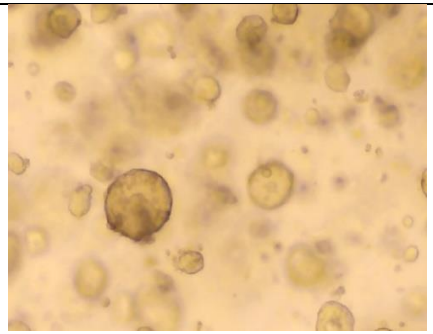
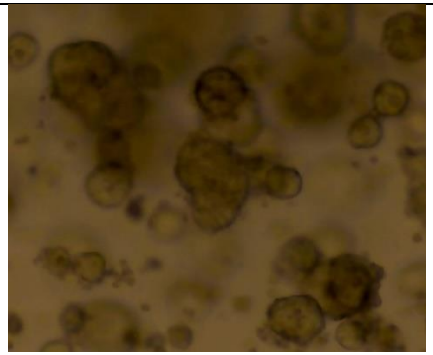
dMMR was detected in 5/15 tumours (33.3%; tumour IHC), RAS mutation in 6/11 (54.5%) tumours assessed and BRAF in 3/15 (20%). Tumour stages from I to IV were represented and therefore the samples are likely to be representative of the range of pathologies encountered.

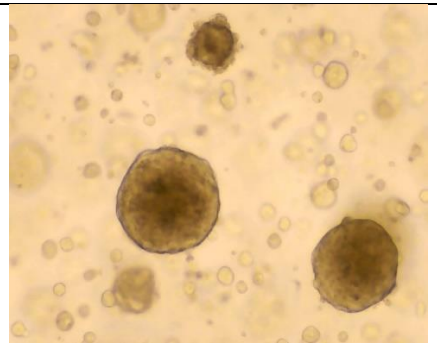
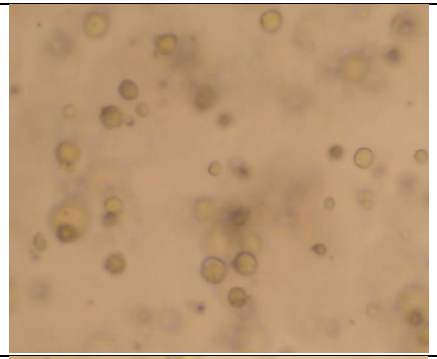
In addition to the baseline pathological data, Class II staining on primary tumours has been performed using a clinically validated antibody, for further details see section 5.2.1. Immunoscore assessment has been performed by HalioDx (France) and is

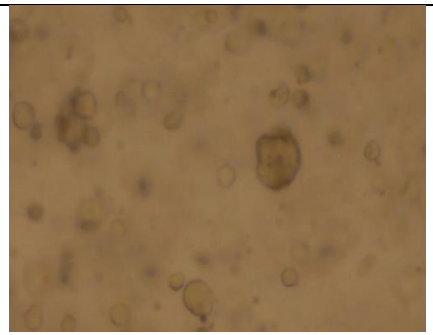
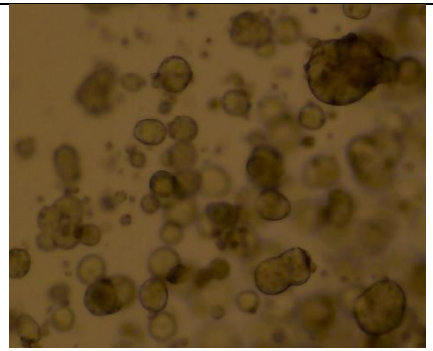
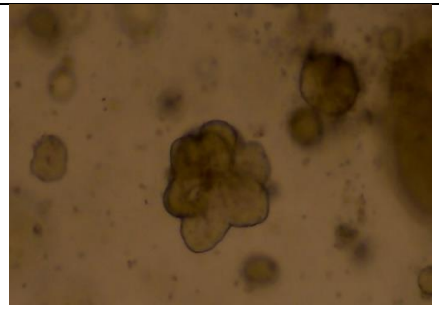
available for ten of the tumours. Full characteristics for each organoid are summarised in **Table 3.1.**

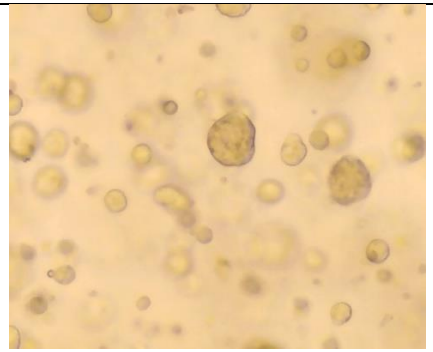
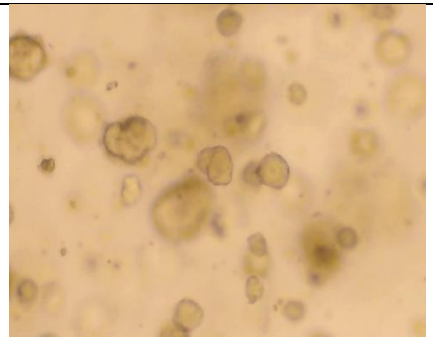
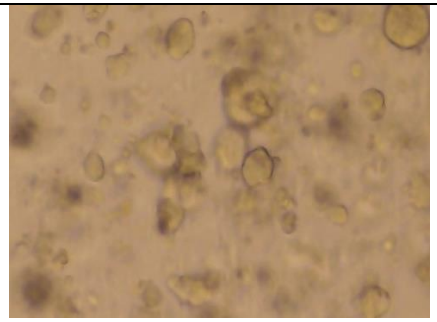
Table 3.1 Characteristics of derived organoids. See overleaf. For each organoid line sample, morphology as well as clinicopathological details are given including age, sex, TNM staging, tumour location, operation, pre-operative treatment received, NHS pathology lab assessment of extended spectrum RAS and BRAF mutation, MMR status assessed by IHC, immunoscore and staining of Class II in the primary tumour. Abbreviations: T/N/M: Tumour, nodal (with positive / total nodes displayed where available) and metastasis status. V/PN/L: details of vascular, perineural and lymphovascular invasion at the site of the primary tumour. WT: Wild-type. LCCRT: Long-course chemoradiotherapy. SCRT: Short-course radiotherapy

Sample Number	Organoid Morphology		
S292064 / 064		Age at presentation/sex	79 / M
		Staging	T2 N1(1/19) M0 V0 PN- L0 R0
		Grade	Moderate
		Location	Rectosigmoid
		Operation	Anterior Resection
		Pre-operative treatment	None
		RAS/BRAF	WT / WT
		MMR status	MSS
		Immunoscore	3 (High)
		Primary Class II IHC	25%
S389080 / 080		Age at presentation/sex	85 / F
		Staging	T3 N0 M0 V0 PN0 L0 R0
		Grade	Well-Moderate
		Location	Rectal
		Operation	Anterior Resection
		Pre-operative treatment	LCCRT
		RAS/BRAF	Not performed
		MMR status	MSS
		Immunoscore	2 (Intermediate)
		Primary Class II IHC	0%
S398157 / 157		Age at presentation/sex	84 / F
		Staging	T3 N2 (4/26) M0 V0 PN0 L0 R1
		Grade	Poor
		Location	Ascending Colon
		Operation	Right Hemicolectomy
		Pre-operative treatment	None
		RAS/BRAF	Not performed / WT
		MMR status	MSI-H (MLH1/PMS2 loss, promoter methylation)
		Immunoscore	4 (High)
		Primary Class II IHC	45%

S403376 / 376		Age at presentation/sex	51 / M
		Staging	T3 N0 (0/41) M0 V1 PN0 L0 R0
		Grade	Poor
		Location	Rectal
		Operation	Anterior Resection
		Pre-operative treatment	LCCRT
		RAS/BRAF	Not performed / Not Performed
		MMR status	MSS
		Immunoscore	Not performed
		Primary Class II IHC	0%
S302389 / 389		Age at presentation/sex	81 / M
		Staging	T4 N2 (6/19) M0 V1 PN0 L0 R0
		Grade	Moderate
		Location	Transverse Colon
		Operation	Right Hemicolectomny
		Pre-operative treatment	None
		RAS/BRAF	WT / WT
		MMR status	MSS
		Immunoscore	0 (Low)
		Primary Class II IHC	0%
S302411 / 411		Age at presentation/sex	74 / F
		Staging	T3 N2 (7/24) M1 V1 PN0 L0 R0
		Grade	Moderate
		Location	Transverse Colon
		Operation	Subtotal Colectomy
		Pre-operative treatment	None
		RAS/BRAF	WT/ V600
		MMR status	MSS
		Immunoscore	2 (Intermediate)
		Primary Class II IHC	1.5%

S366557 / 557		Age at presentation/sex	75 / F
		Staging	T3 N (0/17) M0 V0 PN1 L0 R0
		Grade	Moderate-poor
		Location	Ascending Colon
		Operation	Right Hemicolectomy
		Pre-operative treatment	None
		RAS/BRAF	KRAS Exon 2 Codon 13 (Gly13Arg) / WT
		MMR status	MSI-H (MLH1, PMS2 and MSH6 loss)
		Immunoscore	2 (Intermediate)
		Primary Class II IHC	1%
S332647 / 647		Age at presentation/sex	45 / M
		Staging	T4 N2 (5/52) M0 V1 PN0 L0 R1
		Grade	Poor
		Location	Ascending Colon
		Operation	Extended Right Hemicolectomy
		Pre-operative treatment	None
		RAS/BRAF	KRAS Exon 2 Codon 13 (Gly13Asp) / WT
		MMR status	MSI-H (MSH6 loss)
		Immunoscore	Not Performed
		Primary Class II IHC	75%
S345653 / 653		Age at presentation/sex	55 / F
		Staging	T2 N0 M0 V1 PN0 L0 R0
		Grade	Moderate
		Location	Rectal
		Operation	Abdominoperineal resection
		Pre-operative treatment	LCCRT
		RAS/BRAF	KRAS Exon 2 Codon 12 (Gly12Asp) / WT
		MMR status	MSS
		Immunoscore	2 (Intermediate)
		Primary Class II IHC	60%

S332658 / 658		Age at presentation/sex	59 / F
		Staging	T4 N0 (0/28) M0 V0 PN0 L0 R0
		Grade	Poor
		Location	Ascending Colon
		Operation	Right Hemicolectomy
		Pre-operative treatment	None
		RAS/BRAF	WT / V600
		MMR status	MSI-H (MLH1 and PMS2 loss)
		Immunoscore	Not performed
		Primary Class II IHC	20%
S309884 / 884		Age at presentation/sex	74 / M
		Staging	T3 N2 (4/12) M1 V1 PN0 L1 R0
		Grade	Moderate-Poor
		Location	Rectal
		Operation	Abdominoperineal resection
		Pre-operative treatment	SCRT
		RAS/BRAF	NRAS Exon 2 Codon 13 (Gly13Arg) / WT
		MMR status	MSS
		Immunoscore	0 (Low)
		Primary Class II IHC	0%
S386964 / 964		Age at presentation/sex	53 / M
		Staging	T2 N0 (0/18) M0 V0 PN0 L1 R0
		Grade	Well-Moderate
		Location	Ascending Colon
		Operation	Right Hemicolectomy
		Pre-operative treatment	None
		RAS/BRAF	Not performed
		MMR status	MSS
		Immunoscore	2 (Intermediate)
		Primary Class II IHC	0%

WTSI-COLO151		Age at presentation/sex	71 / M
		Staging	T3 N1 (1/33) M0 V0 PN0 L0 R0
		Grade	Moderate
		Location	Ascending Colon
		Operation	Right Hemicolectomy
		Pre-operative treatment	None
		RAS/BRAF	WT / V600
		MMR status	MSS
		Immunoscore	2 (Intermediate)
		Primary Class II IHC	0%
WTSI-COLO155		Age at presentation/sex	60 / M
		Staging	T4 N0 (0/11) M0 V1 PN1 L0 R1
		Grade	Moderate
		Location	Low Rectal
		Operation	Abdominoperineal resection/Pelvic exenteration
		Pre-operative treatment	LCCRT, 3xFOLFIRI, 6x FOLFOX
		RAS/BRAF	KRAS codon 61 (Gln61His) / WT
		MMR status	MSS
		Immunoscore	2 (Intermediate)
		Primary Class II IHC	7.5%
WTSI-COLO312		Age at presentation/sex	76 / F
		Staging	T3 N0 (0/17)
		Grade	Moderate-poor
		Location	Ascending Colon
		Operation	Right Hemicolectomy
		Pre-operative treatment	None
		RAS/BRAF	KRAS Exon2 Codon13 (Gly13Arg) / WT
		MMR status	MSI-H
		Immunoscore	Not performed
		Primary Class II IHC	0%

3.3 Transcriptional subtypes

Colorectal cancers can be classified based on unsupervised clustering of expression patterns into four main groups, termed the consensus molecular subtypes (CMS) (51). The original algorithm predicts CMS based on cancer and stromal RNA expression, originally designed to call primary CRC tumour extracts. Cell lines and organoids lack this stromal component, leading initially to the theory that 'mesenchymal CMS4' tumours are selected against growing in tissue culture conditions. An R package termed CMScaller was developed by the Lothe lab, designed to use cancer cell-intrinsic expression to more accurately call CMS-type in organoid lines (256). This has been validated in public datasets and is therefore the standard approach to CMS classifying organoids and cell lines. RNA extracted from the 15 organoid lines was analysed using the CMScaller R package and I'm grateful to Dr João Silva for his R expertise. Fourteen of the lines were successfully classified into CMS groups, the results of which are displayed in **Table 3.2**.

Line	CMS Classifier	P value	FDR
064	CMS2	0.015	0.017
080	CMS2	0.001	0.002
157	CMS1	0.001	0.002
376	CMS1	0.002	0.003
389	CMS2	0.001	0.002
411	CMS3	0.013	0.016
557	CMS1	0.001	0.002
647	CMS4	0.002	0.003
653	CMS4	0.001	0.002
658	N/A	0.978	0.978
884	CMS2	0.001	0.002
964	CMS1	0.038	0.041
COLO151	CMS3	0.001	0.002
COLO155	CMS4	0.001	0.002
COLO312	CMS1	0.001	0.002

Table 3.2 CMS Classification of organoids. CMS group with P-value and False Discovery Rate (FDR), based on analysis in CMScaller R package. Line 658 failed to classify.

Though not absolute, most MSI-H lines will classify as CMS1. In this dataset three of the four classified MSI-H lines were classified as CMS1 (157, 557 and COLO312 CMS1, 647 was grouped as CMS4. Note 658 failed to classify) indicating that the analysis is biologically plausible. Additionally, there is a broad representation of CMS groups, therefore a culture-mediated selection of CMS groups is unlikely to have caused significant bias in the organoids that were successfully grown.

3.4 Summary

A collection of fifteen CRC organoids has been developed from local patient samples. Clinicopathological characteristics e.g. MMR, BRAF and RAS status, within these lines appear well balanced and near expected frequencies encountered from surgically resected disease. Furthermore, primary tissue Class II expression in the ten pMMR tumours (6 negative/<1%, 3 weak/1-49%, 1 strong/>50%), closely matches the expected frequencies from previously published data (5).

Over the subsequent chapters, the in vitro characteristics of Class II inducibility will be assessed.

Chapter 4: Characterisation of MHC Class II inducibility in colorectal cancer organoids

4.1 Introduction

Currently, our understanding of MHC Class II expression within CRC comes from two sources: immunohistochemistry (IHC) on archival tissue samples following surgical resection, and a limited number of mechanistic cell stimulation experiments (5, 196). Satoh et al demonstrated that approximately half of colorectal and gastric cancer cell lines were inherently unable to present MHC Class II following IFNγ stimulation. Furthermore, they found that loss of Class II expression was secondary to epigenetic silencing of the *CIITA* promoter in the non-inducible lines (196). The loss of IFNγ inducibility in colorectal cancer cell lines is postulated as an acquired route of immune evasion, as in normal epithelial biology, epithelial cells can freely express Class II under certain conditions, including IFNγ stimulation from both exogenous and endogenous sources e.g. in inflammatory bowel disease (138, 163, 166).

Around half of all colorectal cancer resection specimens show an absence of Class II staining on IHC, with only 11% of MSS-CRC samples strongly (with >50% cells staining positive) expressing Class II (5). Colorectal cancer is often described as an immunologically cold tumour, however, when immune infiltration is observed (for example the presence of tumour infiltrating lymphocytes) it is associated with significantly improved prognosis (53, 55). A Class II negative CRC tumour, therefore, may arise as a result (or combination) of two underlying states:

1. An inadequate ‘activated’ immune presence in the tumour microenvironment, with a resultant failure to promote MHC Class II expression through IFNγ production.
2. A tumour intrinsic defect in MHC Class II expression, for example, *CIITA* promoter methylation, potentially causing a failure to enhance immune cell recruitment to the tumour.

In these two scenarios, it has not possible to establish causality, as we are faced with a ‘chicken and egg’ problem. Are all Class II negative tumours negative because they are unable to upregulate MHC expression appropriately in response to immune cell recognition? Or are some negative tumours Class II inducible, if a TME threshold could be passed to allow immune infiltration and activation?

Our current understanding of this problem is limited by the lack of a model that can relate the microenvironmental background of the cancer with the mechanistic behaviour of the cells that comprise that tumour in vitro. One such model that could bridge this gap is the colorectal cancer organoid as previously outlined. Organoids have been shown to recreate both normal and disease biology more accurately than traditional cell lines (10), and in particular are remarkably epigenetically stable in comparison to the tissue they are derived from (230, 231). Finally, as patient-derived samples, we are able to analyse clinicopathological correlates to the underlying cell behaviour. Patient factors could include tumour side, grade, TNM stage, treatment responses and survival outcomes, all data that is not normally available with traditional cell lines. Additionally, the primary tumours that organoids are derived from can be characterised with in situ MHC expression and other immunological

microenvironmental annotation, providing a sophisticated model which can be compared to the native biology of that tumour.

4.1.1 Aims and Objectives

1. Validate the model system of Class II inducibility:
    a. IFNγ dose
    b. Assess the validity of flow cytometry assessment by performing experiments from Satoh et al using human colorectal cell lines to assess the reproducibility of results
2. Establish the IFNγ responsiveness of human colorectal cancer organoid models:
    a. At cell signalling level (IRF1/STAT1 response)
    b. On cell surface expression of MHC Class I and Class II following IFNγ

4.2 Validation of IFNγ stimulation experiments

4.2.1 Dosing and timing of IFNγ stimulation

A large range of IFNγ doses have been reported in the literature when studying the effects on colorectal cancer immunology, from very low levels (0.1 ng/ml) (108) to significantly higher doses (≥500 IU/ml) (166, 197). Notably, whilst some older papers have used nanogram dosing, this can cause problems with the reproducibility of experiments. IFNγ of the same concentration (ng/ml) from different suppliers can have a range of biological activity (units, or IU/ml). This biological activity is defined as the ability to induce an antiviral state in a cell and can be measured using the Cytopathic Protection Effect Assay (257). In all subsequently documented experiments, where different batches of IFNγ have been used concentrations have

been adjusted to the same activity (IU/ml) using manufacturer supplied specific activity values, to ensure biological equivalence.

In addition to dose, the length of stimulation varies between experiments in the literature, with some treating with IFNγ for up to 24 hours (108), whilst other groups have assessed for as long as seven days (166). In this later example using the colorectal HT29 cell line and flow cytometry assessment, HLA-DR expression was observed after only 24 hours treatment, however, HLA-DQ expression was not seen until seven days (166). Mehta et al studied the epigenetic accessibility and regulation of CIITA in HeLa cervical cancer cells following IFNγ stimulation (this time at 500 IU/ml), demonstrating rapid increases in acetylation after 20 minutes, with maximal acetylation at 18 hours. Similarly, the repressive methylation mark H3K9me3 was decreased significantly after 20 minutes and a maximal reduction was seen at 80 minutes (258). The cell signalling and transcriptional regulation responses to IFNγ are therefore prompt, however, the downstream expression of complete Class II on the cell surface requires several processing steps at protein level (163). The temporal regulation of Class II following IFNγ was assessed in a range of cell lines, including differing metastatic variants of the MDA MB 435 line which are known to harbour a range of Class II expressions. All five cell lines demonstrated Class II induction by 24 hours, but in some lines, this required 72 hours to become maximal (212).

4.2.2 Dose-response assessment

It is apparent from the literature that no standardised approach to IFNγ stimulation has been adopted. IRF1/STAT1 activation downstream of IFNγ receptor activation

can be utilised to assess whether an adequate response to stimulation occurs (108), and is independent of any downstream confounding factors, such as the aforementioned CIITA epigenetic inactivation.

A range of IFNγ doses was therefore trialled in both cell lines and organoids. Initially, the colorectal cell line HCT116 was treated with a range of IFNγ doses from 0-100 ng/ml (750 IU/ml) for 24 hours. Subsequently, the same experiment was performed in S309884, a rectal patient-derived organoid. Interferon was added into fresh media, incubated for 24 hours and cells were lysed for protein extraction. 20 µg total protein was loaded for Western Blotting, and membranes were probed with antibodies to STAT1, IRF1 and GAPDH (loading control). In HCT116, both IRF1 and STAT1 were observed to increase compared to control at doses as low as 1 ng/ml (7.5 IU/ml), further increasing at 10 ng/ml (75 IU/ml). Between 10 and 100 ng/ml (75 to 750 IU/ml) IFNγ, no further increase was seen in protein levels. The experiment was performed in triplicate, with representative blots shown **(Figure 4.1a)**

The experiment was then repeated in S302884, with identical findings. Maximal IFR1 and STAT1 was observed at 10 ng/ml (75 IU/ml) IFNγ, with no notable increase seen at 100 ng/ml (75 IU/ml). The experiment was performed once. **(Figure 4.1b)**

Maximal cell signalling responses in these two experiments occurred at a relatively low level. A standardised dose of 75 IU/ml IFN was therefore chosen for subsequent experiments unless otherwise stated. As previously outlined, the concern in colorectal cancer is that inadequate immune infiltration is seen in many tumours. Higher doses of IFNγ are at risk of therefore becoming supra-physiological, and the

lowest dose to give adequate cell activation was therefore seen as desirable, with this disease biology in mind.

Assessment of cell lines over longer time frames (up to 72 hours) of IFNγ exposure was performed (see section 4.3), with no further Class II upregulation observed with longer exposures. Therefore, a dose of 75 IU/ml for 24 hours was chosen for the main characterisation of IFNγ response experiments.

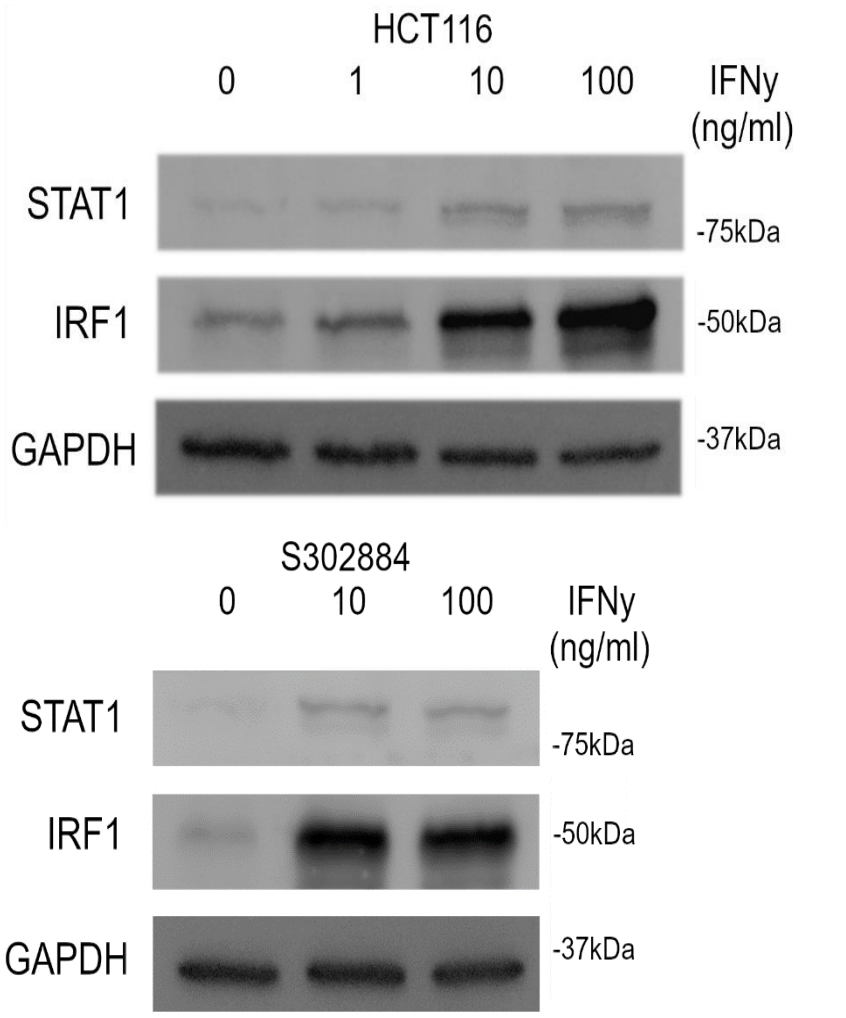


Figure 4.1 Western blot for IFNγ dose confirmation.
Colorectal cell line HCT116 **(a)** and rectal organoid S302884 **(b)** treated for 24 hours with IFNγ at indicated doses (0-100 ng/ml; 0-750 IU/ml). Protein lysates were assessed for STAT1 and IRF1 at each dose, with GAPDH loading control. HCT116 experiment in triplicate with representative blot displayed, S302884 single experiment performed.

4.2.3 Validation of Class II antibody and flow cytometry methodology

In order to confirm the specificity of MHC Class II staining and assessment with flow cytometry, a known positive control was used. HEK293, a human embryonic kidney cell line with stable transfection of *CIITA* (referred to as HEK293+CIITA) was compared to the parental wild-type cells (referred to as HEK293 parental). The HEK293 parental cells have previously been shown to be $CIITA^-$/MHC Class II^- under normal conditions. The HEK+CIITA cells demonstrate constitutive CIITA and MHC Class II expression, independent of the requirement of IFNγ stimulation. The HEK293 cells were produced and generously gifted from Dr Heather Long's laboratory and their usage has previously been published (259).

Cells were cultured, dissociated into single cells and then underwent cell surface staining with antibodies for pan-Class I (HLA-A,B,C), pan-Class II (HLA-DR,DP,DQ) and cell viability stain. Cells were fixed before same-day analysis on a BD LSRFortessa™ X-20 Flow Cytometer. Nearly all cells (>98.5%) expressed Class I. Class II expression was absent in HEK293 parental cells (0.59%), with nearly all transfected cells expressing Class II (99.6%). **(Figure 4.2)** The sensitivity and specificity of the Class II antibody in this validation model, therefore, appeared satisfactory. Fluorescence minus one (FMO) strategy was utilised for gating of Class II expression.

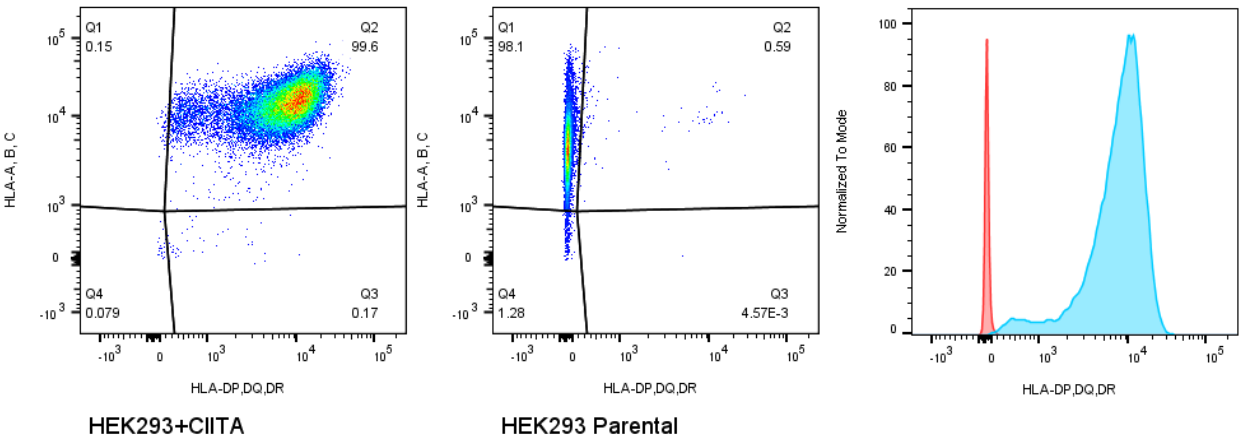


Figure 4.2 Flow Cytometry Class II Antibody Validation in HEK293 ± CIITA cells.
HEK293+CIITA **(left)** and HEK293 parental **(centre)** cells were stained for Class I (HLA-A,B,C) and Class II (HLA-DP,DQ,DR) and analysed by flow cytometry. An overlay **(right)** of Class II histograms is shown, with normalisation to mode. Experiment performed once.

4.3 Cell line assessment

Following on from the initial experimental validation of methodology, the next step was to repeat the experiments on previously published colorectal cell lines. The Satoh et al study remains the largest parallel assessment of colorectal cancer cell line class II inducibility, with five inducible lines and three non-inducible lines (196). Their findings, along with relevant clinicopathological data is summarised in **Table 4.1**.

Cell Line	Class II post IFNγ	CIITA-pIV methylation	Source	Mutation Data	MSI status	CIMP
RKO*	Negative	Methylated	Colon primary	*BRAF* V600E	MSI	+
HCT116*	Negative	Methylated	Right sided colon	*KRAS* G13D	MSI	+
Caco2	Negative	Methylated	Colon	Wild Type	MSS	+/-
HT29*	Positive	Unmethylated	Colon primary	*BRAF* V600E	MSS	+
DLD1*	Positive	Unmethylated	Colon	*KRAS* G13D	MSI	+
LoVo	Positive	Unmethylated	Colon supraclavicular node	*KRAS* G13D and A14V	MSI	-
SW48	Positive	Unmethylated	Colon	Wild-type	MSI	+
Colo320	Positive	Unmethylated	Sigmoid colon primary	Wild-Type	MSS	-

Table 4.1 Summary of known cell line class II inducibility with IFNγ and underlying methylation status of promoter IV of CIITA. Class II expression assessed with flow cytometry. This data has been summarised from Satoh et al (196). Additional data on the site of tumour origin, mutation (*KRAS* and *BRAF*), mismatch repair (microsatellite instability MSI or microsatellite stable MSS) and CpG methylator phenotype (CIMP) status adapted from Ahmed et al (260). Lines with an asterisk (*) have been assessed subsequently in this project.

Two inducible cell lines (HT29 and DLD1) and two non-inducible (HCT116 and RKO) were selected for full assessment. It is worth noting that a high proportion of these cell lines exhibit microsatellite instability and CIMP, with rates of dMMR in patients undergoing resection typically around only 15% (32). The data on Class II inducibility is also qualitative, and it is not clear from this paper what percentage of cells expressed Class II following IFNγ treatment. It is clear however from other papers that a spectrum of Class II inducibility is likely to be observed, with Stoneman et al reporting a 98.1 fold increase in Class II peak fluorescence in HT29 and a smaller, heterogeneous response in HCT116 (a line described by Satoh as non-inducible). Some lines demonstrated low-level inducibility, with LoVo and Caco2 showing a 2.2 and 1.3 fold increase in Class II peak fluorescence respectively. Interestingly, these two ‘low’ inducible lines were differentially categorised as inducible and non-inducible by Satoh et al. A 98.1 and 2.2 fold increase in Class II might satisfy a definition of inducibility, however, these two lines would likely behave very differently biologically;

both in terms of generating an immune response and in the underlying Class II regulatory mechanisms.

Validation in cell lines thereby provides three important purposes: to quantitatively assess Class II upregulation, to demonstrate reproducibility and reliability of the methodology, and to allow detailed comparison of cell line biology with the organoid models.

4.3.1 Cancer cell line IFNγ inducibility

First, cell lines were assessed for IFNγ pathway integrity, with western blot of cell signalling response proteins. Cell lines were treated with 75 IU/ml IFNγ or media control for 24 hours, before undergoing protein extraction. Lysates were purified and quantified, prior to gel resolution and transfer to PVDF membranes. Membranes were sequentially probed for STAT1, IRF1 and GAPDH by western blotting. All four lines demonstrated a statistically significant increase in STAT1 and IRF1 total protein levels compared to control lysates ($P<0.05$). **(Figure 4.3)** Cell signalling response to IFNγ is therefore preserved in all four of these cell lines.

Next, cell lines were assessed for Class I and II inducibility via flow cytometry. Cell lines were again treated with 75 IU/ml IFNγ for 24 hours, before processing into single-cell suspensions. Cells were stained for viability and cell surface staining of HLA-A,B,C and HLA-DR,DP,DQ, prior to fixation and running on a LSRFortessa™ X-20 Flow Cytometer. IFNγ stimulated cells were compared with untreated control cells. A fluorescence minus one (FMO) control was used for purposes of gating Class II positive cells. Further details and gating ancestry in methods. All experiments were performed at least in triplicate.

All cell lines exhibited low levels of Class II positivity (<10%) at baseline prior to IFNγ. All lines except for DLD1 expressed Class I at baseline, with no notable increase in Class I following IFNγ, consistent with prior literature (261). Class II expression was strongly induced in HT29, with expression in over 80% of cells following IFNγ. RKO by contrast was completely unresponsive to IFNγ. DLD1 and HCT116, reported by Satoh et al as inducible and non-inducible respectively, appeared to show a small non-statistically significant increase in Class II expression. Though contradicting Satoh's findings, these behaviours are consistent with other prior published data, with DLD1 characterised by only weak Class II expression (262) and a subpopulation of inducible cells previously demonstrated in the HCT116 line (263). These data are summarised in **Table 4.2** and **Figure 4.4 and Figure 4.5.** Full individual experimental gating selections for all flow cytometry experiments is provided in **Chapter 8 Appendix.**

Cell Line	IFNγ Class II % (SD)	Control Class II % (SD)	Change in Class II % (SD)	P-value
HT29	86.7 (3.04)	2.21 (2.07)	84.56 (5.02)	*0.001
DLD1	8.94 (4.98)	0.977 (0.437)	7.96 (4.98)	0.11
HCT116	10.7 (3.03)	5.61 (1.18)	5.10 (2.46)	0.07
RKO	3.34 (1.89)	2.38 (0.973)	0.957 (0.970)	0.23

Table 4.2 Summary of Flow Cytometry Class II inducibility of colorectal cancer cell lines +/- IFNγ stimulation. Mean expression (percentage positive cells) and standard deviation (SD) given for each line with IFNγ stimulation, untreated control cells and derived percentage change. Minimum of three independent experiments with paired two-tailed T-test performed.

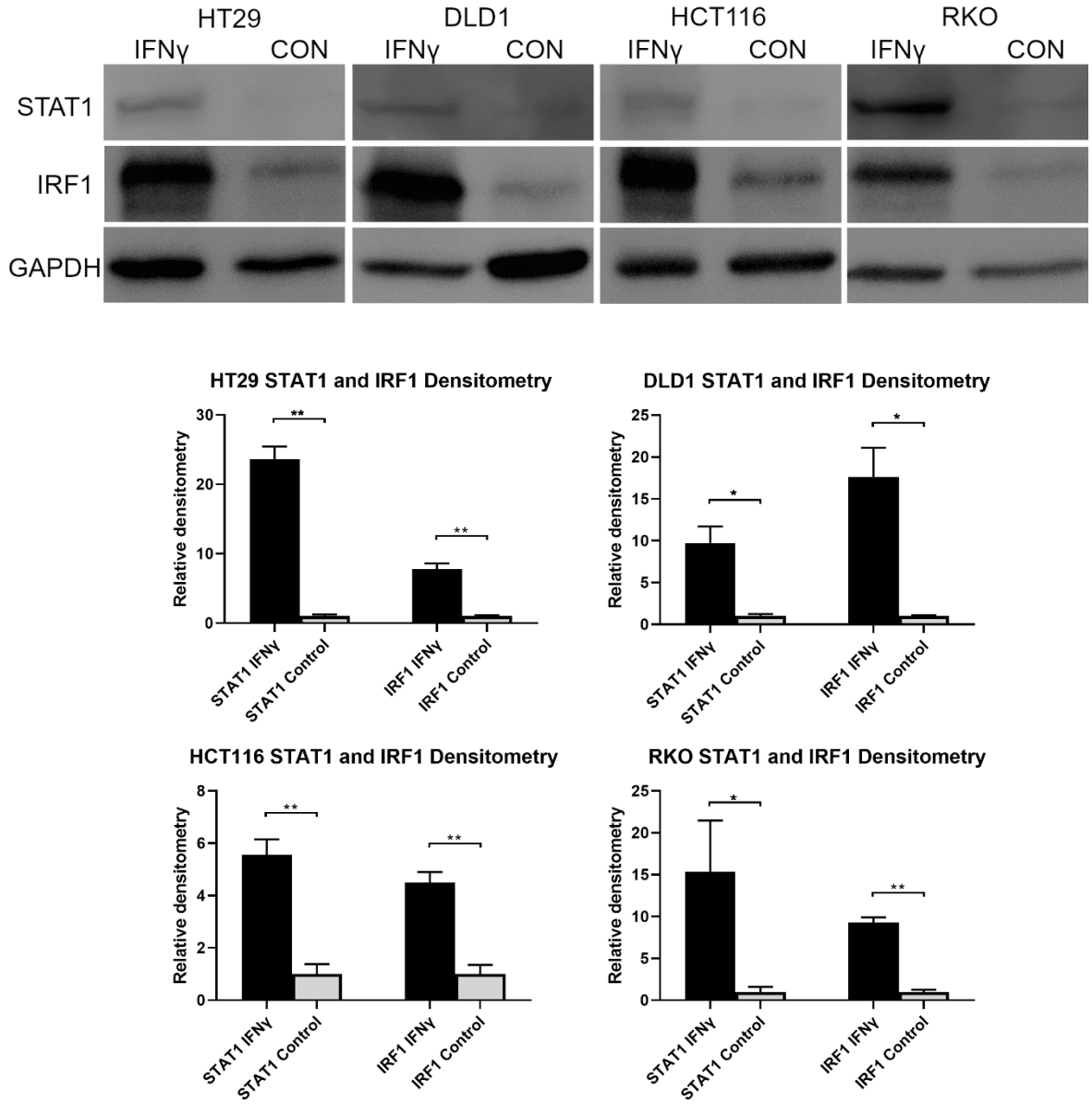


Figure 4.3 Western blot of IFNγ response in colorectal cell lines. Top: Cells were assessed for STAT1, IRF1 and GAPDH protein levels following 24 hours stimulation with 75 IU/ml IFNγ. Unstimulated control cells (CON) displayed alongside. Representative blots shown, experiments performed in triplicate. **Bottom:** Densitometry performed on western images, with area quantification for proteins of interest adjusted by GAPDH loading control. Relative expression compared to control condition given, and mean values with standard deviation displayed. Paired two-tailed T-test performed for statistical analysis: NS $P \geq 0.05$; * $P < 0.05$; ** $P < 0.01$; *** $P < 0.001$; **** $P < 0.0001$.

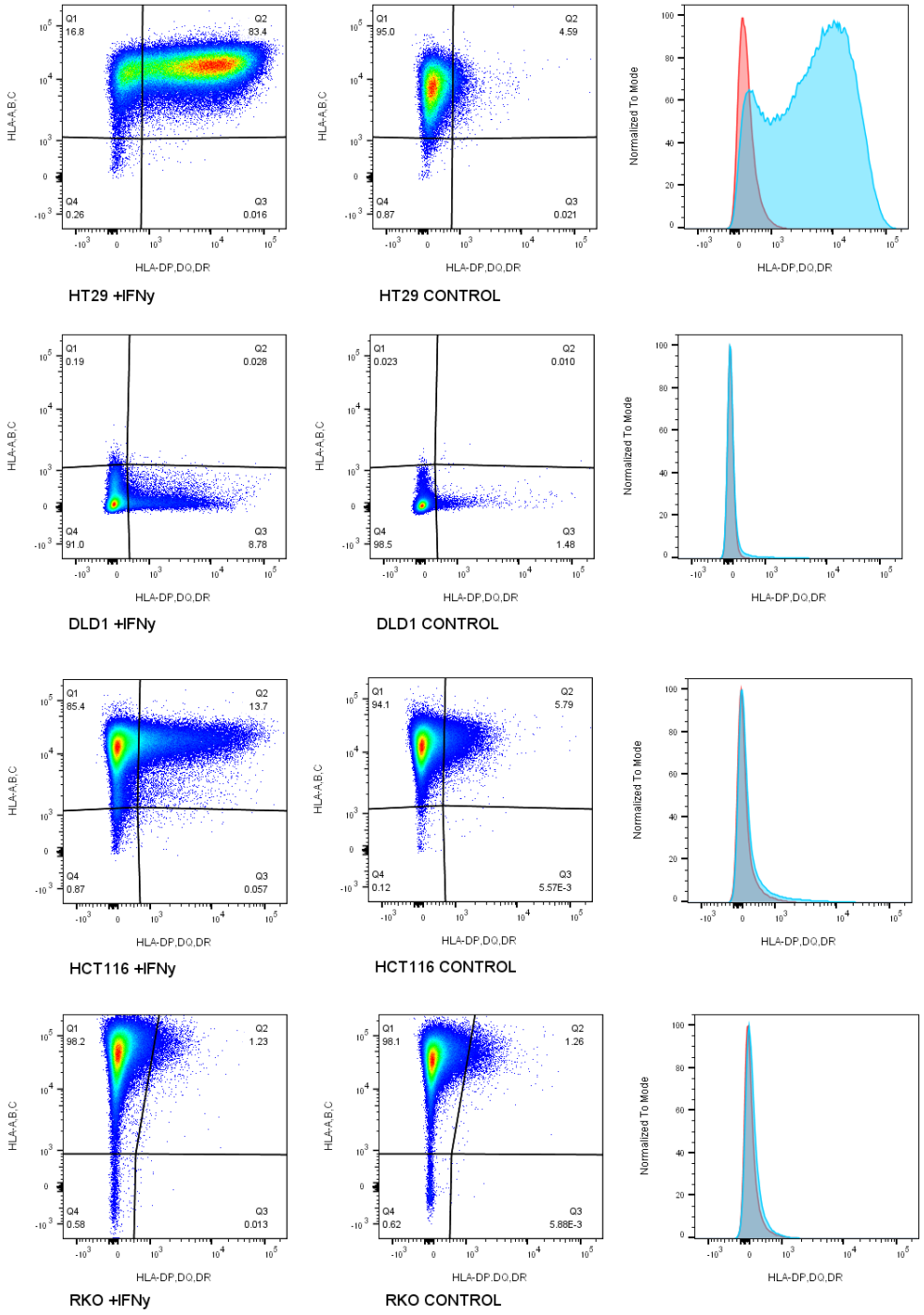


Figure 4.4 Flow cytometry assessment of Class I and Class II expression in four colorectal cancer cell lines. Each line was treated with IFNγ (left) and compared with untreated control cells (centre). Overlay of class II histograms (right) with IFNγ displayed in blue, control in red. Each cell line replicated in triplicate with representative plots shown.

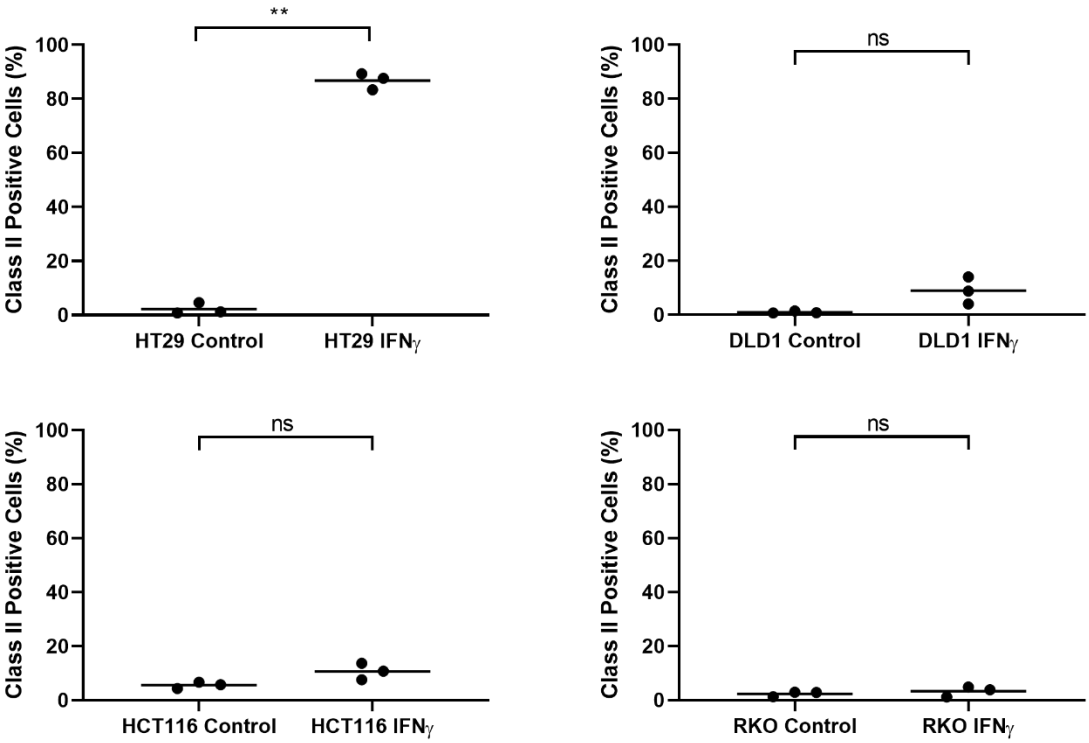


Figure 4.5 Summary of flow cytometry Class II inducibility for colorectal cancer cell lines. Each line treated in triplicate, with Class II expression (percentage of cells positive) displayed with mean (horizontal line). Statistics performed (paired two-tailed T-test): NS $P \geq 0.05$; * $P < 0.05$; ** $P < 0.01$; *** $P < 0.001$; **** $P < 0.0001$.

The three cell lines with minimal Class II expression at 24 hours (DLD1, HCT116 and RKO) were treated over a longer timeframe, as delayed responses requiring 72 hours exposure for maximal Class II upregulation have been reported (212). Cell lines were again treated with 75 IU/ml IFNγ, this time for 72 hours, before cell collection and flow cytometry as previously described. All three lines failed to show any further upregulation of Class II at 72 hours and therefore delayed IFNγ response kinetics are not exhibited by these cell lines. Experiments performed in duplicate with representative flow cytometry displayed in **Figure 4.6**.

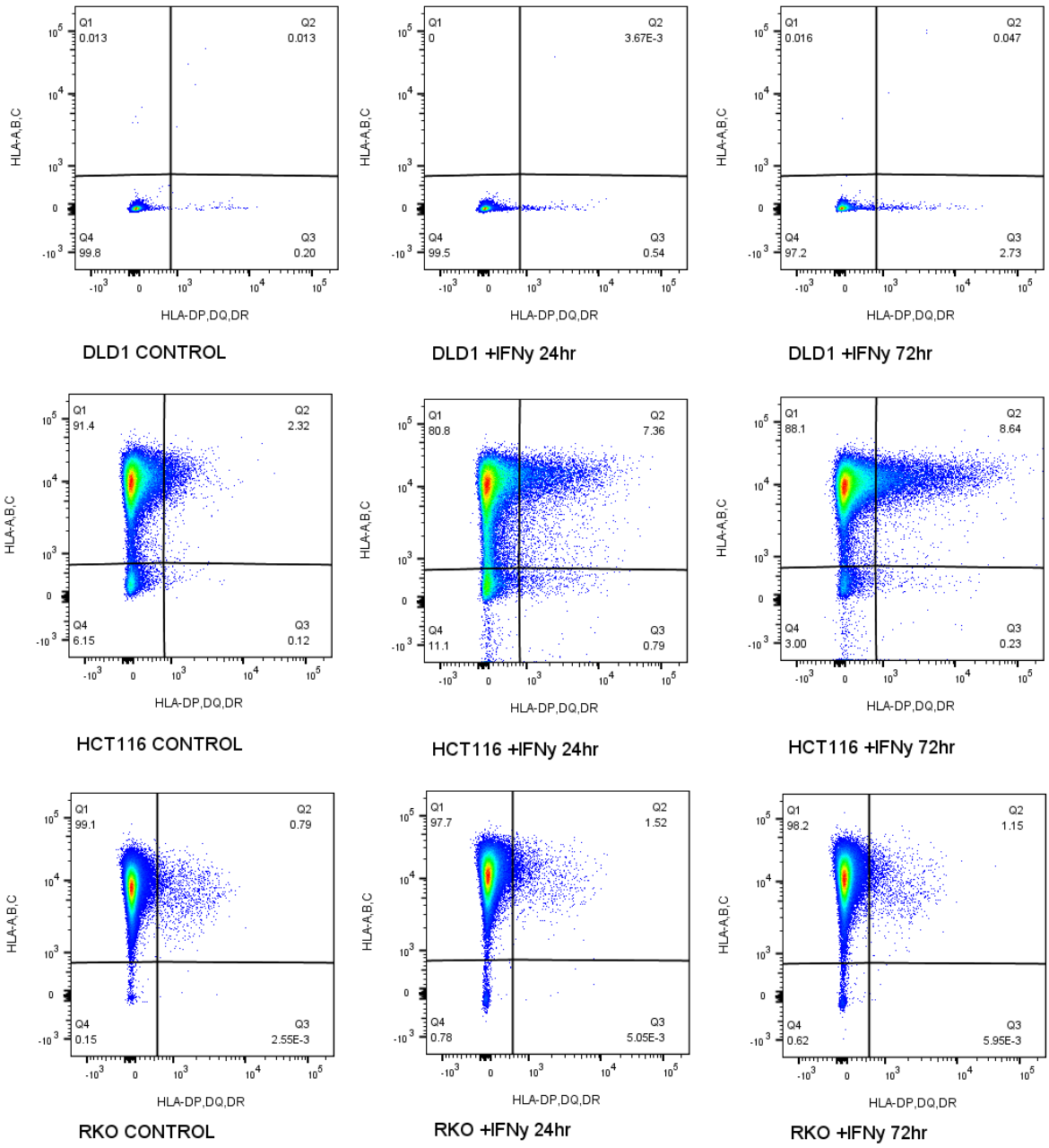


Figure 4.6 Flow cytometry assessment of Class II expression following prolonged IFNγ exposure in three minimally responsive colorectal cell lines. Each line was treated with 75 IU/ml IFNγ for 24 hours **(centre)** and 72 hours **(right)** and compared with untreated control cells **(left)**. Each cell line replicated in duplicate with representative plots shown.

4.3.2 Cancer Cell Line Summary

Data from the four CRC cell lines confirms that IFNγ signalling transduction response is maintained in all lines, with the induction of IRF1 and STAT1 seen. Despite this, a strong induction of Class II expression was only seen in one line (HT29). DLD1, designated unquantifiably by Satoh as an inducible line (196), shows only a small non-statistically increase in Class II following IFNγ ($p=0.11$), in keeping with other literature describing it as only weakly Class II inducible (262). The two non-inducible lines assessed, RKO and HCT116, showed no significant upregulation of Class II, though HCT116 (similarly to the 'inducible' DLD1) showed a non-significant increase ($p=0.07$). These lines, therefore, provide validation of the methodology and also provide a basis for comparison of organoid responses.

4.4 Organoid assessment

A total of 15 colorectal cancer organoids were derived from patient samples and assessed for Class II expression following IFNγ stimulation, following the same methodology as the cell line experiments. For all stimulation experiments, organoids were maintained in 3D culture embedded in matrigel with IFNγ dissolved in organoid culture media, until the point of cell use for downstream applications. For protein extraction, matrigel was removed, pellets of organoids washed before lysis of whole organoids. For flow cytometry, following the stimulation organoids were digested into single-cell suspensions by a combination of mechanical and minimal chemical disruption and then filtered, before immediately proceeding with the staining protocol.

4.4.1 Characterisation of organoid IFNγ responses by flow cytometry

Organoid cultures were stimulated for 24 hours with 75 IU/ml IFNγ and then assessed for Class I and Class II expression by flow cytometry. In order to further characterise and explore mechanisms of Class II regulation, organoids were grouped into three populations:

1. Lines with high levels of Class II expression (>50% of cells) following IFNγ
2. Lines with weak inducibility of Class II expression with IFNγ (10-50% of cells)
3. Lines with negligible inducibility of Class II expression following IFNγ (<10%)

All flow cytometry experiments were performed in a minimum of triplicate, with high reproducibility within models demonstrated, including in lines passaged for greater than six months. Results summarised in **Table 4.3.**

Organoid	IFNγ Class II % (SD)	Control Class II % (SD)	Change in Class II % (SD)	P-value
376	3.32 (0.59)	4.38 (1.06)	-1.05 (0.64)	0.12
557	3.23 (0.38)	5.05 (2.51)	-1.82 (2.18)	0.19
964	2.67 (0.86)	4.21 (0.71)	-1.54 (0.39)	*0.02
389	28.2 (12.3)	3.91 (1.35)	24.3 (13.1)	0.09
658	13.7 (4.11)	3.50 (1.83)	10.2 (5.18)	0.08
884	18.4 (6.79)	2.07 (0.74)	16.4 (7.30)	0.06
COLO312	42.7 (3.30)	15.4 (2.99)	27.3 (4.16)	*0.008
064	69.4 (16.5)	2.27 (1.05)	67.2 (16.7)	*0.02
080	72.5 (4.78)	9.95 (3.49)	62.5 (6.92)	*0.004
157	73.0 (7.82)	25.5 (6.21)	47.5 (12.1)	*0.02
411	76.6 (6.92)	5.12 (3.18)	71.5 (5.51)	*<0.001
647	69.8 (4.82)	7.83 (2.50)	61.9 (4.83)	*0.002
653	83.5 (19.7)	7.2 (1.22)	76.2 (19.5)	*0.02
COLO151	72.9 (23.4)	3.77 (2.69)	69.2 (21.9)	*0.03
COLO155	87.5 (14.5)	25.3 (10.0)	62.2 (5.89)	*0.003

Table 4.3 Summary of Flow Cytometry Class II inducibility of colorectal cancer organoids +/- IFNγ stimulation. Lines have been grouped by Class II expression following IFNγ into no expression (<10%), weak expressers (10-50%) and high expressers (50-100%). Mean expression (percentage positive cells) and standard deviation (SD) given for each line with IFNγ stimulation, untreated control cells and derived percentage change. Minimum of three independent experiments with paired two-tailed T-test performed.

Out of the 15 lines, three were non-inducible, four were weak expressers and eight strongly expressed Class II following IFNγ. The majority of organoids were Class II negative at baseline without stimulation, however low-level positivity (>10% cells expressing Class II) was observed in three lines. The non-inducible lines showed no evidence of any Class II upregulation with stimulation, with 964 showing a significant small, but biologically irrelevant decrease. The weak-inducers, by contrast, had a minimum mean delta (stimulated positive cells % - unstimulated positive cells %) increase of 10%, and whilst these changes only reached statistical significance in 1/4 of the lines (COLO312), the remaining three lines had a clear trend towards an increase (P 0.06-0.09). The strong-inducers had a mean delta increase of over 60% in 7/8 lines, and all lines had statistically significant increases in Class II expression with IFNγ. Flow cytometry results and statistics are summarised in **Figure 4.7-4.9**.

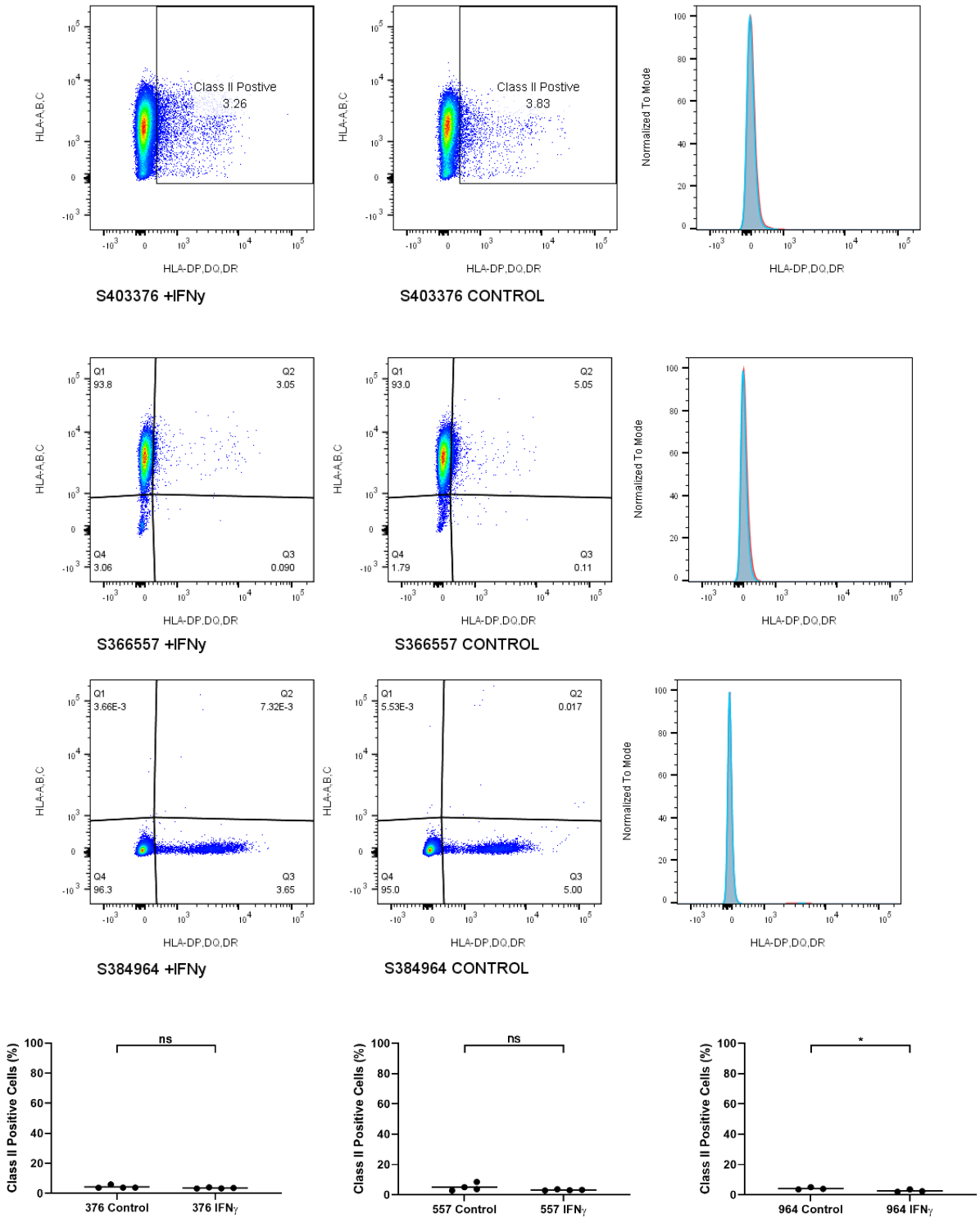


Figure 4.7 Flow cytometry assessment of Class I and Class II expression in three non-inducible organoids lines. Top: Each line was treated with IFNγ **(left)** and compared with untreated control cells **(centre)**. Overlay of class II histograms **(right)** with IFNγ displayed in blue, control in red. Each cell line replicated at least in triplicate, with representative plots shown. **Bottom:** Summary of Class II expression (percentage of cells positive) +/- IFNγ displayed with mean (horizontal line). Statistics performed (paired two-tailed T-test): NS P ≥ 0.05; * P < 0.05; ** P < 0.01; *** P < 0.001; **** P < 0.0001.

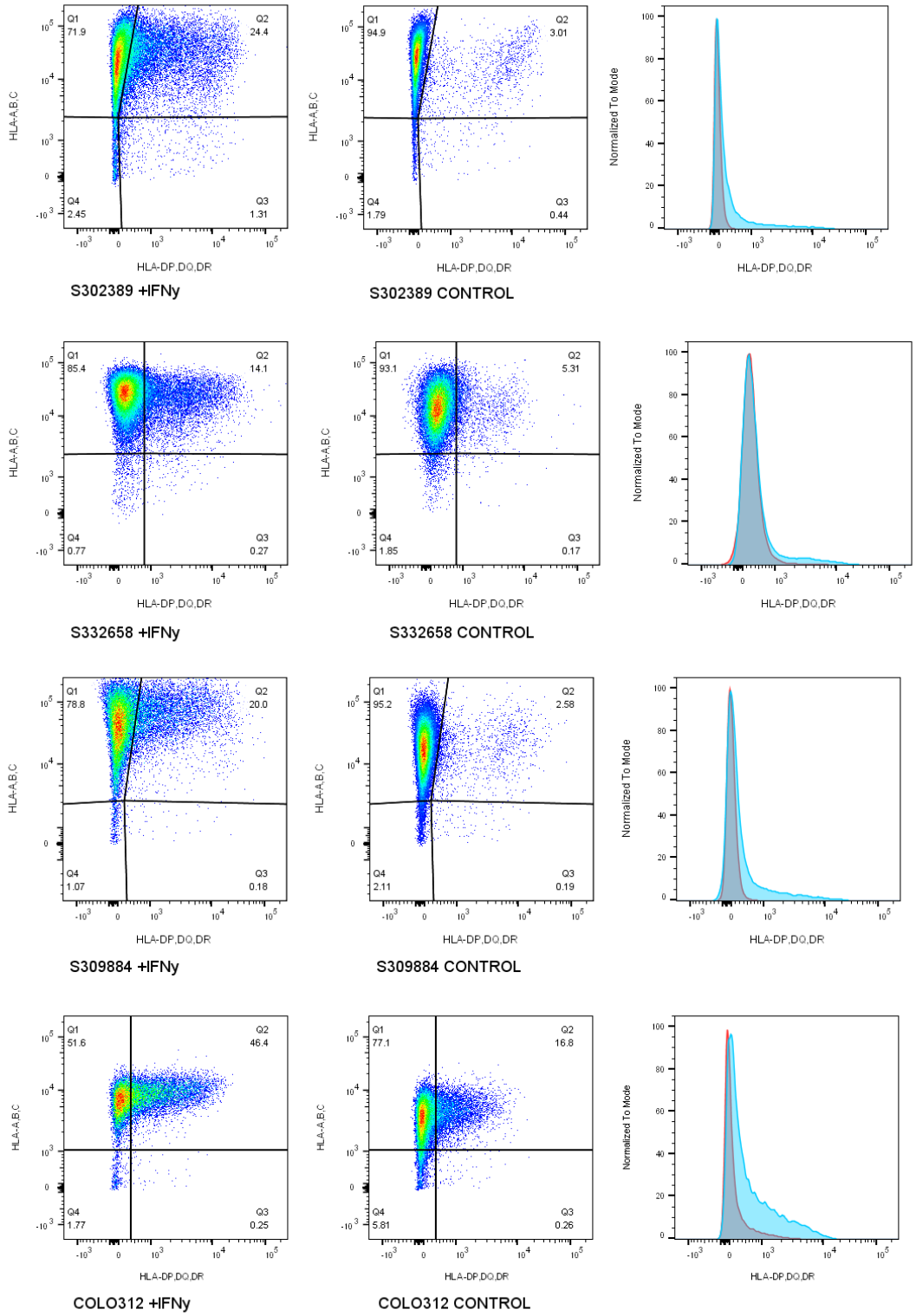


Figure 4.8a Flow cytometry assessment of Class I and Class II expression in four weakly-inducing organoid lines. Above: Each line was treated with IFNγ **(left)** and compared with untreated control cells **(centre)**. Overlay of class II histograms **(right)** with IFNγ displayed in blue, control in red. Each cell line replicated at least in triplicate, with representative plots shown.

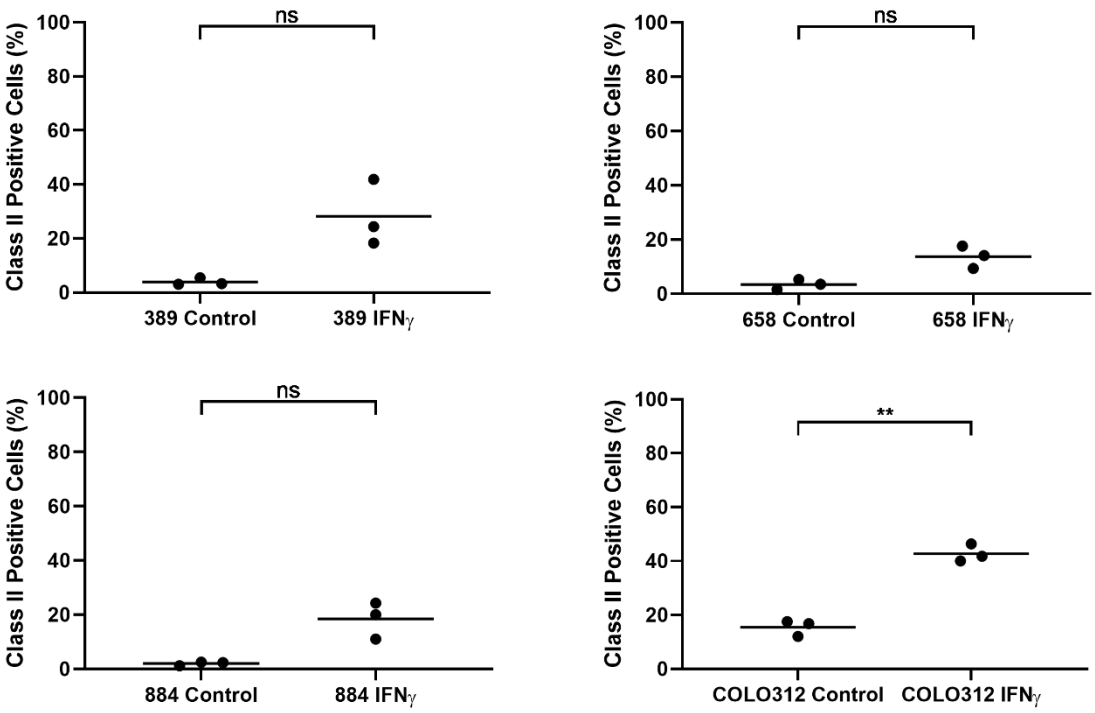


Figure 4.8b: Summary of Class II expression in four weakly-inducing lines. Percentage of cells positive +/- IFNγ displayed with mean value (horizontal line). Statistics performed (paired two-tailed T-test): NS $P \geq 0.05$; * $P < 0.05$; ** $P < 0.01$; *** $P < 0.001$; **** $P < 0.0001$.

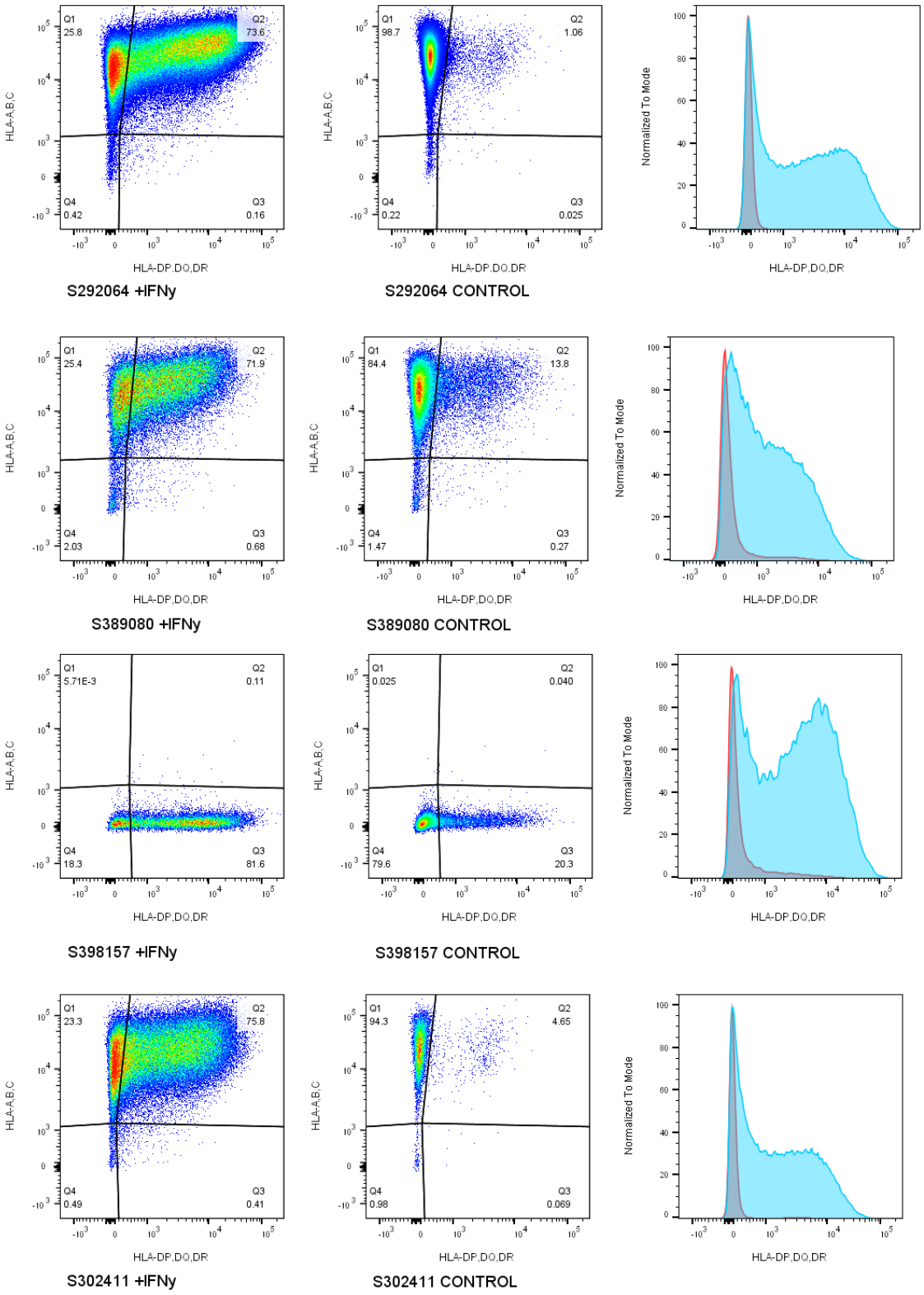


Figure 4.9a Flow cytometry assessment of Class I and Class II expression in strongly-inducing organoid lines. First four of eight lines, continued next page. Each line was treated with IFNγ **(left)** and compared with untreated control cells **(centre)**. Overlay of class II histograms **(right)** with IFNγ displayed in blue, control in red. Each cell line replicated at least in triplicate, with representative plots shown.

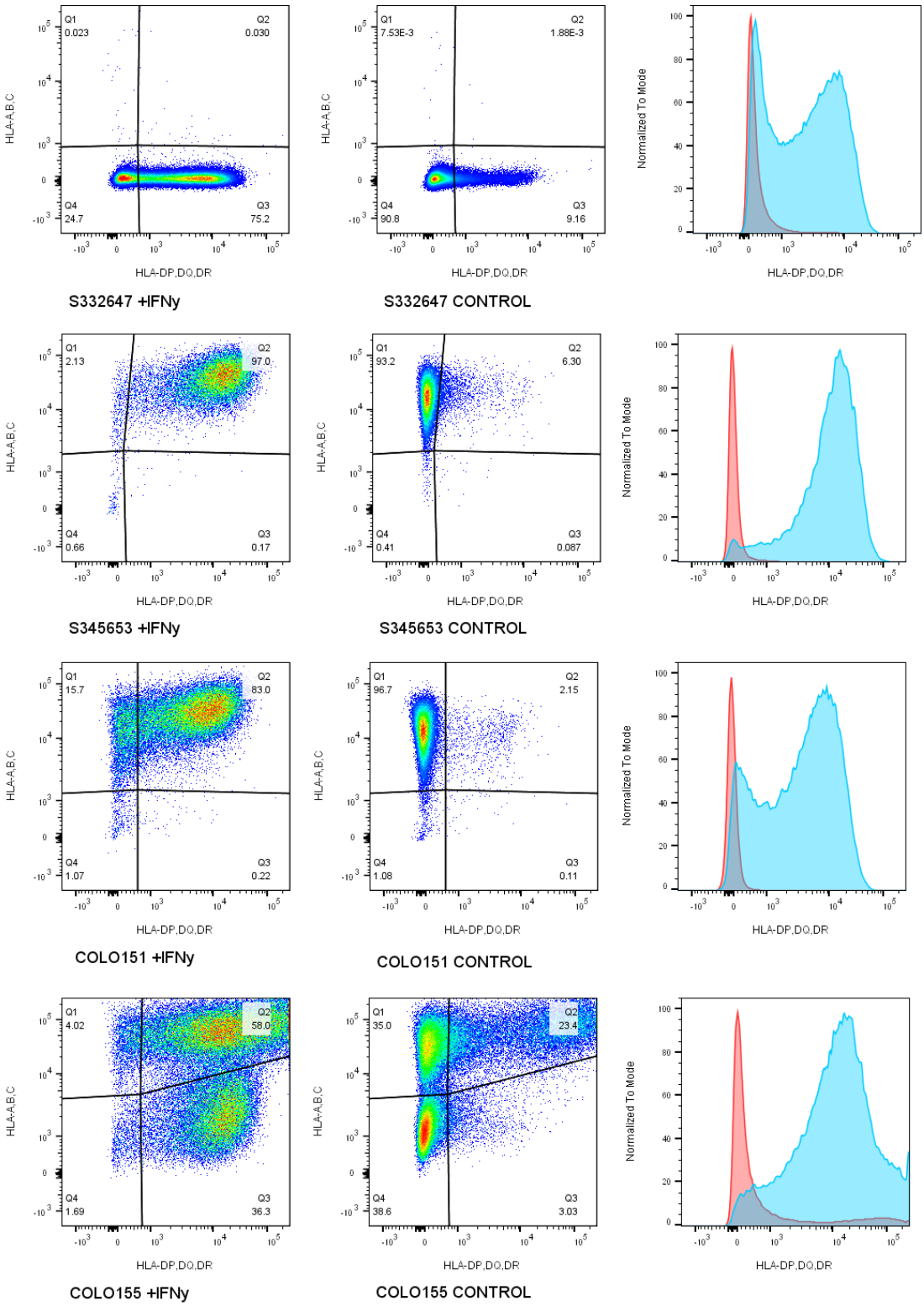


Figure 4.9b Flow cytometry assessment of Class I and Class II expression in strongly-inducing organoid lines. Second group of eight lines. Each line was treated with IFNγ **(left)** and compared with untreated control cells **(centre)**. Overlay of class II histograms **(right)** with IFNγ displayed in blue, control in red. Each cell line replicated at least in triplicate, with representative plots shown.

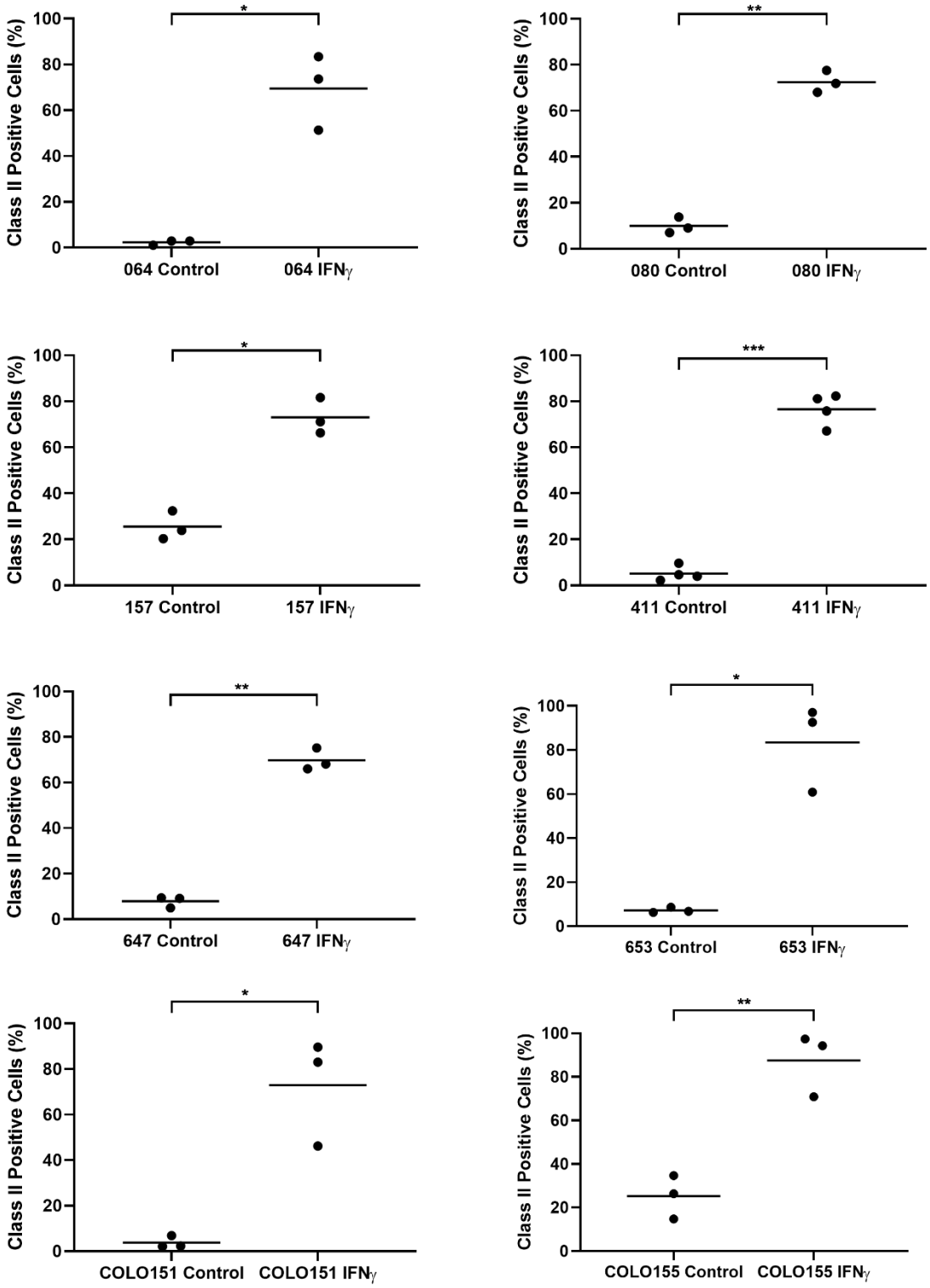


Figure 4.9c Summary of Class II expression in eight strongly-inducing lines. Percentage of cells positive +/- IFNγ displayed with mean value (horizontal line). Statistics performed (paired two-tailed T-test): NS $P \geq 0.05$; * $P < 0.05$; ** $P < 0.01$; *** $P < 0.001$; **** $P < 0.0001$.

Loss of Class I expression was seen in three organoids (647 and 157; both with strong Class II induction, and 964 which also lacked Class II expression). Furthermore, two lines (376 and COLO155) exhibited a Class I 'low' expression, in contrast to the total loss seen in the three lines. 376 demonstrated only low Class I, however, COLO155 interestingly had heterogeneous Class I with a ~40% subgroup showing low expression, with the remaining cells having preserved expression. Class I levels were not increased following IFNγ stimulation in any line.

4.4.2 Characterisation of organoid IRF1/STAT1 responses following IFNγ

Next organoids were assessed for IRF1/STAT1 cell signalling response by western blot following IFNγ stimulation at 75 IU/ml for 24 hours. Following stimulation, matrigel was removed with organoid harvesting solution and non-dissociated organoids were lysed in RIPA buffer, with 20 µg of subsequently processed protein loaded onto gels and then probed with antibodies to STAT1, IRF1 and GAPDH sequentially. Each experiment has been performed in triplicate.

Results are again displayed in the three sub-groups derived from flow cytometry responses to IFNγ. In each case, densitometry has been performed on the blots to allow for quantification, with normalisation of STAT1 and IRF1 protein levels to GAPDH. Increases in protein levels following IFNγ have been compared with untreated control cells, where the mean densitometry values obtained in the controls have been assigned an arbitrary value of 1. Statistical comparison with two-tailed paired T-Test performed. Results displayed in **Figure 4.10-4.12**.

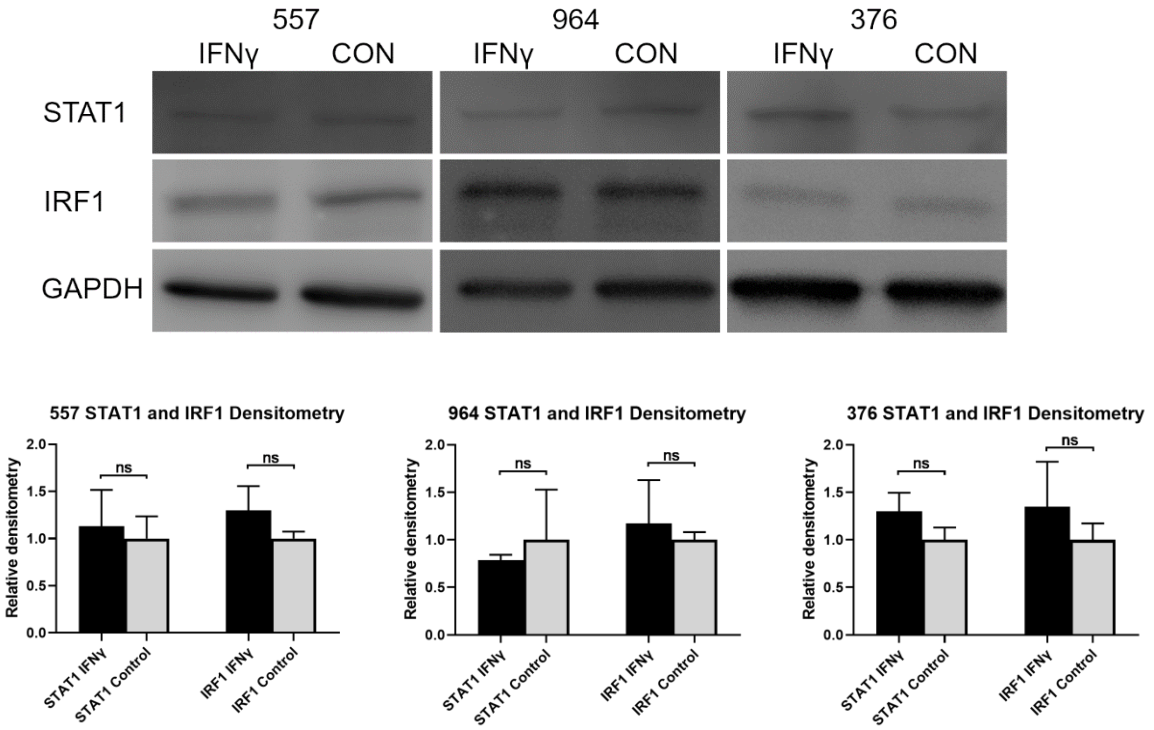


Figure 4.10 Western blot of IFNγ response in non-responding organoid lines. Top: Cells were assessed for STAT1, IRF1 and GAPDH protein levels following 24 hours stimulation with 75 IU/ml IFNγ. Unstimulated control cells (CON) displayed alongside. Representative blots shown, experiments performed in triplicate. **Bottom:** Densitometry performed on western images, with area quantification for proteins of interest adjusted by GAPDH loading control. Relative expression compared to control condition given, and mean values with standard deviation displayed. Paired two-tailed T-test performed for statistical analysis: NS $P \geq 0.05$; * $P < 0.05$; ** $P < 0.01$; *** $P < 0.001$; **** $P < 0.0001$.

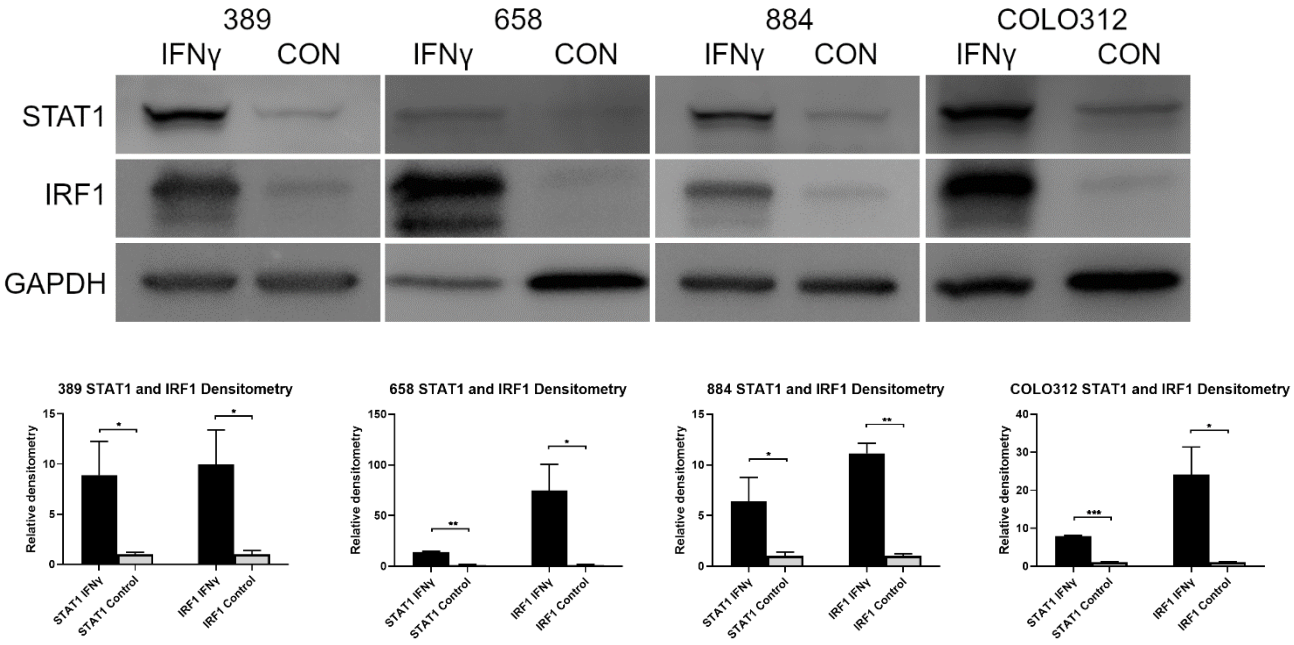


Figure 4.11 Western blot of IFNγ response in weakly-inducing organoid lines. Top: Cells were assessed for STAT1, IRF1 and GAPDH protein levels following 24 hours stimulation with 75 IU/ml IFNγ. Unstimulated control cells (CON) displayed alongside. Representative blots shown, experiments performed in triplicate. **Bottom:** Densitometry performed on western images, with area quantification for proteins of interest adjusted by GAPDH loading control. Relative expression compared to control condition given, and mean values with standard deviation displayed. Paired two-tailed T test performed for statistical analysis: NS $P \geq 0.05$; * $P < 0.05$; ** $P < 0.01$; *** $P < 0.001$; **** $P < 0.0001$.

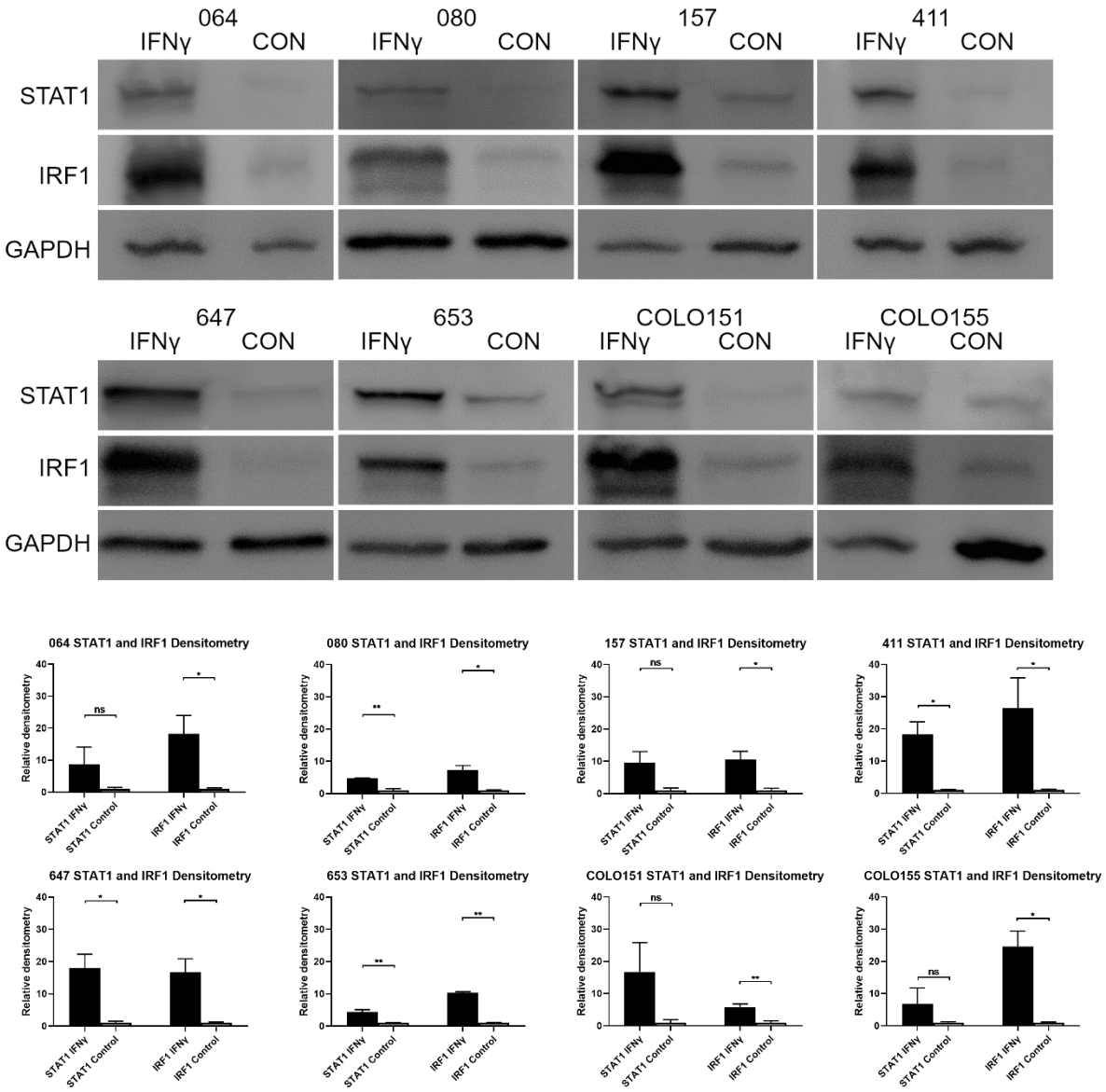


Figure 4.12 Western blot of IFNγ response in strongly-inducing organoid lines. Top: Cells were assessed for STAT1, IRF1 and GAPDH protein levels following 24 hours stimulation with 75 IU/ml IFNγ. Unstimulated control cells (CON) displayed alongside. Representative blots shown, experiments performed in triplicate. **Bottom:** Densitometry performed on western images, with area quantification for proteins of interest adjusted by GAPDH loading control. Relative expression compared to control condition given, and mean values with standard deviation displayed. Paired two-tailed T-test performed for statistical analysis: NS $P \geq 0.05$; * $P < 0.05$; ** $P < 0.01$; *** $P < 0.001$; **** $P < 0.0001$.

In both the weakly **(Figure 4.11)** and strongly **(Figure 4.12)** inducible lines, there was a clear induction of the interferon signalling pathway, with significant increases in IRF1 in all lines. Similarly, STAT1 was significantly increased in all four of the weak lines and 4 out of 8 of the strong lines. By contrast, the group of three non-inducible lines **(Figure 4.10)** all demonstrated lack of IRF1/STAT1 protein upregulation following IFNγ, with no significant change in protein expression.

This difference between the weakly-inducible and non-inducible lines suggests differing biological mechanisms for loss (or reduction) in Class II inducibility. The loss of IFNγ signalling response strongly suggests mutations in the top end of the pathway, at the level of IFNγ receptor (*IFNGR1/2*), *JAK1* or *STAT1* as previously described as a mechanism underlying MHC loss in cancer (104, 182).

Surface expression of IFNγR levels was assessed in two organoid lines, a strongly inducible line (411) and a non-inducible line (557). Surface staining and flow cytometry was performed on organoids both with and without IFNγ pre-treatment (at 75 IU/ml for 24 hours) and results are displayed in **Figure 4.13.** Both lines had highly comparable expression at baseline, albeit at low levels. After IFNγ treatment levels of IFNγR appeared lower in 411 but were maintained in 557. Loss of IFNγR is therefore unlikely to explain the lack of IRF1/STAT1 response in 557. The non-inducible lines will be assessed with whole-genome sequencing subsequently to further interrogate the pathway.

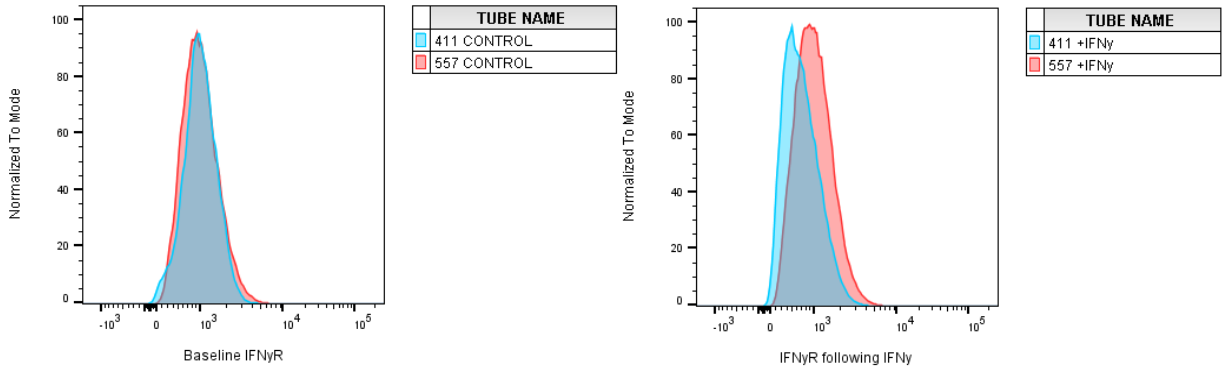


Figure 4.13 Flow cytometry assessment of IFNγ Receptor surface expression. Organoid lines 557 (non-inducible) and 411 (strongly-inducible) were asssessed for surface IFNγR expression bowth without (**left**) and with (**right**) pre-treatment with IFNγ at 75 IU/ml for 24 hours. Histogram of results displayed for both 557 (blue) and 411 (red). Experiment performed once.

4.4.3 Evaluation of higher doses of IFNγ on organoid Class II expression

As discussed at the beginning of this chapter, variable doses of IFNγ have been studied in different disease models. The evaluation of organoid responses so far has been performed using a relatively low dose, a considered approach given immune exclusion is an important part of CRC pathophysiology. In order to assess if higher doses of IFNγ would lead to increased Class II expression in CRC organoids, six lines were treated with an increased dose of IFNγ (150 IU/ml for 24 hours). These six lines included two lines that were weakly inducible (389 and 884) and four strongly inducible. Results of these experiments, performed once on each line, are displayed in **Figure 4.14.** In all these lines, the overlay of Class II histograms appear closely related, and no further dose-dependent increase in Class II expression was observed.

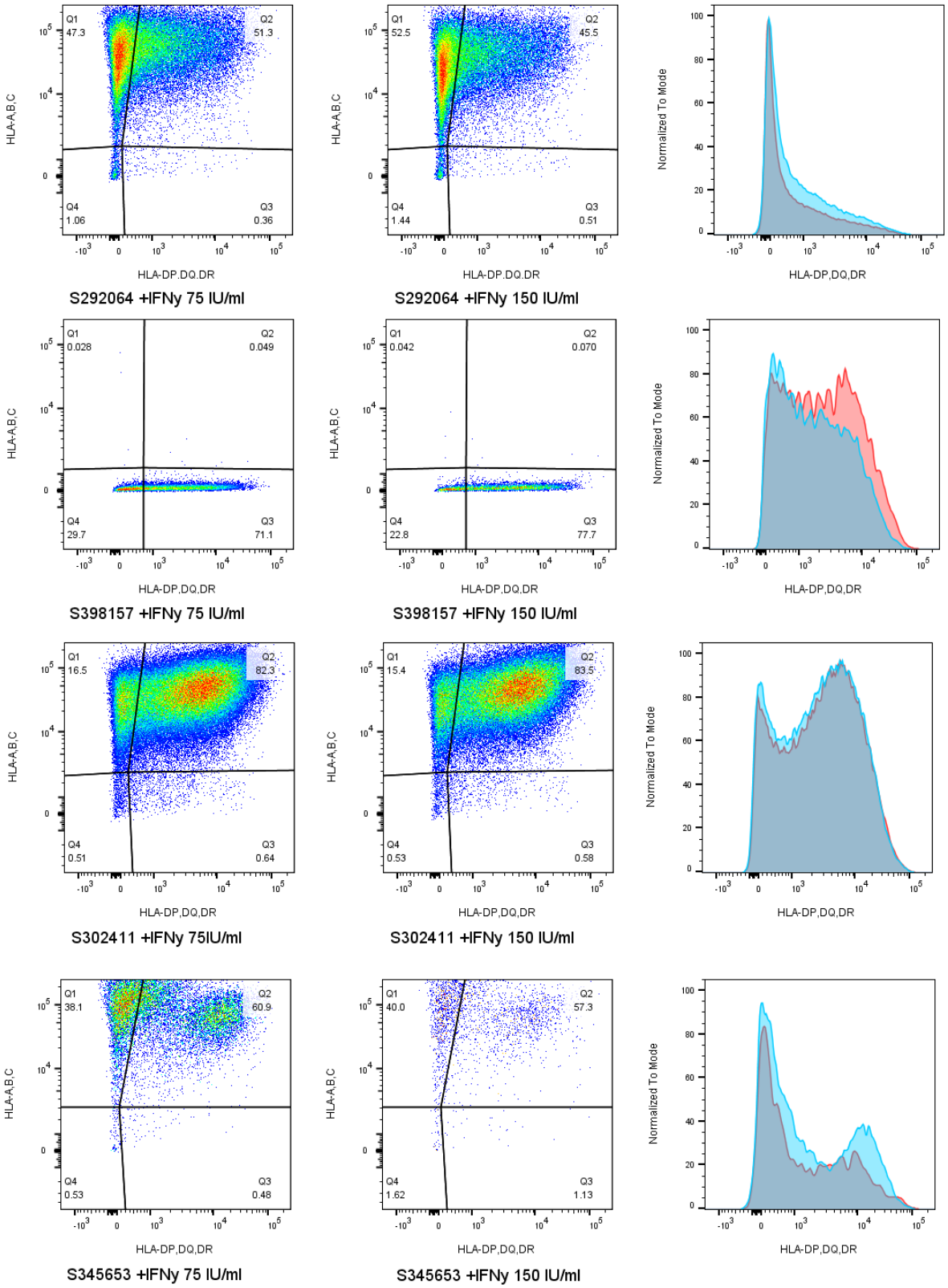


Figure 4.14a Flow cytometry assessment of Class II responses with higher IFNγ doses in strongly inducible lines. Results from four strongly-inducing organoids treated with 75 IU/ml (**left**) or 150 IU/ml (**centre**) IFNγ for 24 hours. Overlay of class II histograms provided **(right)** with 75 IU/ml IFNγ displayed in blue and 150 IU/ml in red. Experiments on each line performed once.

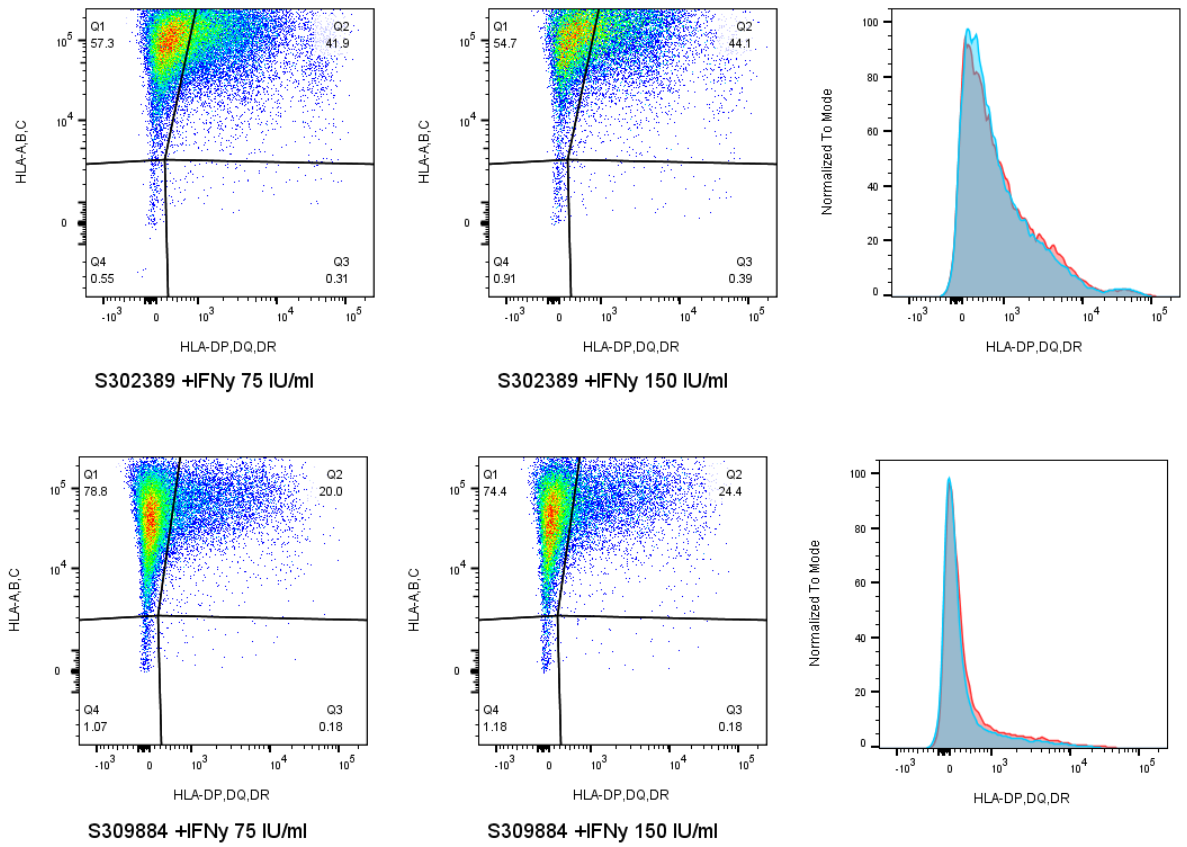


Figure 4.14b Flow cytometry assessment of Class II responses with higher IFNγ doses in weakly inducible lines. Results from two weakly-inducing organoids treated with 75 IU/ml (**left**) or 150 IU/ml (**centre**) IFNγ for 24 hours. Overlay of class II histograms provided **(right)** with 75 IU/ml IFNγ displayed in blue and 150 IU/ml in red. Experiments on each line performed once.

4.5 Conclusions

Assessment of IFNγ responses in these fifteen organoids has provided some clear biological differences between lines, with three subgroups emerging. Firstly, the majority (n=8/15) of these organoid lines demonstrate high levels of Class II expression following stimulation with relatively low doses of interferon. A second group (n=3/15) demonstrate a complete loss of interferon response, with no upregulation of Class II expression observed and an underlying loss of signalling response, with these three lines failing to upregulate IRF1/STAT1. This phenomenon has previously been identified and is known to be more common in MSI-H cancers, with one of these lines (557) known to be mismatch repair deficient (dMMR) with loss of MLH1, PMS2 and MSH6 on IHC. A third group (n=4/15) exhibit weak Class II expression following 24 hours of IFNγ stimulation.

The cell line data provides some further insight into different biological mechanisms controlling Class II expression in cancers. HCT116 and DLD1, a non-inducible line and inducible line respectively according to Satoh et al, show equivalent small increases in Class II expression, with ratification of the findings described here with the other literature. Both of these cell lines maintain IRF1/STAT1 response to IFNγ, indicating an alternative mechanism to the three non-responding organoids. Indeed, this could perhaps be hypothesised from the flow cytometry data alone; the non-inducible organoid lines are completely unchanged when stimulated with IFNγ, compared to the small increases in Class II seen in DLD1 and HCT116. These small increases in Class II expression could point to epigenetic dysregulation of *CIITA* as previously reported, with the Class II pathway essentially intact but repressed via CpG or histone level control, which may allow a small subgroup of cells with less

methylation to express some *CIITA* for example. RKO, the other non-inducible cell line, appears similar to the non-responsive organoids with a delta following IFNγ stimulation of less than one percent. In contrast to the non-responding organoids, however, this line maintains IRF1/STAT1 response, suggesting an alternative mechanism of class II loss, and could represent more complete epigenetic silencing compared to HCT116/DLD1 for example.

Comparison of the weakly-inducible group of organoids with the cell lines again suggests a difference biologically between them. The upregulation of Class II expression in these lines (10-27%) with IFNγ appears more robust than in HCT116 and DLD1. Together these differences suggest alternative mechanisms between cell lines and organoids might be at play. These mechanisms, including the biology of *CIITA* and epigenetic modifications, will be explored in the next chapter.

Chapter 5: Understanding the Mechanisms of MHC Class II Loss in Colorectal Cancer

5.1 Introduction

In the previous chapter, a group of fifteen patient-derived colorectal cancer organoids were characterised by inducibility of surface MHC Class II expression following IFNγ stimulation. In addition, the cell signalling component of the IFNγ-Class II axis was assessed, by quantification of IRF1 and STAT1 protein expression. Just over half of these lines were able to express high levels of Class II. By contrast, three lines showed a complete loss of Class II upregulation, seemingly secondary to a loss of the signal transduction component of IFNγ response. A third group demonstrated only weak Class II expression and had intact IRF1/STAT1 responses. In addition to these findings in organoids, four colorectal cancer cell lines were assessed, with very weak or no upregulation of Class II in three. Notably, the non-inducible cell lines, in contrast to the organoids, maintained IRF1/STAT1 signalling responses, potentially indicating alternate mechanisms of Class II repression between 2D and 3D models.

5.1.1 Revision of MHC Class II presentation

Once a cell is activated with IFNγ, a complex cascade of events occurs **(Figure 1.4)**. JAK1 is phosphorylated causing dimerization and nuclear translocation of the transcription factor STAT1, which targets several genes including *IRF1*. The CIITA-pIV promoter is activated by a combination of STAT1 dimers, USF-1 and IRF1 binding to the GAS, E-box and IRE elements of the promoter respectively. Once *CIITA* is activated it coordinates the DNA-binding *RFX* family of transcription factors to facilitate expression of the HLA-DR/DP/DQ loci, as well as the invariant chain and

non-classical HLA-DM. Class II molecules are assembled in the endoplasmic reticulum, combined with antigen in endosomal compartments, before finally being transported to the cell surface for expression (139, 151, 152). Interestingly, mutations in Class II alleles and other distal parts of the pathway appears relatively uncommon in cancers, with most of the events causing loss of Class II expression occurring at or before the level of CIITA. Secondary resistance to immune checkpoint blockade (ICB) can involve HLA loss, but this more commonly affects Class I, including through loss of β2 microglobulin (*B2M*) (102, 139). In CRC, *JAK1* mutations are described in MSI-H disease, likely as a result of the high levels of immune activation that these hypermutated tumours induce even in the absence of ICB (182).

Binding of transcription factors to *CIITA* alone is not sufficient to cause transcription, with further chromatin modulation required to facilitate expression. BRG1 (also known as *SMARCA4*, part of the SWI/SNF chromatin remodelling complex) enables the recruitment and binding of histone acetyltransferases (HATs) to allow the promoter chromatin to adopt an open conformation and has been shown to keep CIITA-pIV remote enhancer positions primed for activation (151-153).

A number of processes can block CIITA expression. Firstly, promoter CpG sites can be directly methylated, typically through the DNA methyltransferase (DNMT) family of proteins (196). In addition, the associated histones can bear repressive marks, including methylation of Histone 3 Lysine 9 or 27 (H3K9me2/3 and H3K27me2/3). H3K27 methylation is known to be regulated by the polycomb repressive complex 2 (PRC2), which includes the proteins SUZ12 and Enhancer of zeste homolog 2 (EZH2). PRC2 works in direct opposition to the SWI/SNF complex. Histone acetylation conversely is a mark associated with accessibility of chromatin, and a

dynamic increase in H3K9ac and H3K27ac has been reported in the CIITA-pIV IFNγ response (152, 153, 196, 212, 258).

A paper by Truax et al, studied the association between EZH2 and disordered Class II expression in cell lines derived from different metastatic deposits of the MDA-MB-435 tumour. These lines demonstrated differing levels (between 30-50%) of Class II expression following IFNγ, and were found to have low-level CpG methylation, features that subsequently will become relevant when considering the weakly-inducible group of organoids. A differential response was seen in the MDA-MB-435 derivatives compared to cell lines that had high-level Class II expression following IFNγ, with the weak-expressers showing increasing EZH2 binding and resultant increase of the H3K27me3 mark at CIITA-pIV in contrast to decreases of both in highly-inducible lines. Furthermore, the levels of EZH2 binding were greatest in the lines with the lowest Class II expression, suggesting that EZH2-directed H3K27me3 levels may well control the amplitude of response in a subgroup of cancers. This effect was independent of *EZH2* mRNA expression, which remained constant (212).

5.1.2 Aims and objectives

1. Establish associations between baseline tumour characteristics (including in situ Class II expression) and organoid Class II responses
2. Assess *CIITA* mRNA expression following IFNγ
3. Cell sort (FACS) weakly-inducible lines by Class II expression and assess differences between populations

4. Assess cell lineages present in organoids by flow cytometry and effect on Class II inducibility
5. Determine levels of CpG methylation of CIITA-pIV in cell lines and organoids
6. Assess histone acetylation (H3K9ac) and methylation (H3K9me2) in organoid lines
7. Establish if EZH2 occupancy of CIITA-pIV is present in weakly-inducible lines
8. Explore genetic determinants of Class II expression

5.2 Tumour Characteristics and IFNγ responsiveness

A number of known clinicopathological characteristics are of potential relevance to CRC tumour biology, including the immunogenicity of the tumour. For example, a correlation between right-sided primary tumours, female sex, older age, *BRAF* V600E mutant disease, CpG island methylator phenotype (CIMP) and mismatch repair-deficient tumours (dMMR) is widely known (264). Class II expression is known to be present in a greater proportion of dMMR tumours (5), and right-sided tumour have a poorer response to EGFR targeting monoclonal antibody treatments (265). RAS mutation has been linked to decreased immunogenicity in certain Consensus Molecular Subtypes (CMS), as well as with loss of STAT1 response to IFNγ (107, 108).

In order to explore the underlying biology of the organoid models and their response (Class II expression by flow cytometry) following IFNγ, lines have been displayed in order of Class II expression in **Table 5.1**, with associated characteristics.

The number of lines is too small for meaningful statistical correlation, however, clinical characteristics have been colour coded in the table to allow for ease of

comparison. By Class II response, there appears to be fairly even representation of sex and tumour side across the groups, and mutation (*BRAF/RAS*) and MMR status also show no obvious differences.

Tumour staging has been displayed by overall stage, as well as individual TNM components separately. The non-inducible lines notably are composed of only low stage (I-II tumours), but the size of the dataset prevents meaningful evaluation. It is worth noting that two patients were included with stage IV disease. Nearly all cell lines (and organoids) will be derived from surgically resected tumours, e.g. those of a lower stage. These lower stage tumours are more likely to have biologically favourable characteristics, with the potential to miss acquired pathological changes, including immune escape mechanisms. The fifteen organoids here include the two metastatic patients, along with the eight with stage III disease (which carries an approximately 50% chance of future relapse). The sample selection, therefore, includes a relatively broad and representative range of tumour presentation. Although this analysis is limited, it is clear that no singular clinicopathological characteristic can predict Class II expression in the organoid lines.

	Negative			Weak				Strong							
Organoid Line	**964**	**557**	**376**	**658**	**884**	**389**	**COLO312**	**064**	**647**	**080**	**COLO151**	**157**	**411**	**653**	**COLO155**
Flow Class II (% cells)	2.67	3.23	3.32	13.7	18.4	28.2	42.7	69.4	69.8	72.5	72.9	73.0	76.6	78.9	87.5
Mean Class II Primary (%)	0	1	0	20	0	0	0	25	75	0	0	45	1.5	60	7.5
Immunoscore	2	2	n/a	n/a	0	0	n/a	3	n/a	2	2	4	2	2	2
Immunoscore group	Int	Int	n/a	n/a	Low	Low	n/a	High	n/a	Int	Int	High	Int	Int	Int
Sex	M	F	M	F	M	M	F	M	M	F	M	F	F	F	M
Left/Right sided primary	R	R	L	R	L	R	R	L	R	L	R	R	R	L	L
Stage	I	II	II	II	IV	III	II	III	III	II	III	III	IV	I	II
T	2	3	3	4	3	4	3	2	4	3	3	3	3	2	4
N	0	0	0	0	2	2	0	1	2	0	1	2	2	0	0
M	0	0	0	0	1	0	0	0	0	0	0	0	1	0	0
Grade	Mod	Poor	Poor	Poor	Poor	Mod	Poor	Mod	Poor	Mod	Mod	Poor	Mod	Mod	Mod
RAS	n/a	*KRAS* MT	n/a	-	*NRAS* MT	-	*KRAS* MT	-	*KRAS* MT	n/a	-	n/a	-	*KRAS* MT	*KRAS* MT
BRAF	n/a	-	n/a	V600	-	-	-	-	-	n/a	V600	-	V600	-	-
MMR	pMMR	dMMR	pMMR	dMMR	pMMR	pMMR	dMMR	pMMR	dMMR	pMMR	pMMR	dMMR	pMMR	pMMR	pMMR

Table 5.1 Clinicopathological characteristics of organoids and Class II expression. Organoids sorted from left to right by surface Class II expression (mean value of triplicate assessment by flow cytometry following IFNγ). Relevant clinical correlates including mean Class II expression (percentage positive cells) performed by IHC in blinded duplicate by consultant pathologist on different sections of primary tumour. Immunoscore and grouping (Low, Intermediate, High) provided by HalioDx. Sex, side of primary, TNM stage and break-down, grade and extended *RAS*, *BRAF* and mismatch repair status (proficient pMMR vs deficient dMMR) as determined by NHS pathology services.
Clinically 'favourable' characteristics have been colour coded (green for prognostically favourable, yellow for intermediate and red for unfavourable). For 'neutral' characteristics e.g. sex, grey/white colour discrimination has been used.

5.2.1 Primary tumour Class II expression and organoid expression

One aspect of Class II expression in cancer that was discussed in the introduction to the previous chapter is the potential disparity between traditional cell lines and the study of Class II on resected tumours, with no way of assessing concordance between the two sources of data. Staining of primary tumour sections for Class II expression is available for all fifteen organoids, with blind scoring of two unique sections provided by a Consultant Pathologist (with huge thanks to Dr Philippe Taniere, University Hospitals Birmingham for his time and assistance) using a clinically validated HLA-DR,DP,DQ antibody **(Table 5.1)**. Of note, only a small proportion of tumour will be processed for organoids and therefore spatial sampling heterogeneity could provide limitations to this approach if non-representative. Additionally, a different clone of Class II antibody has been used for IHC and flow, with the IHC antibody not available conjugated for flow cytometry.

Importantly, however, no line with absent Class II expression had evidence of significant Class II expression in the primary tumour, with non-inducible cells in vitro consistently non-inducible in vivo. Similarly, the one weakly-inducible line with some Class II staining in the primary is of similar low-level expression in vitro by flow (20 vs 13.7%).

Perhaps unsurprisingly, six out of the eight strongly-inducing lines had evidence of Class II expression in the primary, with the levels of expression seen comparably high in three of these (>50% Class II positive cells). Importantly, however, a number of completely Class II negative primary tumour exhibit strong Class II expression when stimulated with IFNγ ex vivo. Lines 080, COLO151 (with 0% tumour Class II

expression) and lines 411 and COLO155 (with <10% tumour expression) show largely unrestricted ability to upregulate Class II. This suggests that Class II expression within the tumour cannot be used to predict a tumour with loss IFNγ responsiveness, but rather that these tumours are likely to be sites of immune-exclusion and deficiency of IFNγ within the TME.

Conversely, tumours with high levels of primary tissue Class II expression are noted to lose this expression when under basal unstimulated conditions as organoids (**Table 4.3**), with only three lines exhibiting >10% basal Class II expression. This is biologically in keeping with an inducible state of Class II expression (e.g. control via CIITA-pIV following IFNγ stimulation) rather than constitutive expression in these lines. This has previously been demonstrated in a patient derived lung cancer cell line with matched CD4+ T cell culture, where the cell line was Class II positive only in the presence of T cell co-culture (roughly recapitulating the TME and immune/cancer cell interaction) or with the addition of exogenous IFNγ added to culture media, but not under basal conditions (210).

5.3 Assessment of *CIITA* mRNA expression

As *CIITA* accessibility has been identified as a major component of Class II loss in CRC, levels of *CIITA* mRNA were assessed with RT-qPCR, with comparison of expression before and after IFNγ stimulation. As previously, a dose of 75 IU/ml IFNγ was used for a period of 24 hours. Following stimulation, cell lines (grown in 2D culture) were detached, washed in PBS and lysed in RLT Plus Buffer. Organoids first underwent dissociation from matrigel, before generation of single-cell suspensions and then were processed identically to the cell lines. RNA from the cells (+/- IFNγ)

was DNAse treated and underwent cDNA synthesis as a two-step process, before performing the PCR.

5.3.1 Validation of RT-qPCR

Initially, a SYBR Green-based approach was performed, based on the custom CIITA primer sequences used by Satoh et al (196):

CIITA Forward: 5'-AGACTTGCCGCGGCCCCAGAG-3'

CIITA Reverse: 5'-GTAGAGGCACAGGGGGTCAGC-3'

A range of total cDNA from 10-100 ng was loaded from HT29 cells (+/- IFNγ) and PCR results analysed for *CIITA* and *GAPDH* (housekeeping) expression using the Thermofisher Cloud Design and Analysis package. Amplified product was detected, with an adequate concentration gradient seen for *GAPDH*, however, amplification of the *CIITA* region was uniform across the different loading amounts. Melt curve analysis was performed, with clean dissociation seen for the *GAPDH* primer, however, a prolonged melt through high temperatures with two separate peaks was observed for the *CIITA* primer **(Figure 5.1).** This result suggested that non-specific binding of the primer was likely to affect data quality.

Therefore primers were redesigned using a TaqMan based reported system instead. A validated inventoried *CIITA* primer with 5' FAM dye and 3' MGB-NFQ from ThermoFisher (Hs00172106) was chosen. The assay was repeated with 10-100 ng total cDNA input from HT29 cells, with 50 ng selected as the loading amount, based on a strong positive Cycle Threshold (Ct) of 20-21 for *CIITA* mRNA in the IFNγ treated group, and a just detectable (>35 Ct) *CIITA* mRNA expression in the control cells.

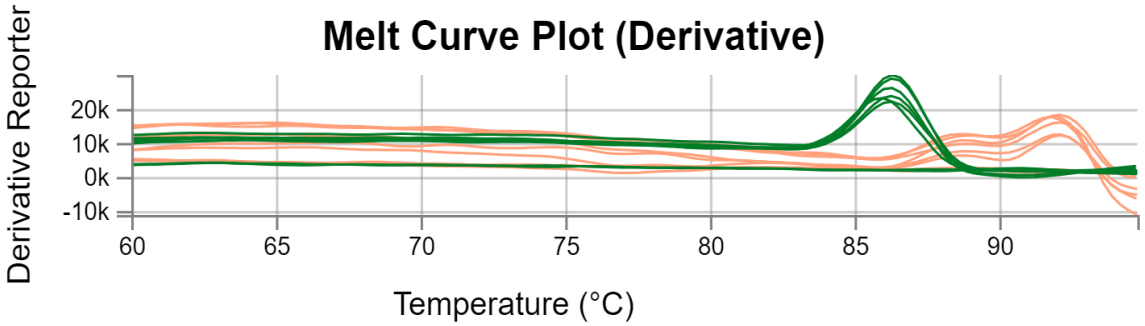


Figure 5.1 Melt Curve from *CIITA*/*GAPDH* SYBR Green Validation. mRNA from HT29 cell (+/- IFNγ) underwent RT-qPCR with SYBR Green primers. Melt curves generated using ThermoFisher Cloud Design and Analysis software, with *GAPDH* (green) and *CIITA* (orange) displayed. A prolonged and double-peak profile is noted in the *CIITA* primer dissociation.

5.3.2 RT-qPCR (TaqMan) for *CIITA* mRNA

50 ng cDNA from the cell lines and organoids was mixed with TaqMan Fast Advanced Mastermix and primers, before running on a Quantstudio 5 qPCR machine on a fast cycling protocol. For each line, with and without IFNγ, both *CIITA* and *GAPDH* were loaded with four technical replicates. Results were analysed using a comparative Ct (ΔΔCt) method, controlling for housekeeping gene (*GAPDH*) and performing relative quantification of *CIITA* mRNA pre- and post-stimulation (2^-(ΔΔCt)) as previously reported (242). Results of relative expression change are displayed in **Figure 5.2**.

Results for three cell lines (HCT116, DLD1 and HT29 representing non-, weakly- and strongly-Class II inducible respectively) demonstrated a small increase in *CIITA* mRNA in HCT116 (relative expression increased 26.7 times) with larger increases

seen in DLD-1 and HT29 (1524 and 36300 times respectively). The cell lines with the strongest Class II expression therefore exhibited the largest relative increases in CIITA-pIV mRNA expression as expected.

CIITA mRNA expression increases in the non-responsive organoid group were markedly lower than both the weak- and strong-responding groups, with all three lines showing relative increases of six-fold or less. By contrast, the responding lines demonstrated relative increases of 30-4241 times **(Figure 5.2)**. One of the limitations of using the comparative Ct method is that a higher *CIITA* mRNA level in the control group can make the relative increase with IFNγ appear smaller. Indeed, when comparing the Ct values for *CIITA* expression at baseline (without IFNγ stimulation) the lines with strong Class II inducibility had a higher mean expression of *CIITA* compared with the weak Class II expressers (mean Ct 31.98 vs 35.36, P=0.0004 unpaired T-Test). The Ct values are given in **Table 5.2**.

Organoid	Relative increase in *CIITA* mRNA following IFNγ	Mean Ct For *CIITA* (IFNγ)	Mean Ct for *CIITA* (Control)
376	2.67	27.1	30.5
557	5.97	31.1	34.6
964	1.24	31.2	33.5
389	4241.7	23.7	37.5
658	30.9	28.6	33.5
884	95.8	24.7	34.5
COLO312	2245.8	23.8	35.00
064	653.0	25.6	36.9
080	38.3	21.3	29.9
157	1221.5	22.0	33.2
411	528.8	24.0	34.0
653	33.3	21.9	28.5
COLO151	206.4	23.2	31.6
COLO155	103.9	22.8	29.8

Table 5.2 Summary of *CIITA* RT-qPCR results. Relative increase in *CIITA* mRNA expression following IFNγ stimulation, mean cycle threshold (Ct) values for *CIITA* expression pre- and post-stimulation as determined by RT-qPCR. Each condition performed with four technical replicates. Relative expression calculated using 2^-(ΔΔCt) method.

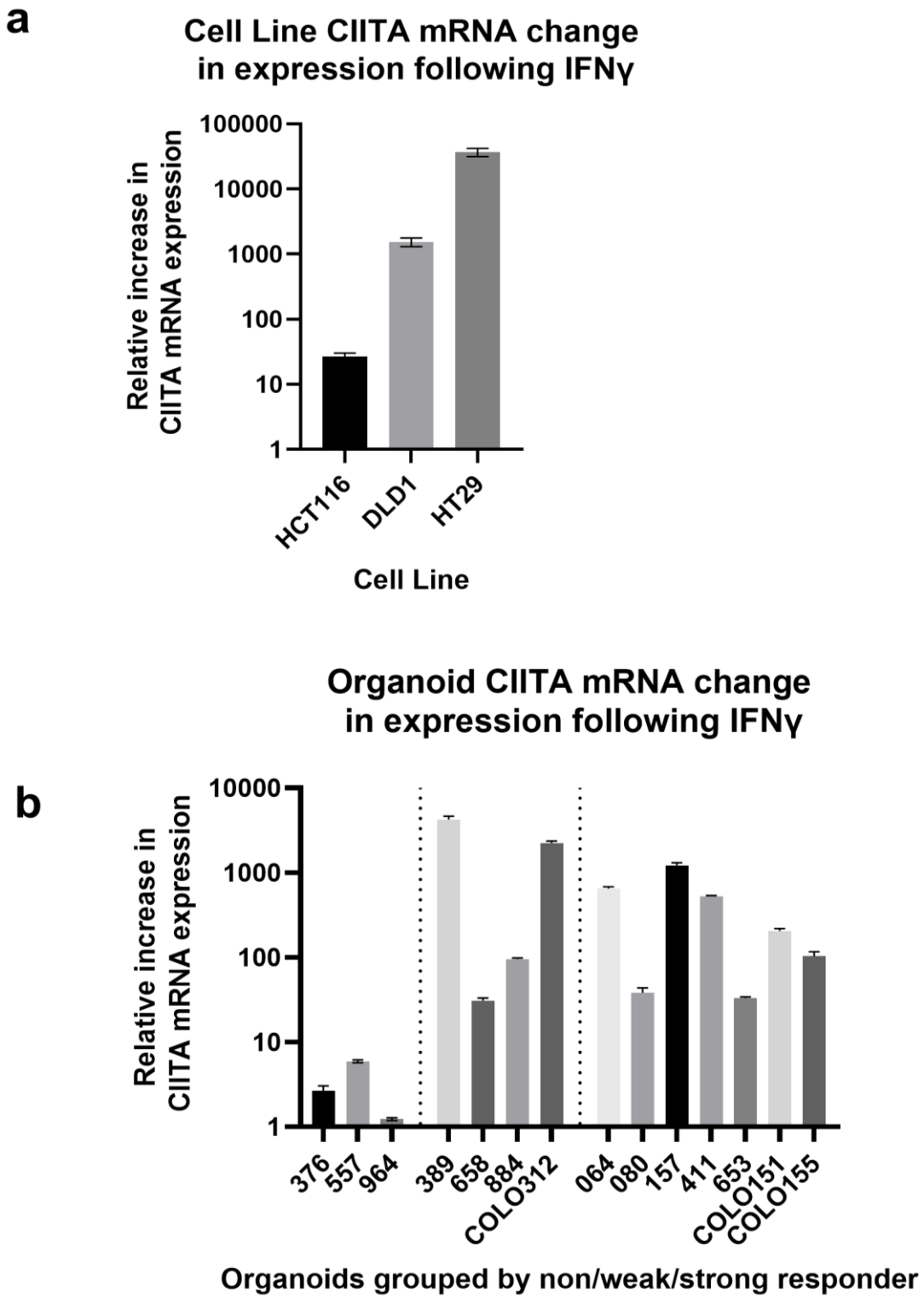


Figure 5.2 RT-qPCR for *CIITA* mRNA expression following IFNγ stimulation. Cell lines **(a)** and organoids **(b)** treated with 75 IU/ml IFNγ for 24 hours prior to RT-qPCR. Expression of *CIITA* mRNA compared with untreated cells and corrected by *GAPDH* expression. Relative increase in expression calculated using ΔΔCt method. Organoid results divided by response groups (dotted lines) with non-, weak- and strong-responders. Results show calculated mean expression change and standard deviation, with a four replicates of each condition for each line. Note logarithmic scale on y-axis.

Additionally, mean Ct values in the IFNγ stimulated organoids were significantly higher between strongly expressing lines compared to the weaker or non-expressers. Mean Ct for stimulated *CIITA* expression was 22.9, 25.2 and 29.7 for strong, weak and negative lines respectively (One-way ANOVA followed by Tukey's post-test: Strong vs Weak P=0.0004, Strong vs Negative P<0.0001, Weak vs Negative P <0.0001). In summary, both the weak and strong Class II expresser lines exhibited large increases in *CIITA* mRNA following IFNγ stimulation. Relative increases in *CIITA* mRNA were of the same relative magnitude in the strong and weak groups, however, the overall expression was likely to be of a higher absolute level in the strong group, based on detection at lower Ct values. Whilst an increase in *CIITA* was seen in the non-inducible lines, with suspected IFNγ signalling derangement, these values were significantly lower. Furthermore, the sensitivity of this assay is likely to be much greater than previously published data (e.g. Satoh et al (196)) where agarose gel quantification was used following the initial PCR. These RT-qPCR results demonstrate a clear correlation of Class II expression (determined by flow cytometry) with levels of *CIITA* mRNA. The mechanism of Class II loss in non-inducible organoids is likely at or proximal to *CIITA*, in comparison to both weakly- and strongly-inducible lines, where CIITA-pIV remains accessible to at least some degree even in the weakly-inducible lines. There is a reduced amplitude of *CIITA* mRNA response seen in the weakly-inducible lines compared with the strongly-inducible lines.

5.4 Cell sorting of positive and negative sub-populations from organoids

In order to assess whether differences in the weakly-inducible lines could be attributed to tumour heterogeneity within the organoid lines, cells were sorted into Class II positive and negative fractions. The weakly-inducible lines 389 and 884 organoids were stimulated for 24 hours with 75 IU/ml IFNγ, dissociated into single cells and stained for live-dead, Class I and Class II prior to fluorescence-activated cell sorting (FACS) using a BD FACSAria Flow Cytometer. FACS was kindly supported by the expertise of Dr Adriana Flores-Langarica in the University of Birmingham flow cytometry facility. Initially, DNA and RNA were extracted directly from the cells obtained following FACS. The resultant DNA/RNA concentration from these directly sorted populations was relatively low, limiting further analysis.

To improve yields and also to allow validation of the success of the sort, sorted cells were instead re-established as organoids. Lines were pre-treated with ROCK inhibitor (Y-27632) for 24 hours to preserve cell viability and the staining procedure was performed in sodium azide free buffer. Cells were directly sorted into organoid media, before being washed briefly in PBSO and resuspended in a single well of matrigel and cultured as per the standard organoid protocol. The following cell numbers were obtained from the sort- 389 2+: $2.95x10^4$, 389 2-: $6.15x10^4$, 884 2+: $2.6x10^4$ and 884 2- $4.2x10^5$. By seven days, organoids had formed in all four conditions and by two weeks lines were expanded to two wells.

The newly established sorted organoid lines were re-characterised by flow cytometry expression of Class I/II by flow cytometry and IRF1/STAT1 expression by western

blot following IFNγ, as per the protocol for the primary lines. DNA and RNA was also extracted for downstream analysis.

Results from the flow cytometry experiments are shown in **Figure 5.3**, with the experiment performed in triplicate and results from the first experiment displayed. The 389 2+ sorted line demonstrated a clear enrichment of Class II inducible cell when re-challenged with IFNγ, with in excess of 60% of cells able to upregulate Class II. The 389 2- continued to show an inducible population of 27.1%, which was nearly identical to the unsorted organoid (mean 28.2% Class II expressing cells). Interestingly, this enrichment of Class II positive cells in 389 Class II positive sort reduced over subsequent experiments, with around 42% present in the second experiment and this dropping further by the third, in contrast to the characterisation results of organoids performed in the previous chapter where results were highly consistent. Conversely, with 884 there was no difference between the 2+ and 2- line, with both showing only weak Class II expression between 8-9% **(Figure 5.4)**.

The negative sorted (2-) lines were next assessed for protein expression of IRF1/STAT1 following IFNγ. IRF1 and STAT1 continued to be upregulated in both of these lines in response to IFNγ, with densitometry confirming significance. Experiments were performed in triplicate with representative blots displayed **(Figure 5.4)**. Overall, these results suggest a temporary enrichment of Class II expressing cells in 389. The ability to recapitulate growing organoid models following FACS from all four groups was pleasing, particularly at the time of the experiment, this had only been reported in the literature in a small number of papers.

The declining enrichment of Class II inducible cells exhibited in the 389 sort suggests that these cells are not maintained in culture. In the organoid culture system, (cancer) stem cells are the self-renewing pool responsible for producing future lineages of cells. There is evidence from the literature that Intestinal Stem Cell (ISC) are Class II positive. In one study using single-cell sequencing of mouse small intestine, Class II was found to be highly upregulated in ISCs compared to other differentiated cells (266). It is therefore possible that the 389 sort contained Class II positive stem cells and an enrichment of Class II positive differentiated cells that over subsequent passages were lost. It is known that organoid cultures maintain a stable proportion of stem cells over time, therefore a rebalancing is likely to have occurred (227). The number and strength of Class II staining in 884 is an order of magnitude lower than 389 and is likely to explain the lack of enrichment observed in this line.

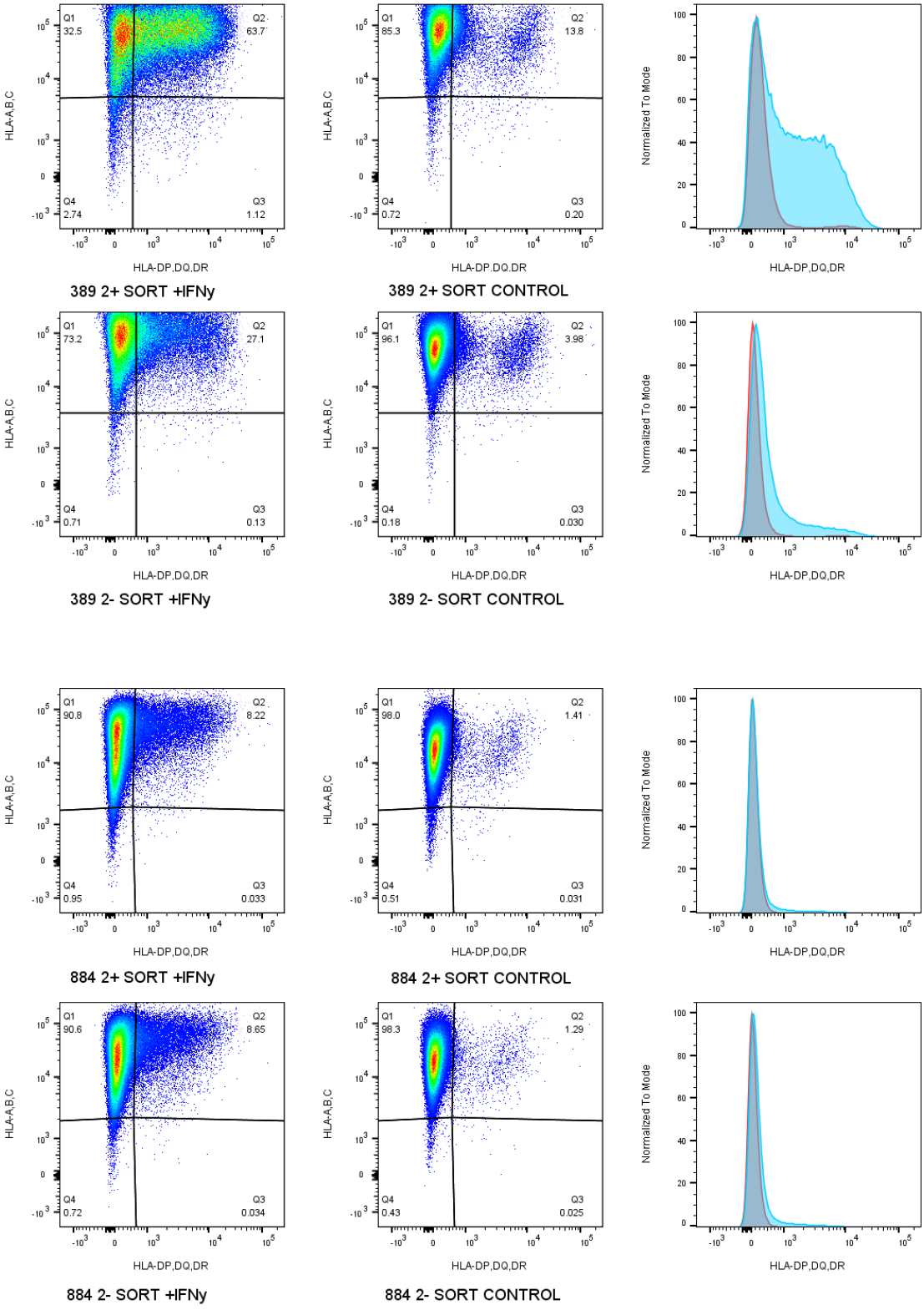


Figure 5.3 Flow cytometry assessment of Class II sorted organoids. Organoids 389 and 884 were FACS sorted into Class II inducible (2+) and non-inducible (2-) populations, with organoids re-established from the sorted cells. Each sorted line was treated with IFNγ **(left)** and compared with untreated control cells **(centre)**. Overlay of class II histograms **(right)** with IFNγ displayed in blue, control in red. Each experiment performed in triplicate, results from first experiment displayed.

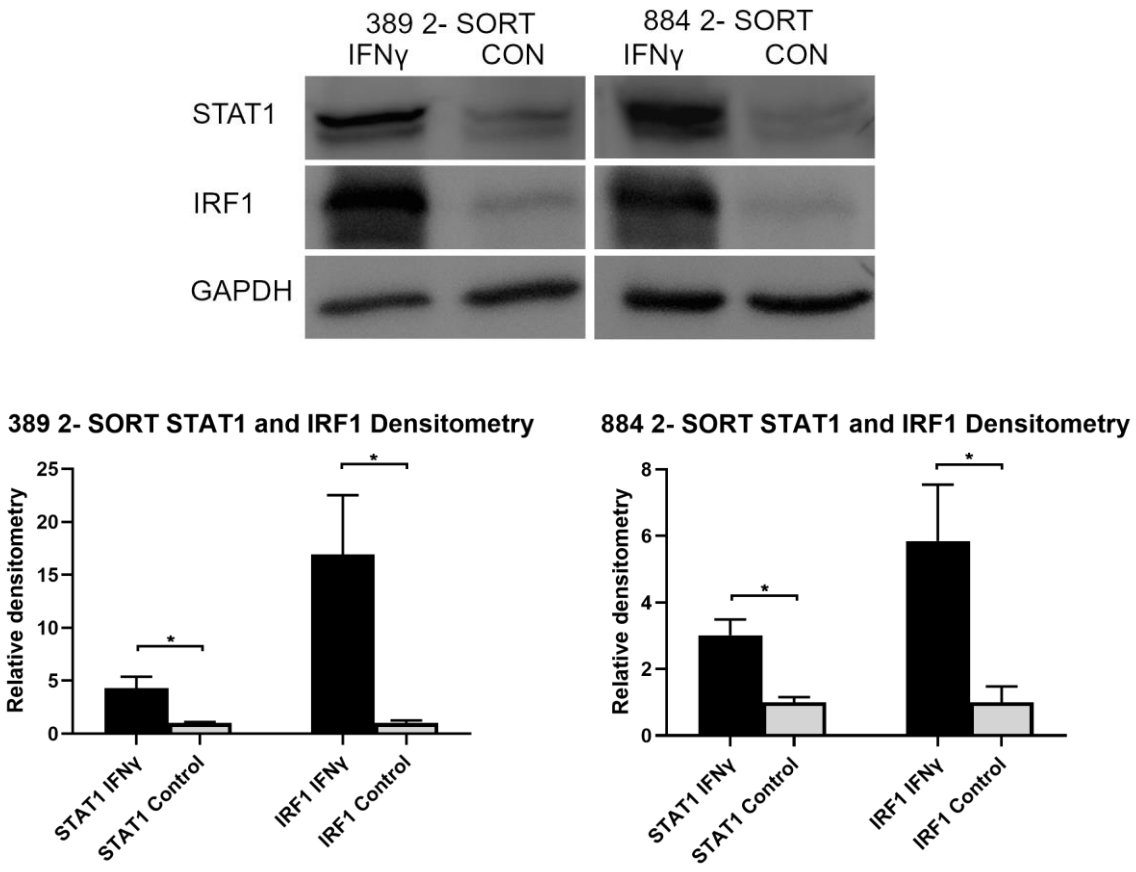


Figure 5.4 Western blot of IFNγ response in Class II sorted lines. Top: Cells were assessed for STAT1, IRF1 and GAPDH protein levels following 24 hours stimulation with 75 IU/ml IFNγ. Unstimulated control cells (CON) displayed alongside. Representative blots shown, experiments performed in triplicate. **Bottom:** Densitometry performed on western images, with area quantification for proteins of interest adjusted by GAPDH loading control. Relative expression compared to control condition given, and mean values with standard deviation displayed. Paired two-tailed T-test performed for statistical analysis: NS $P \geq 0.05$; * $P < 0.05$; ** $P < 0.01$; *** $P < 0.001$; **** $P < 0.0001$.

5.5 Assessment of cell lineages comprising organoids

Intestinal organoid models, in contrast to 2D cultures, contain a stable proportion of LGR5+ stem cells which give rise to multiple lineages of differentiated cell types that are present in the bowel. A mucinous tumour for example would be expected to contain a high proportion of goblet cells compared to a normal tumour. In order to exclude a cell lineage-specific cause for loss of Class II expression, subtypes of cell lineages in organoids were assessed. The most notable cell-type after enterocytes is

the goblet cell, and previously detection of rarer cell types, including LGR5+ stem cells has required enrichment strategies (267, 268). A flow cytometry panel was therefore designed to include several other lineage markers including LGR5, Chromogranin A (CgA; representing enteroendocrine), EPCAM (epithelial cells), Mucin2 (MUC2; representing goblet cells).

An initial experiment was run with 389 and 411, with organoids treated with IFNγ (75 IU/ml for 24 hours) and then stained for Class II expression, live-dead and the above panel of CgA/MUC2/EPCAM/LGR5. As expected, diffuse EPCAM positivity was observed in the majority of cells. LGR5 was not convincingly demonstrated in either line, in keeping with the relative sparsity of this cell type. Similarly, enteroendocrine cells (CgA +ve) were not convincing identified above background signal. MUC2 staining was seen at low levels in nearly all cells (when compared to unstained and subsequent MUC2 FMO), with a distinct small $MUC2^{hi}$ population, hypothesized to represent goblet cells. Class II expression was confined to EPCAM+ cells, whereas Class II inducibility was seen in both $MUC2^{hi}$ and $MUC2^{lo}$ cells **(Figure 5.5)**. Only IFNγ stimulated cells shown, as these experiments were designed specifically to assess if Class II positive cells were confined to a particular lineage of cells e.g. MUC2 non-expressors.

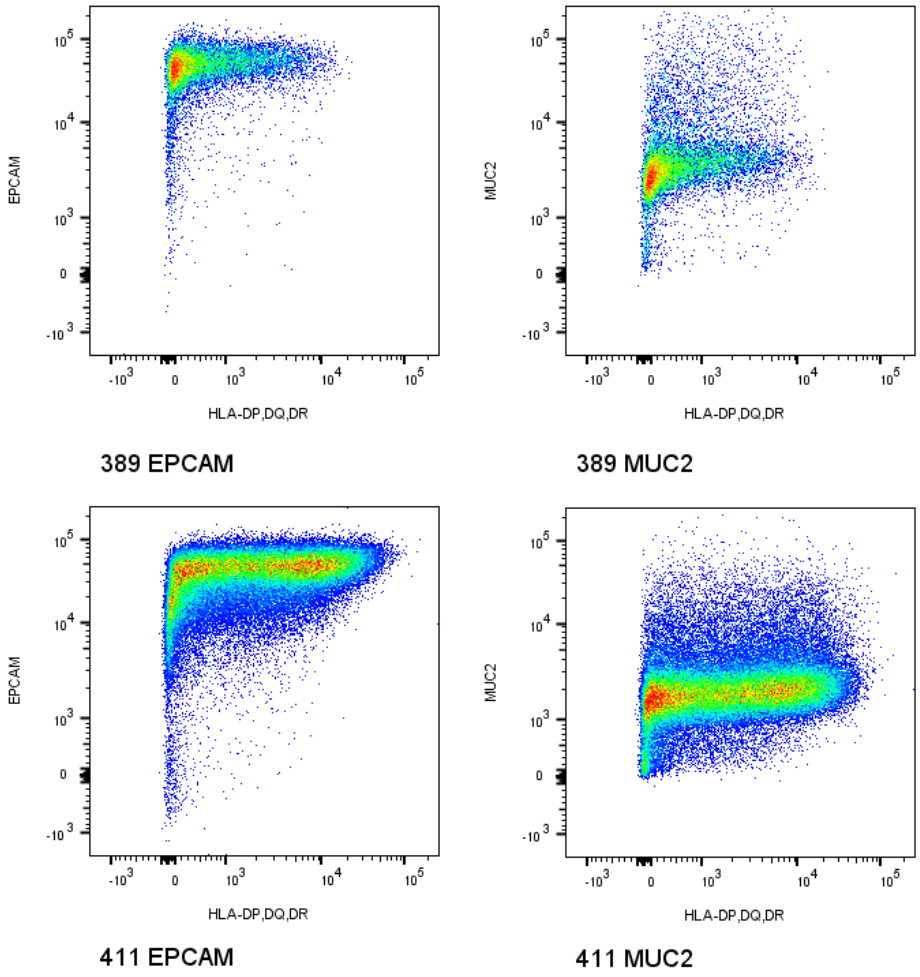


Figure 5.5 Flow cytometry assessment of cell populations within organoids.
Organoids 389 and 411 were stimulated with IFNγ and then stained for a panel of lineage markers and Class II. Results of EPCAM and MUC2 displayed against Class II expression. Results from single experiment.

This experiment was then repeated in the 389 and 884 Class II sorted lines, with just MUC2 staining in addition to Class I/II and live-dead dye. An FMO for both Class II and MUC2 was included to aid with gating. Results in 389 remained consistent with the broader characterisation panel. 389 appeared to have a greater proportion of $MUC2^{hi}$ cells compared to 884, with <0.11% cells staining $MUC2^{hi}$ in 884. The $MUC2^{lo}$ pattern was again confirmed as distinct to negative cells with FMO control. A higher proportion of $MUC2^{hi}$ cells were seen in the Class 2+ sorted 389 2+ line

compared with the 389 2- **(Figure 5.6)**. Class II inducibility was seen in both MUC2^{hi} and MUC2^{lo} cells and therefore loss of Class II inducibility is independent of any organoid lineage effects.

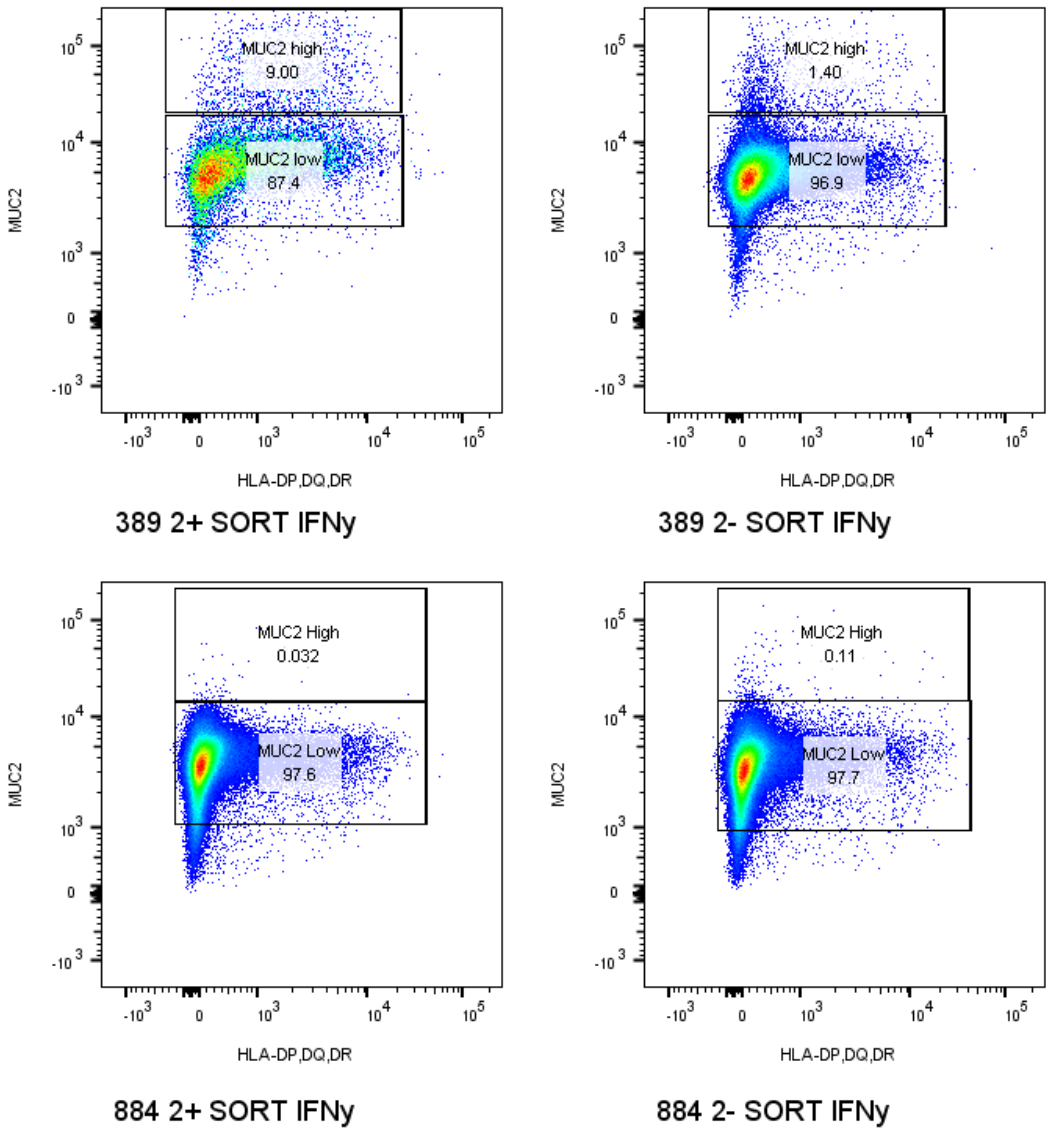


Figure 5.6 Flow cytometry assessment of sorted organoid lines for goblet cell populations. 389 and 884 Class II sorted organoid lines were stimulated with IFNγ prior to staining for MUC2 and MHC expression. MUC2 expression displayed against Class II inducibility. Experiment performed once.

5.6 Assessment of CpG methylation of CIITA-pIV

CpG promoter methylation of CIITA-pIV has previously been reported as a major cause of loss of Class II expression in CRC cell lines. The *CIITA* RT-qPCR experiments confirm that the IFNγ induced *CIITA* mRNA expression in HCT116 (a non-inducible cell line) is several orders of magnitude smaller than HT29 (a strongly-inducible cell line) and there is a dose-response relationship between expressed Class II and *CIITA* mRNA. Whilst induction of *CIITA* mRNA was observed in weakly-inducible organoids, it was at a lower level compared with the strongly-inducible lines. CpG methylation was therefore assessed as a possible cause of either the complete or partial transcriptional repression of *CIITA* observed in these groups. DNA extracted from cell lines and organoids was bisulfite (BS) converted, before undergoing PCR amplification of a 126bp region of the CIITA-pIV CpG island and pyrosequencing performed, targeting eight individual CpG sites.

Before proceeding with pyrosequencing, BS converted DNA from eight of the organoids underwent quality control assessment of BS conversion efficiency using a qPCR-based approach as previously described (244). Two primers, one recognising methylated (hence unconverted by the BS conversion process) β-actin and a second unmethylated (converted) β-actin primer were used on each sample, as well as a negative control of human genomic DNA that had not undergone BS conversion. Analysis (ΔΔCt) of Ct values from the two primers allowed for calculation of the percentage BS conversion efficiency **(Table 5.3)**. Conversion was successful, with >99.1% efficiency in all eight samples validated.

Sample	BS Conversion (%)	Sample	BS Conversion (%)
064	99.7	653	99.8
080	99.3	884	99.4
389	99.6	964	99.1
411	99.5	gDNA control	0
557	99.4	Negative control	-

Table 5.3 Bisulfite conversion efficiency. Eight organoids underwent BS conversion followed by qPCR based assessment of conversion efficiency of β-actin. Genomic DNA (gDNA; unconverted) also run as a control. Each condition performed in technical duplicate with mean Ct values used.

BS DNA from all fifteen organoids and the four cell lines underwent amplification for the CIITA-pIV region followed by pyrosequencing. All samples underwent PCR followed by sequencing in triplicate, and EpiTect Methylated and Unmethylated Control DNA (supplied BS converted) were also run alongside as a sequencing positive and negative control respectively. Further negative PCR controls were run alongside samples on all runs and the five QIAGEN recommended primer controls (see methods) were also run to exclude non-specific primer binding. Samples were run on a QIAGEN Pyromark Q48 Autoprep sequencer, and sequences and percentage methylation values were automatically calculated using the manufacturer's Autoprep software.

Results are displayed in **Table 5.4**. The EpiTect controls validated the accuracy of the sequencing results, with a mean (across all eight CpG) methylation of 86.5% and 6.0% for the methylated and unmethylated control respectively. The cell line data replicated the previously describe findings by Satoh et al (196), with minimal methylation seen in HT29 and DLD1 (mean values 3.8% and 8.0% respectively).

RKO and HCT116 demonstrated moderate and high levels of methylation (29.3% and 81.8% respectively). By contrast, the organoids were found to all be globally hypomethylated (highest mean CpG methylation of 5.1% in 658, with all other lines <5%) **(Table 5.4)**. Results were highly consistent, with low variability seen across replicates.

In conclusion, CpG methylation has been confirmed in the two previously described cell lines as a likely cause of low Class II expression in these lines. DLD1, a line with only very low levels of Class II inducibility demonstrates generally low levels of methylation, suggesting an alternative cause of restriction of Class II expression in this cell line. The organoid results across all response groups demonstrate very low levels of methylation, suggesting that this silencing of the *CIITA* promoter is not responsible for Class II regulation in organoids. Given that previously published findings of CIITA-pIV methylation have been validated in two cell lines reported to be methylated here, the applicability of the methodology used here is likely to be representative. By contrast, the absence of any significant methylation of CIITA-pIV across a panel of fifteen organoids of varying Class II inducibility, strongly indicates that *CIITA* promoter methylation is likely to be an acquired phenomenon of 2D culture, rather than a mechanism of Class II loss in CRC of biological relevance.

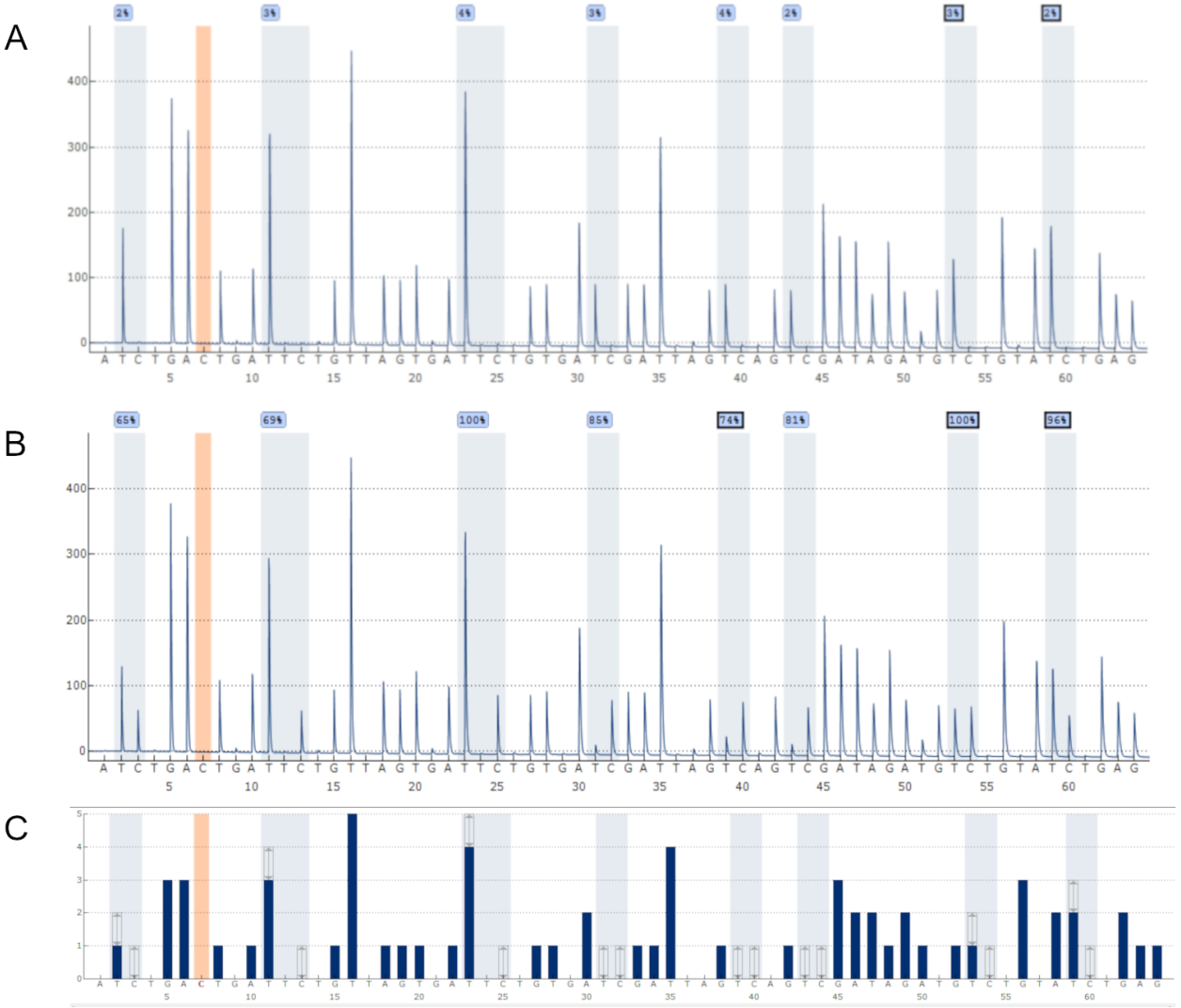


Figure 5.7 Pyrosequencing of CIITA-pIV in organoids and cell lines. Example pyrograms with calculated methylation at each CpG site displayed above (percentage) variable positions (light blue box). Results for organoid 064 **(A)** and cell line HCT116 **(B)**. **(C)** shows dispensation order for bases in pyrosequencing run, with dark blue rectangles showing expected base calls from known sequence. Clear boxes with arrows represent variable positions. Orange cytosine is an internal negative control used by the software.

Line	CpG Methylation % (Standard Deviation)								
	CpG 1	**CpG 2**	**CpG 3**	**CpG 4**	**CpG 5**	**CpG 6**	**CpG 7**	**CpG 8**	**All**
EpiTect Methylated	80.7 (11.3)	89.2 (4.2)	100.0 (0.0)	76.6 (0.8)	69.8 (2.1)	78.4 (1.0)	97.4 (1.2)	100.0 (0.0)	86.5 (1.7)
EpiTect Unmethylated	5.2 (0.7)	9.8 (2.3)	9.3 (0.3)	3.6 (1.2)	2.9 (0.5)	4.0 (1.6)	6.2 (1.4)	7.2 (2.2)	6.0 (0.7)
HT29	3.2 (1.2)	2.6 (0.4)	5.5 (0.4)	4.9 (0.3)	5.1 (0.2)	2.4 (0.7)	3.3 (1.3)	3.2 (1.4)	3.8 (0.4)
DLD1	6.0 (1.7)	7.1 (1.6)	12.9 (0.7)	9.1 (0.5)	13.1 (0.2)	5.4 (0.9)	5.6 (0.3)	4.9 (1.0)	8.0 (0.2)
RKO	13.0 (0.7)	15.7 (1.2)	49.9 (3.3)	44.5 (1.3)	42.3 (2.1)	37.4 (0.4)	15.1 (0.6)	16.6 (0.4)	29.3 (0.8)
HCT116	59.9 (11.0)	65.0 (5.8)	96.8 (5.5)	83.8 (1.0)	74.1 (4.1)	79.8 (1.3)	100.0 (0.0)	94.7 (2.4)	81.8 (2.7)
376	2.3 (0.7)	2.5 (0.3)	1.8 (0.4)	0.9 (0.2)	1.0 (0.1)	0.8 (0.3)	1.1 (0.3)	1.1 (0.2)	1.4 (0.2)
557	3.4 (1.1)	3.0 (0.7)	3.2 (0.4)	1.8 (0.5)	2.6 (0.7)	1.9 (1.1)	2.7 (1.6)	2.5 (1.2)	2.6 (0.7)
964	3.7 (0.6)	3.5 (1.0)	4.5 (0.5)	3.1 (0.7)	6.9 (0.5)	2.8 (1.2)	3.1 (1.5)	2.3 (1.1)	3.7 (0.8)
389	2.8 (0.7)	2.9 (0.9)	3.2 (0.7)	1.7 (0.4)	2.2 (1.1)	1.6 (0.8)	2.3 (1.2)	2.6 (1.5)	2.4 (0.6)
658	3.1 (0.7)	3.2 (1.2)	6.3 (0.4)	5.5 (0.6)	12.7 (0.8)	2.9 (0.1)	3.7 (0.8)	3.5 (1.2)	5.1 (0.3)
884	3.1 (0.4)	2.4 (0.8)	2.5 (0.3)	1.4 (0.4)	1.8 (0.9)	1.8 (1.1)	2.2 (1.2)	2.2 (1.3)	2.2 (0.5)
COLO312	3.4 (0.6)	4.4 (0.7)	11.0 (0.3)	3.0 (0.4)	3.5 (0.2)	1.2 (0.3)	1.7 (0.4)	1.9 (0.3)	3.8 (0.3)
064	2.9 (0.5)	3.7 (0.7)	4.8 (0.7)	3.0 (0.4)	4.3 (0.6)	2.8 (1.2)	3.8 (1.6)	2.7 (1.3)	3.5 (0.8)
080	2.9 (0.9)	2.6 (0.6)	3.2 (0.3)	1.6 (0.3)	5.0 (0.7)	2.4 (1.4)	2.4 (1.1)	2.0 (1.2)	2.8 (0.5)
157	2.1 (1.0)	2.4 (0.7)	3.4 (0.4)	1.6 (0.4)	1.5 (0.6)	1.5 (0.9)	1.9 (1.1)	2.3 (1.5)	2.1 (0.4)
411	3.0 (0.5)	3.3 (0.4)	3.6 (0.5)	2.7 (0.1)	3.8 (1.0)	2.0 (1.3)	3.0 (1.6)	3.3 (1.1)	3.1 (0.6)
647	3.0 (0.6)	2.9 (0.7)	2.8 (1.0)	1.3 (0.4)	1.8 (0.2)	1.1 (0.0)	1.3 (0.3)	1.7 (0.5)	2.0 (0.4)
653	3.3 (0.5)	2.8 (0.6)	2.9 (0.6)	1.8 (0.9)	1.9 (1.2)	1.9 (1.4)	2.6 (1.4)	2.1 (1.5)	2.4 (1.0)
COLO151	2.6 (1.4)	2.8 (0.6)	3.3 (0.9)	1.7 (0.7)	1.8 (0.4)	1.7 (1.1)	2.3 (1.3)	2.7 (1.9)	2.4 (0.6)
COLO155	2.2 (1.0)	2.7 (0.5)	2.9 (0.8)	1.3 (0.8)	1.8 (0.9)	1.3 (0.8)	1.8 (1.0)	1.9 (1.3)	2.0 (0.6)

Table 5.4 Pyrosequencing results for CIITA-pIV methylation. Cell line and organoid (grouped by non-, weak- and strong- responses to IFNγ) DNA was bisulfite converted prior to PCR and determination of CpG methylation status of CIITA-pIV using pyrosequencing. Control EpiTect methylated and unmethylated DNA was run alongside. All experiments performed in triplicate. Results displayed show the mean methylation percentage at each CpG site and standard deviation of data. The final column is a mean value across all CpG sites in that sample.

5.7 Assessment of H3K9ac and H3K9me2 of CIITA-pIV

Histone regulation of *CIITA* is known to be integral to controlling gene expression (151). Acetylation is associated with an open chromatin conformation and chromatin accessibility, whereas H3K9 methylation is associated with repression of gene expression. H3K9me2 is closely correlated with CpG methylation with higher overall levels of this mark observed in a single line with CpG methylation in the Satoh paper (196).

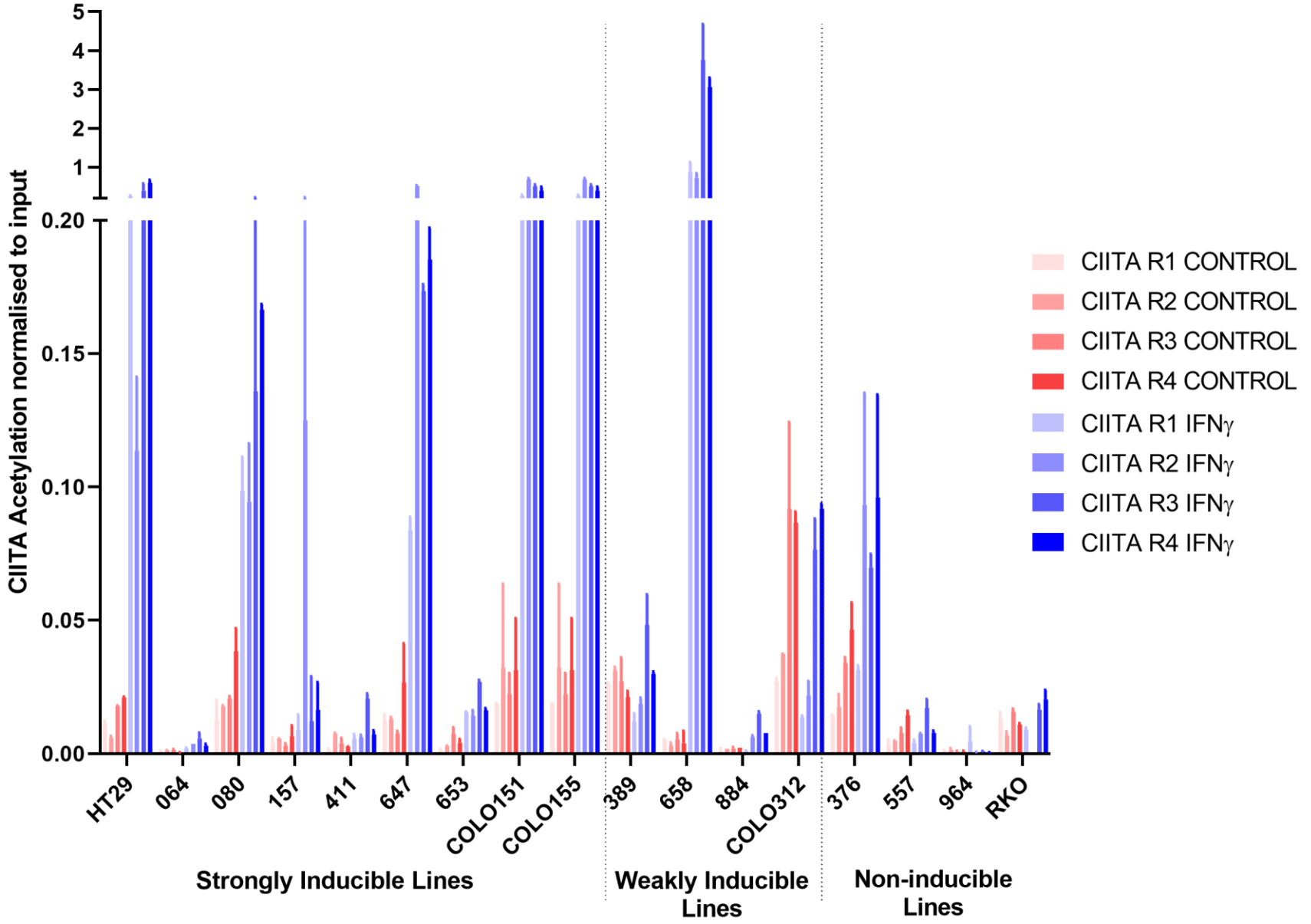
In order to assess if differential acetylation and methylation patterns were observed between the cell lines and organoid Class II response groups, lines were treated for 24 hours with 75 IU/ml IFNγ before generating single-cell suspensions, counting cells and performing cross-linking. All 15 organoids and two cell lines including RKO, a non-inducible CpG methylated example and HT29, a strongly inducible line without CpG methylation were assessed. In order to assess histone modification across CIITA-pIV, a region of around 500 bp, four separate primers pairs were used as described previously (196). Chromatin immunoprecipitation (ChIP) was performed for H3K9ac and H3K9me2 using $1x10^7$ total cells. Eluted DNA underwent SYBR Green qPCR across each of the four *CIITA* regions and was controlled by input DNA. PCR was performed with a standard curve of known concentration of genomic DNA for quantification. Each sample and each region was run in duplicate for both IFNγ stimulated and control cells. Total acetylation was controlled by input DNA and relative change in acetylation with IFNγ (compared to control untreated cells) was calculated for each CIITA-pIV region individually and as a combined mean. Acetylation results are displayed in **Figure 5.8a-c**. Similarly, total methylation

controlled by input, relative H3K9me2 change with IFNγ by region of *CIITA* and as a combined mean across the promoter is given in **Figure 5.9a-c**.

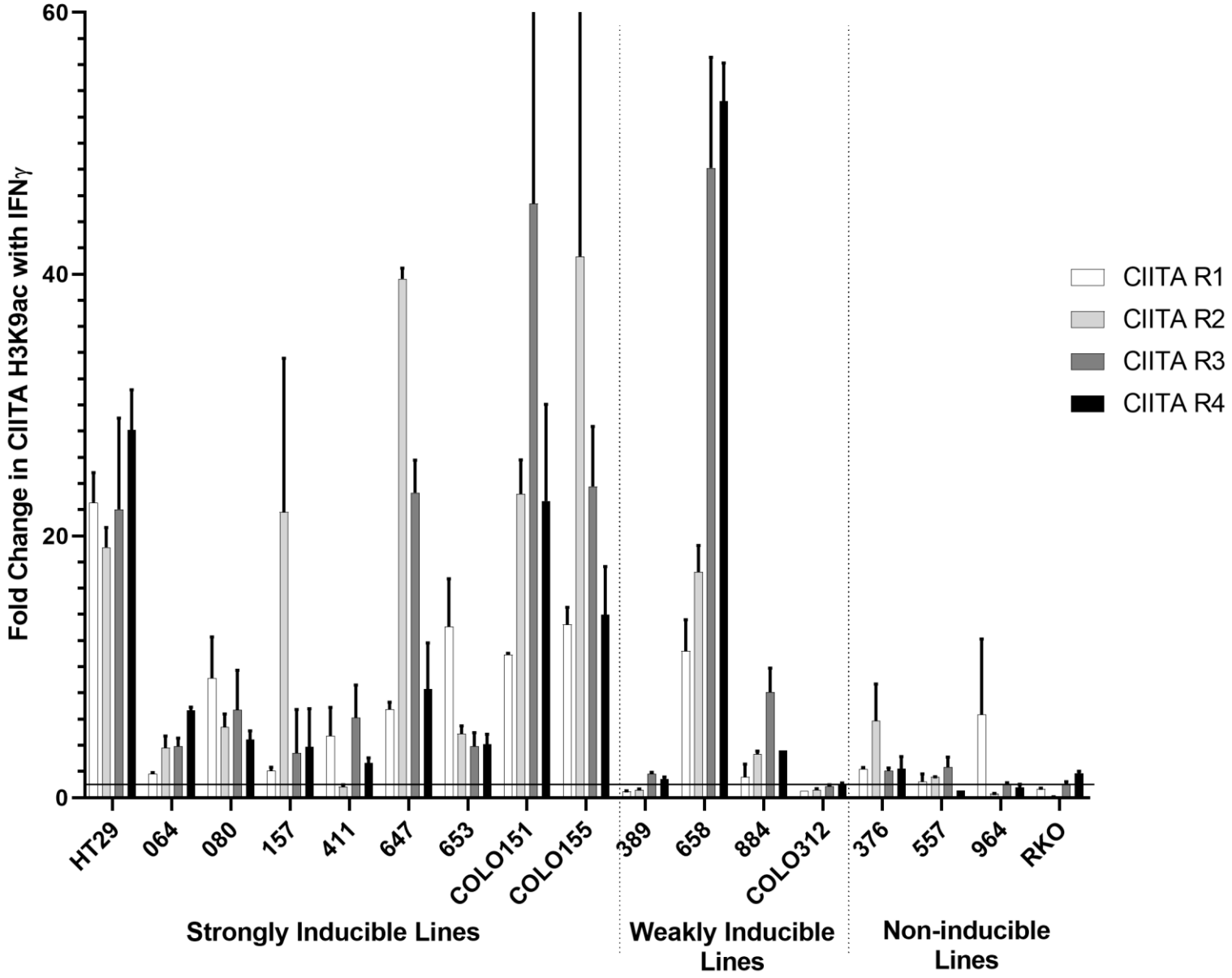
Results of the acetylation ChIP experiments demonstrate substantial induction with IFNγ in the majority of strongly inducible lines when examining total acetylation **(Figure 5.8a)**. Three of the strong lines (064, 411 and 653) have comparably lower levels when reviewing acetylation controlled by input, however, these lines have around a four-fold relative increase in acetylation compared to control (4.1x for 064, 3.6x for 411 and 6.5x for 653; mean fold change in acetylation across CIITA-pIV) (**Figure 5.8c, Table 5.5)**. Conversely, increases in acetylation are reduced in the minimally and non-responsive lines, particularly when considering the relative change **(5.8b&c)**. The one notable exception is 658, which as will be apparent subsequently, appears to have distinct EZH2 occupancy which could explain this high induction of acetylation of *CIITA* despite only minimal Class II surface expression.

Statistical analysis (unpaired T-test) demonstrated statistically significant increases in acetylation in all but two (157 and 411) of the strongly inducible lines, whereas only 658 and 376 from the weak and non-inducible group were significant. **(Table 5.5)**

5.8a


CIITA Acetylation normalised to input
5
4
3
2
1
0.20
0.15
0.10
0.05
0.00
HT29
064
080
157
411
647
653
COLO151
COLO155
389
658
884
COLO312
376
557
964
RKO
Strongly Inducible Lines
Weakly Inducible Lines
Non-inducible Lines
CIITA R1 CONTROL
CIITA R2 CONTROL
CIITA R3 CONTROL
CIITA R4 CONTROL
CIITA R1 IFNγ
CIITA R2 IFNγ
CIITA R3 IFNγ
CIITA R4 IFNγ

5.8b


Fold Change in CIITA H3K9ac with IFNγ
60
40
20
0
CIITA R1
CIITA R2
CIITA R3
CIITA R4
HT29
064
080
157
411
647
653
COLO151
COLO155
389
658
884
COLO312
376
557
964
RKO
Strongly Inducible Lines
Weakly Inducible Lines
Non-inducible Lines

5.8c

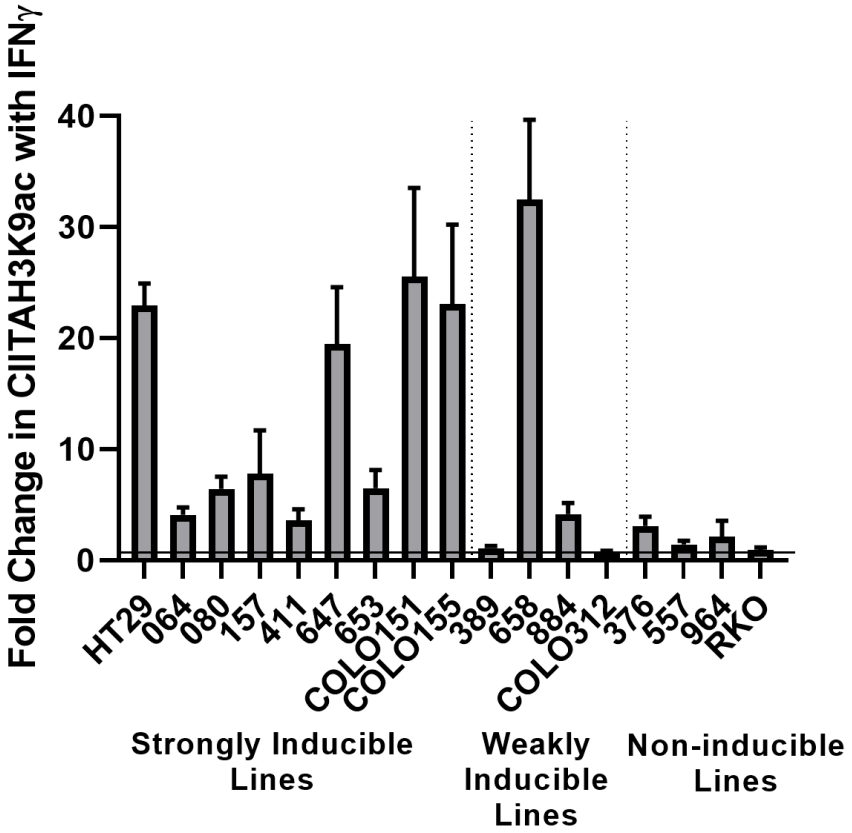
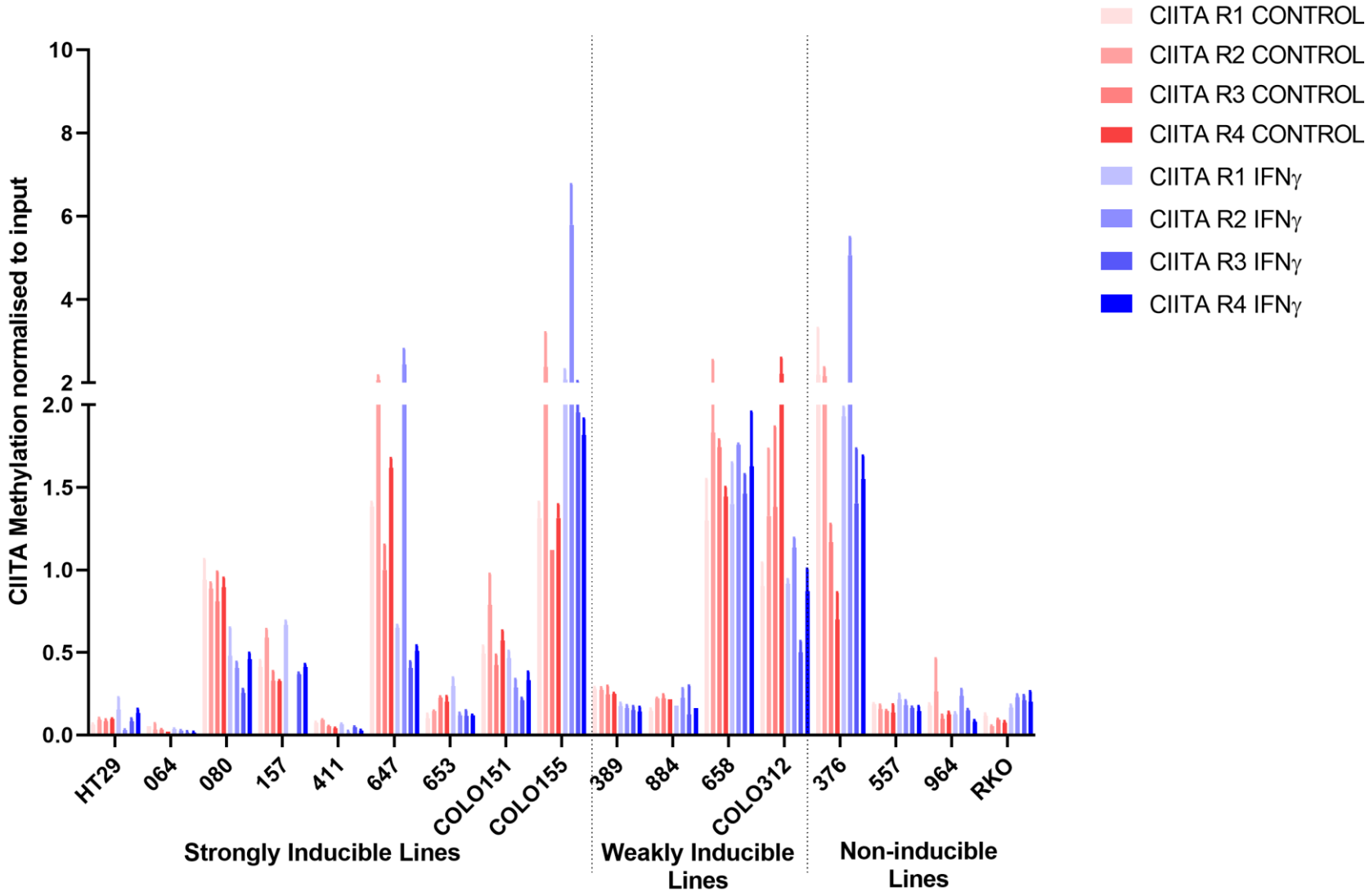
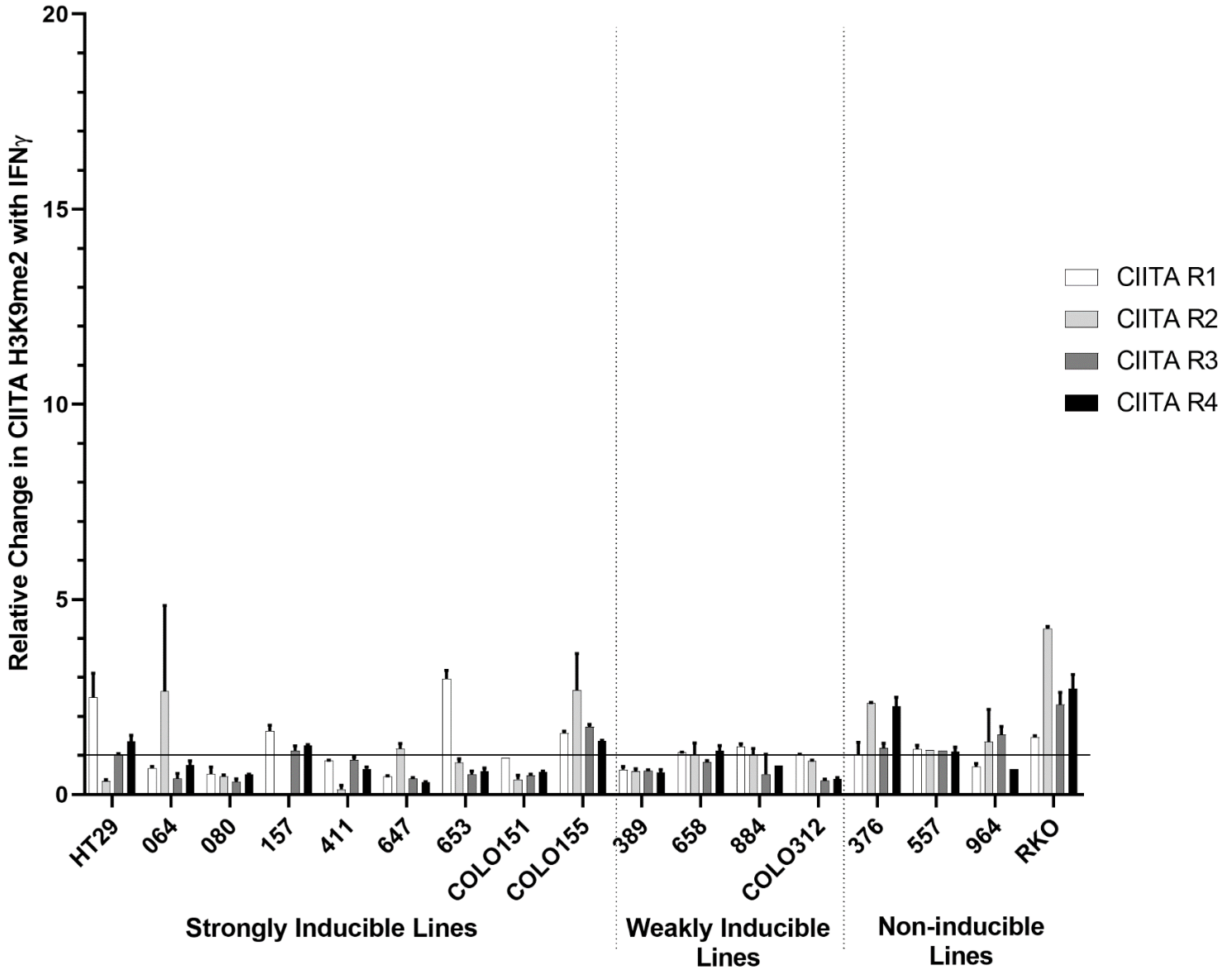


Figure 5.8 CIITA-pIV H3K9 acetylation in cell lines and organoids. (a) Total acetylation for each region of *CIITA* at baseline (red) and following IFNγ (blue) displayed normalised to input DNA. **(b)** Relative change in acetylation for each region of *CIITA* and **(c)** mean relative change in *CIITA* acetylation across all four regions of the promoter. Lines are grouped by Class II flow cytometry response groups and separated by dashed vertical lines. Horizontal lines on relative change graphs represents 1, e.g. the no overall change in acetylation. All results performed in duplicate for both IFNγ and control, with mean and SEM plotted.

5.9a


CIITA R1 CONTROL
CIITA R2 CONTROL
CIITA R3 CONTROL
CIITA R4 CONTROL
CIITA R1 IFNγ
CIITA R2 IFNγ
CIITA R3 IFNγ
CIITA R4 IFNγ
CIITA Methylation normalised to input
10
8
6
4
2
2.0
1.5
1.0
0.5
0.0
HT29
064
080
157
411
647
653
COLO151
COLO155
389
884
658
COLO312
376
557
964
RKO
Strongly Inducible Lines
Weakly Inducible Lines
Non-inducible Lines

5.9b


Relative Change in CIITA H3K9me2 with IFNγ
20
15
10
5
0
CIITA R1
CIITA R2
CIITA R3
CIITA R4
HT29
064
080
157
411
647
653
COLO151
COLO155
389
658
884
COLO312
376
557
964
RKO
Strongly Inducible Lines
Weakly Inducible Lines
Non-inducible Lines

5.9c

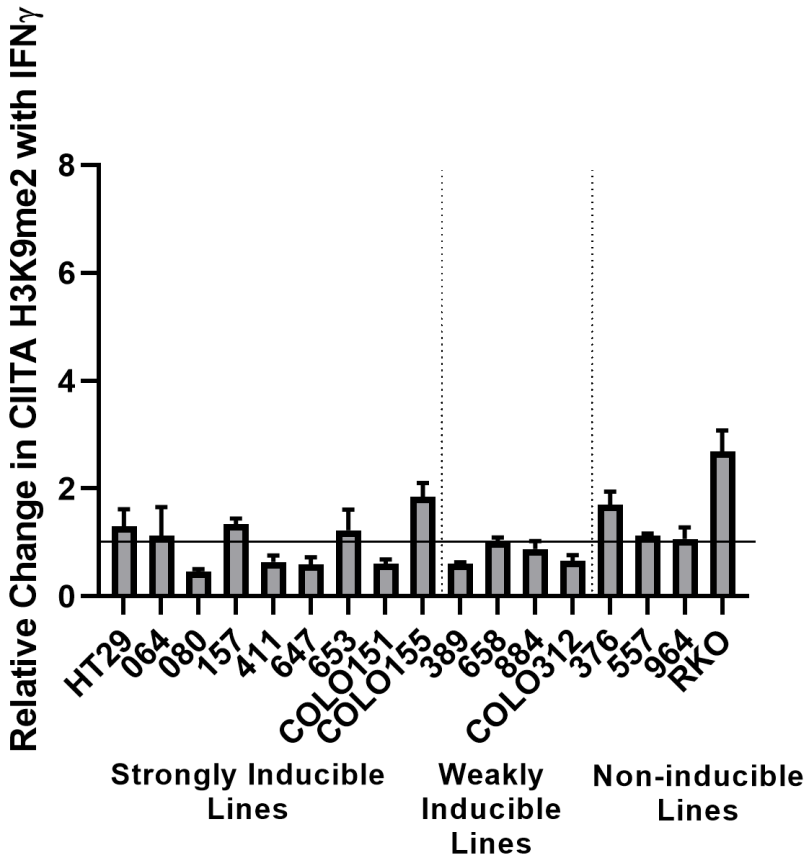


Figure 5.9 CIITA-pIV H3K9me2 in cell lines and organoids. (a) Total methylation for each region of *CIITA* at baseline (red) and following IFNγ (blue) displayed normalised to input DNA. **(b)** Relative change in methylation for each region of *CIITA* and **(c)** mean relative change in *CIITA* methylation across all four regions of the promoter. Lines are grouped by Class II flow cytometry response groups and separated by dashed vertical lines. Horizontal lines on relative change graphs represents 1, e.g. the no overall change in methylation. All results performed in duplicate for both IFNγ and control, with mean and SEM plotted.

Line	Mean Control controlled by input	Mean IFNγ controlled by input	P value	Relative change across *CIITA*
HT29	0.014	0.339	**0.006**	23.0
064	0.001	0.004	**0.012**	4.07
080	0.022	0.124	**<0.001**	6.42
157	0.005	0.041	0.583	7.79
411	0.004	0.010	0.209	3.58
647	0.015	0.241	**0.029**	19.5
653	0.004	0.018	**<0.001**	6.49
COLO151	0.026	0.454	**<0.001**	25.5
COLO155	0.026	0.454	**<0.001**	23.1
389	0.026	0.027	0.988	1.07
658	0.004	2.101	**0.014**	32.4
884	0.002	0.007	0.071	4.15
COLO312	0.061	0.051	0.981	0.753
376	0.028	0.073	**0.046**	3.08
557	0.008	0.009	0.981	1.43
964	0.001	0.002	0.981	2.13
RKO	0.012	0.011	0.988	0.915

Table 5.5 H3K9ac changes with IFNγ. Mean acetylation across all four regions of *CIITA* with and without IFNγ stimulation, mean values represent the proportion of input DNA as determined by qPCR. Statistical significance assessed with unpaired T-test, significant values in bold type. Relative fold change in acetylation expressed as the mean of all four regions of *CIITA*.

Total levels of H3K9me2 were low in the control RKO line (CpG methylated) and were unchanged in the majority of the lines, suggesting minimal role of H3K9me2 in regulating *CIITA* expression. RKO demonstrated the greatest mean increase across *CIITA* (2.7 fold) and was the only line with a statistically significant increase in H3K9me2 following IFNγ, with three lines (080, COLO151 and 389) exhibiting significantly decreased CIITA-pIV H3K9me2 with IFNγ (**Figure 5.9 and Table 5.6)**. The lines with relatively high total H3K9me2 in the strongly inducible group (647 and COLO155) also exhibited some the strongest relative increases in H3K9ac, suggesting that this level of methylation is not relevant to the silencing of *CIITA*, particularly as these lines express high levels of Class II (**Figure 5.9a and 5.8c)**. These findings are consistent with Truax et al, who found a decreasing trend in H3K9me3 with time following IFNγ in inducible lines (212). The lines with only weak expression of Class II show stable or reducing H3K9me2, suggesting no functional

role. The non-inducible lines, with suspected IRF1/STAT1 additionally exhibit no significant change, consistent with loss of regulation at the top of the pathway above the level of *CIITA* and therefore no overall activation of *CIITA* in these lines (**Figure 5.9b,c**).

Line	Mean Control controlled by input	Mean IFNγ controlled by input	P value	Relative change across *CIITA*
HT29	0.084	0.101	0.930	1.29
064	0.035	0.023	0.837	1.12
080	0.882	0.400	**<0.001**	0.45
157	0.415	0.482	0.930	1.34
411	0.065	0.038	0.237	0.639
647	1.518	1.002	0.837	0.593
653	0.168	0.162	0.984	1.22
COLO151	0.570	0.324	**0.044**	0.600
COLO155	1.533	2.912	0.507	1.84
389	0.261	0.157	**<0.001**	0.602
658	0.202	0.173	0.930	1.02
884	1.579	1.562	0.984	0.876
COLO312	1.457	0.855	0.211	0.656
376	1.557	2.489	0.837	1.70
557	0.156	0.176	0.837	1.13
964	0.166	0.147	0.963	1.06
RKO	0.083	0.202	**<0.001**	2.68

Table 5.6 H3K9me2 changes with IFNγ. Mean methylation across all four regions of *CIITA* with and without IFNγ stimulation, mean values represent the proportion of input DNA as determined by qPCR. Statistical significance assessed with unpaired T-test, significant values in bold type. Relative fold change in methylation expressed as the mean of all four regions of *CIITA*.

Strongly inducible lines, therefore, acetylate *CIITA* H3K9 following IFNγ as expected with minimal changes overserved in the non-inducible lines. The group of interest, the lines with only weak responses to IFNγ, do have reduced acetylation (except for 658) compared with the strong lines, but this does not appear to be either secondary to CpG methylation or H3K9 methylation. It is therefore possible that EZH2 (and H3K27me3) is the important regulatory difference in these four lines.

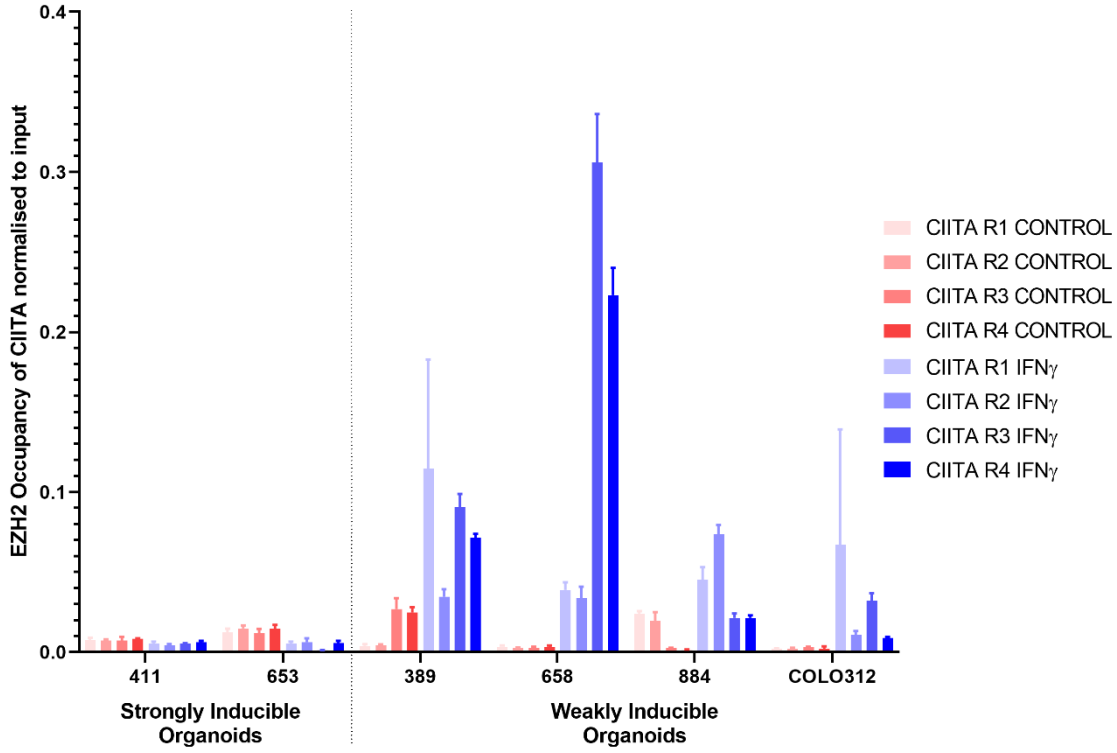
5.8 Assessment of EZH2 occupancy

The four weakly inducible organoid lines (389, 658, 884 and COLO312) bear close resemblance to a group of MDA-MB-435 cell lines described by Truax et al. Cells from this cell line were allowed to metastasise within mouse models, with the variants with greatest metastatic potential exhibiting the lowest Class II expression (212). Interestingly, these lines exhibited weak upregulation of Class II expression with IFNγ, to between 30-50%. Additionally, these lines had delayed kinetics of Class II expression, taking 72 hours to reach maximal levels (which will be assessed in Chapter 6) and were not found to be CpG methylated, nor controlled by H3K9me2. Instead, the weakly-inducible lines were found to have increased CIITA-pIV occupancy by EZH2 following IFNγ in contrast to strongly-inducible cell lines, where occupancy decreased following stimulation.

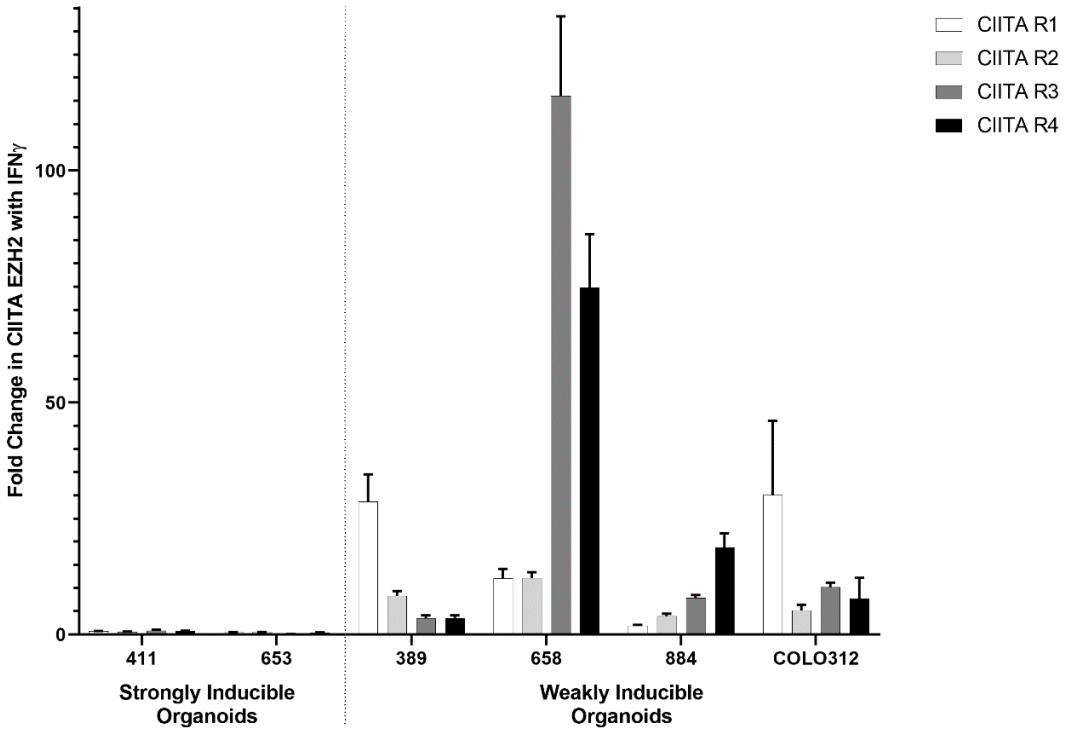
The four weakly-inducible organoid lines therefore were assessed for EZH2 occupancy (of the *CIITA* promoter) following IFNγ stimulation and were run for comparison alongside two strongly-inducible lines (411 and 653). As before, organoids were treated for 24 hours with 75 IU/ml IFNγ, before generating single-cell suspensions, dual-crosslinking and assessing with ChIP PCR. Each line and condition was performed as four replicates and controlled with input DNA. EZH2 binding is highly correlated with the H3K27me3 repressive mark. Previous attempts by our laboratory to assess H3K27me3 have found the previously published antibodies to be unreliable and generated poor quality data. The EZH2 antibody (Abcam, UK, #ab195409) by contrast has been used reliably. As EZH2/H3K27me3 is so strongly correlated, assessment of EZH2 alone has therefore been performed (190, 212). As with the acetylation and methylation data, total EZH2 occupancy of

CIITA and relative change across each region of *CIITA* and total mean change is given in **Figure 5.10**. The strongly inducible lines demonstrated low levels of EZH2 binding and furthermore, this was significantly reduced following IFNγ stimulation (relative change: 411 0.73-fold reduction p<0.001, 653 0.35-fold reduction p<0.001). By contrast, the weakly inducible lines had evidence of increased EZH2 occupancy following IFNγ stimulation, with a relative increase of 11.0-fold for 389 (p<0.001), 8.2-fold for 884 (p=0.001) and 13.3-fold for COLO312 (p=0.025). 658 exhibited a very high level of EZH2 binding, increasing by 53.8-fold (p<0.001) with IFNγ, statistics assessed with an unpaired T-test.

5.10a



5.10b



5.10c

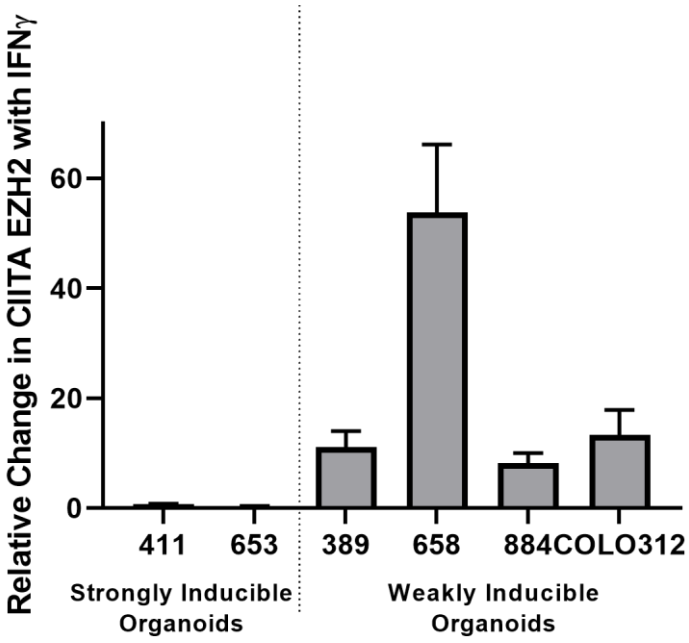


Figure 5.10 CIITA-pIV occupancy by EZH2. (a) Total EZH2 occupancy for each region of *CIITA* at baseline (red) and following IFNγ (blue) displayed normalised to input DNA. **(b)** Relative change in EZH2 occupancy for each region of *CIITA* and **(c)** mean relative change in EZH2 occupancy across all four regions of the CIITA-pIV. Two strongly-inducible lines are displayed for comparison with the four weakly-inducible lines, separated by vertical dashed line. All results performed with four replicates for both IFNγ and control, with mean and SEM plotted.

An attenuated response to IFNγ stimulation caused by increased EZH2 binding to the CIITA-pIV is displayed by the four weakly-inducible organoids. Assessment of longer exposures to IFNγ, as well as the role of EZH2 inhibition, will be assessed in the next chapter.

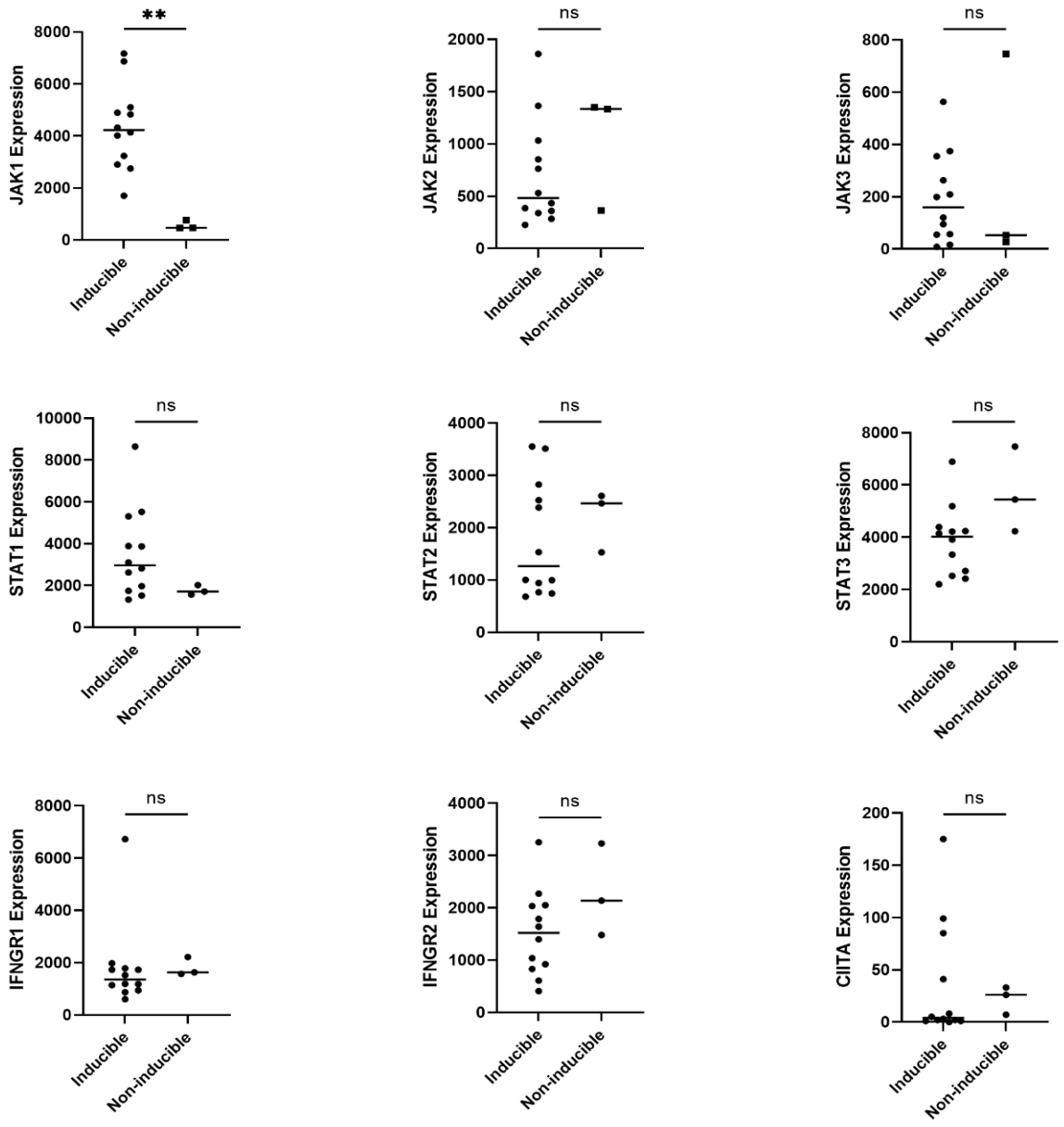
5.9 Genetic determinants of Class II inducibility in organoids

In the non-inducible organoids (376, 557 and 964), whole-genome sequencing data was interrogated for mutations in IFNγ signalling pathway including *IFNGR1/2*, *JAK1/2, STAT1-6, B2M, HLA-A,B,C* and *HLA-DR,DP,DQ*. Results were filtered for either missense or stop-gain mutations within these pathway genes, however, no obvious classical causal mutations were identified, although interestingly all three non-inducible lines had *STAT6* mutations. 964 had evidence of a missense mutation (p.Ala321Glu) within the STAT binding domain according to PFAM data and has been characterised as a somatic mutation in liver cancer previously (COSMIC ID: COSM6267107). It is unlikely to be a single-nucleotide polymorphism (SNP) as it is rarely observed with minor allele frequency (MAF) of 0.000008/2 (rs767707263; according to dbSNP). Both 376 and 557 had evidence of a different missense mutation within the SH2 binding domain of *STAT6* (p.Arg605Gln). Again, this mutation is unlikely to be a SNP with MAF of 0.000004/1 (rs1267549866; dbSNP). STAT6 activation previously has been shown to block IFNγ responsiveness, downregulating and antagonising STAT1 activation, so whilst not classically described there is a potential biological mechanism (269). Whilst these mutations are likely to be functionally important as they involve protein binding domains, this analysis remains speculative at this stage and it is not known whether these mutations would confer gain or loss of function. Potential future work would look to

validate this finding via transfection into cell lines and reassessing IRF1/STAT1 responses following IFNγ stimulation with western blot.

Whilst anticipating that these non-responsive lines would harbour a canonical *JAK1* or *STAT1* mutation as previously described, it is worth noting that these findings have typically been identified as mechanisms of immunotherapy resistance, rather than in an immunologically cold MSS CRC tumour. The finding of *STAT6* mutations in all three tumours of this hitherto unexplored disease subset is nonetheless intriguing. Additionally, loss of STAT1/IRF1 responsiveness has been reported as a functional consequence of *RAS* mutation and in CRC, a MAPK driven tumour, this mechanism is also potentially relevant. Several interferon responsive genes were found to be silenced, with others confirming that this was caused by transcriptional repression that could be reversed with 5-azacytidine (108, 270). In order to identify if loss of expression, rather than mutation, was responsible for loss of IFNγ responsiveness in the non-inducible organoids, an exploratory analysis of RNAseq data was performed. IFNγ pathway genes (including *JAK1-3, STAT1-3 and IFNGR1-2*). Very low levels of *JAK1* expression were observed in the non-inducible lines, with this found to be highly significant (p=0.0044, Mann-Whitney test) compared to the inducible lines, likely indicating loss of *JAK1* expression (**Figure 5.11a**). Lower levels of *JAK3* and *STAT1* were also seen, however these were not significant. *CIITA* expression, under these baseline conditions were also not significantly different between groups. In the Class I negative organoids β2 microglobulin (*B2M*) levels were significantly reduced (**Figure 5.11b**), indicating the likely mechanism for Class I loss in these lines.

a



b

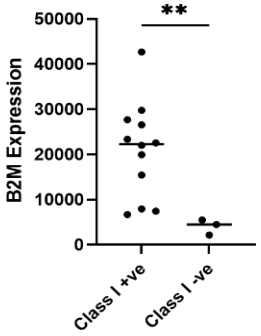


Figure 5.11 RNA expression of IFNγ response pathway genes. RNAseq expression data for IFN**γ** response genes **(a)** in Class II inducible and non-inducible CRC organoids and *B2M* **(b)** expression between Class I positive and negative lines. Individual values with mean displayed, statistical assessment with Mann-Whitney test: NS $P \geq 0.05$; * $P < 0.05$; ** $P < 0.01$

JAK1 loss of expression has previously been implicated in loss of IFNγ response in lung cancer cell lines, with epigenetic silencing of *JAK1*. DNMT and HDAC inhibition restored *JAK1* expression, facilitating STAT1 response to stimulation again. Further analysis of the *JAK1* transcription factor binding site in the organoid WGS data revealed mutations in two of the three non-inducible lines with absent *JAK1* RNA expression. The non-protein coding regions involved were Ch1:64966765 (G>A) in organoid 376 and Ch1:64967061-62 deletion (AA) in line 557. Further validation of the mechanism of *JAK1* loss in these lines is ongoing, including western for protein expression, IHC on tumour sections for JAK1 (to be followed up with multispectral IHC panel) and promoter methylation of *JAK1*.

Further analysis of the transcriptional background of the non-inducible lines was performed, with analysis of total RNA sequencing data from all 15 lines. Gene set analysis (GSA) was performed in Partek Flow, with a comparison of non-inducible lines vs weakly/strongly-inducible lines. Filtering was performed to identify transcripts differentially expressed ≥ or ≤ 2 fold, to a significance of $p<0.05$. Volcano plot of differentially expressed genes is given in **Figure 5.12.** Hierarchical clustering revealed a distinct expression signature between the non-inducible and inducible lines, displayed in **Figure 5.13.** Principal component analysis (PCA; performed in R) of the 15 organoids revealed similarities in transcriptional profiles between non-inducible and inducible lines. 658 was a notable outlier in this initial analysis, and therefore the PCA was repeated excluding 658. **(Figure 5.14)** A total of 1564 differentially expressed genes were identified.

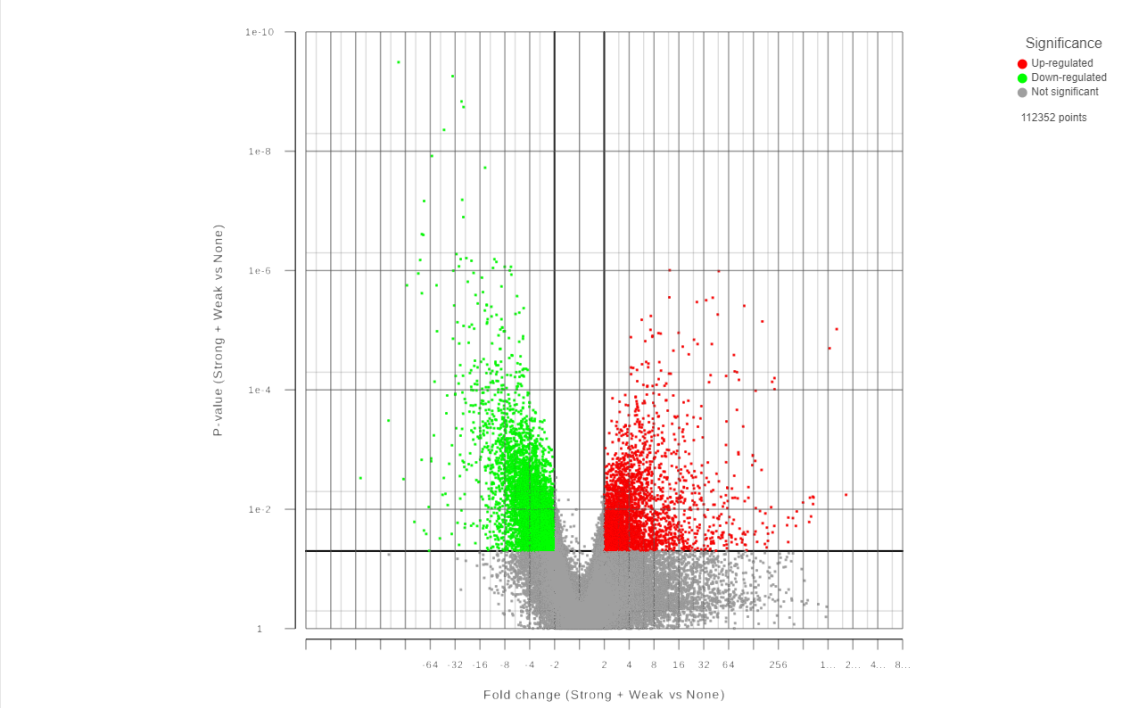


Figure 5.12 Differential RNA expression in non-inducible organoids. Volcano plot of differentially expressed RNA between strongly/weakly inducible organoids vs non-inducible lines. Expression changes filtered by less than or greater than 2 fold change and p≤0.05. Image produced in Partek Flow.

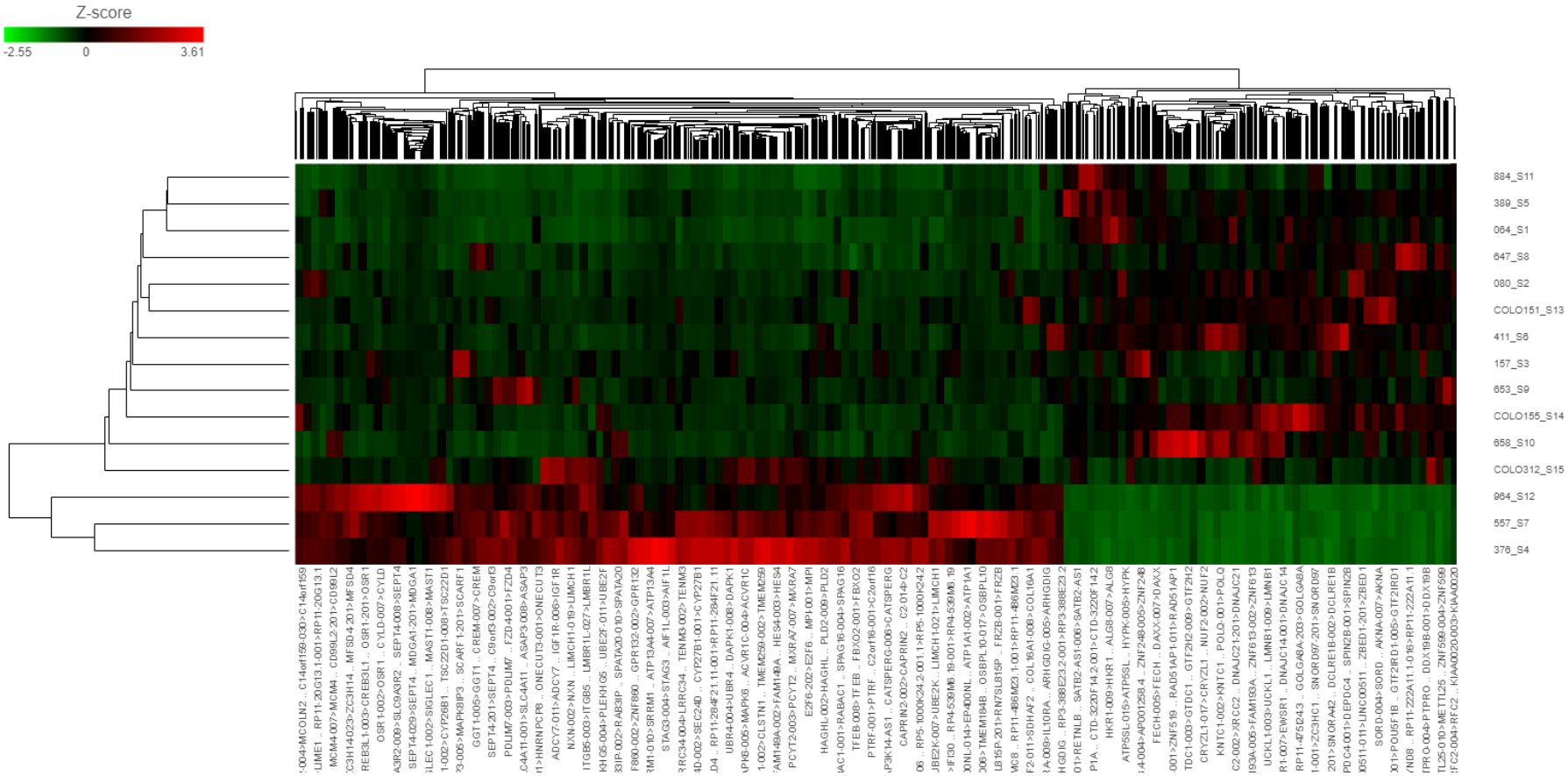


Figure 5.13 Hierarchical clustering of expression data for non-inducible organoids. Differential gene expression reveals distinct transcriptional signature for organoids with Class II non-inducibility. Genes in red upregulated and those in green downregulated.

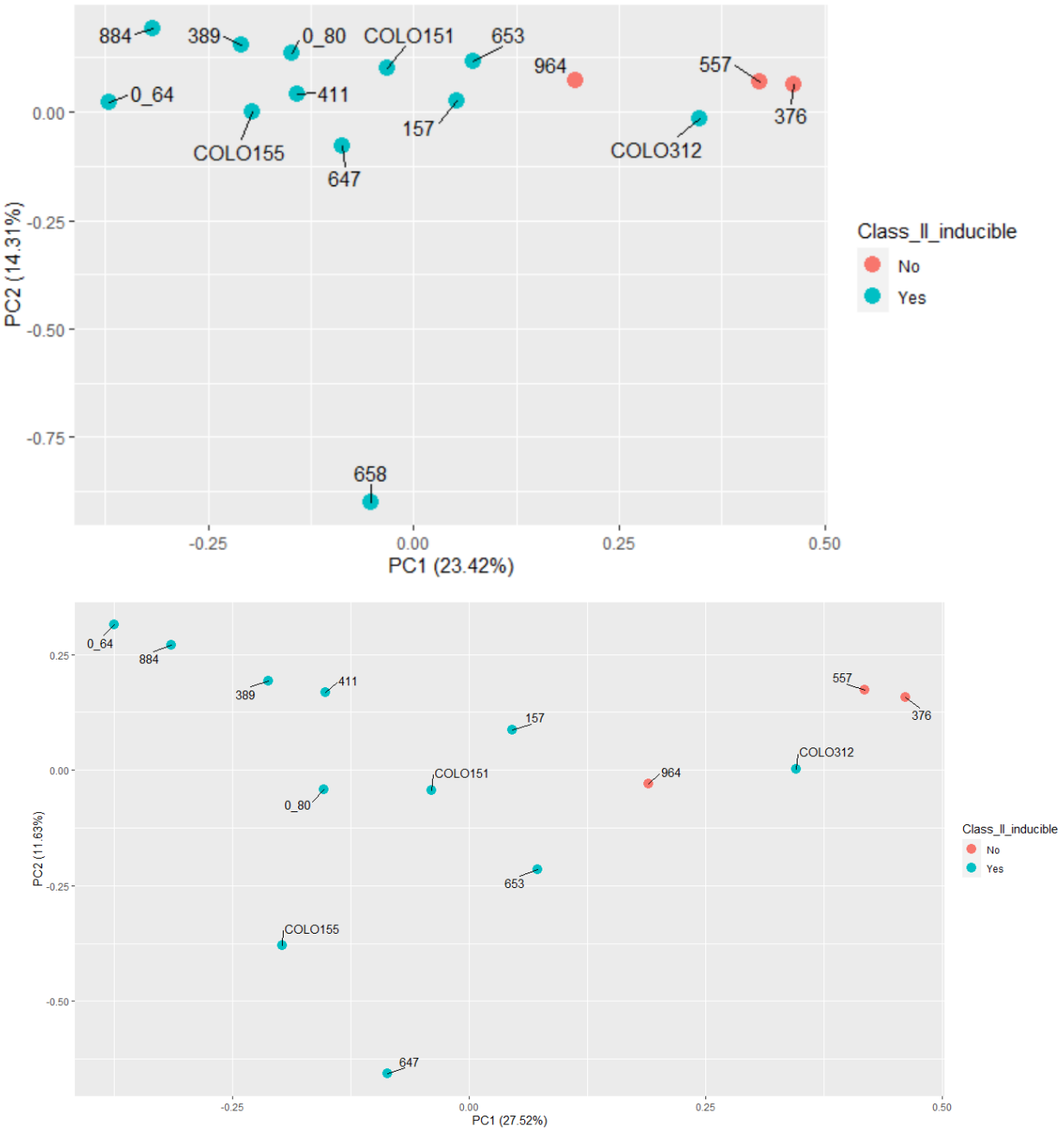


Figure 5.14 Principal Component Analysis (PCA) Analysis of RNA expression profiles of 15 organoids, with non-inducible lines represented in orange, inducible lines in teal. PCA provides a 2D spatial representation of the transcriptional heterogeneity between line characteristics. 658 was found to be a significant outlier **(top)** and therefore analysis was repeated **(bottom)** excluding this line, reducing anomaly. Non-inducible lines are noted to cluster, along with COLO312, with similar findings evident in the hierarchical clustering analysis

Pathway enrichment analysis was then performed using Clusterprofiler package via R, with kind support from Dr Akshay Patel. Kyoto Encyclopaedia of Genes and Genomes (KEGG) and Gene Ontology (GO) enrichment analysis were performed using a cut off of FDR <0.05. Analysis was repeated both with and without the exclusion of 658, the outlier identified on PCA. Few differences were seen between pathway enrichment outputs without 658, other than changing the ordering of 'hits.' A number of steroid synthesis pathway were identified in the non-inducible organoids (**Figure 5.15b**) which were no longer observed after exclusion of 658. GO analysis of Class II inducible organoids demonstrated upregulated DNA repair, recombination and replication pathways. Non-inducible organoids, after 658 exclusion, had upregulated energy pathways, cellular respiration and aerobic metabolism pathways **(Figure 5.15)**. KEGG pathway analysis identified seven pathways **(Table 5.7)** to be enriched. Pathways related to steroid metabolism were again identified, with the most significant hit 'bile secretion,' which is closely related to steroid production and cholesterol metabolism. KEGG pathway for the retinol metabolism pathway is given in **Figure 5.16**. Members of this pathway, including *CYP1A1* are known to be overexpressed in cancers including CRC, with a potential role in carcinogenesis and arachidonic acid metabolism (271). Additionally, steroid metabolism including generation of tissue oestrogens has been implicated in CRC proliferation and progression (272).

KEGG identifier	Descriptor	Gene Ratio	Adjusted P-value
hsa04976	Bile secretion	21/539	0.000132
hsa00040	Pentose and glucuronate interconversions	12/539	0.000188
hsa03030	DNA replication	10/539	0.0104
hsa00860	Porphyrin and chlorophyll metabolism	10/539	0.0311
hsa00830	Retinol metabolism	13/539	0.0314
hsa00053	Ascorbate and aldarate metabolism	8/539	0.0314
hsa00140	Steroid hormone biosynthesis	12/549	0.0314

Table 5.7 KEGG pathway enrichment. Pathway analysis across the 14 organoids (excluding 658) revealed 7 differentially expressed pathways.

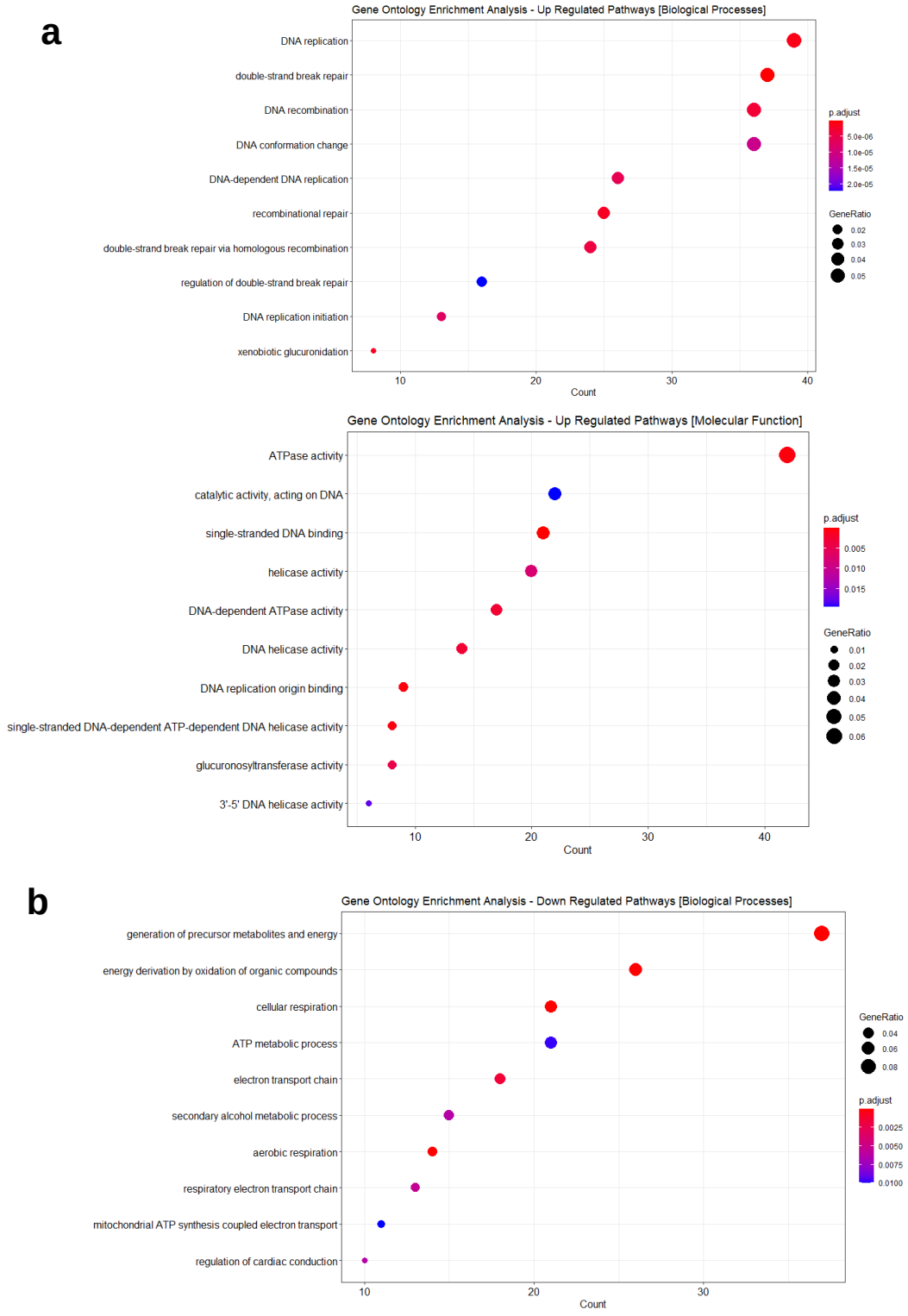


Figure 5.15 Gene Ontology analysis of Class II inducible (strong/weak) vs non-inducible organoids. Upregulated GO terms in inducible **(a)** and non-inducible **(b)** lines. Size of circle represents proportion of genes enriched within the respective GO term, colour represents significance (see legend).

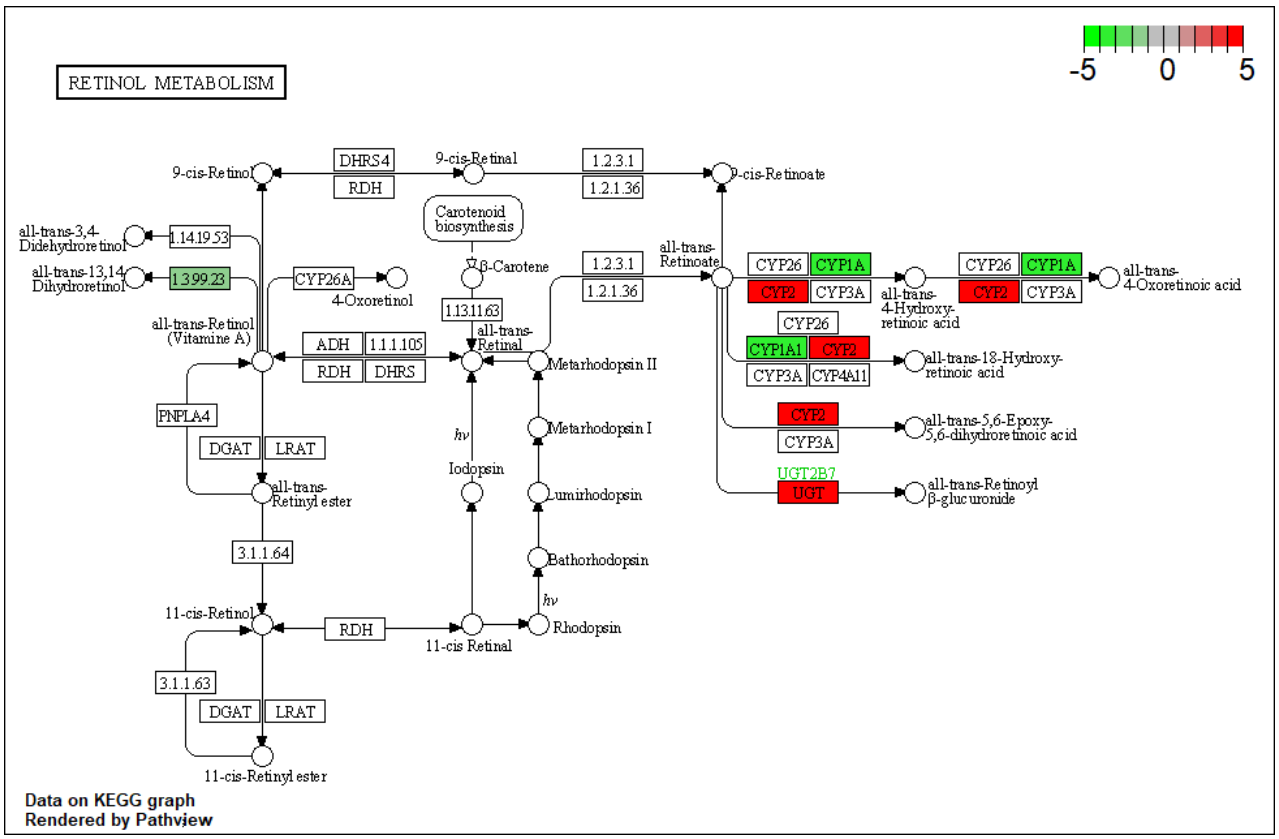


Figure 5.16 KEGG pathway display for retinol metabolism. Retinol metabolism pathway differential expression in organoids. 'Green' transcripts were upregulated in non-inducible organoids, with 'red' upregulated in inducible organoids.

Again these observations remain speculative at this stage and biologically it seems unlikely that local steroid synthesis would lead to complete IFNγ pathway unresponsiveness in these non-inducible organoids. Steroid production however could be more broadly associated with an immunosuppressed TME, which in combination with a cell-intrinsic loss of IFNγ sensitivity, would provide a major barrier to immunotherapy response. Additionally, several GO steroid pathways were no longer significant after the exclusion of 658 and therefore the true significance of these findings is less certain. Early discussions with local groups (PIs Prof Wiebke

Arlt and Dr Paul Foster) with expertise in steroid metabolism are underway and future work will look to validate these findings.

5.10 Summary and discussion

This collection of colorectal organoids has revealed that three groups of responses in Class II expression following IFNγ can be identified. Firstly, a group that completely fail to respond to IFNγ, with no change in Class II expression and a loss of IRF1/STAT1 upregulation, suggesting a defect at the top of the pathway. The mRNA levels of *CIITA* remain low in these lines, in support of a proximal pathway defect. Futhermore, no significant change in acetylation or methylation is observed in these three lines, except for 376 which demonstrates a significant but comparably modest increase in acetylation (3.08-fold) compared to control. There was no evidence of CpG methylation in these lines to account for their unresponsiveness. Whole-genome sequencing failed to identify a clear cause of this, for example, *JAK1* mutation (though two may have promotor mutations) and this may therefore represent a functional loss similar to downregulation of the pathway described in RAS mutant lines (108). Whilst the exact mechanism of *JAK1* expression loss has not been identified, the ongoing work to confirm this finding on IHC (currently being run by Dr Neeraj Lal) could prove valuable. Multiple mechanisms of *JAK1* loss (mutation, promotor mutation, epigenetic) may converge on loss of JAK1 protein on IHC, which could be used as a rapid and affordable biomarker for cancers less likely to respond to ICB. RNAseq demonstrated transcriptional differences between these non-inducible lines and the weakly/strongly inducible lines. Interestingly, steroid synthesis pathways appeared to be upregulated in the non-inducible lines, with future work planned within the group to explore these findings and validate them.

A second group, representing the majority (eight of fifteen lines) exhibit high levels of Class II expression at 24 hours following IFNγ. Unsurprisingly, they have significantly increased responses in *CIITA* mRNA and corresponding H3K9 acetylation and methylation patterns across CIITA-pIV in keeping with chromatin accessibility, with induction of acetylation and stable or decreasing methylation observed following IFNγ. Two of the representative lines from this group also have low levels of EZH2 occupancy across *CIITA* and again this appears to decrease or remain stable at low levels following IFNγ. A number of these strongly-inducible organoids arise from tumours without Class II expression on primary tumour IHC, indicating that IFNγ deficiency and failure of immune cell ingress and activation is likely the functional barrier to immune responses in these tumours.

The final group of four organoids represent an intermediate group, with weak induction at 24 hours of Class II with IFNγ only. Again, no evidence of CpG methylation at *CIITA* can be found to explain this and there is evidence of transcriptional activation of *CIITA* with increasing mRNA following IFNγ, albeit at lower absolute levels compared with the strongly-inducible lines. The ChIP data in these four lines exclude significant H3K9 methylation as the cause of the reduced Class II expression, though low-level acetylation only is observed in three of the lines. The crucial difference across these four lines appears to increased binding of EZH2 to CIITA-pIV following IFNγ (and therefore likely concomitant H3K27me3) causing restriction of Class II expression. Where this mechanism has previously been described (212), delayed responses to IFNγ have also been reported. Time-dependent changes, along with pharmacological reversal of EZH2 effects will be considered in Chapter 6.

The results from the cell lines are as expected from the literature, with evidence of CpG methylation in two lines. The inducible HT29 line shows strong increases in acetylation in the ChIP experiments and minimal H3K9me2. RKO, the CpG methylated line has a minimal change in acetylation and even demonstrates a small increase in H3K9me2. DLD1 is the one slightly unusual line, with minimal CpG methylation and only weak expression of Class II. ChIP has not been performed in this cell line, due to time and cost constraints, but it is possible that EZH2 binding could be the underlying cause of this in this cell line.

The complete absence of CpG methylation in any of the fifteen organoids is important. The two control cell lines (RKO and HCT116) and control methylated DNA were shown to be methylated as previously described, demonstrating that the experimental technique is reliable. CpG methylation is therefore very likely to be a cell culture-induced change in 2D culture, with the reported findings in the literature in cell lines likely to be irrelevant to actual tumour biology. This is in keeping with a paper performing primary tissue assessment of Class II negative MSI-H CRC tumours, which were all shown to be unmethylated unlike the cell lines examined in parallel (185). Similarly, studies of trophoblast cell lines that demonstrated CpG methylation of *CIITA*, failed to show the same in primary trophoblast tissue that had not been subjected to prolonged time in 2D culture (208). The data presented here also demonstrate that *CIITA* methylation is not required to cause loss of Class II inducibility, with total loss observed following IFNγ pathway defects and attenuation of Class II expression through EZH2-mediated control of CIITA-pIV observed. The translational relevance of these findings is that the use of ICB in combination with epigenetic modifiers to increase Class II expression and enhance immunotherapy

response is unlikely to be successful, in keeping with a small number of phase II studies in this area (214, 273).

Chapter 6: Reversing loss of Class II inducibility

6.1 Introduction

Results from Chapters 4 and 5 revealed three main subgroups of IFNγ responsiveness and Class II inducibility in this collection of CRC organoids. The first group, representing the majority (53%) of lines were able to strongly (>50% of cells) express Class II by 24 hours following IFNγ stimulation. Importantly, four of these strongly inducible lines were derived from primary tumour microenvironments with low levels of Class II (<10%) and two of these tumours were completely negative. In these tumours, the lack of Class II expression in the tumour is fundamentally likely to be as a result of inadequate T cell trafficking into tumours or failure to produce IFNγ by intratumoural T cells. The cancer cells comprising these tumours have no cell-intrinsic restriction of Class II inducibility.

The second group of tumours, comprising three organoids (20%), demonstrated a complete failure to upregulate Class II with IFNγ. Importantly, in contrast to previously described cell line models (196), these cell lines were not CpG methylated at the CIITA-pIV locus and they failed to significantly acetylate *CIITA* or express *CIITA* mRNA in response to IFNγ. However, the loss of *CIITA* expression (and failure to acetylate) appeared to be the result of the loss of the STAT1/IRF1 signal transduction response, as has been reported in cancer as a route to immune escape (182).

The final group of four organoids (27%) demonstrated an intermediate response, with weak (<50%) expression of Class II observed at 24 hours. *CIITA* mRNA expression was seen, albeit at a lower magnitude compared with the strongly inducible group.

Whilst acetylation appeared attenuated in two of these lines, the other two demonstrated significant increases in acetylation, with the highest induction of any line seen in 658. These lines also lacked evidence of CpG methylation of CIITA-pIV and in keeping with this, the CpG methylation-linked repressive histone mark, H3K9me2, was not found to be increased. The role of EZH2 occupancy of CIITA-pIV was therefore assessed, as this has been described in cell lines with similar weak expression of Class II, with these cell lines also displaying a delayed IFNγ response, requiring up to 72 hours to reach maximal Class II expression (212). EZH2 occupancy of *CIITA* strikingly increased in all four of these weakly-inducible organoid lines following IFNγ stimulation, in contrast to the strongly inducible lines where EZH2-CIITA occupancy decreased following treatment. This differential EZH2 response appears therefore to determine the speed and amplitude of Class II expression, consistent with the literature.

EZH2 forms part of the polycomb repressive complex 2 (PRC2), with the recruitment of EZH2 to promoters highly correlated to epigenetic silencing through H3K27me3. PRC2 alterations, including *EZH2* overexpression and gain-of-function mutations, have been reported in multiple cancer types and is associated with poorer prognosis and more aggressive cancer phenotype. A broad range of PRC2-related mutations are found in cancers aside from *EZH2*, including mutations in the H3K27 demethylase enzyme (UTX) and loss of function of the SWI/SNF/BRG-1 complex which competes with EZH2 and is particularly important for *CIITA* expression (152, 153, 274). Several inhibitors targeting EZH2 have been developed and therefore to confirm the role of EZH2 in the observed attenuation of IFNγ responsiveness, the pharmacological reversal of EZH2 restriction of Class II expression will be attempted.

6.1.1 Aims and Objectives

1. To assess the effect of longer durations of IFNγ stimulation in lines with increased EZH2 *CIITA* occupancy
2. To assess the potential reversibility of reduced Class II expression using pharmacological EZH2 and HDAC inhibition
3. Examine genomic determinants of EZH2 behaviour in organoids

6.2 Validation of EZH2 inhibitor (GSK126) and HDACi (Entinostat) dose

GSK126 is a highly selective competitive inhibitor of EZH2. It exhibits both direct cytotoxic effects at higher doses, as well as having a role as an epigenetic modifier through reducing levels of H3K27me3 and de-repression of silenced genes. GSK126 possesses similar efficacy against both wild-type and mutated EZH2. GSK126 exhibits activity against the majority of histone methyltransferases, most are >1000 fold-less inhibited than EZH2, with even EZH1 (with highly conserved sequence homology compared with EZH2) inhibited at less than 150 fold sensitivity (236). Although very few compounds have been studied in depth in colorectal organoid panels, surprisingly a panel of twenty CRC organoids was treated with GSK126, revealing variable cytotoxicity between lines. Proficiency of p53 was found to sensitise lines to GSK126 treatment, with these lines exhibiting marked loss of viability even at low doses (<2 μM). Some lines had evidence enhanced growth at low doses (1-2 μM) before exhibiting linear decreases in viability between 2-8 μM. The enhanced growth is thought to potentially be secondary to de-repression of pro-oncogenic genes and interestingly some myelodysplastic syndromes have evidence of *EZH2* loss of function mutations as part of the disease process (238). Similar

results in human colorectal cell lines (HCT116, HT29 and COLO205) were observed, whilst 2 µM doses were tolerated, significant cytotoxicity was observed at 5 µM in all lines and no additional reduction in H3K27me3 was seen between 2 and 5 µM (240). Epigenetically, promoter-specific H3K27me3 levels were reduced effectively at doses of 1.5 µM after four days with no further changes seen with doses up to 20 µM. Minimal increases of target gene expression were seen before three days, with this increasing significantly by day six (239). Given the unpredictable cytotoxicity of GSK126 reported between different cancer lines, the decision was taken to screen drug sensitivity across the lines of interest. This will enable a dose of GSK126 that is likely to cause changes in EZH2 activity but not be overly cytotoxic to be selected.

A range of GSK126 concentrations between 0 and 10 µM was assessed in the four lines with evidence of increased EZH2 binding to CIITA-pIV following IFNγ. Organoids were dissociated to single cells, counted and 1000 cells per well were plated in matrigel, allowing small organoids to reform over 72 hours. GSK126 was added and incubated together with the organoids for a further 72 hours, before the addition of CellTiter-Glo 3D Cell Viability Assay and measurement of luminescence on a microplate reader. An ATP standard curve was performed alongside to ensure assay linearity as per the protocol. Results are displayed in **Figure 6.1**. Viability readings were found to increase at low concentrations (up to 2 µM GSK126) in two of the lines (884 and COLO312) as previously reported (238). 658 was the most sensitive to GSK126, however, viability remained relatively preserved (relative 69%) at the 2 µM dose. A dose of 2 µM for six days was therefore selected for future experiments based on this data and the previously published data outlined above.

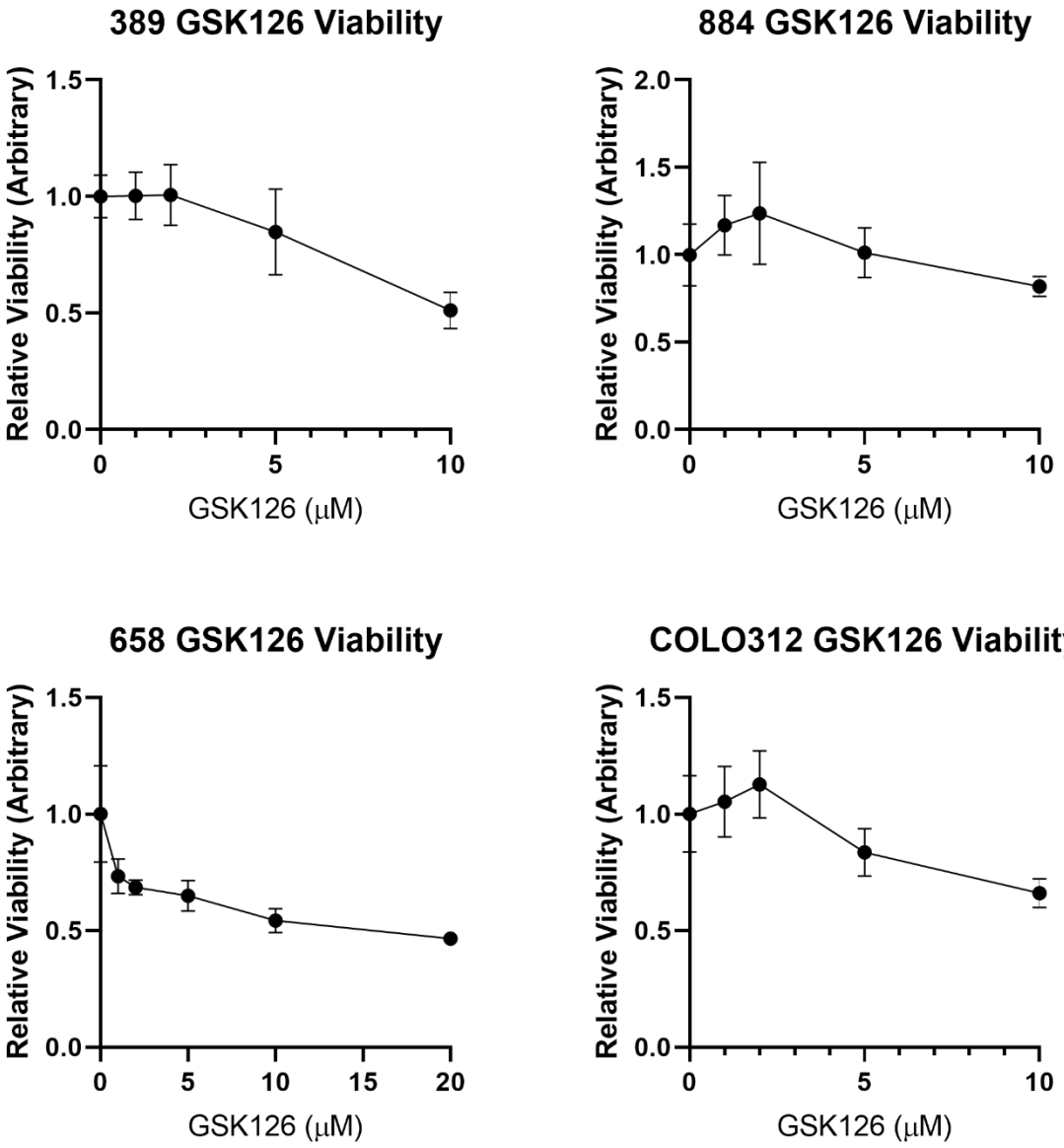


Figure 6.1 GSK126 viability across colorectal cancer organoids. Four colorectal cancer organoids were treated with a range of concentration of GSK126 between 0-10 μM (20 μM uM 658) for 72 hours, prior to determining the cell viability using CellTiter-Glo 3D Cell Viability Assay. Results were scaled relative to untreated control cells (given relative viability of 1.0) and all conditions were based on a minimum of five replicates. Mean values with standard deviation displayed.

In addition to GSK126, HDAC inhibition has been used to increase Class II expression as a result of enhanced CIITA gene expression. Typically doses of 5 μM for 24-72 hours of entinostat have been used for this purpose, though these are notably toxic. In a panel of CRC cell lines, de-repression of a target gene was observed at 5 μM, with minimal activity at 1 μM (275). In a paper examining reversal

of Class II loss in ovarian lines, a range of doses and time points were assessed, with 5 µM for 72 hours appearing most effective (204). Doses of 5 µM for 24 hours have also shown effects on gene expression in colorectal cell lines (276). It should be noted that the levels of cytotoxicity with entinostat are generally high at 5 µM doses, typically with 50-75% reduction in viability observed (204, 241). A dose of 5 µM for 72 hours entinostat will therefore be studied for efficacy in these experiments. The role of entinostat is relatively well studied in this area, however, the combined HDAC and EZH2 inhibition will be assessed for potential synergy.

6.3 Assessment of longer exposures of IFNγ

A key feature of the EZH2-mediated reduction in Class II expression described by Truax et al, was that the weakly-inducible cell lines required 72 hours following IFNγ to reach maximum levels of Class II expression (212). This phenomenon occurred despite acetylation of *CIITA* occurring rapidly (within 20 minutes) and *CIITA* mRNA expression evident after only 40 minutes and continuing to increase through to 18 hours, the latest time point measured (258). To assess if delayed kinetics of IFNγ response were displayed, all of the non- and weakly-inducible cell lines and organoids were treated out to 72 hours with IFNγ, prior to undergoing repeat assessment with flow cytometry.

In the initial validation experiments (Section 4.3), the three cell lines with minimal or no evidence of Class II inducibility (DLD1, HCT116 and RKO) were treated with 75 IU/ml IFNγ for 24 and 72 hours. No significant increase in Class II expression was observed at the later time point, therefore delayed responses to IFNγ were not present in these cell lines (**Figure 4.6**).

The three organoids with no evidence of any Class II upregulation and loss of STAT1/IRF1 signalling response were treated for 24 and 72 hours. Again, these three lines failed to show any further increase in Class II expression, in keeping with a mechanism of loss at a signalling pathway level (**Figure 6.2**).

Therefore no time-dependent increases of Class II expression in either the cell lines or completely non-inducible organoids were observed. Longer IFNγ stimulation next assessed in the weakly-inducible organoids with evidence of enhanced EZH2 occupancy of CIITA-pIV. These results will be assessed alongside the pharmacological reversal experiments in the next section.

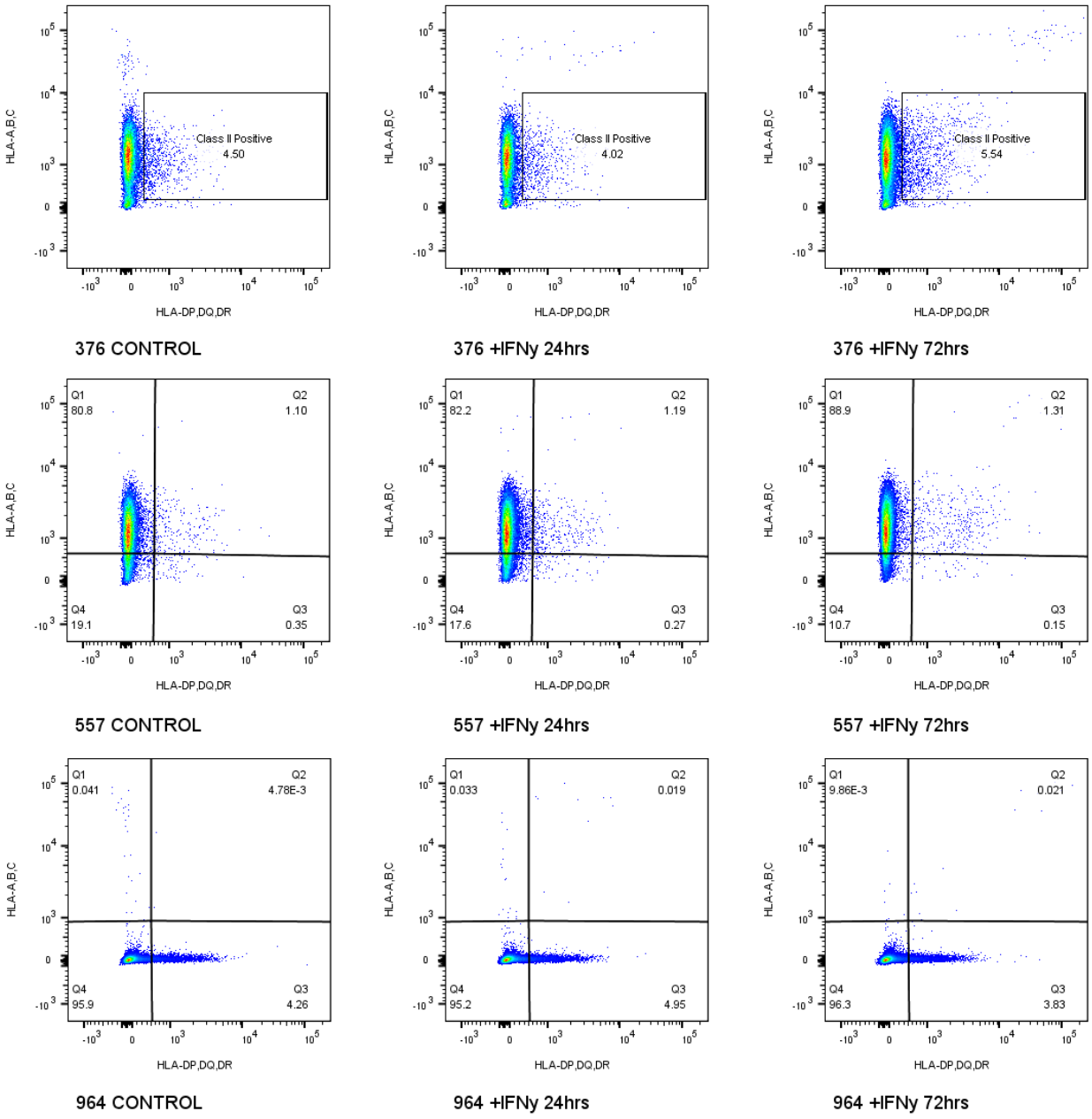


Figure 6.2 Treatment of non-responsive organoids with longer duration of IFNγ. 376, 557 and 964, the three organoids assessed in Chapter 4 as having no responses to IFNγ at 24 hours were stimulated for 72 hours. Flow cytometry results for Class I and Class II displayed for untreated control cells and treated cells (75 IU/ml IFNγ) at 24 and 72 hours. Experiment performed in duplicate with representative blots displayed.

6.4 Pharmacological reversal of Class II loss in organoids

The four weakly-inducible organoid lines were treated with over 24 and 72 hours with 75 IU/ml IFNγ as previously and were exposed to the following additional drug conditions:

- GSK126 2 μM for 144 hours / 6 days
- Entinostat 5 μM for 72 hours
- Combination of both agents together

Surprisingly, three out of four of the lines (389, 884 and COLO312) exhibited strong induction of Class II at 72 hours, with greater than 70% of cells becoming positive, remaining only weakly positive at 24 hours. 658, the line with the greatest increase in EZH2 occupancy of CIITA-pIV following IFNγ, was the only line not to significantly increase levels of Class II by 72 hours (**Figure 6.3a-d**).

In three out of four organoid lines, the addition of GSK126 significantly increased Class II expression at a minimum of one time point assessed. In 389, the 24 hour expression (mean across replicates) was increased with GSK126 from 35.4% to 67.9% ($p=0.0113$), with 72 hour expression going from 85.1% to 91.6% ($p=0.686$). 658 had no significant change at the 24 hours mark (6.25% to 10.4% with GSK126, $p=0.327$), though expression at 72 hours underwent a small but significant increase (11.9% to 24.2%, $p=0.0081$). COLO312 Class II expression was significantly increased with GSK126 at both time points (24 hour: 14.0% to 35.4%, $p<0.0001$. 72 hour: 82.0% to 91.3%, $p=0.0024$). Only 884 failed to show a significant change with GSK126 addition, with 24 hour Class II going from 2.8% to 3.8% ($p=0.909$) and 72 hour Class II going from 75.9% to 81.6% ($p=0.0810$) **(Figure 6.4)**.

Notably, 884 had the smallest increase in EZH2 occupancy of the four weakly inducible lines. It may therefore be that the addition of GSK126 to simply longer periods of IFNγ stimulation offered the smallest benefit in this line, with the least amount of competition of EZH2-CIITA occupancy.

Of note the use of entinostat in these experiments was with the anticipated aim of enhancing CIITA-pIV acetylation, with evidence in the literature that this can enchance Class II expression following IFNγ stimulation (204), rather than directly addressing the issue of EZH2 occupancy of CIITA-pIV.

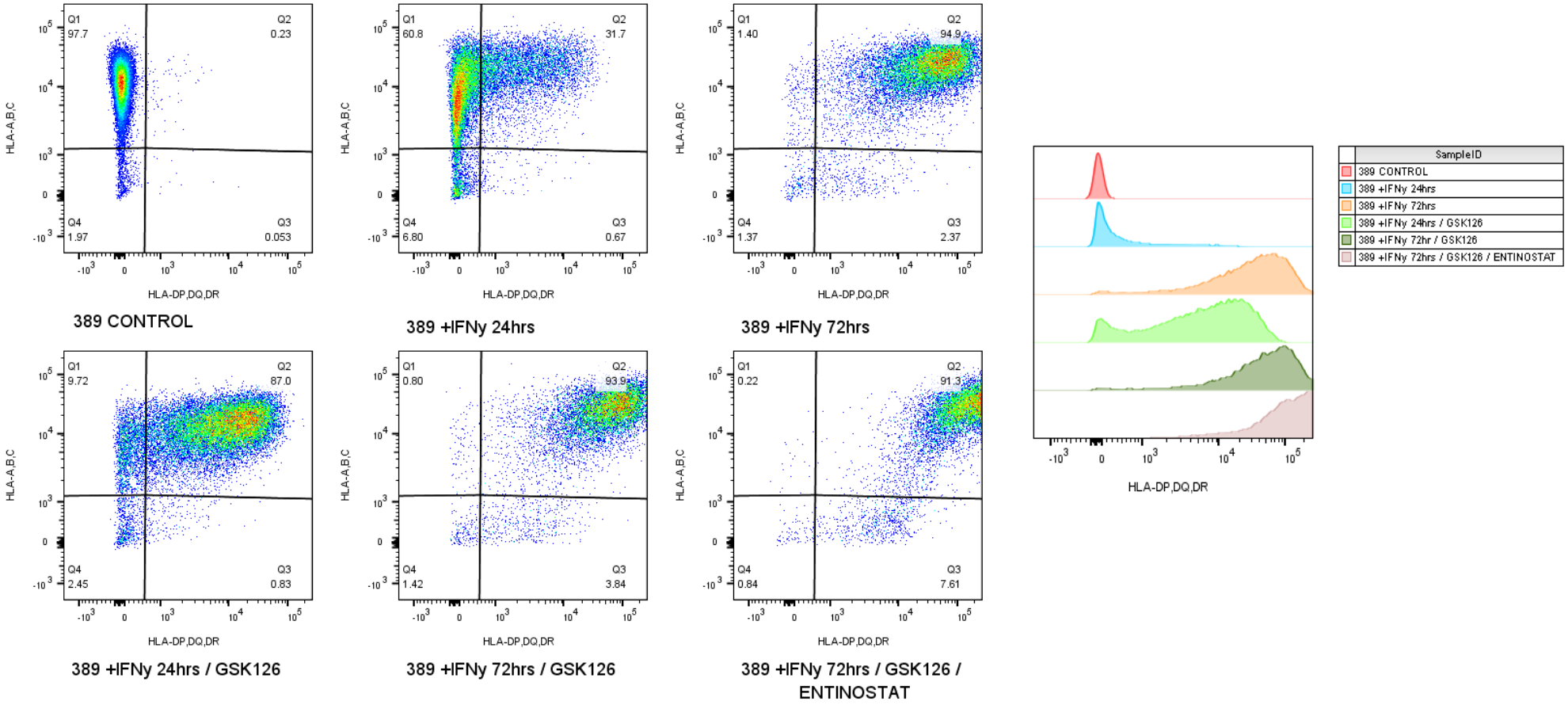


Figure 6.3a Pharmacological reversal of Class II loss and longer IFNγ exposure in weakly inducible organoids. 389 was treated with IFNγ for 24 hours and 72 hours +/- 2 µM GSK126 for 6 days. Additionally, effect of HDAC inhibition was assessed using 5 µM entinostat for 72 hours, in combination with 72 hours IFNγ and 6 days GSK126. Flow cytometry results displayed for Class I and Class II, with Class II offset overlay displayed on right. Experiment performed in triplicate with representative blots displayed.

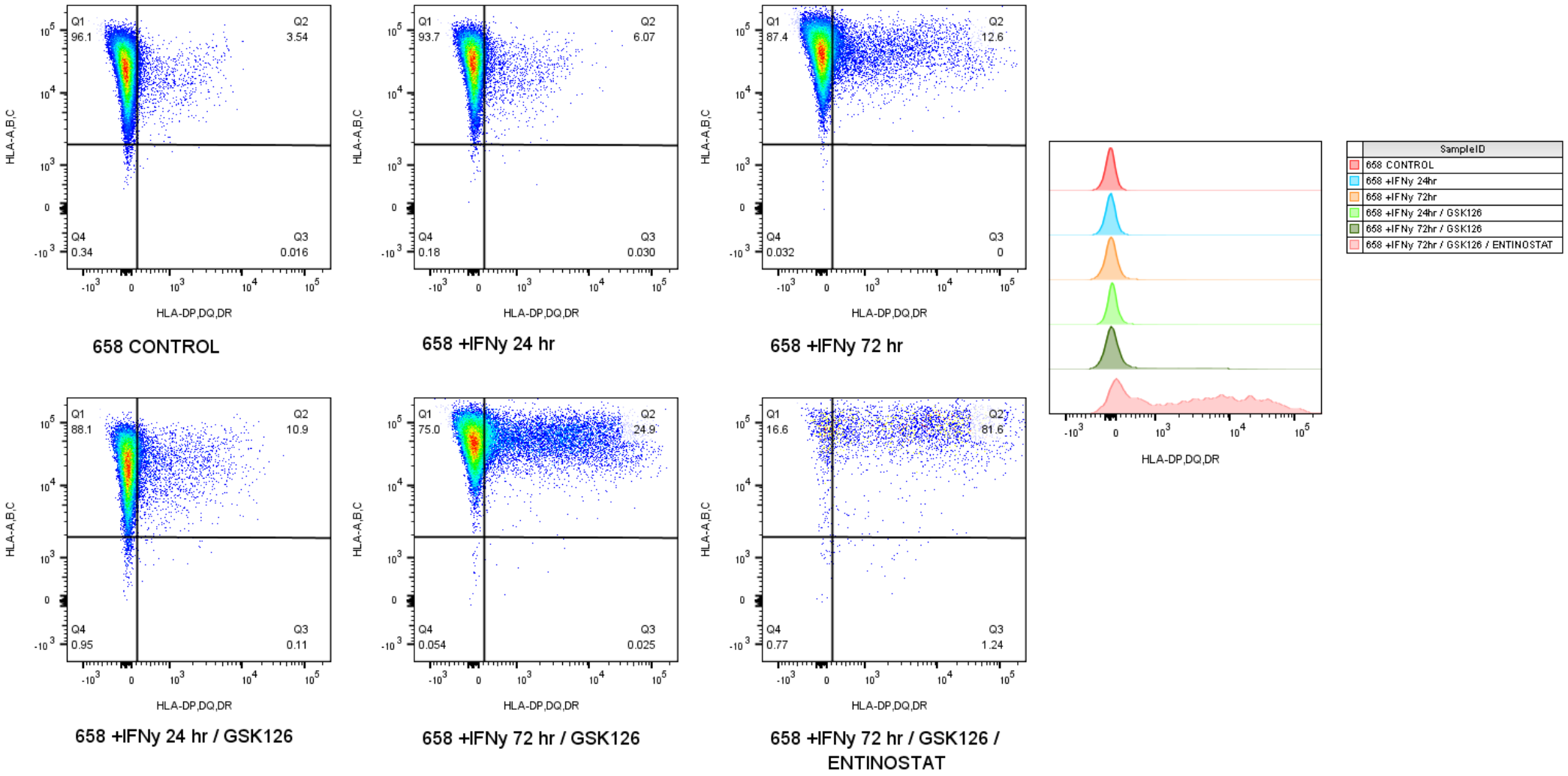


Figure 6.3b Pharmacological reversal of Class II loss and longer IFNγ exposure in weakly inducible organoids. 658 was treated with IFNγ for 24 hours and 72 hours +/- 2 μM GSK126 for 6 days. Additionally, effect of HDAC inhibition was assessed using 5 μM entinostat for 72 hours, in combination with 72 hours IFNγ and 6 days GSK126. Flow cytometry results displayed for Class I and Class II, with Class II offset overlay displayed on right. Experiment performed in duplicate with representative blots displayed.

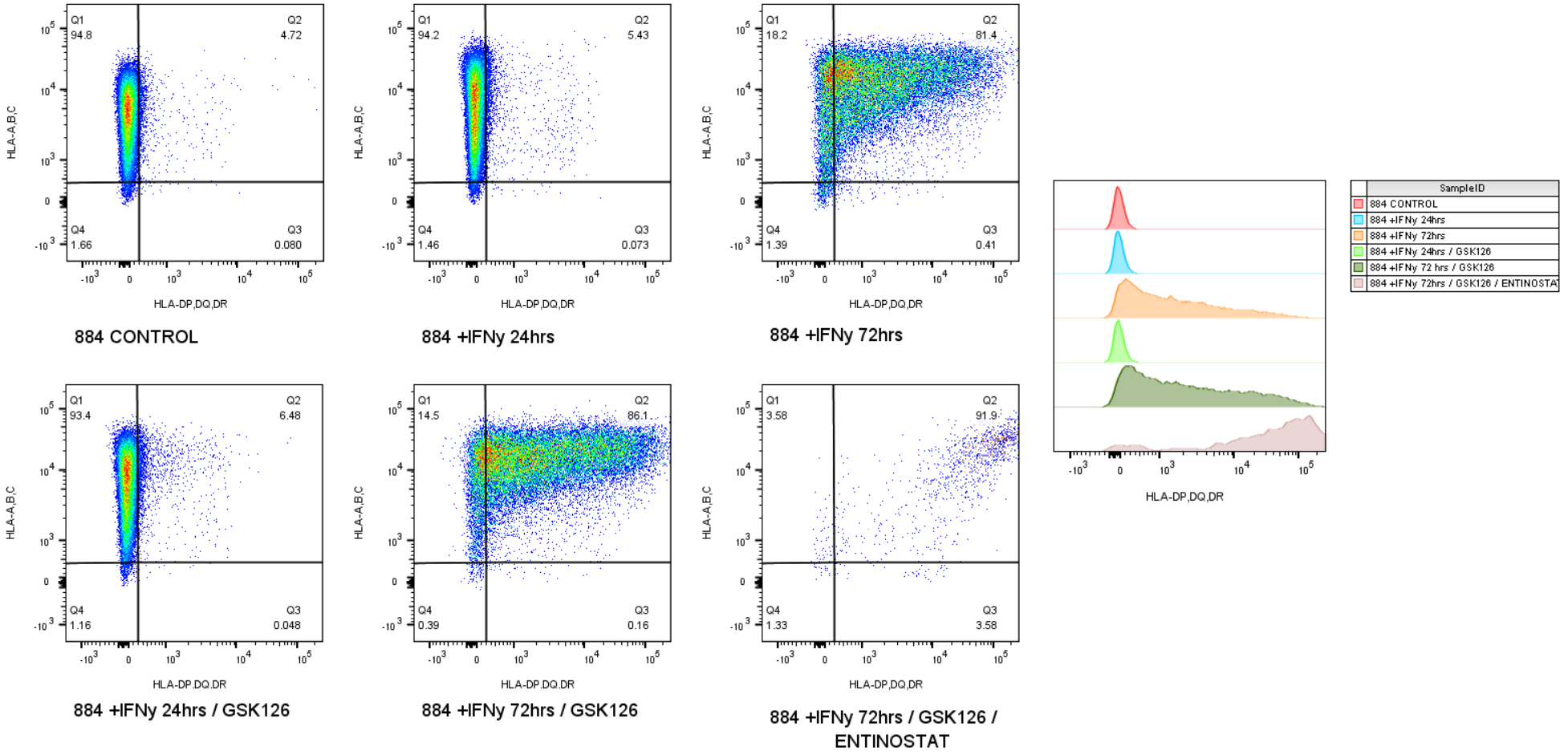


Figure 6.3c Pharmacological reversal of Class II loss and longer IFNγ exposure in weakly inducible organoids. 884 was treated with IFNγ for 24 hours and 72 hours +/- 2 µM GSK126 for 6 days. Additionally, effect of HDAC inhibition was assessed using 5 µM entinostat for 72 hours, in combination with 72 hours IFNγ and 6 days GSK126. Flow cytometry results displayed for Class I and Class II, with Class II offset overlay displayed on right. Experiment performed in triplicate with representative blots displayed.

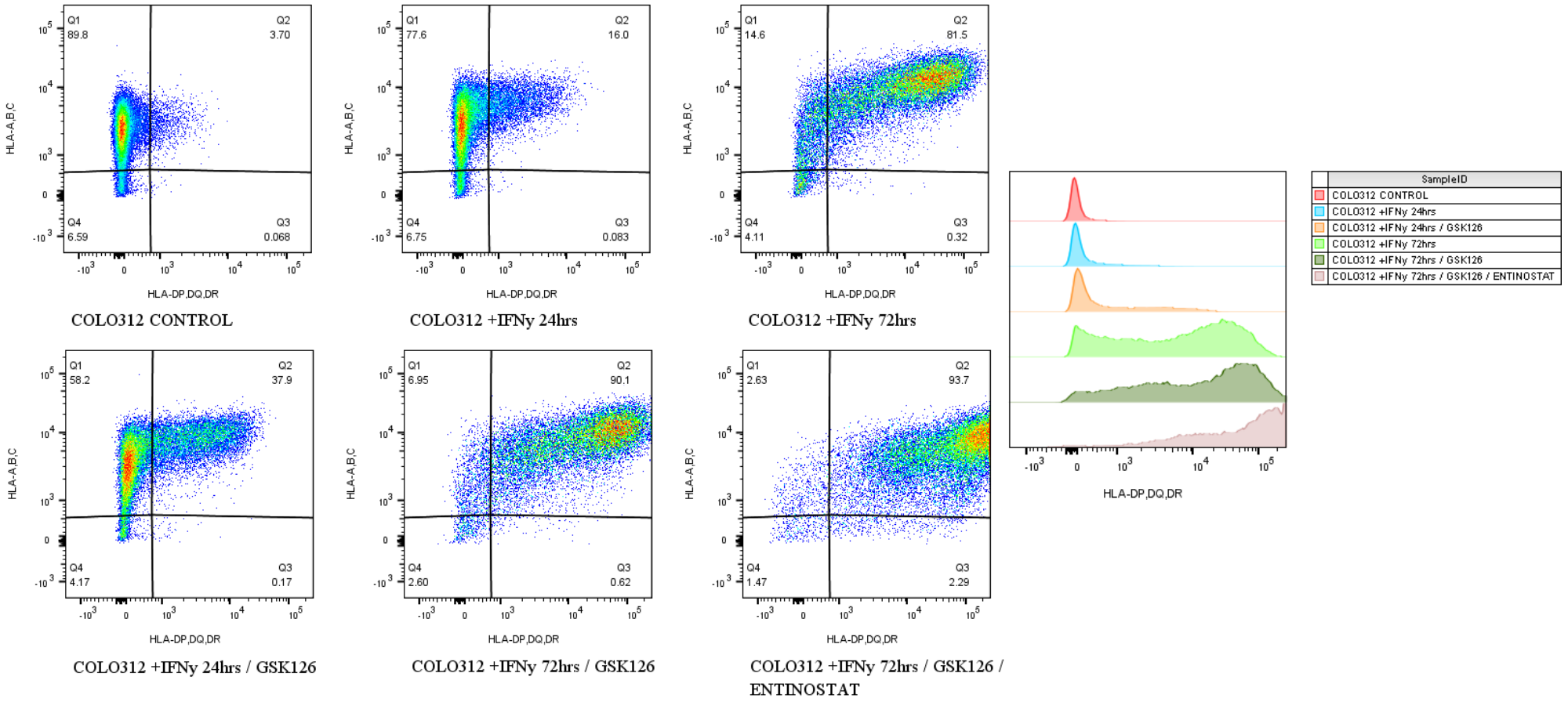


Figure 6.3d Pharmacological reversal of Class II loss and longer IFNγ exposure in weakly inducible organoids. COLO312 was treated with IFNγ for 24 hours and 72 hours +/- 2 μM GSK126 for 6 days. Additionally, effect of HDAC inhibition was assessed using 5 μM entinostat for 72 hours, in combination with 72 hours IFNγ and 6 days GSK126. Flow cytometry results displayed for Class I and Class II, with Class II offset overlay displayed on right. Experiment performed in triplicate with representative blots displayed.

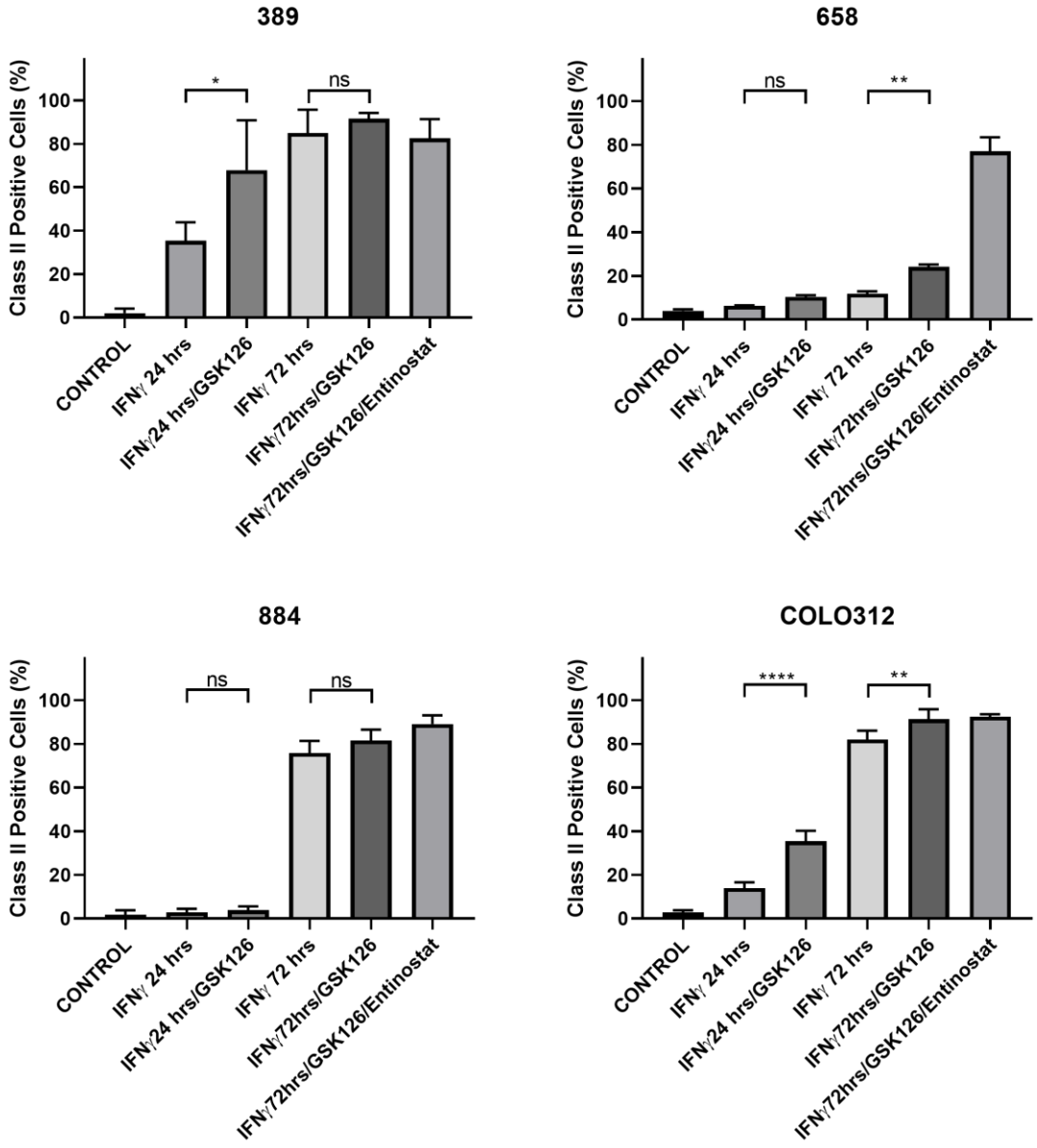


Figure 6.4 Class II expression with longer duration IFNγ, GSK126 and Entinostat. Mean and standard deviation of flow cytometry results. Statistical analysis of results using one-way ANOVA followed by Sidak's multiple comparisons test (planned analysis on 24 hour IFNγ +/- GSK126 and 72 hours IFNγ +/- GSK126 only. NS $P \geq 0.05$; * $P < 0.05$; ** $P < 0.01$; *** $P < 0.001$; **** $P < 0.0001$.

Entinostat appeared to shift the ‘cloud’ of Class II expressing cells to the right of the flow cytometry plot, indicating not only a greater percentage of cells expressing Class II but also greater intensity and therefore likely density of Class II expression. Indeed, the voltages for PE/Cy7 (Class II) have been reduced due to the higher intensity staining compared to the initial characterisation experiments in Chapter 4 (and therefore caution should be taken comparing like-for-like). The effect on cell viability of the entinostat and GSK126 combination, with notably fewer events, indicates this is a likely toxic combination. For these reasons statistics have not been applied to these data and they are provided for exploratory purposes given the relative paucity of events recorded.

6.5 Genomic determinants of differential EZH2 responses

The WGS data from the organoids was analysed for determinants of enhanced EZH2 activity including members of the PRC2 complex and loss of function mutations within the SWI/SNF complex (comprising *ARID1A*, *ARID1B, SMARCA2, SMARCA4* aka BRG1 and *SMARCB1*). No likely causal mutation was identified within three lines, however, 658 had evidence of an *EZH2* mutation (c.1648A>G, p.Lys550Glu) within the CXC domain (277) which is likely to be pathogenic. This would require further mechanistic validation to confirm the functional role of this mutation, as it would typically be expected to cause loss of function. Furthermore, an exploratory analysis of individual gene expression from the RNAseq data failed to show a significant difference in expression levels of relevant genes across any of the organoid Class II response groups. Interestingly, however, 658 had the highest *EZH2, SUZ12* and *ARID1A* expression, potentially indicating overexpression of the PRC2 complex within this line with very high EZH2-CIITA binding (**Figure 6.5**).

Given the distinct behaviour of 658, with weak Class II upregulation at 72 hours even with GSK126, consideration was given to further downstream mechanisms that could limit Class II expression, in addition to the above *EZH2* mutation. This line is derived from an MSI-H tumour and as previously reported, just over a quarter of Class II negative MSI-H tumours have evidence of an *RFX5* mutation (185). 658 was identified as having a highly pathogenic clonal heterozygous (VAF 0.41) D461G mutation, which was predicted to impair protein folding. CIITA coordinates Class II expression via the recruitment of RFX family proteins. Strong Class II expression was only observed in 658 with the combination of HDAC inhibition with GSK126 and 72-hours of IFNγ, hypothetically suggestive that very high levels of CIITA expression are required to overcome reduced functional RFX5 levels, passing a threshold for successful Class II expression.

EZH2 occupancy of *CIITA*, therefore, causes a delayed Class II expression response following IFNγ stimulation. 658, the outlier line, in addition to the distinct transcriptional behaviour delineated in Chapter 5, potentially has a complex composite mechanism of both enhanced EZH2-CIITA occupancy with a downstream *RFX5* mutation. Within the other three lines, it has not been possible to identify a genomic 'biomarker' for this behaviour, for example a *SMARCA4* (BRG-1) mutation, however further exploration including more global methylation assessment is planned subsequently (450K array).

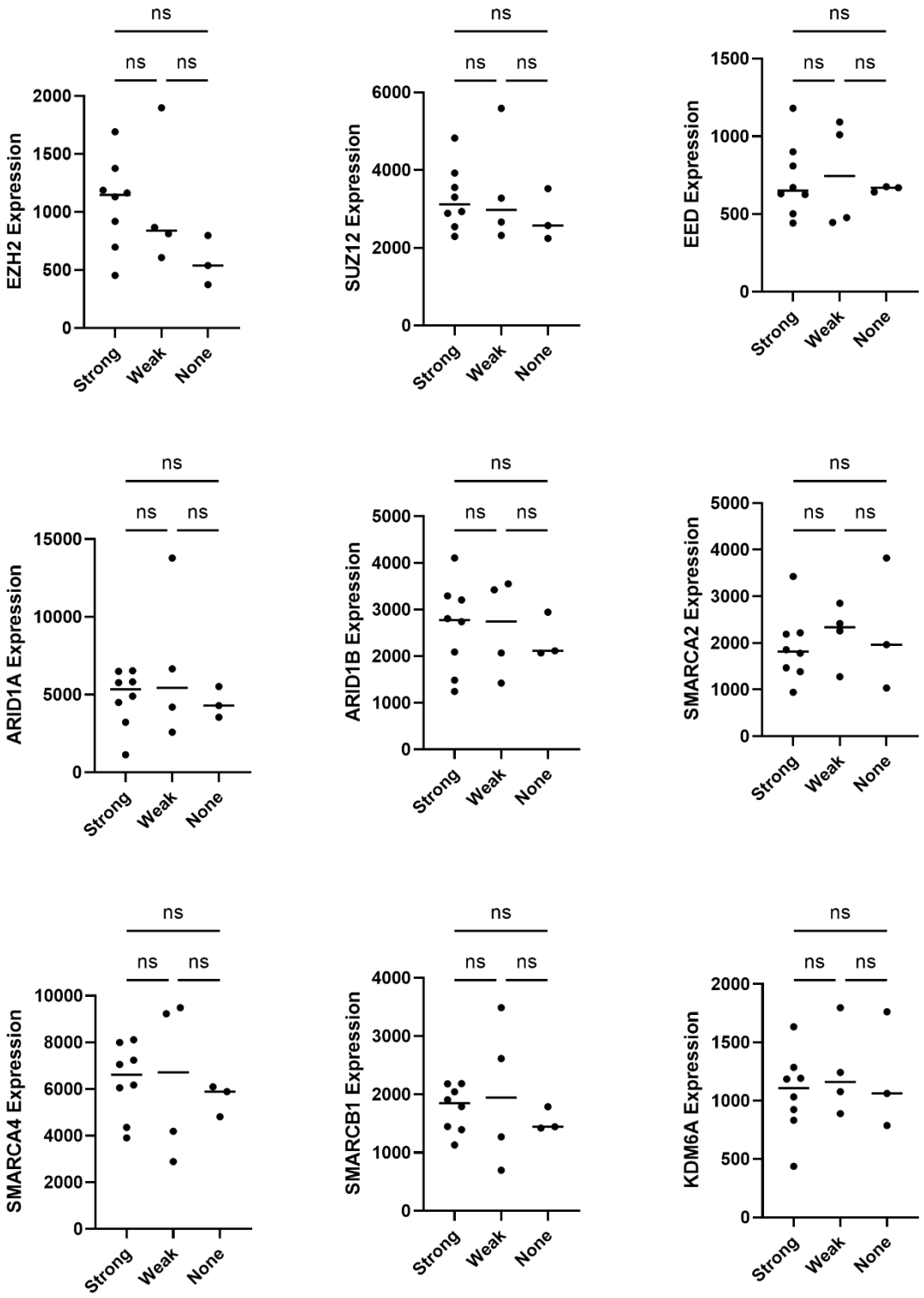


Figure 6.5 RNA expression of PRC2 and SWI/SNF complex proteins. RNAseq expression data for PRC2 and SWI/SNF complex components, in addition to *KDM6A* (aka UTX, responsible for H3K27me3 demethylation), assessed across the three different Class II response groups in CRC organoids. Individual values with mean displayed, statistical assessment with Kruskal-Wallis test and Dunn's post test, ns=non-significant ($p>0.05$).

6.6 Conclusions

The weakly-inducible organoids, with the exception of 658, are capable of expressing very high levels of Class II without pharmacological intervention, instead displaying delayed kinetics of IFNγ response. This is in contrast to the non-inducible organoids, where loss of signalling response to IFNγ stimulation fails to reverse even with prolonged exposures. Likewise, the three cell lines remain unchanged with 72 hours of IFNγ compared to the 24 hour stimulation. With RKO and HCT116, this is likely to be explained by the (cell-culture induced) CpG methylation observed at CIITA-pIV. In DLD1, where only a small increase in Class II observed and CIITA-pIV was not methylated, similar mechanisms to those found in the 658 organoid may be present. Indeed, the Sanger Cosmic database holds mutation data for DLD-1 (sample ID COSS2301972, available from https://cancer.sanger.ac.uk/) and two pathogenic *RFX5* missense mutations are present (p.G399V / c.1196G>T and p.R335Q / c.1004G>A). Again, DLD-1 is an MSI-H cell line and this is, therefore, a recognised route of immune escape (185).

658 interestingly had a significantly increased *CIITA* promoter occupancy by EZH2 (Chapter 5) following IFNγ compared to the other three weakly-inducible lines and was the only line to continue to only weakly express Class II at 72 hours of IFNγ stimulation, potentially caused by a secondary *RFX5* mutation. A small effect was seen from EZH2 inhibition at the 72-hour timepoint, though less than 25% of cells were able to express Class II. It appears that the addition of entinostat to this situation was able to rescue Class II expression. This is consistent with the *CIITA* mRNA expression data for 658 (Chapter 5), with 658 exhibiting both the smallest relative increase in *CIITA* mRNA and the weakest absolute Ct value (28.6 compared

to <25 for the other three weakly-inducible lines) for the detection of *CIITA* mRNA following IFNγ. Conversely, 884 demonstrated no significant benefit for the addition of GSK126 at either time point (though this was close to significance at 72 hours) and also had the smallest relative increase in EZH2 promoter binding following IFNγ. Therefore a spectrum of EZH2 binding behaviour is likely to be observed and may reflect different underlying mechanisms e.g. overexpression, mutation or loss of competition from the SWI/SNF/BRG-1 complex.

Chapter 7: General Discussion

7.1 Development of the organoid collection

Several outputs have been generated from this work. The first has been the generation of a collection of colorectal cancer organoids from local patients. Increasingly, organoid models are being utilised for many experiments that would have traditionally been performed with 2D cell culture (11). Compared to 2D culture, organoids allow recapitulation of precise organ biology, accurate prediction of chemo- and radiotherapy sensitivity and additionally begin to encompass the complexity of tumour heterogeneity. The expansion of this field has been rapid and it is now possible to purchase organoids, produced under licence and intellectual property rights of the Hubrecht Organoid Technology (HUB), from sources such as OrganoidBase (see https://www.crownbio.com/ob-registration). Additionally, the specialised media required for stem cell culture is being commercially produced and this has certainly enabled this work and improved standards through having a uniform quality-controlled media compared with the 'lab-brewed' versions that had until recently been the standard. Through our work and collaboration with the Sanger Institute, we are expanding our collection of organoids and the strength of this collection over even commercially available lines, is the ability to annotate the lines with clinicopathological data from the patients and the microenvironmental characteristics of the tumours. This has enabled the data presented here on the Class II inducibility of each organoid line to be interpreted in the context of the Class II expression found in that patient's tumour in situ. The addition of whole-genome and total RNA sequencing of the organoids leaves a collection of fifteen lines that are completely characterised, allowing future work on related projects to be carried out at

a fraction of the cost and time. We continue to expand this collection and in addition to these primary lines, a collection of liver and peritoneal metastasis-derived organoids has also been produced.

7.2 Class II is frequently inducible in CRC tumours and absence likely represents IFNγ deficiency within the TME

The main output of this work has been the detailed examination of the mechanisms and dysregulation of Class II expression in colorectal cancer, utilising both CRC cell lines and organoids. Each line has been assessed for loss of IFNγ signalling response (STAT1/IRF1 western blotting), *CIITA* expression (RT-qPCR for mRNA) and accessibility of *CIITA* (promoter CpG methylation, H3K9 acetylation, H3K9 methylation and EZH2 occupancy) and surface Class I and II expression following IFNγ (flow cytometry) at 24 hours and 72 hours. Crucially, I have demonstrated that some tumours with an absence of Class II in the microenvironment are fully inducible in vitro. The vast majority of organoid lines (eight strongly-inducible at 24 hours, three further strongly inducible at 72 hours post-IFNγ) are able to express Class II without any evidence of a cell-autonomous block on Class II inducibility and in the absence of epigenetic modifiers. The three non-inducible lines had evidence of IRF1/STAT1 pathway deficits, as has previously been reported in patients as a mechanism of immune escape, with one of these lines MSI-H, suggesting that this very likely represents an adaptive form of immune escape in an immunogenic tumour (182).

It is worth again considering the events that occur within the TME when analysing these results. Approximately half of in situ MSS CRC tumours lack Class II expression, with strong expression seen only in around 10% of samples (5). An early

hypothesis of this work was that these Class II negative tumours represented the approximately 50% of CRC cell lines that were non-inducible in vitro (196). These results, however, disprove this hypothesis. The fact that many of the in situ tumours are negative for Class II and yet strongly induce in vitro instead points to IFNγ deficiency and an absence of functional CD4+ and CD8+ T cells within the TME.

Three out of the four weakly-inducible group of organoids, characterised by <50% Class II expression at 24 hours following IFNγ stimulation, are strongly (>50%) Class II positive at 72 hours. Antigen recognition within the TME, with resultant IFNγ production, of course does not occur in an isolated time-constrained period. An increase in immune surveillance and anti-tumour activity is likely to build over months, as a pre-cancerous adenoma progresses to an increasingly invasive tumour, with this response attenuated by various methods of immune escape evolved by the tumour (94). This delayed IFNγ response could, however, be relevant to the initiation of any immune attack on tumour. IFNγ has a dual role, both ramping up MHC expression and inducing direct cytotoxic effects (103), but also leading to the expression of PD-L1/2 and other immune checkpoints including IDO, on tumour cells (278, 279). This induction of PD-L1 is known to be rapid, with in vitro experiments demonstrating surface expression within 24 hours of IFNγ treatment (280). It is possible therefore that EZH2-mediated delayed IFNγ Class II responsiveness is enough to tip the balance away from a feed-forward amplification of anti-tumour response and instead lead to a tolerant TME with inactivated T cell population, with these T cells known to be resistant to reactivation even following anti-PD-1 checkpoint blockade (121). Conceivably, this initial tumour-immune system interaction could shape the future of that tumour, as we do not generally see

evidence of established tumours being subsequently eradicated by the immune system in absence of ICB or rare events such as abscopal reactions (281).

Antigen recognition within the TME, leading to IFNγ production, is likely to result in a wave of activation across the tumour. For example, a mouse tumour model with an IFNγ reporter revealed that IFNγ action could be detected at 800 μM (around 40 cell depths) away from the initiator event (282). There is further evidence of the broad-acting bystander effects of IFNγ within tumours, with a second paper describing the establishment of 'cytokine fields,' comprised of the cumulative action of T cells across antigen-presenting areas of tumour, with antigen-negative regions typically devoid of T cell infiltrates (283).

We had hoped to perform an analysis of the primary tumour sections from the patients we had derived organoids from using multispectral IHC. The hypothesis was that in tumours with some Class II expression (e.g. 10% of tumour cells), that the expressing tumour cells would be in proximity to activated T cells in support of the IFNγ deficiency theory. A multispectral panel had been designed to include pan-cytokeratin (identifying tumour), Class I and Class II, along with an activated T cell marker panel (CD3+, Ki67 and Granzyme B). This was adapted from a paper describing nearest-neighbour analysis within tumours (284) and would have allowed the relationship between the presence of co-localised activated T cells and the expression of Class II within the primary tumour to be assessed. Unfortunately, this experiment was not possible, firstly because of technical malfunctions and delays in the Vectra imaging facility, followed by the Covid-19 shutdown. This remains an area of interest and is an area for potential future work.

7.2.1 Therapeutic consequences of IFNγ deficiency

A further extension of IFNγ-deficiency is that in CRC tumours with immune-desert microenvironments are unlikely to respond to ICB (285). Instead, increased focus is likely needed to increase T cell trafficking into tumours. So far approaches in CRC have looked to target adverse TME factors in combination with ICB, for example through agents targeting VEGF (Bevacizumab/NCT02982694 and Regorafenib/NCT03657641), Wnt-signalling (Porcupine inhibitors e.g. CGX1321/NCT02675946 and LGK974/NCT01351103) and M2 macrophage depletion (CSF-1R/Pexidartinib/NCT02777710) (286). Other immune checkpoints, most notably TIM-3 and LAG-3, along with co-stimulatory molecules such as OX40 and ICOS are currently being assessed in a number of clinical trials. In the future, this may provide a broad repertoire of agents to enable a more personalised approach in refining the immune response to a given tumour with a given microenvironment, however, doubts remain as to whether these could ever overcome the complete absence of immune infiltration (287). It may also be possible to bypass the need for immune production of anti-tumour cytokines by treating patients with exogenous cytokines. Notably, these approaches provided some limited success in renal cell carcinoma, with IFNα and IL-2 best characterised. These treatments, however, are toxic, expensive and now almost entirely obsolete in the era of ICB. Recent advances, including a novel pegylated IL-2 (NKTR-214), which has triggers effector cell ingress and activation in tumour, with a favourable toxicity profile in an initial phase I study, has renewed some interest in the approach (287, 288).

Other methods to bypass the need for immune infiltration are in continued development, including bispecific antibodies, which bind to a target that is (relatively

specifically) expressed on the tumour cell and which will potently attract effector T cells to the antibody. Numerous such molecules are in development, including a Carcino-Embryonic Antigen (CEA; a colorectal tumour marker) targeting antibody, cibisatamab, which is currently in early phase clinical assessment (289). Chimeric Antigen Receptor T cells (CAR-T) utilise a similar approach and like bispecific antibodies, don't require MHC-bound antigen offering advantages in MHC negative tumours. CAR-T therapies have demonstrated tremendous efficacy in liquid tumours, however, have considerable risks (75). A CAR-T directed against HER2 mutated CRC, which led to a cytokine release storm, respiratory compromise and death of a patient, was linked to low-level pulmonary expression of HER2 in the normal tissue (290). Finally, approaches using oncolytic viral therapies have shown some promise, albeit largely in immunogenic tumours including melanoma. Viral replication is facilitated in malignant cells with disordered cell cycle control and oncolytic therapies are likely to be further refined in the coming decade (291).

7.3 Tumour-specific Class II expression: a biomarker for ICB responsiveness?

The mere presence of effector T cells in the TME does not guarantee a response to ICB. Tumours with markedly inflamed microenvironments may respond poorly if effector cells are countered by large numbers of Treg and MDSC populations (287). On the other hand, tumour-specific Class II expression, in the context of colorectal epithelium which is typically Class II negative except for in the presence of IFNγ, implies that a functional and uninhibited immune response against tumour is ongoing. Class II expression is one of the last steps that would be expected in the chain of events: the presence of adequately immunogenic mutation(s), MHC Class I or II presentation of that antigen, subsequent activation and priming of CD4/CD8 T cells

through the direct or indirect presentation by tumour or APC, T cells activated to produce IFNγ, finally leading to MHC upregulation including Class II (178). As previously discussed, it is known that Class II positive melanomas and Hodgkin lymphoma have improved survival and better response rate to ICB than their Class II negative counterparts. Both PD-L1 and Class I expression were non-predictive (6, 161). There is potentially an issue of cause vs effect; if a tumour is highly immunogenic it may well have high levels of Class II expression non-specifically, caused by the overspill of cytokine fields within the TME (283). These highly immunogenic tumours would likely exhibit superior responses to ICB, even if the Class II expression itself was not the cause of this. Ultimately, whether causative or not, tumour-specific Class II expression has the potential to identify tumours with favourable TME, and could therefore serve as a biomarker of ICB treatment selection in typically non-responsive tumours, of which MSS CRC is an archetypical example.

This theory underpins the single-arm Phase II clinical trial ANICCA (NCT03981146, Prof G Middleton, Chief Investigator) which we have launched in parallel to this body of work. This study builds on the premise that around 10% of MSS CRC has high Class II expression on IHC, with a further 40% exhibiting weak expression (5). The study aims to establish the responses to anti-PD-1 (nivolumab) therapy in the high Class II group, to see if Class II expression has merits as a biomarker. As of late 2020, the first patients have commenced treatment. An important observation has already been generated from the study, requiring a substantial amendment of the protocol to allow entry for any patient with >1% Class II expression, rather than the >50% originally planned. This follows the finding that over the first fifty patients screened, none had greater than 50% Class II expression, and far fewer had weak

(1-49%) expression (personal communication, Prof G Middleton) than expected. Importantly, the patients entering this study have metastatic (Stage IV) CRC with poor prognosis, whereas the data from Lovig et al above is comprised of resected patients, generally with Stage II or III disease (5). This observation potentially adds weight to the prognostic impact of Class II expression. The adapted protocol now aims to treat 36 patients, with results likely over the next two years.

7.4 Tumour-specific Class II expression: the in-situ vaccination approach?

Previous studies have demonstrated that mice injected with cancer cells with constitutively expressed CIITA (and therefore high levels of surface Class II expression) rapidly cleared the tumours. Furthermore, these animals generated effective memory CD4 and CD8 T cell pools. These immune responses were highly effective, with subsequent rechallenge of these animals with the same tumour, even when lacking CIITA expression, also leading to rapid tumour clearance, as did the transfer of CD4 and CD8 T cells into naïve mice with established tumours. Switching on CIITA expression in these tumours effectively caused delivery of an in situ, tumour-specific vaccine in these mice (179, 180, 292).

Given the difficulties inducing expression of Class II classically, via IFNγ production in proximity to the tumour, we have formed a collaboration with CRUK Therapeutic Discovery Laboratories at the Babraham (Cambridge). This forms part of the Functional Genomics Centre and the CRUK-ONO-LifeArc Immuno-oncology Alliance, aiming to accelerate therapeutic development of new compounds, shortening development times and bringing together specialist genomics services and pharma industry expertise. We submitted our proposal in January 2020, with the subsequent

approval of the project which would hope to identify genes that could upregulate Class II expression, independently of IFNγ. We have identified several MSS CRC cell lines without evidence of *CIITA* methylation. These cell lines will undergo whole genome CRISPR screening to identify potential 'hits,' with screening facilitated by selection of Class II positive cells by FACS. An advantage of the CRISPR screen approach is the unbiased exploration of biology, without the requirement for pre-requisite biological knowledge. Potential hits will be validated in CRC organoids to confirm the effectiveness in restoring Class II expression within our group. Any discoveries will benefit from the input of the alliance into compound discovery and rapid development into early phase clinical trials. This future work will provide an additional direction for this work and even potentially lead to new drug discovery.

7.4 Epigenetics: the pitfalls of 2D cell culture and epigenetic modifiers

In the introduction chapter, the background literature on epigenetic control of CIITA was explored in some detail. There have been some notable inconsistencies in the literature, including the presence of *CIITA* CpG methylation in established trophoblast cultures, but not in primary cells (208). Whilst mechanistically the cell line findings of *CIITA* methylation have been convincingly demonstrated in a number of different cancer types (196, 201, 203), there has been an absence of confirmation in primary tissue. Indeed, one of the few papers studying primary MSI-H CRC tumours did not find evidence of *CIITA* methylation in any of the Class II negative tumours (185). This work has assessed methylation across fifteen CRC organoids, with none demonstrating evidence of CpG methylation of *CIITA*. Previously identified methylated cell lines, by contrast, have been confirmed as methylated, validating

both previously published findings and confirming that the underlying methodology utilised here is reliable (196).

These results perhaps should not be surprising. It has been known for some time that the majority of promoters identified as hypermethylated in cell lines are not corroborated with primary tissue samples and that in CRC, CIMP is significantly overrepresented in cell lines, again comparing to primary tissue (205, 206). By contrast, organoids are increasingly recognised as high fidelity models for the study of epigenetics (230, 231). When considering the role of epigenetic modifiers in CRC, for example, the DNMT1 inhibitor 5-azacytidine in combination with pembrolizumab immunotherapy, a trial failed to show any meaningful activity for this combination in MSS disease (214). Furthermore, the addition of 5-azacytidine to immunotherapy in lung cancer (an established effective treatment), led to worse outcomes in the patients receiving 5-azacytidine (273). The rationale of ICB-DNMT1 combination is not just to re-express Class II, but also to increase immunogenicity through other means including re-expression of tumour suppressor genes, cancer-testis antigens and endogenous retroviral species (194, 214). These few clinical examples, however, show how difficult this approach is and these compounds are highly non-specific in action.

The results from this work however add a clear caution to utilising 2D cell culture epigenetic data, without prior corroboration with primary tissue samples or organoids, to design clinical studies. This data convincingly demonstrates that CIITA methylation is not a mechanism for Class II loss in CRC. To our knowledge, this is the first side-by-side analysis of a postulated epigenetic mechanism in cell lines vs organoids. We

strongly suggest that in future in vitro epigenetic studies, organoids represent the gold standard mechanistic disease model.

The non-specific nature of these epigenetic compounds is a concern, as these studies demonstrate. Data presented here on EZH2 inhibition using GSK126 should also be considered with caution prior to clinical assessment. It is known for example that GSK126 can polarise the TME towards immune tolerance via the generation of MDSCs, albeit with the potential to ameliorate this effect through combining treatment with an anti-GR-1 antibody, neutralising this myeloid differentiation antigen (293). There is also the functional impact on immune cells directly. Additionally, de-repressing oncogenes can cause potential pro-oncogenic effects of and increase stemness in cancer cells. The data here, in confirmation with the prior literature (238), demonstrates that low doses of GSK126 enhance the growth of some CRC organoids. Finally, the role of EZH2 inhibition with GSK126 has been explored here in the weakly Class II inducible group. Even in the absence of GSK126 however, three out of these four lines were able to strongly express Class II by 72 hours. The biological relevance of 24 vs 72 hours IFNγ stimulation in the lab is of course pure conjecture to immune activity within the TME. The potent combination of an HDAC inhibitor (entinostat) with GSK126 appeared to have a synergistic effect and further enhanced Class II expression significantly. This combination, however, was toxic, with few viable cells remaining on flow cytometry and there is a high likelihood it would be overly toxic in clinical practice.

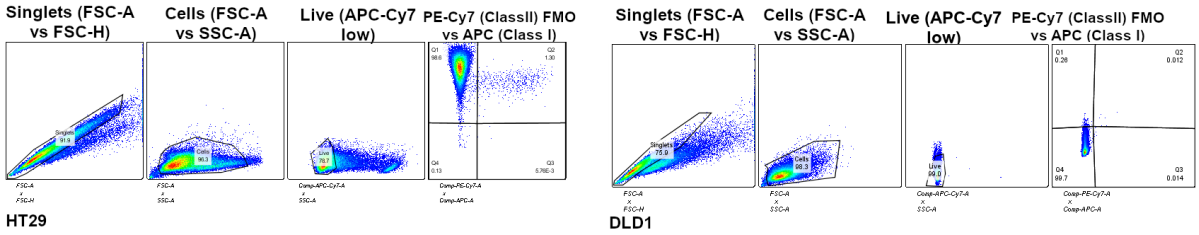
7.5 Summary

The work here has generated a collection of highly annotated CRC organoids, with further expansion likely over the coming years, providing a hugely valuable resource for future research efforts. Organoids remain a new methodology and have several disadvantages compared to traditional 2D cell culture, not least the highly time-consuming nature of experiments and prolonged culture times to generate enough cells for experiments. The media remains prohibitively expensive to many groups. However, the fidelity of the data that has been generated here and in the literature, provides an opportunity to understand the true biology of cancers and other diseases, and may lead to novel discoveries as a result. This work would support a move away from 2D culture for epigenetics in future work. This is important not only to generate ‘true’ scientific discoveries, but also more importantly to protect patients from clinical trials of non-efficacious, toxic treatments based on inaccurate models of disease.

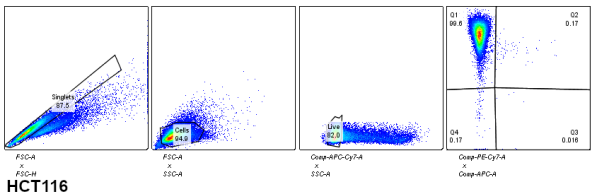
The multiple mechanisms of Class II loss displayed by CRC provide clinically meaningful insight into the difficulties of expanding ICB into this disease site. The dichotomy of MSI vs MSS CRC is likely to be hugely important in further dissecting immunotherapy responses in many cancers. The importance of immune exclusion in CRC has been outlined here, with IFNγ deficiency a key obstacle to overcome. The continuing work in ANICCA and the CRISPR screen collaboration offer two opportunities to deliver a therapeutic benefit to patients with MSS CRC. Ultimately, I hope this work offers further progress in expanding response rates to immunotherapy across all cancers, bringing with it the hope of durable, long-lasting disease remissions for increasing numbers of patients with metastatic disease.

Chapter 8: Appendix- Flow cytometry gating

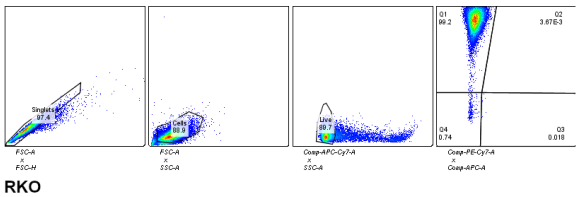
FIG 4.4



HT29



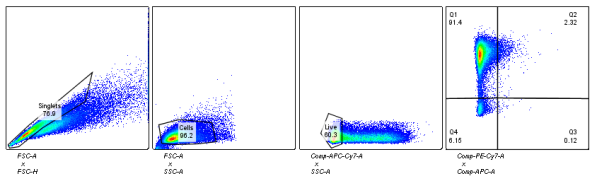
HCT116



DLD1

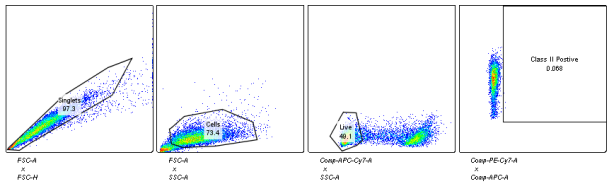
RKO

FIG 4.6

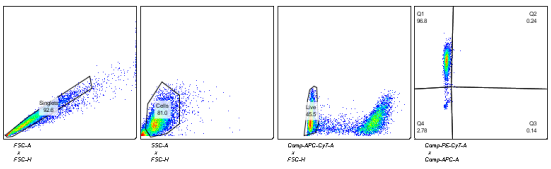


Cell line 72 hours

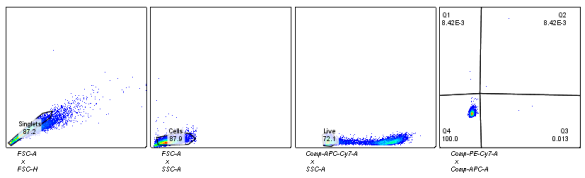
FIG 4.7



376

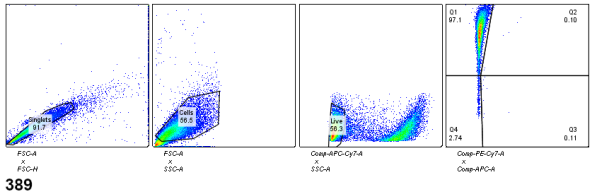


557

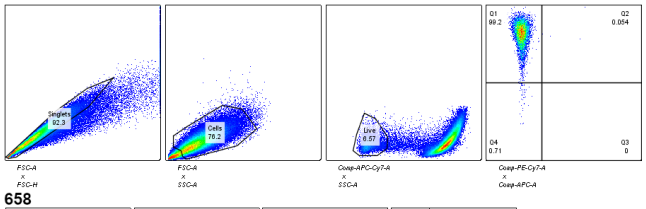


964

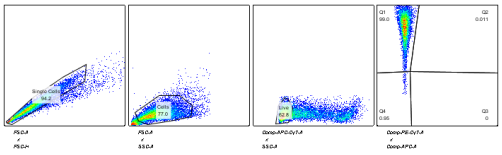
FIG 4.8



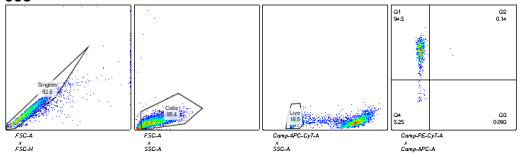
389



658

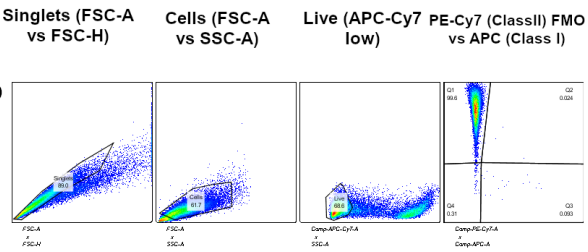


884

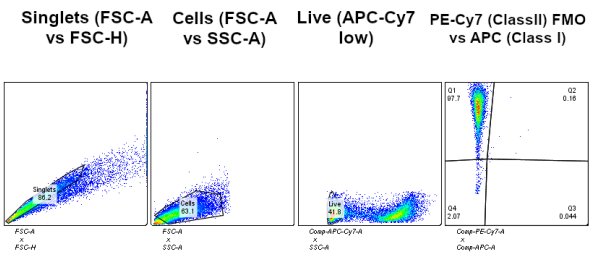


COLO312

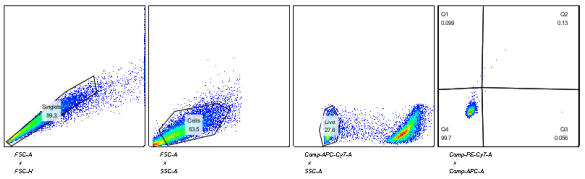
FIG 4.9



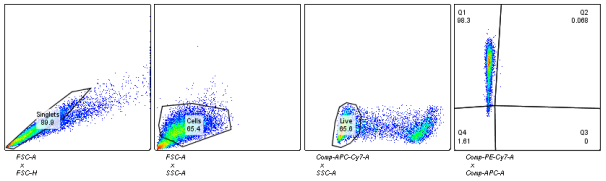
064



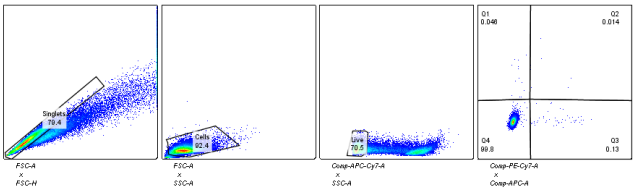
080



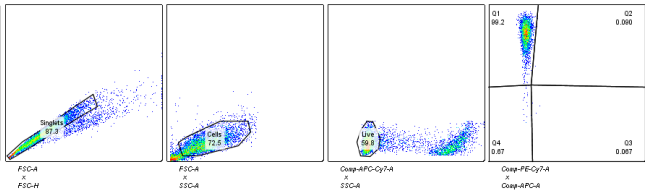
157



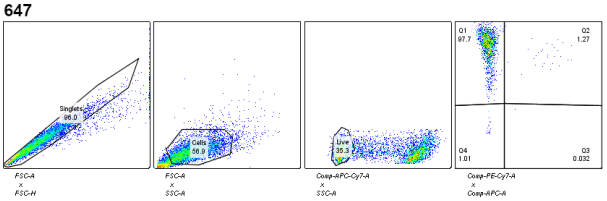
411



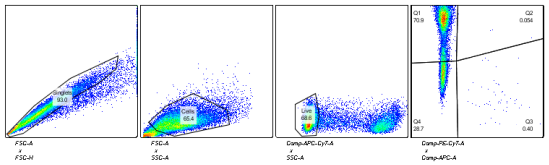
647



653

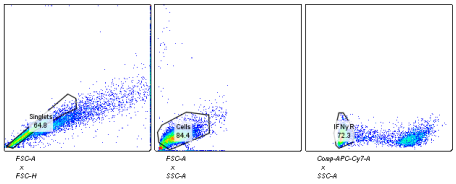


COLO151



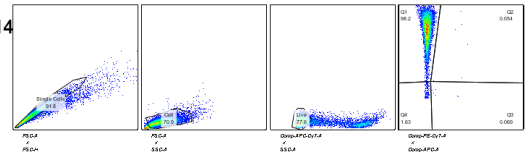
COLO155

FIG 4.13

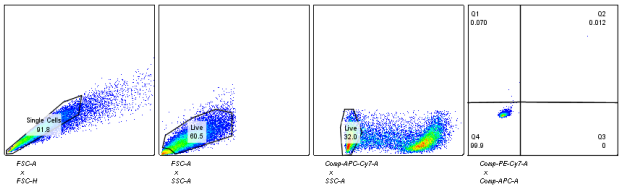


IFNy Receptor only

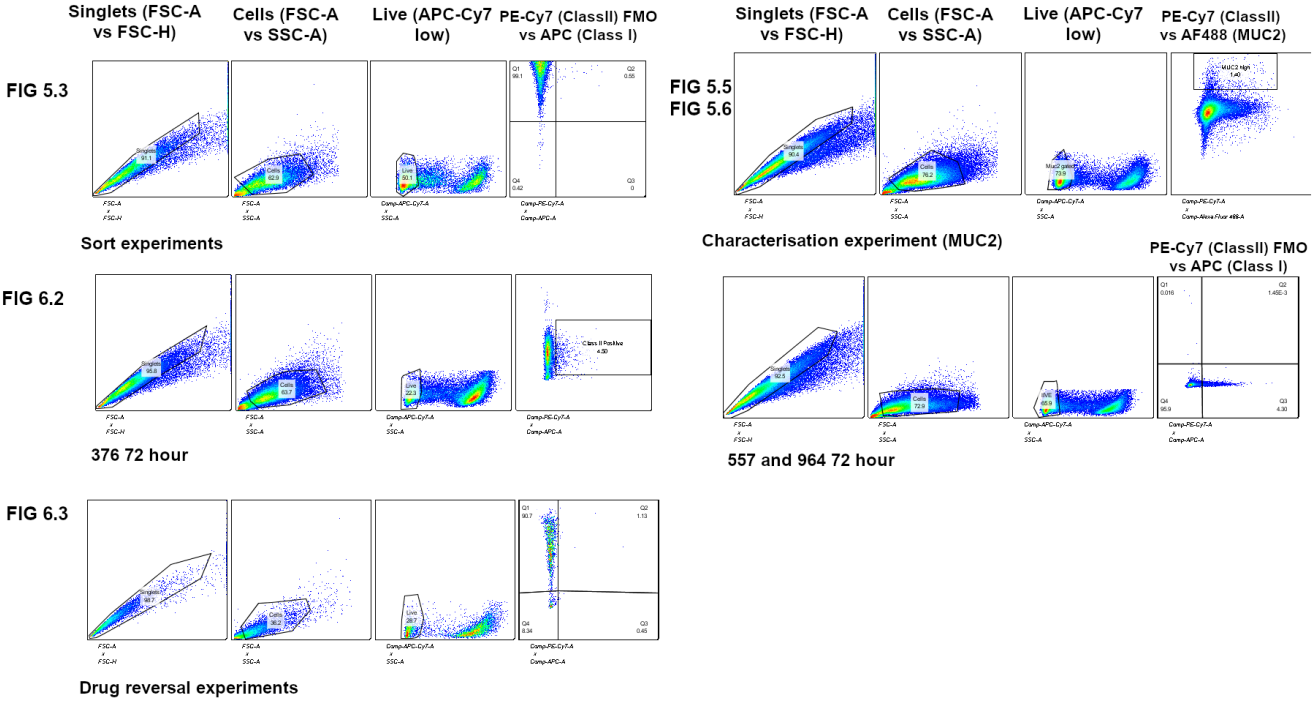
FIG 4.14



All lines except 157



157 for Fig 4.14



Gating conditions for all flow cytometry experiments is provided above in this appendix. For each figure gating has occurred in the following order:

1. Singlet selection (FSC-A vs FSC-H)
2. Selection of cells (FSC-A vs SSC-A)
3. Live cell selection using viability dye selected on APC-Cy7 channel vs SSC-A
4. Selection of Class II (PE-Cy7) using a Class II FMO stain vs Class I (APC)

Chapter 9: References

1. Van Cutsem E, Cervantes A, Adam R, Sobrero A, Van Krieken JH, Aderka D, et al. ESMO consensus guidelines for the management of patients with metastatic colorectal cancer. Ann Oncol. 2016;27(8):1386-422.
2. Okazaki T, Honjo T. PD-1 and PD-1 ligands: from discovery to clinical application. Int Immunol. 2007;19(7):813-24.
3. Hodi FS, Chiarion-Sileni V, Gonzalez R, Grob JJ, Rutkowski P, Cowey CL, et al. Nivolumab plus ipilimumab or nivolumab alone versus ipilimumab alone in advanced melanoma (CheckMate 067): 4-year outcomes of a multicentre, randomised, phase 3 trial. Lancet Oncol. 2018;19(11):1480-92.
4. Le DT, Uram JN, Wang H, Bartlett BR, Kemberling H, Eyring AD, et al. PD-1 Blockade in Tumors with Mismatch-Repair Deficiency. N Engl J Med. 2015;372(26):2509-20.
5. Lovig T, Andersen SN, Thorstensen L, Diep CB, Meling GI, Lothe RA, et al. Strong HLA-DR expression in microsatellite stable carcinomas of the large bowel is associated with good prognosis. Br J Cancer. 2002;87(7):756-62.
6. Johnson DB, Estrada MV, Salgado R, Sanchez V, Doxie DB, Opalenik SR, et al. Melanoma-specific MHC-II expression represents a tumour-autonomous phenotype and predicts response to anti-PD-1/PD-L1 therapy. Nat Commun. 2016;7:10582.
7. Lal N, Beggs AD, Willcox BE, Middleton GW. An immunogenomic stratification of colorectal cancer: Implications for development of targeted immunotherapy. Oncoimmunology. 2015;4(3):e976052.
8. Ben-David U, Siranosian B, Ha G, Tang H, Oren Y, Hinohara K, et al. Genetic and transcriptional evolution alters cancer cell line drug response. Nature. 2018;560(7718):325-30.
9. Prasad VV, Gopalan RO. Continued use of MDA-MB-435, a melanoma cell line, as a model for human breast cancer, even in year, 2014. NPJ Breast Cancer. 2015;1:15002.
10. Sato T, Stange DE, Ferrante M, Vries RG, Van Es JH, Van den Brink S, et al. Long-term expansion of epithelial organoids from human colon, adenoma, adenocarcinoma, and Barrett's epithelium. Gastroenterology. 2011;141(5):1762-72.
11. Drost J, Clevers H. Organoids in cancer research. Nat Rev Cancer. 2018;18(7):407-18.
12. Cancer Research UK. Bowel Cancer Statistics 2014-2016 [cited 2020 Feb 22]. Available from: https://www.cancerresearchuk.org/health-professional/cancer-statistics/statistics-by-cancer-type/bowel-cancer.
13. Ballester V, Rashtak S, Boardman L. Clinical and molecular features of young-onset colorectal cancer. World J Gastroenterol. 2016;22(5):1736-44.
14. Irving MH, Catchpole B. ABC of colorectal diseases. Anatomy and physiology of the colon, rectum, and anus. BMJ. 1992;304(6834):1106-8.
15. Costigan DC, Dong F. The extended spectrum of RAS-MAPK pathway mutations in colorectal cancer. Genes Chromosomes Cancer. 2020;59(3):152-9.
16. Fleming M, Ravula S, Tatishchev SF, Wang HL. Colorectal carcinoma: Pathologic aspects. J Gastrointest Oncol. 2012;3(3):153-73.
17. Armaghany T, Wilson JD, Chu Q, Mills G. Genetic alterations in colorectal cancer. Gastrointest Cancer Res. 2012;5(1):19-27.
418. Vogelstein B, Fearon ER, Hamilton SR, Kern SE, Preisinger AC, Leppert M, et al. Genetic alterations during colorectal-tumor development. N Engl J Med. 1988;319(9):525-32.
19. Bodmer WF, Bailey CJ, Bodmer J, Bussey HJ, Ellis A, Gorman P, et al. Localization of the gene for familial adenomatous polyposis on chromosome 5. Nature. 1987;328(6131):614-6.
20. Solomon E, Voss R, Hall V, Bodmer WF, Jass JR, Jeffreys AJ, et al. Chromosome 5 allele loss in human colorectal carcinomas. Nature. 1987;328(6131):616-9.

21. Knudson AG, Jr. Mutation and cancer: statistical study of retinoblastoma. Proc Natl Acad Sci U S A. 1971;68(4):820-3.
22. Fearon ER, Vogelstein B. A genetic model for colorectal tumorigenesis. Cell. 1990;61(5):759-67.
23. Zhan T, Rindtorff N, Boutros M. Wnt signaling in cancer. Oncogene. 2017;36(11):1461-73.
24. Kinzler KW, Vogelstein B. Lessons from hereditary colorectal cancer. Cell. 1996;87(2):159-70.
25. Giannakis M, Hodis E, Jasmine Mu X, Yamauchi M, Rosenbluh J, Cibulskis K, et al. RNF43 is frequently mutated in colorectal and endometrial cancers. Nat Genet. 2014;46(12):1264-6.
26. Batlle E, Clevers H. Cancer stem cells revisited. Nat Med. 2017;23(10):1124-34.
27. Barker N, Ridgway RA, van Es JH, van de Wetering M, Begthel H, van den Born M, et al. Crypt stem cells as the cells-of-origin of intestinal cancer. Nature. 2009;457(7229):608-11.
28. Matano M, Date S, Shimokawa M, Takano A, Fujii M, Ohta Y, et al. Modeling colorectal cancer using CRISPR-Cas9-mediated engineering of human intestinal organoids. Nat Med. 2015;21(3):256-62.
29. Drost J, van Jaarsveld RH, Ponsioen B, Zimberlin C, van Boxtel R, Buijs A, et al. Sequential cancer mutations in cultured human intestinal stem cells. Nature. 2015;521(7550):43-7.
30. Ionov Y, Peinado MA, Malkhosyan S, Shibata D, Perucho M. Ubiquitous somatic mutations in simple repeated sequences reveal a new mechanism for colonic carcinogenesis. Nature. 1993;363(6429):558-61.
31. Ellegren H. Microsatellites: simple sequences with complex evolution. Nat Rev Genet. 2004;5(6):435-45.
32. Raut CP, Pawlik TM, Rodriguez-Bigas MA. Clinicopathologic features in colorectal cancer patients with microsatellite instability. Mutat Res. 2004;568(2):275-82.
33. Alexander J, Watanabe T, Wu TT, Rashid A, Li S, Hamilton SR. Histopathological identification of colon cancer with microsatellite instability. Am J Pathol. 2001;158(2):527-35.
34. Murphy KM, Zhang S, Geiger T, Hafez MJ, Bacher J, Berg KD, et al. Comparison of the microsatellite instability analysis system and the Bethesda panel for the determination of microsatellite instability in colorectal cancers. J Mol Diagn. 2006;8(3):305-11.
35. Lynch HT, Lynch PM, Lanspa SJ, Snyder CL, Lynch JF, Boland CR. Review of the Lynch syndrome: history, molecular genetics, screening, differential diagnosis, and medicolegal ramifications. Clin Genet. 2009;76(1):1-18.
36. Gausachs M, Mur P, Corral J, Pineda M, González S, Benito L, et al. MLH1 promoter hypermethylation in the analytical algorithm of Lynch syndrome: a cost-effectiveness study. Eur J Hum Genet. 2012;20(7):762-8.
37. Sargent DJ, Marsoni S, Monges G, Thibodeau SN, Labianca R, Hamilton SR, et al. Defective mismatch repair as a predictive marker for lack of efficacy of fluorouracil-based adjuvant therapy in colon cancer. J Clin Oncol. 2010;28(20):3219-26.
38. André T, de Gramont A, Vernerey D, Chibaudel B, Bonnetain F, Tijeras-Raballand A, et al. Adjuvant Fluorouracil, Leucovorin, and Oxaliplatin in Stage II to III Colon Cancer: Updated 10-Year Survival and Outcomes According to BRAF Mutation and Mismatch Repair Status of the MOSAIC Study. J Clin Oncol. 2015;33(35):4176-87.
39. Seligmann JF. FOxTROT: neoadjuvant FOLFOX chemotherapy with or without panitumumab (Pan) for patients (pts) with locally advanced colon cancer (CC). J Clin Oncol. 2020;38(15_suppl):4013-.
40. Germano G, Amirouchene-Angelozzi N, Rospo G, Bardelli A. The Clinical Impact of the Genomic Landscape of Mismatch Repair-Deficient Cancers. Cancer Discov. 2018;8(12):1518-28.
41. Koopman M, Kortman GA, Mekenkamp L, Ligtenberg MJ, Hoogerbrugge N, Antonini NF, et al. Deficient mismatch repair system in patients with sporadic advanced colorectal cancer. Br J Cancer. 2009;100(2):266-73.

42. Llosa NJ, Cruise M, Tam A, Wicks EC, Hechenbleikner EM, Taube JM, et al. The vigorous immune microenvironment of microsatellite instable colon cancer is balanced by multiple counter-inhibitory checkpoints. Cancer Discov. 2015;5(1):43-51.
43. Smyrk TC, Watson P, Kaul K, Lynch HT. Tumor-infiltrating lymphocytes are a marker for microsatellite instability in colorectal carcinoma. Cancer. 2001;91(12):2417-22.
44. Gong J, Wang C, Lee PP, Chu P, Fakih M. Response to PD-1 Blockade in Microsatellite Stable Metastatic Colorectal Cancer Harboring a POLE Mutation. J Natl Compr Canc Netw. 2017;15(2):142-7.
45. Palles C, Cazier JB, Howarth KM, Domingo E, Jones AM, Broderick P, et al. Germline mutations affecting the proofreading domains of POLE and POLD1 predispose to colorectal adenomas and carcinomas. Nat Genet. 2013;45(2):136-44.
46. Vasen HF, Watson P, Mecklin JP, Lynch HT. New clinical criteria for hereditary nonpolyposis colorectal cancer (HNPCC, Lynch syndrome) proposed by the International Collaborative group on HNPCC. Gastroenterology. 1999;116(6):1453-6.
47. Cunningham D, Atkin W, Lenz HJ, Lynch HT, Minsky B, Nordlinger B, et al. Colorectal cancer. Lancet. 2010;375(9719):1030-47.
48. Oruç Z, Kaplan MA. Effect of exercise on colorectal cancer prevention and treatment. World J Gastrointest Oncol. 2019;11(5):348-66.
49. Ullman TA, Itzkowitz SH. Intestinal inflammation and cancer. Gastroenterology. 2011;140(6):1807-16.
50. Kim ER, Chang DK. Colorectal cancer in inflammatory bowel disease: the risk, pathogenesis, prevention and diagnosis. World J Gastroenterol. 2014;20(29):9872-81.
51. Guinney J, Dienstmann R, Wang X, de Reynies A, Schlicker A, Soneson C, et al. The consensus molecular subtypes of colorectal cancer. Nat Med. 2015;21(11):1350-6.
52. Becht E, de Reyniès A, Giraldo NA, Pilati C, Buttard B, Lacroix L, et al. Immune and Stromal Classification of Colorectal Cancer Is Associated with Molecular Subtypes and Relevant for Precision Immunotherapy. Clin Cancer Res. 2016;22(16):4057-66.
53. Roelands J, Kuppen PJK, Vermeulen L, Maccalli C, Decock J, Wang E, et al. Immunogenomic Classification of Colorectal Cancer and Therapeutic Implications. Int J Mol Sci. 2017;18(10).
54. Isella C, Brundu F, Bellomo SE, Galimi F, Zanella E, Porporato R, et al. Selective analysis of cancer-cell intrinsic transcriptional traits defines novel clinically relevant subtypes of colorectal cancer. Nat Commun. 2017;8:15107.
55. Galon J, Costes A, Sanchez-Cabo F, Kirilovsky A, Mlecnik B, Lagorce-Pages C, et al. Type, density, and location of immune cells within human colorectal tumors predict clinical outcome. Science. 2006;313(5795):1960-4.
56. Mlecnik B, Bindea G, Angell HK, Maby P, Angelova M, Tougeron D, et al. Integrative Analyses of Colorectal Cancer Show Immunoscore Is a Stronger Predictor of Patient Survival Than Microsatellite Instability. Immunity. 2016;44(3):698-711.
57. National Institute for Health and Care Excellence. Colorectal cancer NICE guideline [NG151] 2020 [cited 2020 7th August]. Available from: https://www.nice.org.uk/guidance/ng151/.
58. Loughrey MB, Kent O, Moore M, Coghlin C, Kelly P, McVeigh G, et al. Impact on colorectal cancer pathology reporting practice of migration from TNM 5 to TNM 8. Histopathology. 2020.
59. Morris EJ, Maughan NJ, Forman D, Quirke P. Who to treat with adjuvant therapy in Dukes B/stage II colorectal cancer? The need for high quality pathology. Gut. 2007;56(10):1419-25.
60. Abelson JS, Michelassi F, Sun T, Mao J, Milsom J, Samstein B, et al. Simultaneous Resection for Synchronous Colorectal Liver Metastasis: the New Standard of Care? J Gastrointest Surg. 2017;21(6):975-82.
61. Van Cutsem E, Cervantes A, Nordlinger B, Arnold D. Metastatic colorectal cancer: ESMO Clinical Practice Guidelines for diagnosis, treatment and follow-up. Ann Oncol. 2014;25 Suppl 3:iii1-9.
62. Fang JY, Richardson BC. The MAPK signalling pathways and colorectal cancer. Lancet Oncol. 2005;6(5):322-7.

63. Bokemeyer C, Van Cutsem E, Rougier P, Ciardiello F, Heeger S, Schlichting M, et al. Addition of cetuximab to chemotherapy as first-line treatment for KRAS wild-type metastatic colorectal cancer: pooled analysis of the CRYSTAL and OPUS randomised clinical trials. Eur J Cancer. 2012;48(10):1466-75.
64. Van Cutsem E, Lenz HJ, Kohne CH, Heinemann V, Tejpar S, Melezinek I, et al. Fluorouracil, leucovorin, and irinotecan plus cetuximab treatment and RAS mutations in colorectal cancer. J Clin Oncol. 2015;33(7):692-700.
65. Allegra CJ, Rumble RB, Hamilton SR, Mangu PB, Roach N, Hantel A, et al. Extended RAS Gene Mutation Testing in Metastatic Colorectal Carcinoma to Predict Response to Anti-Epidermal Growth Factor Receptor Monoclonal Antibody Therapy: American Society of Clinical Oncology Provisional Clinical Opinion Update 2015. J Clin Oncol. 2016;34(2):179-85.
66. Cremolini C, Loupakis F, Antoniotti C, Lupi C, Sensi E, Lonardi S, et al. FOLFOXIRI plus bevacizumab versus FOLFIRI plus bevacizumab as first-line treatment of patients with metastatic colorectal cancer: updated overall survival and molecular subgroup analyses of the open-label, phase 3 TRIBE study. Lancet Oncol. 2015;16(13):1306-15.
67. Giantonio BJ, Catalano PJ, Meropol NJ, O'Dwyer PJ, Mitchell EP, Alberts SR, et al. Bevacizumab in combination with oxaliplatin, fluorouracil, and leucovorin (FOLFOX4) for previously treated metastatic colorectal cancer: results from the Eastern Cooperative Oncology Group Study E3200. J Clin Oncol. 2007;25(12):1539-44.
68. Heinemann V, von Weikersthal LF, Decker T, Kiani A, Vehling-Kaiser U, Al-Batran SE, et al. FOLFIRI plus cetuximab versus FOLFIRI plus bevacizumab as first-line treatment for patients with metastatic colorectal cancer (FIRE-3): a randomised, open-label, phase 3 trial. Lancet Oncol. 2014;15(10):1065-75.
69. Hurwitz H, Fehrenbacher L, Novotny W, Cartwright T, Hainsworth J, Heim W, et al. Bevacizumab plus irinotecan, fluorouracil, and leucovorin for metastatic colorectal cancer. N Engl J Med. 2004;350(23):2335-42.
70. NHS England. Bevacizumab in combination with 2nd/3rd line oxaliplatin–based combination chemotherapy for metastatic colorectal cancer. 2015 [Accessed 4th July 2016]. Available from: https://www.england.nhs.uk/wp-content/uploads/2015/09/cdf-decision-summ-bevacizumab_2nd3rdlinemcrc-oxaliplatin.pdf.
71. Mayer RJ, Van Cutsem E, Falcone A, Yoshino T, Garcia-Carbonero R, Mizunuma N, et al. Randomized trial of TAS-102 for refractory metastatic colorectal cancer. N Engl J Med. 2015;372(20):1909-19.
72. Kopetz S, Grothey A, Yaeger R, Van Cutsem E, Desai J, Yoshino T, et al. Encorafenib, Binimetinib, and Cetuximab in BRAF V600E-Mutated Colorectal Cancer. N Engl J Med. 2019;381(17):1632-43.
73. Seligmann JF, Fisher D, Smith CG, Richman SD, Elliott F, Brown S, et al. Investigating the poor outcomes of BRAF-mutant advanced colorectal cancer: analysis from 2530 patients in randomised clinical trials. Ann Oncol. 2017;28(3):562-8.
74. Corcoran RB, André T, Atreya CE, Schellens JHM, Yoshino T, Bendell JC, et al. Combined BRAF, EGFR, and MEK Inhibition in Patients with BRAF(V600E)-Mutant Colorectal Cancer. Cancer Discov. 2018;8(4):428-43.
75. Locke FL, Ghobadi A, Jacobson CA, Miklos DB, Lekakis LJ, Oluwole OO, et al. Long-term safety and activity of axicabtagene ciloleucel in refractory large B-cell lymphoma (ZUMA-1): a single-arm, multicentre, phase 1-2 trial. Lancet Oncol. 2019;20(1):31-42.
76. Darvin P, Toor SM, Sasidharan Nair V, Elkord E. Immune checkpoint inhibitors: recent progress and potential biomarkers. Exp Mol Med. 2018;50(12):1-11.
77. Waldman AD, Fritz JM, Lenardo MJ. A guide to cancer immunotherapy: from T cell basic science to clinical practice. Nat Rev Immunol. 2020:1-18.

78. Motzer RJ, Tannir NM, McDermott DF, Aren Frontera O, Melichar B, Choueiri TK, et al. Nivolumab plus Ipilimumab versus Sunitinib in Advanced Renal-Cell Carcinoma. N Engl J Med. 2018;378(14):1277-90.
79. Pardoll DM. The blockade of immune checkpoints in cancer immunotherapy. Nat Rev Cancer. 2012;12(4):252-64.
80. Garcia-Diaz A, Shin DS, Moreno BH, Saco J, Escuin-Ordinas H, Rodriguez GA, et al. Interferon Receptor Signaling Pathways Regulating PD-L1 and PD-L2 Expression. Cell Rep. 2017;19(6):1189-201.
81. Kruger S, Ilmer M, Kobold S, Cadilha BL, Endres S, Ormanns S, et al. Advances in cancer immunotherapy 2019 – latest trends. J Exp Clin Cancer Res [Internet]. 2019 2019/06/19; 38(1):[268 p.]. Available from: https://doi.org/10.1186/s13046-019-1266-0

https://jeccr.biomedcentral.com/track/pdf/10.1186/s13046-019-1266-0.
82. McGranahan N, Furness AJ, Rosenthal R, Ramskov S, Lyngaa R, Saini SK, et al. Clonal neoantigens elicit T cell immunoreactivity and sensitivity to immune checkpoint blockade. Science. 2016;351(6280):1463-9.
83. Yarchoan M, Hopkins A, Jaffee EM. Tumor Mutational Burden and Response Rate to PD-1 Inhibition. N Engl J Med. 2017;377(25):2500-1.
84. Chan TA, Yarchoan M, Jaffee E, Swanton C, Quezada SA, Stenzinger A, et al. Development of tumor mutation burden as an immunotherapy biomarker: utility for the oncology clinic. Ann Oncol. 2019;30(1):44-56.
85. Goodman AM, Kato S, Bazhenova L, Patel SP, Frampton GM, Miller V, et al. Tumor Mutational Burden as an Independent Predictor of Response to Immunotherapy in Diverse Cancers. Mol Cancer Ther. 2017;16(11):2598-608.
86. Marcus L, Lemery SJ, Keegan P, Pazdur R. FDA Approval Summary: Pembrolizumab for the Treatment of Microsatellite Instability-High Solid Tumors. Clin Cancer Res. 2019;25(13):3753-8.
87. Le DT, Durham JN, Smith KN, Wang H, Bartlett BR, Aulakh LK, et al. Mismatch repair deficiency predicts response of solid tumors to PD-1 blockade. Science. 2017;357(6349):409-13.
88. Ganesh K, Stadler ZK, Cercek A, Mendelsohn RB, Shia J, Segal NH, et al. Immunotherapy in colorectal cancer: rationale, challenges and potential. Nat Rev Gastroenterol Hepatol. 2019;16(6):361-75.
89. Boland PM, Ma WW. Immunotherapy for Colorectal Cancer. Cancers (Basel). 2017;9(5).
90. Lenz HJ, editor Nivolumab plus low-dose ipilimumab as first-line therapy in microsatellite instability-high/DNA mismatch repair deficient metastatic colorectal cancer: Clinical update2020; Gastrointestinal Cancers Symposium: American Society of Clinical Oncology.
91. Overman MJ, Lonardi S, Wong KYM, Lenz HJ, Gelsomino F, Aglietta M, et al. Durable Clinical Benefit With Nivolumab Plus Ipilimumab in DNA Mismatch Repair-Deficient/Microsatellite Instability-High Metastatic Colorectal Cancer. J Clin Oncol. 2018;36(8):773-9.
92. Reck M, Rodríguez-Abreu D, Robinson AG, Hui R, Csőszi T, Fülöp A, et al. Pembrolizumab versus Chemotherapy for PD-L1-Positive Non-Small-Cell Lung Cancer. N Engl J Med. 2016;375(19):1823-33.
93. Zaretsky JM, Garcia-Diaz A, Shin DS, Escuin-Ordinas H, Hugo W, Hu-Lieskovan S, et al. Mutations Associated with Acquired Resistance to PD-1 Blockade in Melanoma. N Engl J Med. 2016;375(9):819-29.
94. Dunn GP, Bruce AT, Ikeda H, Old LJ, Schreiber RD. Cancer immunoediting: from immunosurveillance to tumor escape. Nat Immunol. 2002;3(11):991-8.
95. Syn NL, Teng MWL, Mok TSK, Soo RA. De-novo and acquired resistance to immune checkpoint targeting. Lancet Oncol. 2017;18(12):e731-e41.
96. Shin DS, Zaretsky JM, Escuin-Ordinas H, Garcia-Diaz A, Hu-Lieskovan S, Kalbasi A, et al. Primary Resistance to PD-1 Blockade Mediated by JAK1/2 Mutations. Cancer Discov. 2017;7(2):188-201.

97. Schrock AB, Ouyang C, Sandhu J, Sokol E, Jin D, Ross JS, et al. Tumor mutational burden is predictive of response to immune checkpoint inhibitors in MSI-high metastatic colorectal cancer. Ann Oncol. 2019;30(7):1096-103.
98. Cornel AM, Mimpen IL, Nierkens S. MHC Class I Downregulation in Cancer: Underlying Mechanisms and Potential Targets for Cancer Immunotherapy. Cancers (Basel). 2020;12(7).
99. McGranahan N, Rosenthal R, Hiley CT, Rowan AJ, Watkins TBK, Wilson GA, et al. Allele-Specific HLA Loss and Immune Escape in Lung Cancer Evolution. Cell. 2017;171(6):1259-71.e11.
100. Anfossi N, André P, Guia S, Falk CS, Roetynck S, Stewart CA, et al. Human NK cell education by inhibitory receptors for MHC class I. Immunity. 2006;25(2):331-42.
101. Giannakis M, Mu XJ, Shukla SA, Qian ZR, Cohen O, Nishihara R, et al. Genomic Correlates of Immune-Cell Infiltrates in Colorectal Carcinoma. Cell Rep. 2016;15(4):857-65.
102. Kalbasi A, Ribas A. Tumour-intrinsic resistance to immune checkpoint blockade. Nat Rev Immunol. 2019.
103. Fish EN, Platanias LC. Interferon receptor signaling in malignancy: a network of cellular pathways defining biological outcomes. Mol Cancer Res. 2014;12(12):1691-703.
104. Gao J, Shi LZ, Zhao H, Chen J, Xiong L, He Q, et al. Loss of IFN-γ Pathway Genes in Tumor Cells as a Mechanism of Resistance to Anti-CTLA-4 Therapy. Cell. 2016;167(2):397-404.e9.
105. Manguso RT, Pope HW, Zimmer MD, Brown FD, Yates KB, Miller BC, et al. In vivo CRISPR screening identifies Ptpn2 as a cancer immunotherapy target. Nature. 2017;547(7664):413-8.
106. Patel SJ, Sanjana NE, Kishton RJ, Eidizadeh A, Vodnala SK, Cam M, et al. Identification of essential genes for cancer immunotherapy. Nature. 2017;548(7669):537-42.
107. Lal N, White BS, Goussous G, Pickles O, Mason MJ, Beggs AD, et al. KRAS Mutation and Consensus Molecular Subtypes 2 and 3 Are Independently Associated with Reduced Immune Infiltration and Reactivity in Colorectal Cancer. Clin Cancer Res. 2018;24(1):224-33.
108. Klampfer L, Huang J, Corner G, Mariadason J, Arango D, Sasazuki T, et al. Oncogenic Ki-ras inhibits the expression of interferon-responsive genes through inhibition of STAT1 and STAT2 expression. J Biol Chem. 2003;278(47):46278-87.
109. Loi S, Dushyanthen S, Beavis PA, Salgado R, Denkert C, Savas P, et al. RAS/MAPK Activation Is Associated with Reduced Tumor-Infiltrating Lymphocytes in Triple-Negative Breast Cancer: Therapeutic Cooperation Between MEK and PD-1/PD-L1 Immune Checkpoint Inhibitors. Clin Cancer Res. 2016;22(6):1499-509.
110. Liao W, Overman MJ, Boutin AT, Shang X, Zhao D, Dey P, et al. KRAS-IRF2 Axis Drives Immune Suppression and Immune Therapy Resistance in Colorectal Cancer. Cancer Cell. 2019;35(4):559-72.e7.
111. Hu-Lieskovan S, Mok S, Homet Moreno B, Tsoi J, Robert L, Goedert L, et al. Improved antitumor activity of immunotherapy with BRAF and MEK inhibitors in BRAF(V600E) melanoma. Sci Transl Med. 2015;7(279):279ra41.
112. Khalili JS, Liu S, Rodriguez-Cruz TG, Whittington M, Wardell S, Liu C, et al. Oncogenic BRAF(V600E) promotes stromal cell-mediated immunosuppression via induction of interleukin-1 in melanoma. Clin Cancer Res. 2012;18(19):5329-40.
113. Pai SG, Carneiro BA, Mota JM, Costa R, Leite CA, Barroso-Sousa R, et al. Wnt/beta-catenin pathway: modulating anticancer immune response. J Hematol Oncol. 2017;10(1):101.
114. Luke JJ, Bao R, Sweis RF, Spranger S, Gajewski TF. WNT/β-catenin Pathway Activation Correlates with Immune Exclusion across Human Cancers. Clin Cancer Res. 2019;25(10):3074-83.
115. Gabrilovich DI. Myeloid-Derived Suppressor Cells. Cancer Immunol Res. 2017;5(1):3-8.
116. Alkasalias T, Moyano-Galceran L, Arsenian-Henriksson M, Lehti K. Fibroblasts in the Tumor Microenvironment: Shield or Spear? Int J Mol Sci. 2018;19(5).
117. Chaudhary B, Elkord E. Regulatory T Cells in the Tumor Microenvironment and Cancer Progression: Role and Therapeutic Targeting. Vaccines (Basel). 2016;4(3).

118. Kuwahara T, Hazama S, Suzuki N, Yoshida S, Tomochika S, Nakagami Y, et al. Intratumoural-infiltrating CD4 + and FOXP3 + T cells as strong positive predictive markers for the prognosis of resectable colorectal cancer. Br J Cancer. 2019;121(8):659-65.
119. Ladoire S, Martin F, Ghiringhelli F. Prognostic role of FOXP3+ regulatory T cells infiltrating human carcinomas: the paradox of colorectal cancer. Cancer Immunol Immunother. 2011;60(7):909-18.
120. Zhang X, Kelaria S, Kerstetter J, Wang J. The functional and prognostic implications of regulatory T cells in colorectal carcinoma. J Gastrointest Oncol. 2015;6(3):307-13.
121. Pauken KE, Sammons MA, Odorizzi PM, Manne S, Godec J, Khan O, et al. Epigenetic stability of exhausted T cells limits durability of reinvigoration by PD-1 blockade. Science. 2016;354(6316):1160-5.
122. Ebert PJR, Cheung J, Yang Y, McNamara E, Hong R, Moskalenko M, et al. MAP Kinase Inhibition Promotes T Cell and Anti-tumor Activity in Combination with PD-L1 Checkpoint Blockade. Immunity. 2016;44(3):609-21.
123. Guo JJ, Li QL, Zhang J, Huang AL. Histone deacetylation is involved in activation of CXCL10 upon IFNgamma stimulation. Mol Cells. 2006;22(2):163-7.
124. Vitetta L, Vitetta G, Hall S. Immunological Tolerance and Function: Associations Between Intestinal Bacteria, Probiotics, Prebiotics, and Phages. Front Immunol. 2018;9:2240.
125. Tilg H, Adolph TE, Gerner RR, Moschen AR. The Intestinal Microbiota in Colorectal Cancer. Cancer Cell. 2018;33(6):954-64.
126. Li YY, Ge QX, Cao J, Zhou YJ, Du YL, Shen B, et al. Association of Fusobacterium nucleatum infection with colorectal cancer in Chinese patients. World J Gastroenterol. 2016;22(11):3227-33.
127. Chaput N, Lepage P, Coutzac C, Soularue E, Le Roux K, Monot C, et al. Baseline gut microbiota predicts clinical response and colitis in metastatic melanoma patients treated with ipilimumab. Ann Oncol. 2017;28(6):1368-79.
128. Ueda K, Yonekura S, Ogasawara N, Matsunaga Y, Hoshino R, Kurose H, et al. The Impact of Antibiotics on Prognosis of Metastatic Renal Cell Carcinoma in Japanese Patients Treated With Immune Checkpoint Inhibitors. Anticancer Res. 2019;39(11):6265-71.
129. Bullman S, Pedamallu CS, Sicinska E, Clancy TE, Zhang X, Cai D, et al. Analysis of Fusobacterium persistence and antibiotic response in colorectal cancer. Science. 2017;358(6369):1443-8.
130. Yu L, Wang L, Chen S. Dual character of Toll-like receptor signaling: pro-tumorigenic effects and anti-tumor functions. Biochim Biophys Acta. 2013;1835(2):144-54.
131. Kesselring R, Glaesner J, Hiergeist A, Naschberger E, Neumann H, Brunner SM, et al. IRAK-M Expression in Tumor Cells Supports Colorectal Cancer Progression through Reduction of Antimicrobial Defense and Stabilization of STAT3. Cancer Cell. 2016;29(5):684-96.
132. Brown JH, Jardetzky TS, Gorga JC, Stern LJ, Urban RG, Strominger JL, et al. Three-dimensional structure of the human class II histocompatibility antigen HLA-DR1. Nature. 1993;364(6432):33-9.
133. Jones EY, Fugger L, Strominger JL, Siebold C. MHC class II proteins and disease: a structural perspective. Nat Rev Immunol. 2006;6(4):271-82.
134. Auffray C, Kuo J, DeMars R, Strominger JL. A minimum of four human class II alpha-chain genes are encoded in the HLA region of chromosome 6. Nature. 1983;304(5922):174-7.
135. Chicz RM, Urban RG, Gorga JC, Vignali DA, Lane WS, Strominger JL. Specificity and promiscuity among naturally processed peptides bound to HLA-DR alleles. J Exp Med. 1993;178(1):27-47.
136. Guo HC, Jardetzky TS, Garrett TP, Lane WS, Strominger JL, Wiley DC. Different length peptides bind to HLA-Aw68 similarly at their ends but bulge out in the middle. Nature. 1992;360(6402):364-6.
137. Drozina G, Kohoutek J, Jabrane-Ferrat N, Peterlin BM. Expression of MHC II genes. Curr Top Microbiol Immunol. 2005;290:147-70.

138. Mayer L, Eisenhardt D, Salomon P, Bauer W, Plous R, Piccinini L. Expression of class II molecules on intestinal epithelial cells in humans. Differences between normal and inflammatory bowel disease. Gastroenterology. 1991;100(1):3-12.
139. Seliger B, Kloor M, Ferrone S. HLA class II antigen-processing pathway in tumors: Molecular defects and clinical relevance. Oncoimmunology. 2017;6(2):e1171447.
140. Neefjes JJ, Stollorz V, Peters PJ, Geuze HJ, Ploegh HL. The biosynthetic pathway of MHC class II but not class I molecules intersects the endocytic route. Cell. 1990;61(1):171-83.
141. Roche PA, Cresswell P. Invariant chain association with HLA-DR molecules inhibits immunogenic peptide binding. Nature. 1990;345(6276):615-8.
142. Wieczorek M, Abualrous ET, Sticht J, Álvaro-Benito M, Stolzenberg S, Noé F, et al. Major Histocompatibility Complex (MHC) Class I and MHC Class II Proteins: Conformational Plasticity in Antigen Presentation. Front Immunol. 2017;8:292.
143. Anders AK, Call MJ, Schulze MS, Fowler KD, Schubert DA, Seth NP, et al. HLA-DM captures partially empty HLA-DR molecules for catalyzed removal of peptide. Nat Immunol. 2011;12(1):54-61.
144. Guce AI, Mortimer SE, Yoon T, Painter CA, Jiang W, Mellins ED, et al. HLA-DO acts as a substrate mimic to inhibit HLA-DM by a competitive mechanism. Nat Struct Mol Biol. 2013;20(1):90-8.
145. Rocha N, Neefjes J. MHC class II molecules on the move for successful antigen presentation. EMBO J. 2008;27(1):1-5.
146. Muhlethaler-Mottet A, Otten LA, Steimle V, Mach B. Expression of MHC class II molecules in different cellular and functional compartments is controlled by differential usage of multiple promoters of the transactivator CIITA. EMBO J. 1997;16(10):2851-60.
147. Feng XM, Chen XL, Liu N, Chen Z, Zhou YL, Han ZB, et al. Interleukin-27 upregulates major histocompatibility complex class II expression in primary human endothelial cells through induction of major histocompatibility complex class II transactivator. Hum Immunol. 2007;68(12):965-72.
148. Accolla RS, Scarpellino L, Carra G, Guardiola J. Trans-acting element(s) operating across species barriers positively regulate expression of major histocompatibility complex class II genes. J Exp Med. 1985;162(4):1117-33.
149. Accolla RS, Jotterand-Bellomo M, Scarpellino L, Maffei A, Carra G, Guardiola J. aIr-1, a newly found locus on mouse chromosome 16 encoding a trans-acting activator factor for MHC class II gene expression. J Exp Med. 1986;164(1):369-74.
150. Steimle V, Otten LA, Zufferey M, Mach B. Complementation cloning of an MHC class II transactivator mutated in hereditary MHC class II deficiency (or bare lymphocyte syndrome). Cell. 1993;75(1):135-46.
151. Wright KL, Ting JP. Epigenetic regulation of MHC-II and CIITA genes. Trends Immunol. 2006;27(9):405-12.
152. Ni Z, Abou El Hassan M, Xu Z, Yu T, Bremner R. The chromatin-remodeling enzyme BRG1 coordinates CIITA induction through many interdependent distal enhancers. Nat Immunol. 2008;9(7):785-93.
153. Abou El Hassan M, Yu T, Song L, Bremner R. Polycomb Repressive Complex 2 Confers BRG1 Dependency on the CIITA Locus. J Immunol. 2015;194(10):5007-13.
154. de Bruin EC, van de Velde CJ, van Krieken JH, Marijnen CA, Medema JP. Epithelial human leukocyte antigen-DR expression predicts reduced recurrence rates and prolonged survival in rectal cancer patients. Clin Cancer Res. 2008;14(4):1073-9.
155. Matsushita K, Takenouchi T, Shimada H, Tomonaga T, Hayashi H, Shioya A, et al. Strong HLA-DR antigen expression on cancer cells relates to better prognosis of colorectal cancer patients: Possible involvement of c-myc suppression by interferon-gamma in situ. Cancer Sci. 2006;97(1):57-63.

156. Sconocchia G, Eppenberger-Castori S, Zlobec I, Karamitopoulou E, Arriga R, Coppola A, et al. HLA class II antigen expression in colorectal carcinoma tumors as a favorable prognostic marker. Neoplasia. 2014;16(1):31-42.
157. Esteban F, Ruiz-Cabello F, Concha A, Perez-Ayala M, Sanchez-Rozas JA, Garrido F. HLA-DR expression is associated with excellent prognosis in squamous cell carcinoma of the larynx. Clin Exp Metastasis. 1990;8(4):319-28.
158. Hilders CG, Houbiers JG, van Ravenswaay Claasen HH, Veldhuizen RW, Fleuren GJ. Association between HLA-expression and infiltration of immune cells in cervical carcinoma. Lab Invest. 1993;69(6):651-9.
159. Samuels S, Spaans VM, Osse M, Peters LAW, Kenter GG, Fleuren GJ, et al. Human Leukocyte Antigen-DR Expression is Significantly Related to an Increased Disease-Free and Disease-Specific Survival in Patients With Cervical Adenocarcinoma. Int J Gynecol Cancer. 2016;26(8):1503-9.
160. Shi B, Vinyals A, Alia P, Broceno C, Chen F, Adrover M, et al. Differential expression of MHC class II molecules in highly metastatic breast cancer cells is mediated by the regulation of the CIITA transcription Implication of CIITA in tumor and metastasis development. Int J Biochem Cell Biol. 2006;38(4):544-62.
161. Roemer MGM, Redd RA, Cader FZ, Pak CJ, Abdelrahman S, Ouyang J, et al. Major Histocompatibility Complex Class II and Programmed Death Ligand 1 Expression Predict Outcome After Programmed Death 1 Blockade in Classic Hodgkin Lymphoma. J Clin Oncol. 2018;36(10):942-50.
162. Johnson DB, Bordeaux J, Kim JY, Vaupel C, Rimm DL, Ho TH, et al. Quantitative Spatial Profiling of PD-1/PD-L1 Interaction and HLA-DR/IDO-1 Predicts Improved Outcomes of Anti-PD-1 Therapies in Metastatic Melanoma. Clin Cancer Res. 2018;24(21):5250-60.
163. Wosen JE, Mukhopadhyay D, Macaubas C, Mellins ED. Epithelial MHC Class II Expression and Its Role in Antigen Presentation in the Gastrointestinal and Respiratory Tracts. Front Immunol. 2018;9:2144.
164. Arnaud-Battandier F, Cerf-Bensussan N, Amsellem R, Schmitz J. Increased HLA-DR expression by enterocytes in children with celiac disease. Gastroenterology. 1986;91(5):1206-12.
165. Hershberg RM, Cho DH, Youakim A, Bradley MB, Lee JS, Framson PE, et al. Highly polarized HLA class II antigen processing and presentation by human intestinal epithelial cells. J Clin Invest. 1998;102(4):792-803.
166. Hershberg RM, Framson PE, Cho DH, Lee LY, Kovats S, Beitz J, et al. Intestinal epithelial cells use two distinct pathways for HLA class II antigen processing. J Clin Invest. 1997;100(1):204-15.
167. Olaussen RW, Johansen FE, Lundin KE, Jahnsen J, Brandtzaeg P, Farstad IN. Interferon-gamma-secreting T cells localize to the epithelium in coeliac disease. Scand J Immunol. 2002;56(6):652-64.
168. Wosen JE, Ilstad-Minnihan A, Co JY, Jiang W, Mukhopadhyay D, Fernandez-Becker NQ, et al. Human Intestinal Enteroids Model MHC-II in the Gut Epithelium. Front Immunol. 2019;10:1970.
169. Koyama M, Mukhopadhyay P, Schuster IS, Henden AS, Hülsdünker J, Varelias A, et al. MHC Class II Antigen Presentation by the Intestinal Epithelium Initiates Graft-versus-Host Disease and Is Influenced by the Microbiota. Immunity. 2019;51(5):885-98.e7.
170. Xie Y, Akpinarli A, Maris C, Hipkiss EL, Lane M, Kwon EK, et al. Naive tumor-specific CD4(+) T cells differentiated in vivo eradicate established melanoma. J Exp Med. 2010;207(3):651-67.
171. Tran E, Turcotte S, Gros A, Robbins PF, Lu YC, Dudley ME, et al. Cancer immunotherapy based on mutation-specific CD4+ T cells in a patient with epithelial cancer. Science. 2014;344(6184):641-5.
172. Kreiter S, Vormehr M, van de Roemer N, Diken M, Lower M, Diekmann J, et al. Mutant MHC class II epitopes drive therapeutic immune responses to cancer. Nature. 2015;520(7549):692-6.
173. Arnold PY, La Gruta NL, Miller T, Vignali KM, Adams PS, Woodland DL, et al. The majority of immunogenic epitopes generate CD4+ T cells that are dependent on MHC class II-bound peptide-flanking residues. J Immunol. 2002;169(2):739-49.

174. Linnemann C, van Buuren MM, Bies L, Verdegaal EM, Schotte R, Calis JJ, et al. High-throughput epitope discovery reveals frequent recognition of neo-antigens by CD4+ T cells in human melanoma. Nat Med. 2015;21(1):81-5.
175. Marty Pyke R, Thompson WK, Salem RM, Font-Burgada J, Zanetti M, Carter H. Evolutionary Pressure against MHC Class II Binding Cancer Mutations. Cell. 2018;175(2):416-28.e13.
176. Corthay A, Skovseth DK, Lundin KU, Rosjo E, Omholt H, Hofgaard PO, et al. Primary antitumor immune response mediated by CD4+ T cells. Immunity. 2005;22(3):371-83.
177. Haabeth OAW, Fauskanger M, Manzke M, Lundin KU, Corthay A, Bogen B, et al. CD4(+) T-cell-Mediated Rejection of MHC Class II-Positive Tumor Cells Is Dependent on Antigen Secretion and Indirect Presentation on Host APCs. Cancer Res. 2018;78(16):4573-85.
178. Axelrod ML, Cook RS, Johnson DB, Balko JM. Biological Consequences of MHC-II Expression by Tumor Cells in Cancer. Clin Cancer Res. 2019;25(8):2392-402.
179. Frangione V, Mortara L, Castellani P, De Lerma Barbaro A, Accolla RS. CIITA-driven MHC-II positive tumor cells: preventive vaccines and superior generators of antitumor CD4+ T lymphocytes for immunotherapy. Int J Cancer. 2010;127(7):1614-24.
180. Mortara L, Castellani P, Meazza R, Tosi G, De Lerma Barbaro A, Procopio FA, et al. CIITA-induced MHC class II expression in mammary adenocarcinoma leads to a Th1 polarization of the tumor microenvironment, tumor rejection, and specific antitumor memory. Clin Cancer Res. 2006;12(11 Pt 1):3435-43.
181. Bou Nasser Eddine F, Forlani G, Lombardo L, Tedeschi A, Tosi G, Accolla RS. CIITA-driven MHC class II expressing tumor cells can efficiently prime naive CD4(+) TH cells in vivo and vaccinate the host against parental MHC-II-negative tumor cells. Oncoimmunology. 2017;6(1):e1261777.
182. Albacker LA, Wu J, Smith P, Warmuth M, Stephens PJ, Zhu P, et al. Loss of function JAK1 mutations occur at high frequency in cancers with microsatellite instability and are suggestive of immune evasion. PLoS One. 2017;12(11):e0176181.
183. Lu Y, Ussery GD, Muncaster MM, Gallie BL, Blanck G. Evidence for retinoblastoma protein (RB) dependent and independent IFN-gamma responses: RB coordinately rescues IFN-gamma induction of MHC class II gene transcription in noninducible breast carcinoma cells. Oncogene. 1994;9(4):1015-9.
184. Mottok A, Woolcock B, Chan FC, Tong KM, Chong L, Farinha P, et al. Genomic Alterations in CIITA Are Frequent in Primary Mediastinal Large B Cell Lymphoma and Are Associated with Diminished MHC Class II Expression. Cell Rep. 2015;13(7):1418-31.
185. Michel S, Linnebacher M, Alcaniz J, Voss M, Wagner R, Dippold W, et al. Lack of HLA class II antigen expression in microsatellite unstable colorectal carcinomas is caused by mutations in HLA class II regulatory genes. Int J Cancer. 2010;127(4):889-98.
186. Yazawa T, Ito T, Kamma H, Suzuki T, Okudela K, Hayashi H, et al. Complicated mechanisms of class II transactivator transcription deficiency in small cell lung cancer and neuroblastoma. Am J Pathol. 2002;161(1):291-300.
187. Strahl BD, Allis CD. The language of covalent histone modifications. Nature. 2000;403(6765):41-5.
188. Rice JC, Briggs SD, Ueberheide B, Barber CM, Shabanowitz J, Hunt DF, et al. Histone methyltransferases direct different degrees of methylation to define distinct chromatin domains. Mol Cell. 2003;12(6):1591-8.
189. Stewart MD, Li J, Wong J. Relationship between histone H3 lysine 9 methylation, transcription repression, and heterochromatin protein 1 recruitment. Mol Cell Biol. 2005;25(7):2525-38.
190. Cao R, Wang L, Wang H, Xia L, Erdjument-Bromage H, Tempst P, et al. Role of histone H3 lysine 27 methylation in Polycomb-group silencing. Science. 2002;298(5595):1039-43.
191. Fuks F, Hurd PJ, Deplus R, Kouzarides T. The DNA methyltransferases associate with HP1 and the SUV39H1 histone methyltransferase. Nucleic Acids Res. 2003;31(9):2305-12.

192. Segovia C, San José-Enériz E, Munera-Maravilla E, Martínez-Fernández M, Garate L, Miranda E, et al. Inhibition of a G9a/DNMT network triggers immune-mediated bladder cancer regression. Nat Med. 2019;25(7):1073-81.
193. Chiappinelli KB, Strissel PL, Desrichard A, Li H, Henke C, Akman B, et al. Inhibiting DNA Methylation Causes an Interferon Response in Cancer via dsRNA Including Endogenous Retroviruses. Cell. 2015;162(5):974-86.
194. Roulois D, Loo Yau H, Singhania R, Wang Y, Danesh A, Shen SY, et al. DNA-Demethylating Agents Target Colorectal Cancer Cells by Inducing Viral Mimicry by Endogenous Transcripts. Cell. 2015;162(5):961-73.
195. Saito Y, Nakaoka T, Sakai K, Muramatsu T, Toshimitsu K, Kimura M, et al. Inhibition of DNA Methylation Suppresses Intestinal Tumor Organoids by Inducing an Anti-Viral Response. Sci Rep. 2016;6:25311.
196. Satoh A, Toyota M, Ikeda H, Morimoto Y, Akino K, Mita H, et al. Epigenetic inactivation of class II transactivator (CIITA) is associated with the absence of interferon-gamma-induced HLA-DR expression in colorectal and gastric cancer cells. Oncogene. 2004;23(55):8876-86.
197. Ramia E, Chiaravalli AM, Bou Nasser Eddine F, Tedeschi A, Sessa F, Accolla RS, et al. CIITA-related block of HLA class II expression, upregulation of HLA class I, and heterogeneous expression of immune checkpoints in hepatocarcinomas: implications for new therapeutic approaches. Oncoimmunology. 2019;8(3):1548243.
198. Croce M, De Ambrosis A, Corrias MV, Pistoia V, Occhino M, Meazza R, et al. Different levels of control prevent interferon-gamma-inducible HLA-class II expression in human neuroblastoma cells. Oncogene. 2003;22(49):7848-57.
199. Morimoto Y, Toyota M, Satoh A, Murai M, Mita H, Suzuki H, et al. Inactivation of class II transactivator by DNA methylation and histone deacetylation associated with absence of HLA-DR induction by interferon-gamma in haematopoietic tumour cells. Br J Cancer. 2004;90(4):844-52.
200. Taylor AW. Ocular Immune Privilege and Transplantation. Front Immunol. 2016;7:37.
201. Radosevich M, Jager M, Ono SJ. Inhibition of MHC class II gene expression in uveal melanoma cells is due to methylation of the CIITA gene or an upstream activator. Exp Mol Pathol. 2007;82(1):68-76.
202. van den Elsen PJ, van der Stoep N, Viëtor HE, Wilson L, van Zutphen M, Gobin SJ. Lack of CIITA expression is central to the absence of antigen presentation functions of trophoblast cells and is caused by methylation of the IFN-gamma inducible promoter (PIV) of CIITA. Hum Immunol. 2000;61(9):850-62.
203. van der Stoep N, Biesta P, Quinten E, van den Elsen PJ. Lack of IFN-gamma-mediated induction of the class II transactivator (CIITA) through promoter methylation is predominantly found in developmental tumor cell lines. Int J Cancer. 2002;97(4):501-7.
204. Turner TB, Meza-Perez S, Londono A, Katre A, Peabody JE, Smith HJ, et al. Epigenetic modifiers upregulate MHC II and impede ovarian cancer tumor growth. Oncotarget. 2017;8(27):44159-70.
205. Smiraglia DJ, Rush LJ, Fruhwald MC, Dai Z, Held WA, Costello JF, et al. Excessive CpG island hypermethylation in cancer cell lines versus primary human malignancies. Hum Mol Genet. 2001;10(13):1413-9.
206. Suter CM, Norrie M, Ku SL, Cheong KF, Tomlinson I, Ward RL. CpG island methylation is a common finding in colorectal cancer cell lines. Br J Cancer. 2003;88(3):413-9.
207. Nestor CE, Ottaviano R, Reinhardt D, Cruickshanks HA, Mjoseng HK, McPherson RC, et al. Rapid reprogramming of epigenetic and transcriptional profiles in mammalian culture systems. Genome Biol. 2015;16(1):11.
208. Holtz R, Choi JC, Petroff MG, Piskurich JF, Murphy SP. Class II transactivator (CIITA) promoter methylation does not correlate with silencing of CIITA transcription in trophoblasts. Biol Reprod. 2003;69(3):915-24.

209. Kanaseki T, Ikeda H, Takamura Y, Toyota M, Hirohashi Y, Tokino T, et al. Histone deacetylation, but not hypermethylation, modifies class II transactivator and MHC class II gene expression in squamous cell carcinomas. J Immunol. 2003;170(10):4980-5.
210. Kondo H, Sahara H, Miyazaki A, Nabeta Y, Hirohashi Y, Kanaseki T, et al. Natural antigenic peptides from squamous cell carcinoma recognized by autologous HLA-DR8-restricted CD4+ T cells. Jpn J Cancer Res. 2002;93(8):917-24.
211. Holling TM, Bergevoet MW, Wilson L, Van Eggermond MC, Schooten E, Steenbergen RD, et al. A role for EZH2 in silencing of IFN-gamma inducible MHC2TA transcription in uveal melanoma. J Immunol. 2007;179(8):5317-25.
212. Truax AD, Thakkar M, Greer SF. Dysregulated recruitment of the histone methyltransferase EZH2 to the class II transactivator (CIITA) promoter IV in breast cancer cells. PLoS One. 2012;7(4):e36013.
213. Herviou L, Jourdan M, Martinez AM, Cavalli G, Moreaux J. EZH2 is overexpressed in transitional preplasmablasts and is involved in human plasma cell differentiation. Leukemia. 2019;33(8):2047-60.
214. Lee JJ, Sun W, Bahary N, Ohr J, Rhee JC, Stoller RG, et al. Phase 2 study of pembrolizumab in combination with azacitidine in subjects with metastatic colorectal cancer. J Clin Oncol. 2017;35(15_suppl):3054-.
215. Levy BP, Giaccone G, Besse B, Felip E, Garassino MC, Domine Gomez M, et al. Randomised phase 2 study of pembrolizumab plus CC-486 versus pembrolizumab plus placebo in patients with previously treated advanced non-small cell lung cancer. Eur J Cancer. 2019;108:120-8.
216. Jeong HM, Kwon MJ, Shin YK. Overexpression of Cancer-Associated Genes via Epigenetic Derepression Mechanisms in Gynecologic Cancer. Front Oncol. 2014;4:12.
217. Jung P, Sato T, Merlos-Suarez A, Barriga FM, Iglesias M, Rossell D, et al. Isolation and in vitro expansion of human colonic stem cells. Nat Med. 2011;17(10):1225-7.
218. Sato T, Vries RG, Snippert HJ, van de Wetering M, Barker N, Stange DE, et al. Single Lgr5 stem cells build crypt-villus structures in vitro without a mesenchymal niche. Nature. 2009;459(7244):262-5.
219. Buzzelli JN, Ouaret D, Brown G, Allen PD, Muschel RJ. Colorectal cancer liver metastases organoids retain characteristics of original tumor and acquire chemotherapy resistance. Stem Cell Res. 2018;27:109-20.
220. Ganesh K, Wu C, O'Rourke KP, Szeglin BC, Zheng Y, Sauve CG, et al. A rectal cancer organoid platform to study individual responses to chemoradiation. Nat Med. 2019.
221. van de Wetering M, Francies HE, Francis JM, Bounova G, Iorio F, Pronk A, et al. Prospective derivation of a living organoid biobank of colorectal cancer patients. Cell. 2015;161(4):933-45.
222. Vlachogiannis G, Hedayat S, Vatsiou A, Jamin Y, Fernández-Mateos J, Khan K, et al. Patient-derived organoids model treatment response of metastatic gastrointestinal cancers. Science. 2018;359(6378):920-6.
223. Yao Y, Xu X, Yang L, Zhu J, Wan J, Shen L, et al. Patient-Derived Organoids Predict Chemoradiation Responses of Locally Advanced Rectal Cancer. Cell Stem Cell. 2019.
224. Ganesh K, Wu C, O'Rourke KP, Szeglin BC, Zheng Y, Sauve CG, et al. A rectal cancer organoid platform to study individual responses to chemoradiation. Nat Med. 2019;25(10):1607-14.
225. Ooft SN, Weeber F, Dijkstra KK, McLean CM, Kaing S, van Werkhoven E, et al. Patient-derived organoids can predict response to chemotherapy in metastatic colorectal cancer patients. Sci Transl Med. 2019;11(513).
226. Weiswald LB, Bellet D, Dangles-Marie V. Spherical cancer models in tumor biology. Neoplasia. 2015;17(1):1-15.
227. Zhao H, Yan C, Hu Y, Mu L, Huang K, Li Q, et al. Sphere-forming assay vs. organoid culture: Determining long-term stemness and the chemoresistant capacity of primary colorectal cancer cells. Int J Oncol. 2019;54(3):893-904.

228. Tsai S, McOlash L, Palen K, Johnson B, Duris C, Yang Q, et al. Development of primary human pancreatic cancer organoids, matched stromal and immune cells and 3D tumor microenvironment models. BMC Cancer. 2018;18(1):335.
229. Dijkstra KK, Cattaneo CM, Weeber F, Chalabi M, van de Haar J, Fanchi LF, et al. Generation of Tumor-Reactive T Cells by Co-culture of Peripheral Blood Lymphocytes and Tumor Organoids. Cell. 2018;174(6):1586-98.e12.
230. Kraiczy J, Nayak KM, Howell KJ, Ross A, Forbester J, Salvestrini C, et al. DNA methylation defines regional identity of human intestinal epithelial organoids and undergoes dynamic changes during development. Gut. 2019;68(1):49-61.
231. Kraiczy J, Zilbauer M. Intestinal Epithelial Organoids as Tools to Study Epigenetics in Gut Health and Disease. Stem Cells Int. 2019;2019:7242415.
232. Howell KJ, Kraiczy J, Nayak KM, Gasparetto M, Ross A, Lee C, et al. DNA Methylation and Transcription Patterns in Intestinal Epithelial Cells From Pediatric Patients With Inflammatory Bowel Diseases Differentiate Disease Subtypes and Associate With Outcome. Gastroenterology. 2018;154(3):585-98.
233. Joshi R, Castro De Moura M, Piñeyro D, Alvarez-Errico D, Arribas C, Esteller M. The DNA methylation landscape of human cancer organoids available at the American type culture collection. Epigenetics. 2020:1-11.
234. Weeber F, van de Wetering M, Hoogstraat M, Dijkstra KK, Krijgsman O, Kuilman T, et al. Preserved genetic diversity in organoids cultured from biopsies of human colorectal cancer metastases. Proc Natl Acad Sci U S A. 2015;112(43):13308-11.
235. Han SH, Shim S, Kim MJ, Shin HY, Jang WS, Lee SJ, et al. Long-term culture-induced phenotypic difference and efficient cryopreservation of small intestinal organoids by treatment timing of Rho kinase inhibitor. World J Gastroenterol. 2017;23(6):964-75.
236. McCabe MT, Ott HM, Ganji G, Korenchuk S, Thompson C, Van Aller GS, et al. EZH2 inhibition as a therapeutic strategy for lymphoma with EZH2-activating mutations. Nature. 2012;492(7427):108-12.
237. Xiong X, Zhang J, Li A, Dai L, Qin S, Wang P, et al. GSK343 induces programmed cell death through the inhibition of EZH2 and FBP1 in osteosarcoma cells. Cancer Biol Ther. 2020;21(3):213-22.
238. Koppens MA, Bounova G, Cornelissen-Steijger P, de Vries N, Sansom OJ, Wessels LF, et al. Large variety in a panel of human colon cancer organoids in response to EZH2 inhibition. Oncotarget. 2016;7(43):69816-28.
239. Bradley WD, Arora S, Busby J, Balasubramanian S, Gehling VS, Nasveschuk CG, et al. EZH2 inhibitor efficacy in non-Hodgkin's lymphoma does not require suppression of H3K27 monomethylation. Chem Biol. 2014;21(11):1463-75.
240. Maryan N, Statkiewicz M, Mikula M, Goryca K, Paziewska A, Strzałkowska A, et al. Regulation of the expression of claudin 23 by the enhancer of zeste 2 polycomb group protein in colorectal cancer. Mol Med Rep. 2015;12(1):728-36.
241. Flis S, Gnyszka A, Flis K, Spławiński J. MS275 enhances cytotoxicity induced by 5-fluorouracil in the colorectal cancer cells. Eur J Pharmacol. 2010;627(1-3):26-32.
242. Livak KJ, Schmittgen TD. Analysis of relative gene expression data using real-time quantitative PCR and the 2(-Delta Delta C(T)) Method. Methods. 2001;25(4):402-8.
243. Wang RY, Gehrke CW, Ehrlich M. Comparison of bisulfite modification of 5-methyldeoxycytidine and deoxycytidine residues. Nucleic Acids Res. 1980;8(20):4777-90.
244. Butcher LM, Ito M, Brimpari M, Morris TJ, Soares FAC, Ährlund-Richter L, et al. Non-CG DNA methylation is a biomarker for assessing endodermal differentiation capacity in pluripotent stem cells. Nat Commun. 2016;7:10458.
245. Ronaghi M, Uhlén M, Nyrén P. A sequencing method based on real-time pyrophosphate. Science. 1998;281(5375):363, 5.

246. Bolger AM, Lohse M, Usadel B. Trimmomatic: a flexible trimmer for Illumina sequence data. Bioinformatics. 2014;30(15):2114-20.
247. Dunn T, Berry G, Emig-Agius D, Jiang Y, Lei S, Iyer A, et al. Pisces: an accurate and versatile variant caller for somatic and germline next-generation sequencing data. Bioinformatics. 2019;35(9):1579-81.
248. McLaren W, Gil L, Hunt SE, Riat HS, Ritchie GR, Thormann A, et al. The Ensembl Variant Effect Predictor. Genome Biol. 2016;17(1):122.
249. Auton A, Brooks LD, Durbin RM, Garrison EP, Kang HM, Korbel JO, et al. A global reference for human genetic variation. Nature. 2015;526(7571):68-74.
250. Karczewski KJ, Francioli LC, Tiao G, Cummings BB, Alföldi J, Wang Q, et al. The mutational constraint spectrum quantified from variation in 141,456 humans. Nature. 2020;581(7809):434-43.
251. Sherry ST, Ward M, Sirotkin K. dbSNP-database for single nucleotide polymorphisms and other classes of minor genetic variation. Genome Res. 1999;9(8):677-9.
252. Abyzov A, Urban AE, Snyder M, Gerstein M. CNVnator: an approach to discover, genotype, and characterize typical and atypical CNVs from family and population genome sequencing. Genome Res. 2011;21(6):974-84.
253. Chen X, Schulz-Trieglaff O, Shaw R, Barnes B, Schlesinger F, Källberg M, et al. Manta: rapid detection of structural variants and indels for germline and cancer sequencing applications. Bioinformatics. 2016;32(8):1220-2.
254. Dilthey AT, Mentzer AJ, Carapito R, Cutland C, Cereb N, Madhi SA, et al. HLA*LA-HLA typing from linearly projected graph alignments. Bioinformatics. 2019;35(21):4394-6.
255. Berkers G, van Mourik P, Vonk AM, Kruisselbrink E, Dekkers JF, de Winter-de Groot KM, et al. Rectal Organoids Enable Personalized Treatment of Cystic Fibrosis. Cell Rep. 2019;26(7):1701-8.e3.
256. Eide PW, Bruun J, Lothe RA, Sveen A. CMScaller: an R package for consensus molecular subtyping of colorectal cancer pre-clinical models. Sci Rep. 2017;7(1):16618.
257. Crisafulli S, Pandya Y, Moolchan K, Lavoie T. Interferon gamma: activity and ELISA detection comparisons. Biotechniques. 2008;45(1):101-2.
258. Mehta NT, Truax AD, Boyd NH, Greer SF. Early epigenetic events regulate the adaptive immune response gene CIITA. Epigenetics. 2011;6(4):516-25.
259. Zuo J, Thomas WA, Haigh TA, Fitzsimmons L, Long HM, Hislop AD, et al. Epstein-Barr virus evades CD4+ T cell responses in lytic cycle through BZLF1-mediated downregulation of CD74 and the cooperation of vBcl-2. PLoS Pathog. 2011;7(12):e1002455.
260. Ahmed D, Eide PW, Eilertsen IA, Danielsen SA, Eknaes M, Hektoen M, et al. Epigenetic and genetic features of 24 colon cancer cell lines. Oncogenesis. 2013;2:e71.
261. Miyagi T, Tatsumi T, Takehara T, Kanto T, Kuzushita N, Sugimoto Y, et al. Impaired expression of proteasome subunits and human leukocyte antigens class I in human colon cancer cells. J Gastroenterol Hepatol. 2003;18(1):32-40.
262. Ferroni P, Guadagni F, Spila A, Martini F, Gazzaniga PP. Evaluation of the potential role of class II histocompatibility antigen HLA-DR in platelet/tumor cell interaction. Cancer Res. 1994;54(3):623-5.
263. Stoneman V, Morris A. Induction of intercellular adhesion molecule 1 and class II histocompatibility antigens in colorectal tumour cells expressing activated ras oncogene. Clin Mol Pathol. 1995;48(6):M326-32.
264. Advani SM, Advani P, DeSantis SM, Brown D, VonVille HM, Lam M, et al. Clinical, Pathological, and Molecular Characteristics of CpG Island Methylator Phenotype in Colorectal Cancer: A Systematic Review and Meta-analysis. Transl Oncol. 2018;11(5):1188-201.
265. Tejpar S, Stintzing S, Ciardiello F, Tabernero J, Van Cutsem E, Beier F, et al. Prognostic and Predictive Relevance of Primary Tumor Location in Patients With RAS Wild-Type Metastatic Colorectal Cancer: Retrospective Analyses of the CRYSTAL and FIRE-3 Trials. JAMA Oncol. 2017;3(2):194-201.

266. Biton M, Haber AL, Rogel N, Burgin G, Beyaz S, Schnell A, et al. T Helper Cell Cytokines Modulate Intestinal Stem Cell Renewal and Differentiation. Cell. 2018;175(5):1307-20.e22.
267. Cramer JM, Thompson T, Geskin A, LaFramboise W, Lagasse E. Distinct human stem cell populations in small and large intestine. PLoS One. 2015;10(3):e0118792.
268. Dame MK, Attili D, McClintock SD, Dedhia PH, Ouillette P, Hardt O, et al. Identification, isolation and characterization of human LGR5-positive colon adenoma cells. Development. 2018;145(6).
269. Baus D, Nonnenmacher F, Jankowski S, Döring C, Bräutigam C, Frank M, et al. STAT6 and STAT1 are essential antagonistic regulators of cell survival in classical Hodgkin lymphoma cell line. Leukemia. 2009;23(10):1885-93.
270. Karpf AR, Peterson PW, Rawlins JT, Dalley BK, Yang Q, Albertsen H, et al. Inhibition of DNA methyltransferase stimulates the expression of signal transducer and activator of transcription 1, 2, and 3 genes in colon tumor cells. Proc Natl Acad Sci U S A. 1999;96(24):14007-12.
271. Androutsopoulos VP, Spyrou I, Ploumidis A, Papalampros AE, Kyriakakis M, Delakas D, et al. Expression profile of CYP1A1 and CYP1B1 enzymes in colon and bladder tumors. PLoS One. 2013;8(12):e82487.
272. Gilligan LC, Rahman HP, Hewitt AM, Sitch AJ, Gondal A, Arvaniti A, et al. Estrogen Activation by Steroid Sulfatase Increases Colorectal Cancer Proliferation via GPER. J Clin Endocrinol Metab. 2017;102(12):4435-47.
273. Wrangle J, Wang W, Koch A, Easwaran H, Mohammad HP, Vendetti F, et al. Alterations of immune response of Non-Small Cell Lung Cancer with Azacytidine. Oncotarget. 2013;4(11):2067-79.
274. Kim KH, Roberts CW. Targeting EZH2 in cancer. Nat Med. 2016;22(2):128-34.
275. Azad NS, El-Khoueiry A, Yin J, Oberg AL, Flynn P, Adkins D, et al. Combination epigenetic therapy in metastatic colorectal cancer (mCRC) with subcutaneous 5-azacitidine and entinostat: a phase 2 consortium/stand up 2 cancer study. Oncotarget. 2017;8(21):35326-38.
276. Lucas J, Hsieh TC, Halicka HD, Darzynkiewicz Z, Wu JM. Upregulation of PD-L1 expression by resveratrol and piceatannol in breast and colorectal cancer cells occurs via HDAC3/p300-mediated NF-κB signaling. Int J Oncol. 2018;53(4):1469-80.
277. Wu H, Zeng H, Dong A, Li F, He H, Senisterra G, et al. Structure of the catalytic domain of EZH2 reveals conformational plasticity in cofactor and substrate binding sites and explains oncogenic mutations. PLoS One. 2013;8(12):e83737.
278. Mojic M, Takeda K, Hayakawa Y. The Dark Side of IFN-γ: Its Role in Promoting Cancer Immunoevasion. Int J Mol Sci. 2017;19(1).
279. Castro F, Cardoso AP, Gonçalves RM, Serre K, Oliveira MJ. Interferon-Gamma at the Crossroads of Tumor Immune Surveillance or Evasion. Front Immunol. 2018;9:847.
280. Abiko K, Matsumura N, Hamanishi J, Horikawa N, Murakami R, Yamaguchi K, et al. IFN-γ from lymphocytes induces PD-L1 expression and promotes progression of ovarian cancer. Br J Cancer. 2015;112(9):1501-9.
281. Ngwa W, Irabor OC, Schoenfeld JD, Hesser J, Demaria S, Formenti SC. Using immunotherapy to boost the abscopal effect. Nat Rev Cancer. 2018;18(5):313-22.
282. Hoekstra ME, Bornes L, Dijkgraaf FE, Philips D, Pardieck IN, Toebes M, et al. Long-distance modulation of bystander tumor cells by CD8(+) T cell-secreted IFNγ. Nat Cancer. 2020;1(3):291-301.
283. Thibaut R, Bost P, Milo I, Cazaux M, Lemaître F, Garcia Z, et al. Bystander IFN-γ activity promotes widespread and sustained cytokine signaling altering the tumor microenvironment. Nature Cancer. 2020;1(3):302-14.
284. Si Y, Merz SF, Jansen P, Wang B, Bruderek K, Altenhoff P, et al. Multidimensional imaging provides evidence for down-regulation of T cell effector function by MDSC in human cancer tissue. Sci Immunol. 2019;4(40).
285. Hegde PS, Chen DS. Top 10 Challenges in Cancer Immunotherapy. Immunity. 2020;52(1):17-35.

286. Turkes F, Mencel J, Starling N. Targeting the immune milieu in gastrointestinal cancers. J Gastroenterol. 2020;55(10):909-26.
287. Murciano-Goroff YR, Warner AB, Wolchok JD. The future of cancer immunotherapy: microenvironment-targeting combinations. Cell Res. 2020;30(6):507-19.
288. Bentebibel SE, Hurwitz ME, Bernatchez C, Haymaker C, Hudgens CW, Kluger HM, et al. A First-in-Human Study and Biomarker Analysis of NKTR-214, a Novel IL2Rβγ-Biased Cytokine, in Patients with Advanced or Metastatic Solid Tumors. Cancer Discov. 2019;9(6):711-21.
289. Gonzalez-Exposito R, Semiannikova M, Griffiths B, Khan K, Barber LJ, Woolston A, et al. CEA expression heterogeneity and plasticity confer resistance to the CEA-targeting bispecific immunotherapy antibody cibisatamab (CEA-TCB) in patient-derived colorectal cancer organoids. J Immunother Cancer. 2019;7(1):101.
290. Morgan RA, Yang JC, Kitano M, Dudley ME, Laurencot CM, Rosenberg SA. Case report of a serious adverse event following the administration of T cells transduced with a chimeric antigen receptor recognizing ERBB2. Mol Ther. 2010;18(4):843-51.
291. Ott PA, Hodi FS. Talimogene Laherparepvec for the Treatment of Advanced Melanoma. Clin Cancer Res. 2016;22(13):3127-31.
292. Accolla RS, Frangione V, De Lerma Barbaro A, Mortara L. New strategies of mammary cancer vaccination. Breast J. 2010;16 Suppl 1:S42-4.
293. Huang S, Wang Z, Zhou J, Huang J, Zhou L, Luo J, et al. EZH2 Inhibitor GSK126 Suppresses Antitumor Immunity by Driving Production of Myeloid-Derived Suppressor Cells. Cancer Res. 2019;79(8):2009-20.